CAPILLARY ELECTROPHORESIS AND RELATED TECHNIQUES FOR THE ANALYSIS OF FRESH WATER ALGAL TOXINS

by

Wilson John

Submitted in partial fulfillment of the requirements
for the degree of Master of Science
in the
Department of Chemistry and Applied Chemistry
University of Natal
Durban

1997

Abstract

As cyanobacteria (also known as blue green algae) produce a range of cyclic peptides which are highly toxic, capillary electrophoresis and associated techniques have been investigated to assess their applicability for toxin monitoring in the water bodies of kwaZulu Natal, South Africa. Capillary electrophoresis (CE) is a technique in which charged molecules can be efficiently separated in a buffer solution within a capillary tube under the influence of a strong electric field. Two CE modes, namely capillary zone electrophoresis (CZE) and micellar electrokinetic capillary chromatography (MECC) were initially evaluated using a laboratory-built CE instrument. The former mode lacked selectivity due to the similar charge to size ratio of the algal toxins. However, with the latter mode, incorporation of a surfactant (sodium dodecyl sulphate) into the buffer, produced sufficient resolution between components. Parameters including surfactant concentration, buffer ionic strength, buffer pH and operating voltage were systematically optimized to separate the four algal toxins under investigation (microcystin YR, microcystin LR, microcystin RR and nodularin). The optimum separation conditions were: 30 mM borax, 9 mM sodium dodecyl sulphate, pH 9.18, 30 kV applied voltage, 10 s hydrodynamic injection, 70 cm x 50 μm i.d. bare fused silica capillary (L_{EFF} 40 cm) and UV detection at 238 nm. Under these conditions, typical detection limits were in the low ng/μL range (14.13 ng/μL for microcystin LR to 29.85 ng/μL for nodularin).

The MECC method was evaluated in terms of migration time precision, efficiency and resolution, peak area and normalised peak area precision. Standard deviation values for retention times acquired using replicate electrokinetic injections ranged from 0.018 to 0.054 and 0.069 to 0.148 for hydrodynamic injections. Normalised peak area precision for replicate hydrodynamic injections were in the range 84 to 97 % RSD, while improved % RSD values of 11.5 to 18.7 were achieved for electrokinetic injections. Due to poor precision resulting from the lack of automation on the laboratory built CE system, poor correlation between increasing concentration and a corresponding change in normalised peak areas were achieved. The MECC method developed was applied to the analysis of an algal scum extract to illustrate the technique.

A general problem with CE is that it suffers from poor detection sensitivity. Hence in this study, alternative injection modes, sample concentration strategies and alternative detection techniques were investigated in an attempt to improve detection limits for algal toxins. Using optimized electrokinetic injection conditions, detection limits were five to ten times better than those obtained with hydrodynamic injections. On-line sample concentration methods were partially successful. Field amplified back and forth MECC in which analyte injected in the entire column volume and subsequently focused in a narrow band by manipulating the electric field, resulted in an enormous sensitivity enhancement that ranged from 197 times for microcystin RR to 777 times for microcystin YR when compared to hydrodynamic injections. Field amplified sample stacking (FASI) was ineffective for toxin preconcentration, while electro-extraction produced detection limits ranging from 0.27 ng/μL for microcystin YR to 1.08 ng/μL for microcystin RR. Solid phase extraction, in which analytes are first trapped and concentrated on HPLC material in a cartridge and then eluted in a more concentrated form for injection, was found to be practical only in the off-line mode. A concentration detection limit of less than 0.002 ng/μL was obtained. Attempts with on-line solid phase extraction failed due to problems associated with coupling the cartridge with the separation capillary. Finally, laser induced fluorescence (LIF) detection was investigated as an alternative to UV detection. Unfortunately, the algal toxins were not amenable to LIF detection because tagging with the fluorescent moiety, fluorescein isothiocyanate (FITC), was prevented by the stereochemistry of these cyclic peptides.

A comparative study between HPLC and MECC revealed that the former displayed poor efficiency peaks and long analysis times for toxin analysis. However HPLC was superior in terms of retention time precision (0.12 to 0.64 % RSD) and area precision (1.78 to 2.86 % RSD). Mass detection limits for MECC (0.0142 to 0.0603 ng) were far superior to those achieved by HPLC (0.55 to 1.025 ng). In addition to HPLC and MECC, a preliminary investigation of micro-high performance liquid chromatography (μHPLC) and capillary electrochromatography (CEC) for the analysis of algal toxins was made using 50 μm i.d. capillary columns packed in-house, with reverse phase HPLC packing material.

Preface

This thesis presents work carried out by the author and has not been submitted in part or in whole to any other university. Where use has been made of the work of others, it has been duly acknowledged and referenced in the text. The work described in this thesis was carried out in the Division of Applied Chemistry of the Department of Chemistry and Applied Chemistry, University of Natal, Durban, from February 1995 to July 1996 under the supervision of Professor Mark W. Raynor. Parts of Chapter 4 and 5 were presented at a poster session at the 17th International Symposium on Capillary Chromatography in Riva del Garda, Italy, May 1996. An oral presentation covering work from these chapters was also presented at Euroanalysis 1X, Bologna, Italy, September 1996. The major part of Chapter 4 was published recently in the Journal of High Resolution Chromatography (volume 20, 1997, page 34-38).

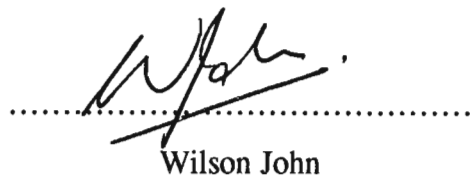

Wilson John

I certify that the above statements are correct.

.....

Mark W. Raynor

Associate Professor, Applied Chemistry

Acknowledgments

I thank a number of people for making this work possible.

Firstly my sincere gratitude goes to my supervisor Professor Mark Raynor for his close guidance, constructive criticism and words of encouragement during the course of my studies. The invaluable contribution toward the publication, presentations and the writing up of the thesis is gratefully acknowledged.

I am greatly indebted to Professor Mike Dutton and Mr Mark Wagner of the Physiology Department of the University of Natal Medical School, Durban, for the use of their HP ^{3D}CE instrumentation and also Mr Rajan Moodley of the Department of Applied Sciences, M.L. Sultan Technikon, Durban for the use of their Beckman P/ACE Laser Induced Fluorescence instrumentation.

Special thanks goes to my colleagues Mr Vikash Sewram and Miss Manomayi Venayagamoorthy, the technical staff, Mrs Saroj Naidoo and Mr Selwyn Peterson and administrative staff Mrs Jenny Hardman for their assistance. My gratitude goes also to Miss Vasti Williams for her support, encouragement, patience and assisting with the typing of this thesis. Sincere thanks goes to Miss Sharon Mei for her support and assistance during the course of my studies. Most important, I thank God for giving me strength and the blessing of good health to complete my studies.

Lastly my sincere appreciation goes to the Department of Chemistry and Applied Chemistry, University of Natal, Durban, Foundation for Research Development and Umgeni Water for financial assistance.

Table of Contents

List of Abbreviations

ADDA	3-amino-9-methoxy-2,6,8-trimethyl-10-phenyldeca-4,6-dienoic acid
Ala	alanine
Arg	arginine
CBQCA	3-(4-carboxybenzoyl)-2-quinoline carboxaldehyde
CE	capillary electrophoresis
CEC	capillary electrochromatography
CE-MS	capillary electrophoresis mass-spectrometry
CE-ICP-MS	capillary electrophoresis-inductively coupled plasma mass-spectrometry
CF-FAB	continuous flow-fast atom bombardment
CGE	capillary gel electrophoresis
CIEF	capillary isoelectric focusing
CITP	capillary isotachophoresis
CMC	critical micelle concentration
CZE	capillary zone electrophoresis
Dns-Cl	dansyl chloride
DQF-COSY	double quantum filter correlation spectroscopy
ELISA	enzyme linked immunosorbent assay
EOF	electroosmotic flow
ESI	electrospray ionization
FABMS	fast atom bombardment mass spectrometry
FASI	field amplified sample injection
FITC	fluorescein isothiocyanate
FMOC	9-fluorenylmethyl-chloroformate
FTC	fluorescein thiocarbamyl
GAC	granular activated carbon
GC	gas chromatography
Glu	glutamic acid
HMBC	heteronuclear multiple bond correlation
HMQC	proton detected multiple quantum coherence
^{1}HNMR	proton nuclear magnetic resonance

HPCE	high performance capillary electrophoresis
HPLC	high performance liquid chromatography
HRFABMS	high resolution fast atom bombardment mass spectrometry
i.d.	internal diameter
LD_{50}	lethal dose fatal to 50 % of organisms
LIF	laser induced fluorescence
LOD	limit of detection
LSIMS	liquid secondary ion mass spectrometry
MAPS	multiple antigen peptide
MAPT	ϒ-methacryloxypropyl trimethoxysilane
MC LR	microcystin LR
MC RR	microcystin RR
MC YR	microcystin YR
Mdha	methyl dehydro alanine
MeAsp	methyl aspartic acid
MECC	micellar electrokinetic capillary chromatography
μHPLC	micro-high performance liquid chromatography
MLD_{100}	minimum lethal dose
NDA	naphthalene dialdehyde
NMR	nuclear magnetic resonance
2D-NMR	two dimensional nuclear magnetic resonance
ODS	octadecyl silane
OPA	*ortho*-phthaldialdehyde
PAC	powdered activated carbon
PAGE	polyacrylamide gel electrophoresis
PDA	photodiode array detection
PEEK	polyetheretherketone
PEG	polyethylene glycol
PTFE	polytetrafluoroethylene
RSD	relative standard deviation
RI	refractive index
SDS	sodium dodecyl sulphate

SFC	supercritical fluid chromatography
SFE	supercritical fluid extraction
STDEV	standard deviation
SDB	styrene divinylbenzene
TLC	thin layer chromatography
TRIS	tris (hydroxymethyl) aminomethane
UV	ultraviolet
UV-VIS	ultraviolet-visible

List of Symbols

c	concentration
D_m	diffusion coefficient
d	particle diameter
e	electronic charge
eo	electroosmotic
ep	electrophoretic
E	electric field
Λ	equivalent conductance
g	gravitational acceleration
h	plate height
i	current density
inj	related to injection
k	Boltzmann's constant
k'	capacity factor
κ	specific conductance
L_T	total column length
L_{EFF}	effective column length
l_{inj}	injection plug length
N	efficiency
ΔP	pressure drop
q	ionic charge
R	resolution
t_m	migration time (CZE)
t_{mc}	micelle migration time
t_r	retention time (MECC)
t_o	retention time of neutral marker
T	temperature
v_{eo}	electroosmotic velocity
v_{ep}	electrophoretic velocity
V	voltage

w_b	peak width
ε	permittivity
ζ	zeta potential
η	viscosity
μ_{eo}	electroosmotic mobility
μ_{ep}	electrophoretic mobility
φ	potential/total porosity
σ^2	variance
Q	heat generated per unit volume

List of Figures

List of Tables

Chapter One

Introduction

1.1 Significance of Cyanobacterial Toxin Monitoring

The occurrence of toxic cyanobacterial blooms and scums in water bodies is a world wide phenomenon [1-3]. Cyanobacteria (also known as blue-green algae) were for many years classified as true algae. However, electron microscopy has revealed that these "algae" are in fact Gram-negative photosynthetic prokaryotes and hence this assembly of organisms has been reclassified as bacteria. Even so, the terms "blue green algae" and "algal toxins" (the toxic substances produced by these organisms) are still widely used and will be referred to in this thesis.

The first cases of cyanobacterial intoxication date back to 1853 causing the death of livestock and wildlife after drinking water from Lake Alexandrina in South Australia. Since then numerous other cases were reported [3,4,5]. In 1992 a kill of approximately 2000 brown trout in Loch Leven and the River Leven, Scotland, occurred shortly after the mass accumulation of the cyanobacterium *Anabaena flos-aquae* began to break open, releasing toxins into the water [6]. Laboratory work demonstrated that the cyanobacterial cells were lethal to mice and the liver damage was consistent with hepatotoxin intoxication. Dog fatalities occurred at Loch Insh, Scotland, in the early 1990s [7]. Human illness and health problems have also been reported [1,3,8]. The first case was published in 1931 after stagnation of the Ohio River in the USA resulted in a cyanobacterial bloom [9]. Another case in the UK involved soldiers who were hospitalized after canoeing in Rudyard Lake, England, which contained a toxic bloom of *Microcystis* at the time [10]. An outbreak of hepatoenteritis at Palm Island, Australia, occurred when 139 children and 10 adults were affected after drinking from a supply reservoir containing cyanobacteria [10]. Recent studies in the People's Republic of China have demonstrated a higher incidence of primary liver cancer in a population taking drinking water from open ditches and ponds containing cyanobacterial hepatotoxins, compared with a neighbouring population receiving its drinking water from wells [11].

Algal poisoning in South Africa (Figure 1.1A) was first diagnosed by Steyn in 1927 [12]. Stevens later reported that the most serious cases occurred in the Vaal Dam in the 1940s while no serious cases were documented in the 1950s and 1960s [13]. It was only in the 1970s that a multidisciplinary research program was initiated by the CSIR, the Medical Research Council, the University of the Orange Free State and the Department of Health to investigate the nature and extent of algal toxins. Studies conducted on the Midmar impoundment, which is the most important impoundment in the Umgeni Water operational area (Figure 1.1B), showed an increase in phosphorus loading and a significant increase in the frequency of occurrence and concentration of blue-green algae, indicating that not only had the water quality deteriorated over the last 15 years but also that phosphorus promotes algal growth. Data collected from 1989 to 1994 for total and soluble phosphorous show that rainfall and flow-rate affect loading (Figure 1.2). The general trend observed is that during periods of high rainfall (1989,1991,1994), there was a corresponding high inflow into the impoundment, resulting in increased phosphorus loading. However, these studies have shown that the relationship between phosphorus loading and algal count is non-linear and has been attributed to factors such as turbidity, temperature and retention time.

Carmichael *et al.* have studied blue-green algal toxins extensively and have categorized them into three main groups according to their mode of action [15]. Neurotoxins are fast-acting neuromuscular blocking agents that can cause respiratory distress or death in mice within minutes to hours of ingestion. Hepatotoxins cause haemorrhage necrosis of the liver and cause death within one to three hours after the toxin is consumed. Contact irritants cause severe dermatitis following direct contact [16]. The microcystins and nodularin are a group of hepatotoxins produced most abundantly by various strains of *Microcystis, Anabaena, Oscillatoria* and *Nostoc* [17].

1.2 Structure of Algal Toxins

The complexity of the algal toxin structures has resulted in a number of different studies in which various elucidation techniques have been employed. Botes *et al.* used mainly NMR

SOUTH AFRICA

(A)

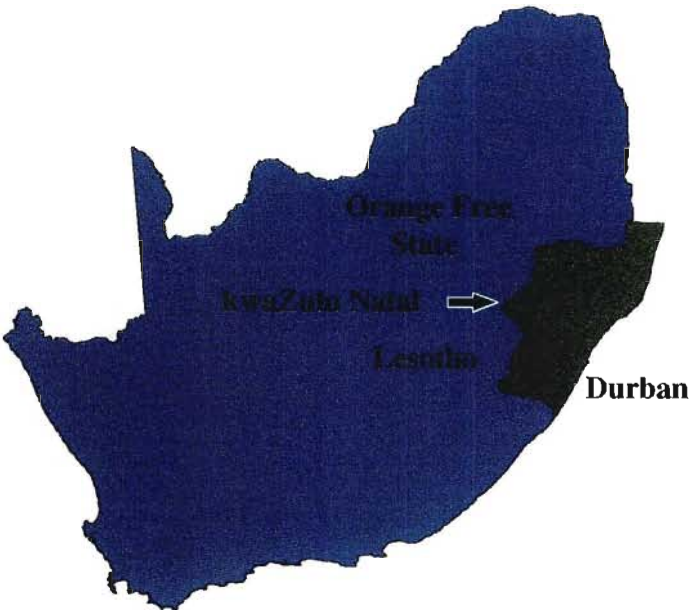

EXISTING OPERATIONAL BOUNDARY

(B)

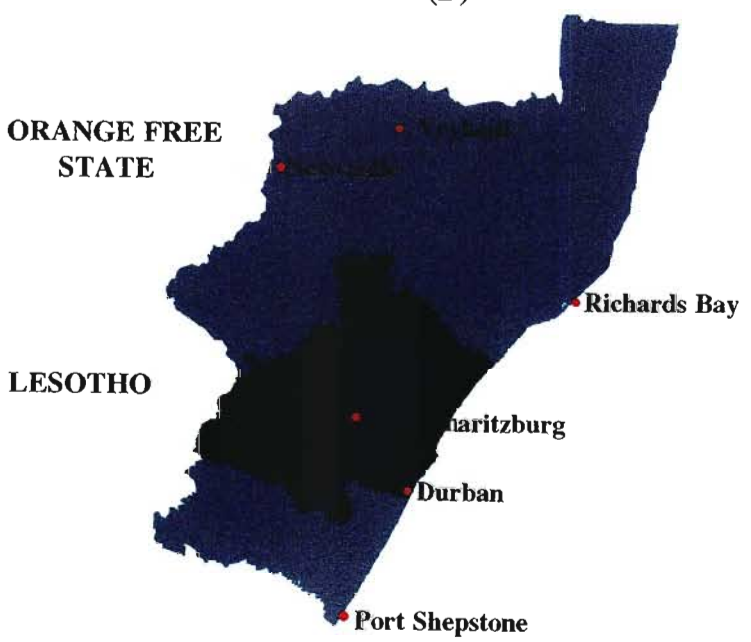

Figure 1.1 (A) Map of South Africa indicating the relative position of the province of kwaZulu Natal and (B) Existing Umgeni Water operational area (marked in dark green) with respect to kwaZulu Natal.

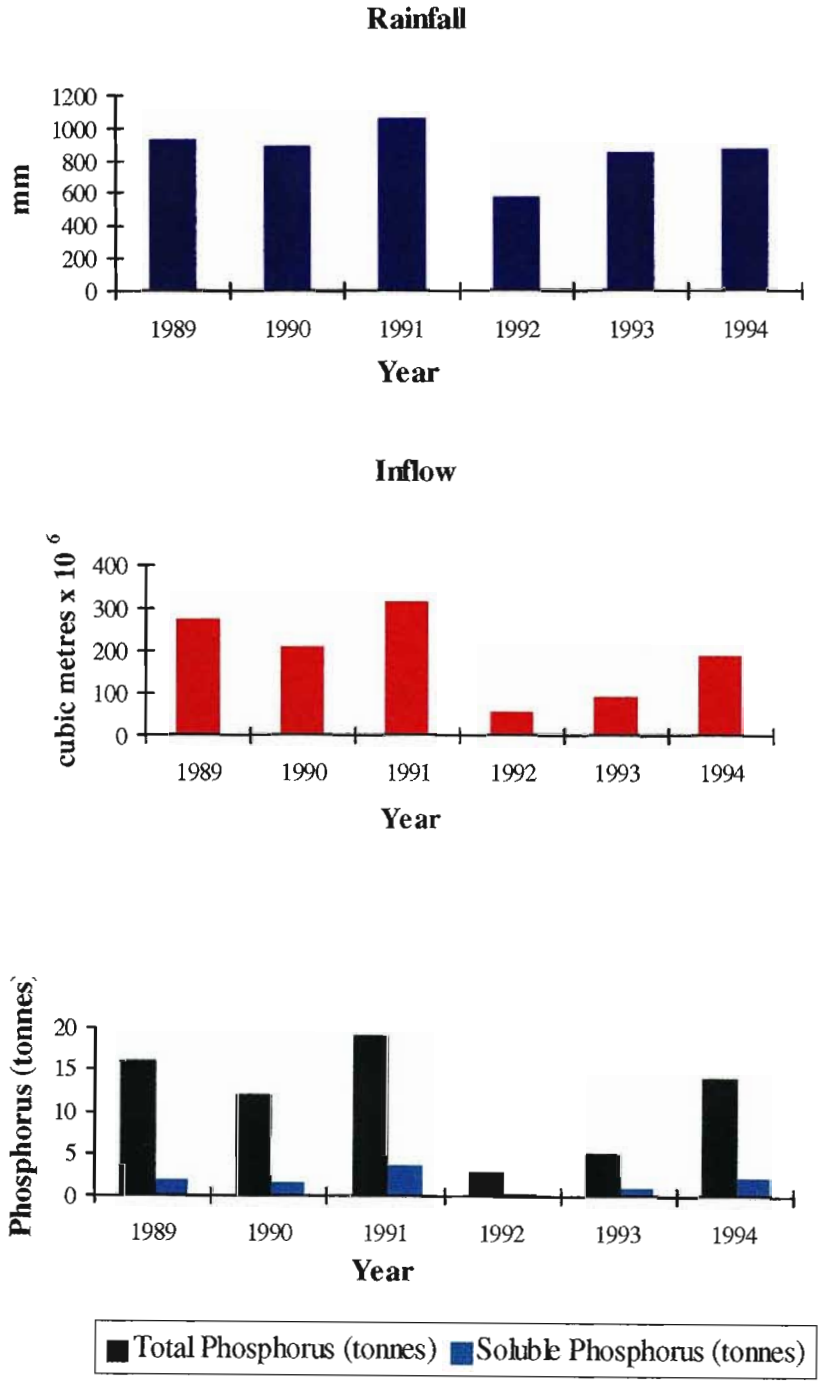

Figure 1.2 Bar graph of rainfall, inflow, total and soluble phosphorus loading in the Midmar Impoundment [14].

spectroscopy, but found it impractical to apply routinely because several milligrams of pure toxins are required [18].

Harada *et al.* established a non-destructive method using a combination of 2D-NMR techniques: double quantum filter correlation spectroscopy (DQF-COSY), ^{1}H-detected multiple quantum coherence (HMQC) and heteronuclear multiple bond correlation (HMBC), for structure determination of the microcystins [19]. The method was successfully applied to assign all carbons and protons of microcystins so that the sequence of constituent amino acids in the microcystins was confirmed.

Mass spectrometry has also been used for structure elucidation. Fast atom bombardment mass spectrometry (FABMS) and liquid secondary ion mass spectrometry (LSIMS) are particularly powerful techniques for obtaining molecular weight information on these polar involatile compounds. However, it is difficult to obtain sequence information of the constituent amino acids. In addition, background interference in the low mass region makes structure elucidation difficult.

Luukainen *et al.* characterized microcystins from eight different Finnish lakes by amino acid analysis, FABMS, and tandem FABMS [20]. From a total of 8 compounds, 5 were known microcystins. The structure of one of the remaining 3 was assigned. Namikoshi *et al.* isolated 12 hepatotoxins from *Microcystis* collected from Homer Lake, Illinois, in 1988 [21]. The components were characterized by amino acid analysis, HRFABMS, FABMS/MS, ^{1}H NMR and UV spectroscopic methods. MC LR was the principal toxin and the presence of MC YR and MC RR was also detected. In addition 9 new microcystins were found, of which the structures of seven were assigned.

Structure elucidation has revealed that these compounds are cyclic peptides, with the microcystins being heptapeptides (Figure 1.3A,B,C) [18,22] and nodularin a pentapeptide (Figure 1.4) The general structure of the microcystins are cyclo (-D-Ala-X-D-MeAsp-Z-Adda-D-Glu-Mdha-), with X and Z being the two variable L-amino acids. About 40 variants have been reported [23,24,25,26]. The pentapeptide, nodularin, is cyclo (-D-

A

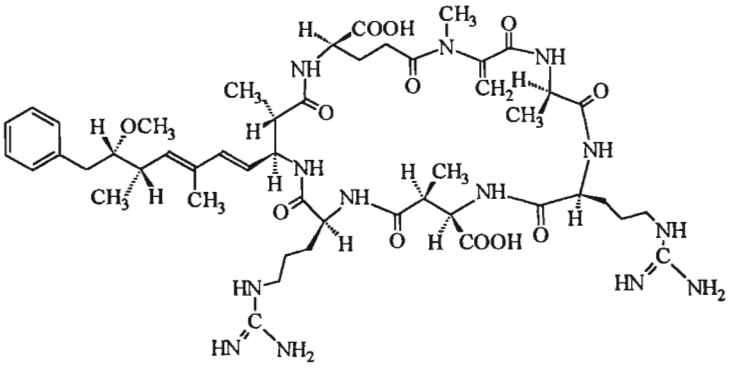

B

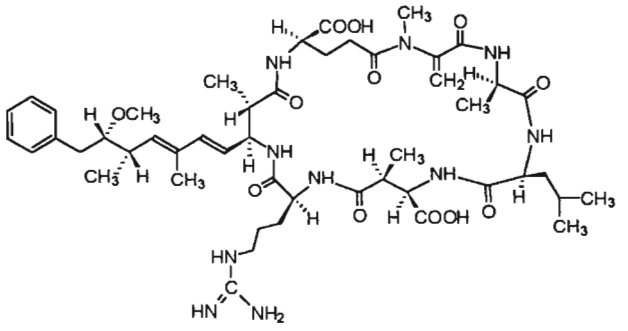

C

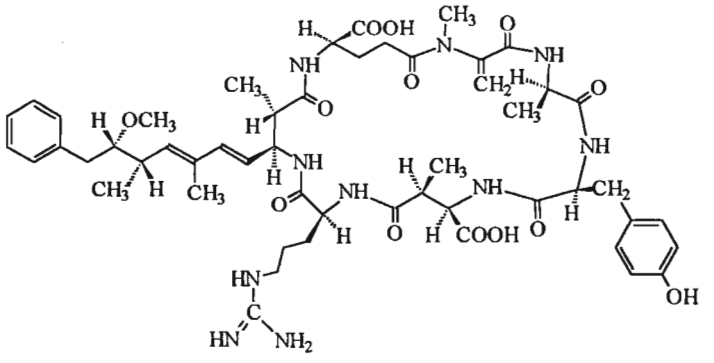

Figure 1.3 (A) Structure of microcystin YR (MC YR), (B) microcystin LR (MC LR), and (C) microcystin RR (MC RR).

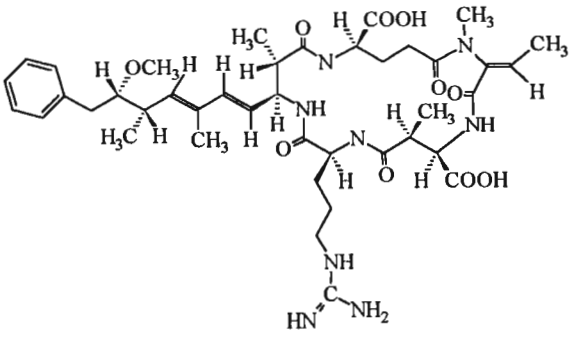

Figure 1.4 Structure of Nodularin.

MeAsp-L-Arg-Adda-D-Glu-Mdhb) [27]. Only one form has been reported so far [23,27,28]. Their high toxicity (LD_{50}=50-600 μg/kg) [17,29], as demonstrated by intraperitoneal mouse bioassay studies, and their impact on water quality are a cause of great concern to water authorities world-wide, particularly as the microcystins cause hepatocyte necrosis [30]. More recent studies suggest that these compounds inhibit the enzymes, protein phosphatases 1 and 2A, and act as tumor promoters in rat liver.

1.3 Toxicity and Factors Affecting Toxicity

The potent hepatotoxicity of algal toxins has serious implications on human health. Five pathways may be considered to contribute to the natural route of detoxification of these toxins including dilution, adsorption, thermal decomposition aided by temperature and pH, photolysis and biological degradation. Namikoshi *et al.* demonstrated that mice given the mono ester of the alpha carboxyl on the glutamic acid unit of MC LR at 1 mg/kg, lived for one week [24]. The compound failed to induce any clinical signs of toxicosis during the week of observation. Studies by Dahlem *et al.* demonstrated that removal of saturation of the 3-amino-9-methoxy-2,6,8-trimethyl-10-phenyldeca-4,6-dienoic acid (ADDA) structure greatly reduces the toxicity of MC LR [31]. A possible explanation for this finding is that the ADDA group of the toxin may provide the necessary steric configuration required for the inhibition of protein phosphatase.

A number of laboratory experiments investigated the influence of environmental factors such as light, temperature, pH, aeration, culture age, and nutrients [32-44]. Wicks *et al.* conducted such studies on the scum samples collected from Hartbeesport Dam, South Africa [45]. The results showed that the toxin concentration was positively correlated to chlorophyll "a" concentration, solar radiation, surface water temperature, pH, and percent oxygen saturation. The growth rate and toxicity of *Microcystis* cultures increased with light intensity, temperature (18-25°C), and pH (8-9).

1.4 Toxin Removal from Potable Water

A number of researchers have shown that conventional water treatment techniques such as coagulation, sedimentation, filtration and chlorination are not effective for removing microcystins from raw water [46-48]. However they showed that while powdered activated carbon (PAC), afforded some removal of the microcystins, granular activated carbon (GAC) was very effective. Only two water treatment plants in Australia currently use GAC filters because of the high costs. The remaining plants use PAC to control the relatively infrequent occurrences of taste and odour problems.

James *et al.* assessed the effect of various oxidants including ozone, chlorine, chlorine dioxide, hydrogen peroxide, and potassium permanganate for the removal of MC LR [49]. Ozone doses of about 2.5 mg/L almost totally removed MC LR from raw and clarified water. The use of a polymeric nanofiltration membrane with a nomimal molecular weight cut-off of 200 resulted in a complete rejection of MC LR. Chlorine and hydrogen peroxide were shown to be ineffective. Chlorine dioxide was ineffective when applied to raw water but resulted in significant removal when applied to clarified water at high doses (>6 mg/L). Potassium permanganate was the most effective oxidant for toxin removal.

1.5 Extraction, Analysis and Detection

Because of the world-wide recognition of the potential health problems caused by toxic cyanobacteria, the need for suitable analytical techniques for toxin monitoring purposes has been highlighted. Methods for the detection and analysis of cyanobacterial toxins fall into two broad categories: biological systems, including protein phosphatase inhibition and biochemical methods, and physicochemical methods.

1.5.1 *Biological Assays*

The mouse bioassay is the longest established and most extensively used method for toxicity determination of cyanobacterial toxins. Its implementation relies on the use of laboratory animals which are dosed orally or intraperitoneally. Quantification of toxicity is determined as the concentration of test material which is lethal to 50% of the test population (LD_{50}) or as the minimum lethal dose for the population (MLD_{100}). Other bioassay methods have employed and evaluated alternatives to the mouse bioassay such as Daphnia, Artemia, bacterial and cytotoxicity bioassays [50-52]. Assays involving the use of bacteria for toxin detection and quantification include assays for the inhibition of bioluminescence, pigment production and growth [53].

In vitro cytotoxicity assays using isolated cells have also been used for toxicity testing [54-57]. Lastly at a molecular level, microcystins are potent inhibitors of protein phosphatases 1 and 2A and microcystins can be detected by measuring the inhibition of phosphate release [58]. Jones *et al.* used protein phosphatase inhibition assay for the detection of the presence of MC LR in filtered samples of *Microcystis* [59].

Chu *et al.* developed an enzyme-linked immunosorbent assay (ELISA) method for the freshwater microcystin detection [60]. The assay involves coating anti-MC LR antibody to the ELISA plate and the use of MC LR peroxidase as the enzyme marker. The antibodies reacted in the presence of the microcystins. The detection limit for microcystins in dried algae was 0.25- 0.5 μg/g lyophilized algae sample.

1.5.2 *Physicochemical Assays*

In addition to toxicity detection in samples, quantification and identification of the toxins present are also important. Gregson and Lohr used reversed phase high performance liquid chromatography (HPLC) with a variable wavelength ultraviolet absorbance (UV) detector in the early 1980s for toxin analysis [61]. More recently HPLC with photodiode-array (PDA UV) detection has been used. This instrumentation allows the UV spectrum of peaks separated by HPLC to be measured. As microcystins have characteristic absorption profiles in the wavelength range 200-300 nm, these can be used as an indication of the identity. A HPLC PDA analytical method has also been devised for measurement of intracellular and extracellular microcystins in water samples containing cyanobacteria [62].

Luukainen *et al.* extracted toxins from lyophilized *Oscillatoria* cells with n-butanol-methanol-water [20]. The organic solvents were evaporated and the toxins applied to a preconditioned C_{18} silica gel cartridge and then eluted with 80 to 100% methanol. Analysis was performed using reversed phase HPLC, thin layer chromatography (TLC), FABMS and gas chromatography (GC). Lawton, Edward and Codd found that repeated methanol extraction was the most versatile solvent for the extraction of microcystins from cyanobacterial cells [62]. The filtered water was subjected to trace enrichment using a C_{18} solid phase extraction cartridge, followed by determination and identification by reversed phase HPLC and photodiode-array UV detection. This is the most frequently used method for the toxin analysis.

Lui *et al.* developed a capillary zone electrophoretic (CZE) technique for the separation of 3 microcystin toxins [63]. 52 different buffer solutions were evaluated and conditions such as pH, applied voltage and concentration were optimised. Their findings were that an acetate buffer at pH 4 produced best results. Precision for apparent mobility ($\mu_{app}=\mu_{ep}+\mu_{eo}$) was 0.8% and 8% for corrected peak areas. The limit of detection (LOD) for microcystin LR was 2 ng/μL. This method was used to monitor the purity of microcystin LR prepared by preparative LC. Wright *et al.* applied CZE to the separation of 3 highly polar naturally occurring marine toxins that are normally difficult to analyse by conventional chromatographic methods [64]. A phosphate buffer at pH 8.7 and a separation voltage of 40 kV was used. Three different derivatization reagents (dansyl chloride, fluorescamine

and ortho-phthaldialdehyde) were used to improve detection sensitivity. The dansyl derivatives were neutral and could not be separated. In contrast, the charged fluorescamine-labelled toxins were easily separated and again the neutral ortho-phthaldialdehyde (OPA) derivatives could not be separated. An LOD of less than 0.1 attomole of the OPA derivative of saxitoxin was achieved. Lastly Lindner *et al.* reported the separation of mycotoxins by CZE, using a phosphate buffer at pH 7 [65]. In addition to the influence of various kinds of buffer additives (β-cyclodextrin, γ-cyclodextrin and cyclodextrin derivatives), reversed electroosmotic flow was evaluated for improving selectivity. Changes in selectivity were attributed to the combined effect of mobility changes resulting from buffer viscosity changes, as well as the different "host-guest" interactions occurring in the cyclodextrin-modified buffer system used. The LOD of the mycotoxins were 1 ng/μL.

Up to now the most popular analytical methods for the determination of these toxins have involved the use of high performance liquid chromatography [62,66,67]. The drawbacks of HPLC include long analysis times, low chromatographic efficiency and poor resolving power. Further, the low diffusion coefficients (D_m) of large biomolecules in liquid mobile phases increase the contribution to the resistance to the mass transfer term in the van Deemter equation resulting in band broadening. The gradient elution program recommended in a publication by Lawton, Edward and Codd requires a total analysis time of one hour to allow for proper equilibration of the column [62]. On the other hand, as shown by other workers, capillary electrophoretic techniques are more efficient at separating these types of molecules [63-65]. From the equation

$$N = \frac{\mu V}{2D_m} \qquad 1.1$$

where μ is the electrophoretic mobility and V is the applied voltage, it is clear that a greater number of theoretical plates (N) will be produced from solutes with a low D_m [68]. For this reason, this thesis focuses on the investigation of capillary electrophoretic methods for the analysis of algal toxins. The following four chapters therefore deal with the theory of

CE methods, experimental details, the optimization of CE conditions for separating algal toxins and the methods used to improve detection sensitivity. A comparative study between CE, HPLC and various micro-liquid separation techniques is made in Chapter 6. The concluding chapter outlines all the important results of the study and recommendations are made for future developments in the analysis of algal toxins by CE. Comments on recent advances and future trends in CE technology are also given.

Chapter Two

Capillary Electrophoretic Methods and Related Techniques
Literature Review

2.1 Introduction

Electrophoresis is a process in which electrically charged species in solution are separated based upon differential migration rates in an electrical field. The principles have been established for over 100 years, however the first sophisticated apparatus was developed by Tiselius in the 1930's for which he was awarded a Nobel Prize in 1948. Jorgenson was the first to demonstrate the power of capillary zone electrophoresis (CZE) in narrow bore capillaries utilizing the effect of electroosmotic flow and it was only in the mid 1980's that commercial instruments for performing electrophoresis in capillary columns were introduced and the technique is now called capillary electrophoresis (CE) or high-performance capillary electrophoresis (HPCE).

2.2 Theory of Capillary Electrophoresis

In this chapter the theory and principles of capillary electrophoretic techniques are discussed. Injection and detection methods are described and factors affecting band broadening are highlighted. Finally some applications which show the analytical potential of CE techniques are presented.

Typically, electrophoresis is carried out in a fused silica capillary, 20 to 100 cm long with an internal diameter ranging from 25 to 100 μm filled with an appropriate buffer solution. A small volume of sample (1 to 30 nL) is introduced into the capillary after which opposite ends of the capillary together with the respective electrodes are immersed into the buffer solution. An electric potential (200 to 300 V DC/cm) is then applied across the capillary causing charged species inside the capillary to migrate toward the electrode of opposite polarity according to the equation

$$v_{ep} = \mu_{ep} E = \frac{\mu_{ep} V}{L} \qquad 2.1$$

where v_{ep} is the migration velocity, μ_{ep} the electrophoretic mobility, E the electric field strength and V the voltage applied across the column of length L. Separation is based on the differences in their electrophoretic mobilities which in turn are governed by the solute charge, size, shape and properties of the buffer solution. Each component migrates in a relatively narrow band and can be monitored and quantified using an on-column detector. A short section of the polyimide coating on one end of the capillary column is removed to form a suitable window for detection of the separated components. Provided that the electroosmotic velocity is high enough, positive, neutral and negative species can be separated in the same run.

2.3 Electroosmosis

Electroosmosis is one of the oldest electrokinetic effects discovered. It can be described as the relative motion of a liquid to a fixed charged surface caused by an electric field. In the case of fused silica in contact with an aqueous solution, its surface hydrolyses to form silanol groups. These groups may be positively charged ($SiOH_2^+$), neutral (SiOH), or negatively charged (SiO^-), depending on the buffer pH. Typically SiO^- groups exist for most applications and are counterbalanced by adsorption of buffer cations. Some of these cations are free to move in solution while others are considered to be fixed to the silica surface. This combination of negative charges on the surface and positive charges in the liquid is called the electrical double layer (Figure 2.1).

Stern's model describes the double or the Helmhlotz layer as consisting of a rigid double layer of adsorbed ions and a diffuse double layer or the Gouy-Chapman layer (sometimes called the Debye-Huckel layer). An electric potential is set up at the interface between the electrolyte solution and the silica surface. The potential of the diffuse double layer is called the zeta potential, ζ, the magnitude of which is given by

$$\zeta = \frac{4\pi\eta\mu_{eo}}{\varepsilon} \qquad 2.2$$

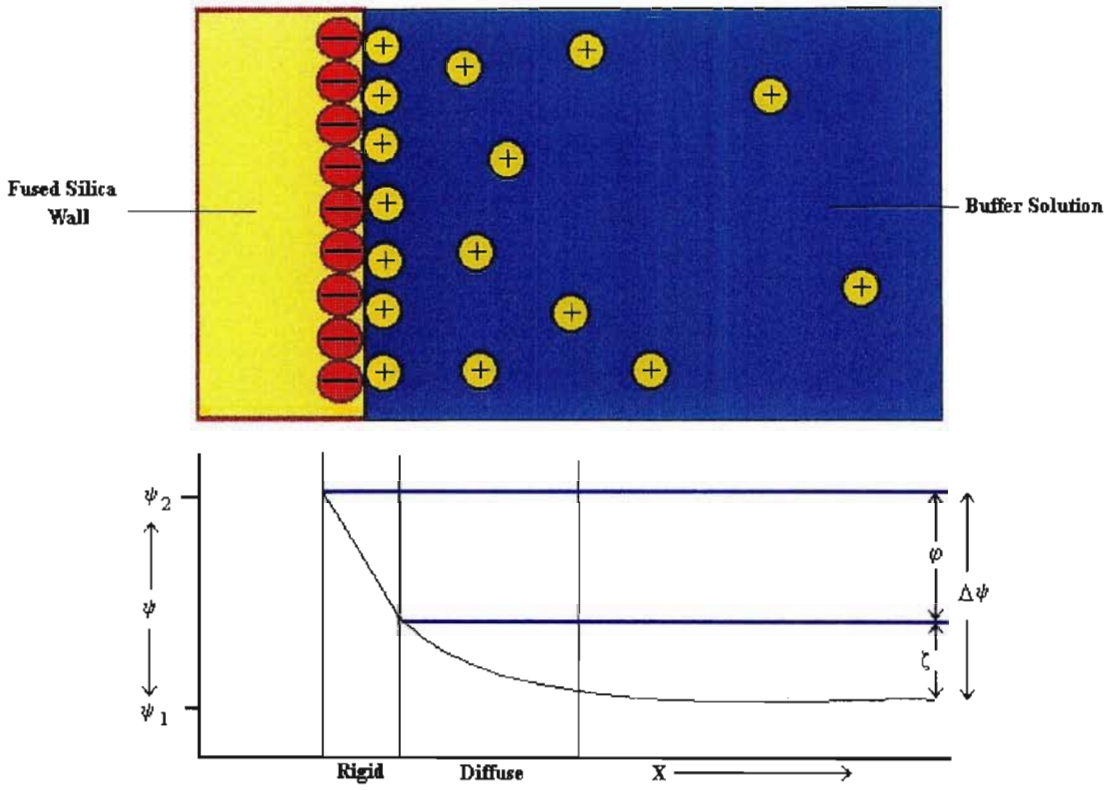

Figure 2.1 Stern's model of the electrical double layer occurring at the interface between an electrolyte solution and the surrounding surface [69].

where η is the solution viscosity, μ_{eo} is the coefficient of electroosmotic flow (EOF) and ε the dielectric constant of the solution. Within the Helmholtz layer, the potential φ drops linearly with distance x from the silica surface while in the diffuse region of the double layer, ζ decreases exponentially. The excess cations in the diffuse double layer forms a charged sheath which encloses the main bulk of the electrolyte. When an electric field is applied parallel to the silica surface, the positive ions together with their hydration spheres experience a force toward the negative electrode. Bulk flow induced by the field is generated over the surface and is called electroosmosis. The electroosmotic velocity v_{eo} is given by

$$v_{eo} = \frac{\varepsilon E \zeta}{4\pi\eta} \qquad 2.3$$

The thickness of the double layer is extremely small (up to several hundred nanometers) relative to the radius of the capillary (25 to 100 μm) and therefore EOF may be considered to originate at the walls of the capillary resulting in the production of a plug flow profile (Figure 2.2). In the infant stages of CE many attempts were made to suppress electrophoresis because it hindered the development of a practical method for the performance of electrophoresis on a microscale. However Jorgenson exploited this

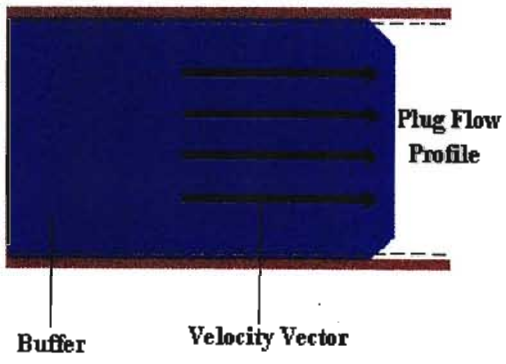

Figure 2.2 Flow profile of an electrically driven system. Arrows indicate flow velocity vectors.

phenomenon to advantage and introduced contemporary electrophoresis to the world. Since 1981, the CE revolution began. The explosion of CE in the 1980's was a result of two factors that had come together. Fused silica tubing coated with polyimide was developed by Dandeneau working at Hewlett Packard Laboratories (Little Falls Site, DE, USA). These capillaries are robust and offer a non-conducting tube with useful heat dissipation properties. Instrumentation was the second factor. In the late 1970's new rapid response UV detectors with improved electronics were introduced for μHPLC and supercritical fluid chromatography. From the perspective of an alternative separation technique, CE gained increasing popularity as it offered several advantages over established separation methods and showed potential of being the next major instrument technique. This is evidenced by the large number of publications, scientific meetings, new commercial instruments and separation methodologies. The tremendous interest in CE stems from the fact that

extraordinary high peak efficiencies are achieved and is attributable to the characteristic flat flow profile. In addition CE is noted for relatively short analysis times, high peak capacity and simple instrumentation due to the absence of an injector, a pump, solvent mixers, and special detection cell. Also CE has a wide range of applications in greatly diverse fields such as chemical, biotechnological, environmental and pharmaceutical analysis as shown in Section 2.10.

2.4 Electroseparation Modes

2.4.1 *Capillary Zone Electrophoresis (CZE)*

CZE is the easiest and most commonly used technique in CE. Individual ions move at a velocity v_{ep}, given by equation 2.1 in a plug of buffer which itself moves at a velocity v_{eo}, given by equation 2.3. Separation of charged species results from differences in their electrophoretic velocities while transport of the species along the tube is primarily by electroosmosis. The electroosmotic flow is usually significantly greater than the electrophoretic mobility of the individual ions and consequently anions, neutrals and cations can be separated in the same run (Figure 2.3A). The separated components form sharp zones and are directed toward a detector.

2.4.2 *Capillary Isotachophoresis (CITP)*

CITP is carried out in a discontinuous buffer system in which the sample components are sandwiched between a leading electrolyte and a terminating electrolyte. Cations of the leading electrolyte must have a higher mobility than the cations that have to be separated. The terminating electrolyte must have a lower mobility than that of the cationic species in the sample. Consequently, the resistance and field strength varies along the separation axis. Upon the application of a potential, leading cations move faster than sample ions creating a region of low conductivity and high electric field strength. This speeds up the faster moving sample ions, pulling them along to prevent the formation of a non-conductive gap in the solvent. In turn they act as leading electrolyte for the slower moving ions and eventually a steady state is reached in which each ion occupies its own zone, adjacent to a zone with higher mobility on one side and one with lower mobility on the other side.

Suppression of EOF is vital and the sample containing only cations or anions can be separated per run. The technique failed to become widespread because successful application is dependent on the judicious control of separation conditions, knowledge of mobility and pK values of the sample components. Steghuis *et al.* used CITP as an on-line concentration pretreatment technique for the CE analysis of FITC derivatized amino acids [70]. Other applications include purity control of synthetic peptides [71,72], separation of commercial immunoglobin preparations for intravenous administration [73] and the determination of calcium ions in the presence of phosphate anion and collagen [74].

2.4.3 *Capillary Gel Electrophoresis (CGE)*

The separation mechanism in CGE is based on molecular sieving which in turn is determined by the differences in solute size (Figure 2.3B). The gel also minimises solute diffusion and adsorption on the capillary walls and helps eliminate electroosmosis. This results in extremely high efficiencies, as demonstrated by Karger *et al.* [75,76], and high resolution. The capillaries are normally filled with polyacrylamide gels containing sodium dodecyl sulphate (SDS), and the technique is referred to as SDS-PAGE. Some of its applications include the separation of proteins, polynucleotides and DNA fragments [75-77]. The limitation of the technique is that neutral molecules cannot be separated.

2.4.4 *Capillary Isoelectric Focusing (CIEF)*

CIEF is limited to amphoteric molecules like proteins. Separation is achieved due to their differences in isoelectric points (pI), where pI is the pH at which an ampholyte has no net charge. At that pH, it is present mainly in the zwitterionic form and does not migrate in an electric field. At high pH (pH > pI), the ampholyte is negatively charged and at low pH (pH < pI), it takes a positive charge. A linear pH gradient is generated across the capillary by a mixture of carrier ampholytes like polyaminopolycarboxylic acids, having pI values covering the desired pH range. After sample introduction, the anodic end of the column is placed in an acidic solution (anolyte) and the cathodic end in a basic solution (catholyte). Under the influence of an applied electric field, sample components will migrate until they reach a region of pH where they become neutral. Zones are focused until a steady state is reached. The focused zones are mobilized past the detector by using pressure as the driving

force. Some applications of CIEF include the analysis of proteins [77-81] and the fractionation of the human recombinant tissue, plasminogen activator glycoforms [82].

2.4.5 *Capillary Electrochromatography (CEC)*

CEC is the least developed of all the electroseparation methods, but is receiving great attention at the present time. The earliest demonstration of CEC was by Pretorius *et al.* in 1974 and it involves packing the separation column with chromatographic material [83]. No further work was reported in this area until the method was revived by Jorgenson and Lukacs in 1981 [84]. Mobility due to electrophoretic properties and sorptive interactions arising from chromatographic behaviour are used simultaneously to produce high resolution separations. CEC in essence exhibits behaviour that is a hybrid between chromatography and electrophoresis (Figure 2.3D). However, the two characteristics, electroosmosis and electrophoresis, from CEC are absent in conventional liquid chromatography. Researchers have used this technique in two ways, with [85-88] and without pressurized flow [89-91]. Pretorius described the relationship between the velocity of a liquid in an applied electric field by the equation

$$\mu = \frac{\varepsilon \zeta E}{4\pi\eta} \qquad 2.4$$

where μ is the linear velocity, ε the dielectric constant, E the electric field strength, η the solution viscosity and ζ the zeta potential. He pointed out that the equation predicts that μ is independent of both the channel and particle size, resulting in a flow which should be uniform across a column irrespective of any inhomogeneities [83]. For a pressure driven system, Knox used the equation

$$\mu = \frac{d^2 \Delta p}{\varphi \eta L} \qquad 2.5$$

where d is the particle diameter, φ is the pressure resistance factor for packed columns, L is the column length and Δp is the pressure drop across the column, to describe the linear flow rate [92]. Numerous problems have been encountered by these researchers, the main ones being bubble formation, flow interruptions accompanied by breakages in current, increased joule heating and sample introduction difficulties. Jorgenson remarked that CEC in packed

columns is difficult and expressed doubt whether increased performance would justify increased difficulty [84].

2.4.6 *Micellar Electrokinetic Capillary Chromatography (MECC)*

MECC was developed by Terabe for the electrokinetic analysis of neutral molecules [93,94]. Studies have shown that it can be applied equally well to the analysis of ionic compounds [95-110]. Using the same instrumentation as CZE, MECC requires only the addition of a charged surfactant to the background electrolyte at or above its critical micelle concentration (CMC). The surfactant molecules form aggregates with typical lifetimes of < 10 μs. During this period, solute molecules partition themselves between the aqueous phase and micellar phase, based on their hydrophobicity. The separation mechanism is analogous to reversed phase liquid chromatography except for the fact that the micelles are referred to as a pseudo-stationary phase. Sodium dodecyl sulphate (SDS), with a critical micelle concentration of 0.0082 M and an aggregate number of 64 at 25°C, is the preferred surfactant in MECC because it possess a negative charge and moves against the bulk EOF although more slowly, so that the net direction of movement is the same as that of the bulk flow. Neutral as well as ionic solutes with similar mobilities that cannot be resolved by CZE are effectively separated by MECC (Figure 2.3C). They elute within a time window starting with species which are least partitioned and finishing with species that are most strongly partitioned into the micelles. Other surfactants used are shown in Table 2.1.

2.5 Sample Injection

The sample must be introduced on column with minimum volume in order to preserve the separation efficiency by restricting the initial zone broadness of the analytes. The total length of the sample plug is therefore limited by the impact of the plug length on peak width. The relationship between injection plug volume and the contribution to standard deviation is given by

$$\sigma_{q_{inj}} = \frac{q_{inj}}{\sqrt{12}} \qquad 2.6$$

Table 2.1 Critical micelle concentration and aggregation numbers of some surfactants

Surfactant	CMC (mM)	Aggregation Number
Sodium decyl sulphate	33	41
Sodium dodecyl sulphate	8.2	64
Sodium tetradecyl sulphate	2.05	80
Sodium hexadecyl sulphate	0.45	100
Sodium lauroylmethyl taurate	8.7	< 10
Sodium cholate	13	< 10
Sodium dehydrocholate	10	< 10
Sodium taurocholate	10	< 10
Sodium taurodehydrocholate	6	< 10
Decyltrimethylammonium bromide	65	< 10
Dodecyltrimethylammonium bromide	15	50
Tetradecyltrimethylammonium bromide	3.5	75
Hexadecyltrimethylammonium bromide	0.92	61

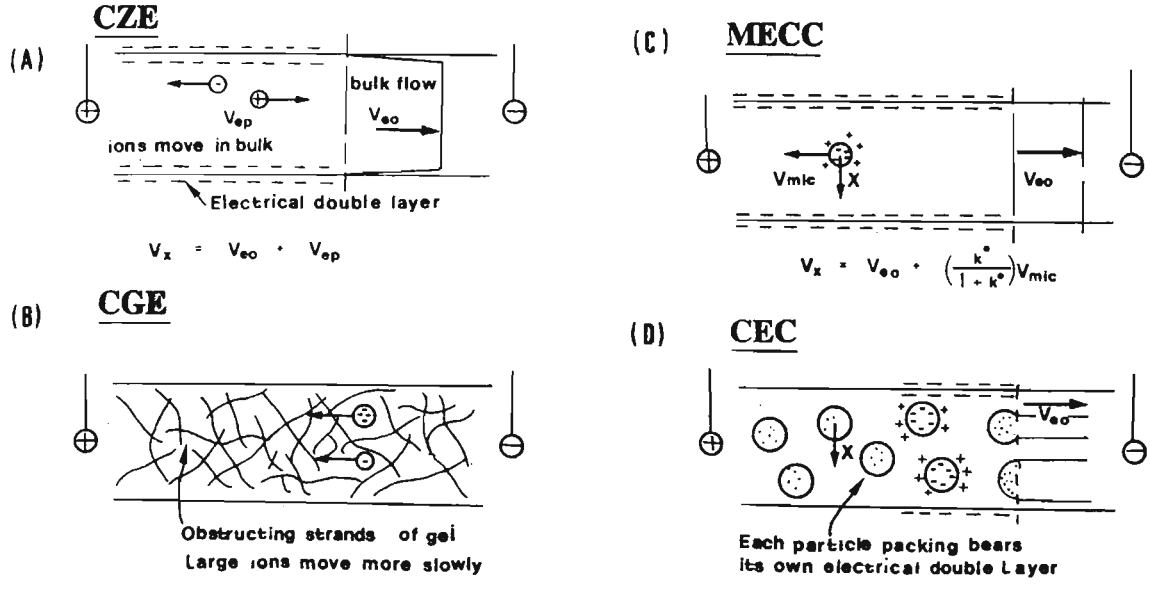

Figure 2.3 Diagrammatic representation of (A) CZE, (B) CGE, (C) MECC, and (D) CEC. v_x is the linear migration velocity of analyte X, v_{eo} is the electroosmotic velocity, v_{ep} is the electrophoretic velocity and k^* is the phase capacity ratio.

where $\sigma_{q_{inj}}$ is the standard deviation of the injection plug and q_{inj} is the volume of sample injected [111]. Therefore, if q_{inj} becomes too large, $\sigma_{q_{inj}}$ can negatively influence the separation efficiency. Grushka and McCormick demonstrated that insertion, withdrawal or both actions could result in sample penetration into the capillary [112]. This is another contributor to peak broadening because sample enters the capillary in an uncontrolled manner. The mechanism of extraneous injection was identified as being due to the displacement of a small volume of the sample into the capillary during insertion into the sample solution, convective movements between buffer and sample due to differences in viscosity, surface tension and density and lastly diffusion of solutes into the capillary. Convective movements attributable to the density difference between the buffer and sample have been thought to play the major part.

Numerous techniques have been developed for sample introduction including the electric sample splitter [113], the split flow syringe injector [114], the rotary type injector [115], freeze plug injector, sampling device with feeder [116], micro injectors [117-120], optical gating [121], on column fracture, and field amplified sample injection (FASI) [122-124]. However, two of the most commonly used injection techniques are on-column hydrodynamic and electrokinetic injections.

2.5.1 *Hydrodynamic Injection*

This injection technique involves a pressure drop along the length of the capillary by either high pressure at the injection end, vacuum at the detector end or hydrostatic pressure by utilizing gravity. The injection volume can be calculated by Poiseuille's law for liquid flow

$$V_i = \frac{\Delta p \, \pi \, r^4 t}{8 \, \eta L_T} \qquad 2.7$$

where V_i is the injection volume (m^3), Δp the pressure difference (Pa), r the inner radius of the capillary (m), t the injection time (s), η the viscosity (Pa s) and L_T the total capillary length (m) [69].

2.5.2 *Electrokinetic Injection*

This mode is based on the fact that voltage causes electrophoretic and electroosmotic movement. The electrode and column inlet are removed from the buffer vial and immersed into the sample vial. An injection voltage is applied for a brief period causing the sample to enter the column by electromigration. From the equation

$$W = \frac{\left(\mu_{ep} + \mu_{eo}\right) \pi r^2 V_i t_i c}{L} \qquad 2.8$$

where V_i is the injection voltage, t_i the injection time, c the sample concentration and other symbols have their usual meanings, the amount of solute injected, W, can be determined. During electrokinetic injection, two types of bias may occur, discrimination as a result of the differences in the electrophoretic mobilities of the various solute species in solution and discrimination by virtue of the conductivity differences between sample solution and operating buffer [125].

With automated systems, peak area reproducibility of 2-3% RSD can be achieved [127]. Hydrodynamic injection is not suitable for viscous samples nor can it be used for CGE because of suppression of hydrodynamic flow. Electrokinetic injections can, however, overcome this problem. Other injection techniques suffer from practical limitations, such as the need to design devices for introducing the sample into the capillary without creating dead volume problems or causing overloading.

2.6 Detection

In CE on-column UV or fluorescence detection is achieved by creating a window on a small section of the capillary by charring, alkaline etching or mechanical scraping of the polyimide. The path length is defined by the internal diameter of the capillary. A wide range of detection techniques have been employed in CE, including UV-visible absorption (UV-VIS), photodiode array (PDA) and multi-wavelength lamp based fluorescence, laser-based thermo-optical and refractive index (RI), electrochemical, indirect detection, radioisotope detection and mass spectrometric detection. The most frequently used is UV-visible absorption followed by fluorescence detection. Multi-wavelength detection can be

performed, making peak identification easier. The main problem in CE detection arises as a direct consequence of the low sample capacity to be detected. Further, the optical pathlength is defined by the internal diameter of the capillary (Figure 2.4), adding to poor detection sensitivity.

Figure 2.4 Schematic diagram of the standard on-column cell.

In recent years, a considerable amount of research has been reported on methods to overcome this limitation. Some approaches include the use of axial beam illumination, the Z-shaped flow cell (Figure 2.5A), the multi reflection flow cell (Figure 2.5B) and the bubble cell which was first introduced by Hewlett Packard (Figure 2.5C). Recently Hewlett Packard designed a high sensitivity cell for their HP ^{3D}CE system. This cell design is based on the Z-shaped cell which improves detection sensitivity by more than 10-fold over standard capillaries [111]. Figure 2.6A&B shows the electropherogram of brilliant green obtained with a single pass cell and a multi-reflection cell respectively [126].

A

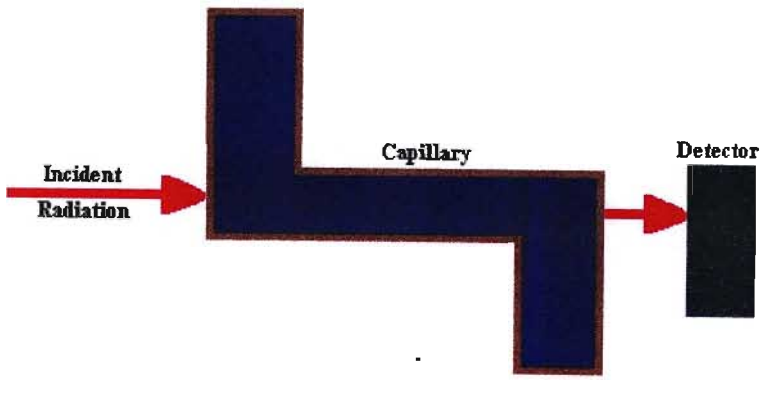

Figure 2.5 (A) Schematic representation of the Z-cell.

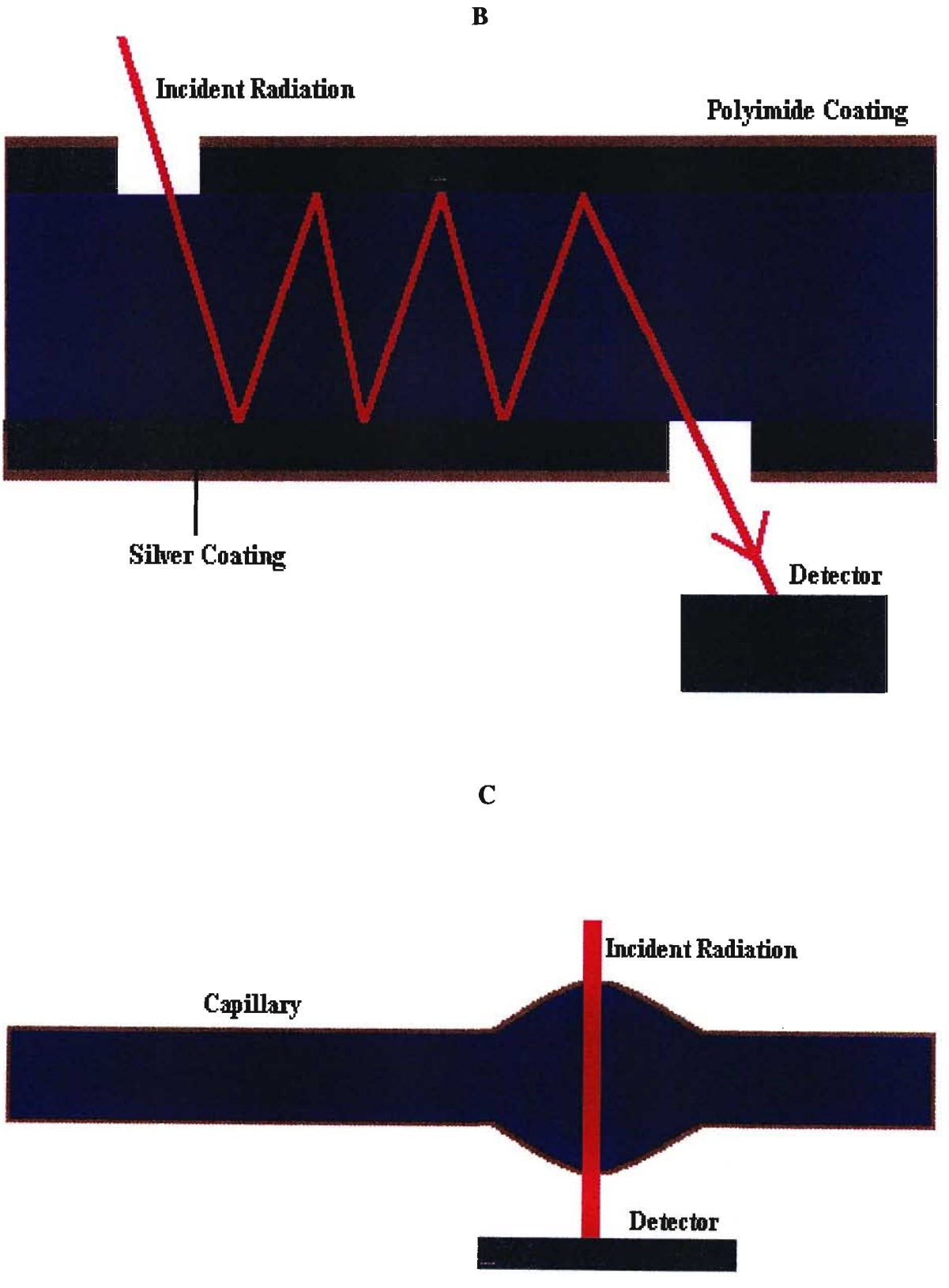

Figure 2.5 (B) Schematic representation of the multi-reflection cell and (C) The bubble cell.

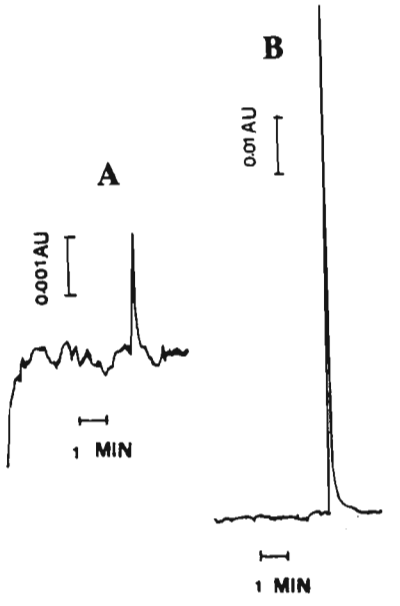

Figure 2.6 (A) Electropherogram of 1.1 x 10^{-5} M brilliant green obtained from a single pass cell and (B) from a multi-reflection cell [126].

2.6.1 *UV-Visible Detectors*

The use of UV-VIS absorbance has remained the most popular detection principle although it suffers from low sensitivity compared to other detection modes developed for CE. The main reason for its popularity include its relatively universal nature and its wide spread availability. The small capillary i.d. presents two problems in CE; namely difficulty in focusing sufficient amount of light onto the on column window and reduced sensitivity arising from a short pathlength. It is therefore essential to use high intensity lamps, optimum slit width (too high cause stray light problems, too little reduces sensitivity), correct and stable positioning of the capillary in the light path. Optical fibers can also be used to maximize light intensity passing through the sample.

2.6.2 *Photodiode Array and Multiwavelength UV Detectors*

Photodiode array detection provides multi-wavelength spectral information which is a powerful tool for the identification of unknown compounds. Furthermore, peak purity

check and absorbance ratio at different wavelengths can be performed to confirm the presence or absence of overlapping peaks in a single electropherogram.

2.6.3 *Fluorescence Detection*

Fluorescence detection enables extremely high sensitivity, however relatively few molecules exhibit intense native fluorescence. Non fluorescent molecules require pre- or post-column

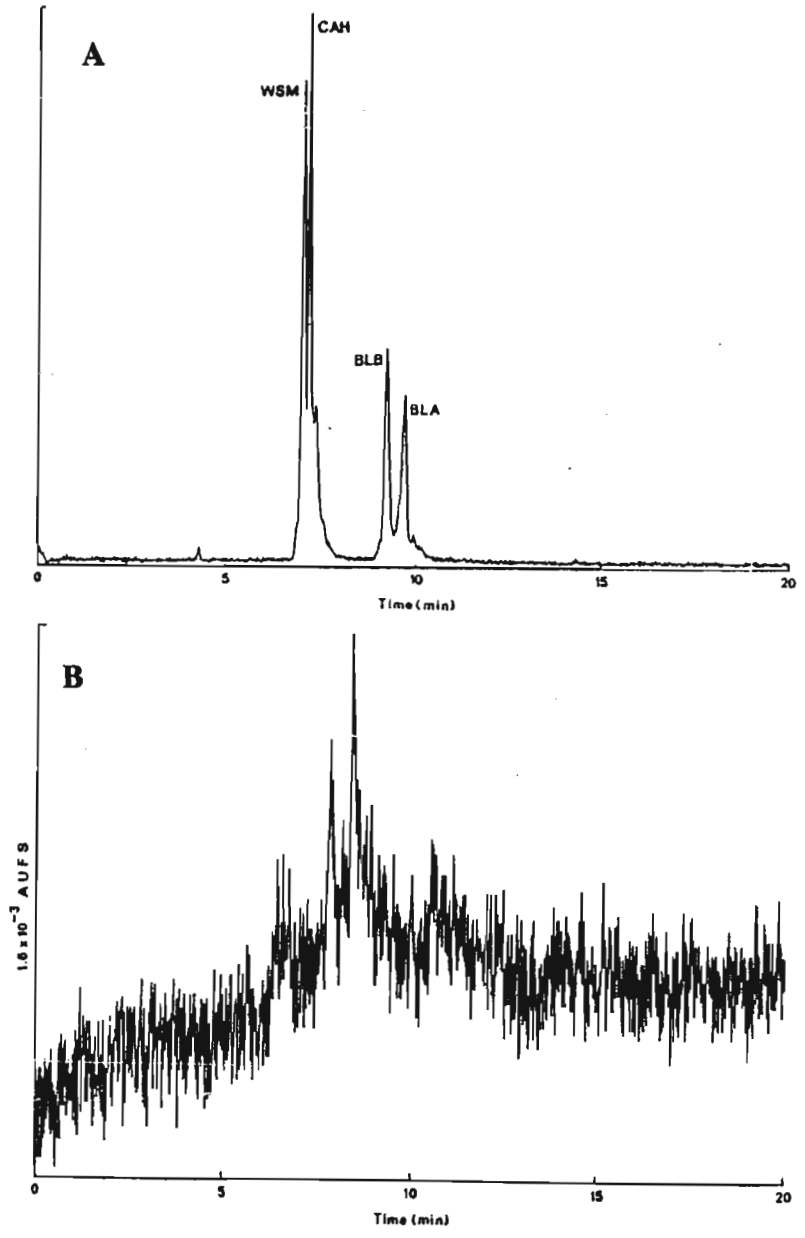

Figure 2.7 (A) Post-capillary fluorescence detection and (B) UV detection at 229 nm. Operating conditions: 50 mm borate-50 mM KCl; pH 9.5; OPA derivatization reagent; 30 kV operating voltage [127].

derivatization to introduce fluorophores to the analyte. Figure 2.7A&B shows a comparison of post-capillary fluorescence and UV detection of whale skeletal muscle (WSM), carbonic anhydrase (CAH), β-lactoglobulin B (BLB) and β-lactoglobulin A (BLA).

The high sensitivity of this technique can be attributed to low background noise and the direct proportionality between excitation power and emission signal intensity. For fluorescein, a detection limit of *ca.* 10^{-8} M (s/n=2) has been found for conventional fluorescence [128], while using laser induced fluorescence (LIF) detection, LODs of as low as 2 x 10^{-12} M (*ca.* 1000 analyte molecules) have been realized for the fluorescein thiohydantoin derivatives of amino acids [129]. The most commonly used lasers are He-Cd and argon-ion lasers. In contrast to arc lamps, lasers emit a highly coherent beam of light, however the limitation of LIF detection is the lack of spectral lines matching the analyte absorption bands. It is therefore vital to introduce fluorophores to match the available laser lines. Numerous fluorescent reagents are readily available. 3-(4-carboxybenzoyl)-2-quinoline carboxaldehyde (CBQCA), dansyl chloride (Dns-Cl), 4-phenylspiro [furan-2(3H)1'-phthalan]-3,3'-dione (fluorescamine), fluorescein isothiocyanate (FITC), naphthalene dialdehyde (NDA) and o-phthaldialdehyde (OPA) have been used extensively for amino acid, peptide, protein and DNA analysis.

2.7 Column Technology

Borosilicate glass, fused silica and various polymers such as Teflon have been used as the column material in CE. The high UV cut-off of glass (280 nm) and poor thermal conductivity of Teflon made these materials unpopular for CE work. Fused silica on the other hand is by far the most frequently used material because it is easy to fabricate into capillaries, optically transparent (UV cut-off 170 nm), available in internal diameters ranging from 10 to 300 nm, mechanically strong, flexible when coated with polyimide, inexpensive, and has good electrical insulating properties.

The major limitation of fused silica is that the surface has unreacted silanol groups that give rise to electroosmosis. Electroosmosis tends to elute components before electrophoretic

resolution is complete. Low pH buffers and acidic additives provide one of the simplest methods to suppress EOF. At a pH<3, there is essentially no silanol ionization and EOF approaches zero (Figure 2.8). Another approach to reduce the effect of the silanol groups is to use coated columns. Coating with organic compounds or polymers occur by absorption or covalent bonding to the fused silica surface. Commonly used coatings in CE include methylcellulose [130,131], polyacrylamide [132,133], polyacrylic acid, polyvinylpyrrolidone [134] and polyethylene glycol [131,135]. The advantages of coated columns is that adsorption is suppressed; the EOF is constant over a wide pH range; the coating is stable over a wide pH range; the coating is stable for long periods and that migration times are reproducible.

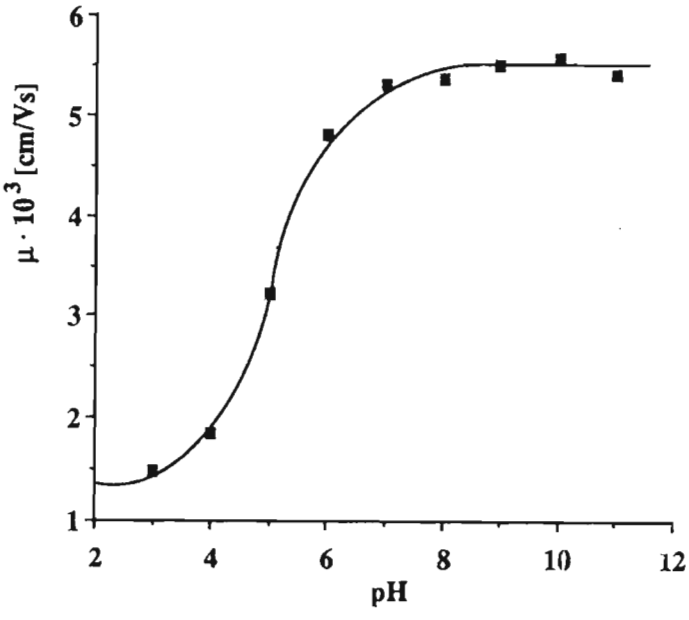

Figure 2.8 Plot of electroosmotic mobility versus pH. Operating conditions: 50 mM phosphate buffer, 263 V/cm applied voltage, UV detection at 200 nm [136].

2.8 Factors Affecting Performance

Capillary electrophoretic techniques are inherently efficient. From equation 1.1, clearly the column length does not influence the number of theoretical plates that can be obtained for any particular separation. However there are factors which result in band broadening.

2.8.1 *Fundamental Dispersive Effects*

Band spreading can be expressed by the variance σ^2 if the peak shapes are assumed to be Gaussian. Thus the total variance is given by the expression

$$\sigma_t^2 = \sigma_D^2 + \sigma_A^2 + \sigma_J^2 + \sigma_E^2 + \sigma_I^2 + \sigma_W^2 + \sigma_O^2 \qquad 2.9$$

where the terms on the right hand side represent the variances due to diffusion, adsorption, Joule heating, electrophoretic dispersion, injection, the width of the injection zone and other effects respectively.

2.8.2 *Diffusion*

In CE, self-diffusion or Brownian molecular motion, and diffusion due to concentration gradients occur. The latter contributes far more significantly to band broadening than the former. During migration of species through the capillary, diffusion occurs along the axis and is termed axial diffusion. The extent of diffusion is related directly to the diffusion coefficient D_m at the time t by

$$\sigma_D^2 = 2D_m t \qquad 2.10$$

This equation dictates large spectral variance for solutes with high diffusion coefficients while the reverse applies to solutes possessing low values of D_m. It is for this reason that CE is especially suited to the separation of large molecules with low diffusion coefficients. This is a significant advantage of CE over HPLC. In HPLC large D_m means greater resistance to mass transfer causing band broadening. From the equation

$$N = \frac{\mu E \ell}{D_m} \qquad 2.11$$

relating efficiency (N) and diffusion (D_m), high electric fields (E) can reduce the effects of axial diffusion because the solute spends less time inside the column.

2.8.3 *Adsorption*

Solid surfaces are never completely indifferent with regards to sample components, with the result that reversible and irreversible adsorption can occur. The former process causes0 a reduction in performance and is seen as band tailing. Furthermore, adsorption can lead to losses of sample particularly given the high surface area/volume ratios in the capillary column. Adsorption of any component can change the local zeta potential at the wall and hence change the performance of all species. Many attempts were made to reduce adsorption in fused silica capillaries by derivatization of the silanol groups. Novotny and Cobb used $SOCl_2$ to convert silanol groups into SiCl groups [137]. Subsequent reaction with the Grignard reagent vinyl magnesium bromide produced a double bond at the surface. The double bonds were then copolymerized with polyacrylamide chains to produce a stable coating for use at high pH.

Hjerten was the first to modify fused silica surfaces with γ-methacryloxypropyl trimethoxysilane (MAPT) [132,138], thereby introducing a molecule to the surface that contained a double bond. This functional group could then be copolymerized with acrylamide to form linear or cross linked polyacrylamide coatings. Bruin *et al.* chemically bonded polyethylene glycol to the silica surface and used the column for the separation of standard proteins [139]. Swedberg used aminopropyltrialkoxysilane as the derivatization reagent after which the amino group was reacted with pentafluorobenzoylchloride [140]. Another approach dealing with the reduction of analyte adsorption involves the use of buffers whose effective pH range is such that the analyte and silica have the same charge signs. Coulombic repulsion suppresses wall adsorption. In the analysis of ampholytes, the buffer pH should be higher than the isoelectric point resulting in both analyte and wall having negative charges. Dynamic capillary coatings involve the use of buffer additives such as surfactants [141], high salt concentrations (100-200 mM) [142], polymer additives (methylcellulose) [143] and polyamines [144], to reduce adsorption.

Static coating is a more sophisticated technique for reducing adsorption. Hjerten [145] described static coating with a polymer layer. Conventional coatings include alkylsilanes [146], arylpentafluoro coatings [147], diols, polyethylene glycol (PEG) and polysaccharides [148], other biomolecules such as α-lactalbumin [149], non crosslinked polyacrylamide

coatings, poly(vinyl-pyrrolidone) [132], polyethyleneimine [150] and poly (methylglutamate) [151].

2.8.4 *Joule Heating*

During the passage of a current in a capillary, electrical energy is partially converted to heat energy. The rate of heat generation per unit volume Q is given by

$$Q = E^2 \Lambda c \varphi \qquad 2.12$$

where E is the field strength, Λ the equivalent conductance of the electrolyte solution, c the electrolyte concentration and φ the total porosity of the medium. Heat transfer is by conduction, convection and radiation. Heat transport out of the tube takes place through the capillary walls and cause a parabolic gradient directed radially from the center to the wall (Figure 2.9) The temperature drops logarithmically in the wall and in the surrounding medium while heat dissipation through the wall takes place mainly by conduction, heat is transferred through the surrounding air by convection and radiation. As a rule of thumb, a power of 0.1 W increases the temperature by 1.1 K for natural convection and 0.6 K for forced air convection [152].

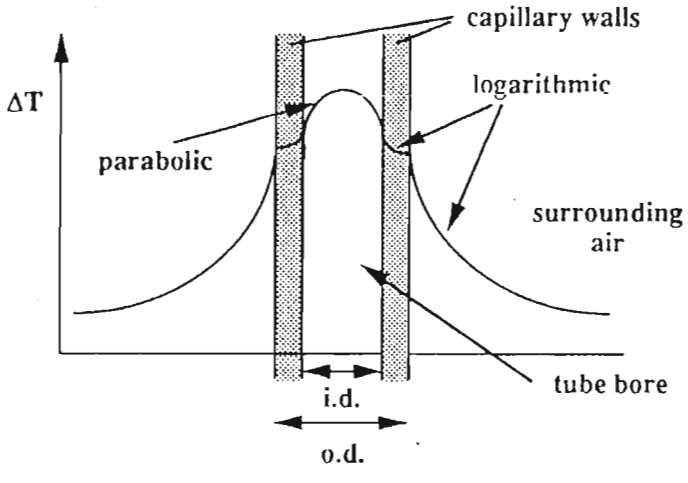

Figure 2.9 Schematic diagram of the temperature profile caused by a current flow across the capillary [153].

Joule heating cause alterations in solute migration due to changes in solution viscosity and density or changes in partition ratios between two phases or a change in the rates of kinetic processes. Excessive Joule heating cause boiling and bubble formation. There is also the possibility of degradation to thermally labile compounds.

2.8.5 *Electrophoretic Dispersion*

Two factors are responsible for peak broadening by electrophoretic dispersion, namely the differences in specific conductance κ between the sample and the buffer zone and the concentration ratio of the sample constituent to the buffer co-ions C_S/C_B. Both factors have their origin in the mobility difference between sample and the buffer co-ion. In the presence of an electric field, the sample zone begins to migrate out of the sampling compartment and is mixed with the buffer constituents. Depending on the mobility of the sample constituents, three cases can be distinguished. If the conductivity of the sample is lower than that of the buffer co-ion, the electric field strength will be higher in the sample zone than in the buffer. Sample molecules that enter the buffer zone by diffusion and convection will experience a lower field strength because of its conductivity and will slow

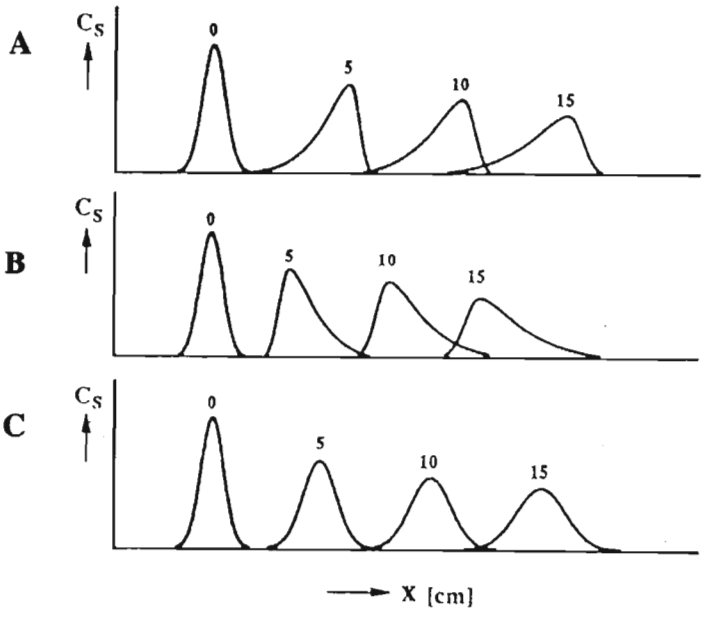

Figure 2.10 (A) Dispersion as a result of diffusion and electromigration when $\mu_{solute} < \mu_{buffer}$ (B) $\mu_{solute} > \mu_{buffer}$ (C) $\mu_{solute} = \mu_{buffer}$ [157].

down. This is seen as a sharpening of the front boundary and a diffuse trailing boundary in an electropherogram. Peak tailing and a reduction in peak height is a pronounced feature in the electropherogram (Figure 2.10A). If the mobility of the sample constituents is higher than that of the buffer, the electric field strength in the sample zone will be lower than in the buffer zone. Sample ions diffusing into the buffer zone will be accelerated resulting in peak fronting (Figure 2.10B). If the sample and buffer have equal conductivities, the electric field strength is constant across the entire capillary. Only diffusion broadening is observed (Figure 2.10C).

2.8.6 *Injection Width*

The variance due to injection (σ_I^2) is given by

$$\sigma_I^2 = \frac{I^2}{12} \qquad 2.13$$

where I is the width of the initial sample pulse [154]. Typical injection lengths in a 75 μm i.d. column are in the range of 1-2 mm. Huang, Coleman and Zare [155] have found that the length of the injection plug is the most significant factor in respect to peak broadening. Vinther and Soeberg have made similar findings in their studies [156].

2.9 Other Effects

2.9.1 *Field Strength*

Field strength is related to the applied voltage by the equation

$$E = \frac{V}{L} \qquad 2.14$$

Since both electrophoretic migration and electroosmosis are directly proportional to the electric field, high field strengths will produce short analysis times, and high efficiency peaks as shown by examples in Figure 2.11. However, a plot of I versus E shows a deviation from linearity at higher values of E (Figure 2.12), which is attributed to Joule heating.

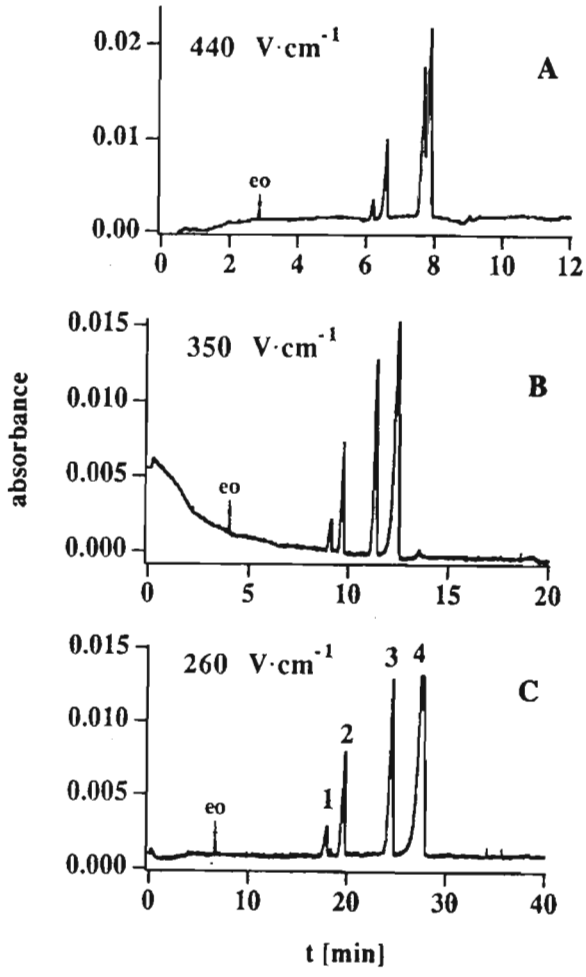

Figure 2.11 Influence of the field strength on the electrophoretic separation of four positional isomers of dihydroxybenzoic acid. Operating conditions: 25 mM phosphate-25 mM borate buffer; pH 9.0; UV detection at 200 nm and field strength (A) 440 V.cm^{-1}, (B) 350 V.cm^{-1} and (C) 260 V.cm^{-1} [158].

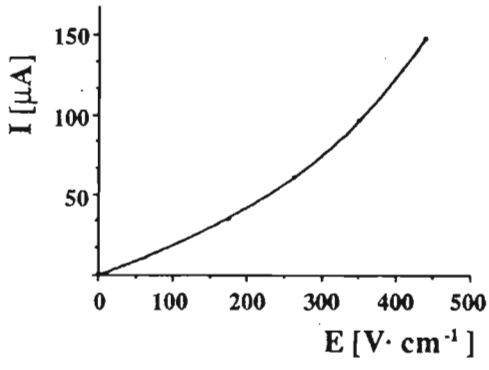

Figure 2.12 Plot of the field strength versus the resulting current for the system in Figure 2.11 (A-C) above [158].

From the equation

$$v_{eo} = \frac{\varepsilon \zeta i}{4\pi\kappa\eta} \qquad 2.15$$

where ε is the permittivity of the medium, i the current density, κ the specific conductance, η the solution viscosity, and ζ the zeta potential, it can be seen that a plot of v_{eo} versus i is a straight line independent of temperature. Therefore a constant current mode is preferred to a constant voltage mode for good precision of v_{eo} and v_{ep}.

2.9.2 *Capillary Dimensions*

The capillary dimensions affect migration time, resolution, detection sensitivity, heat dissipation and adsorption. Colburn *et al.* showed that the migration time of a peptide increases from 18 to 48 minutes on increasing the column length from 50 cm (25 cm effective) to 100 cm (75 cm effective) [159]. There was a dramatic improvement in peak resolution and efficiency. Jorgenson found that there was no significant improvement in peak efficiency in columns longer than 100 cm but considerably longer analysis times resulted [160]. Short capillaries produced a sharp decrease in plate numbers which was attributed to thermal effects.

2.9.3 *Temperature*

In CE, temperature is usually considered in a negative context due to the loss in efficiency by excessive Joule heating. However, there are some promising aspects of the influence of temperature on CE (Figure 2.13). The major effect of temperature is to shorten the analysis time due to an increase in the EOF and the effect it has on chemical equilibria such as metal chelation, micelle partitioning, complex formation and dissociation. Hoffstetter-Kuhn *et al.* studied the influence of temperature on the electrophoretic behaviour of carbohydrates in borate solutions [161]. It was observed that by increasing the column temperature, equilibrium was reached faster, resulting in narrow peaks, and improved sensitivity and resolution.

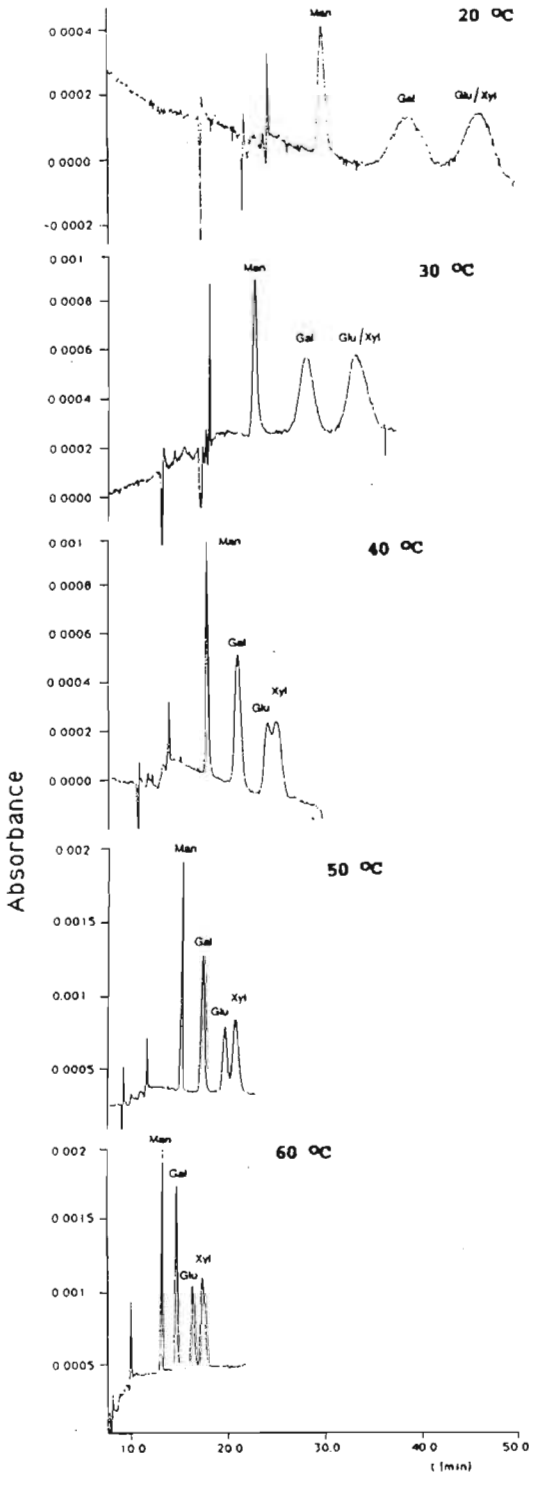

Figure 2.13 Effect of temperature on the separation of underivatized monosaccharides. Operating conditions: 50 mM borax; pH 9.3; 20 kV applied voltage; UV detection at 195 nm [161].

2.10 Application

Capillary electrophoresis has developed into an extremely powerful analytical technique with a wide range of applications in greatly diverse fields. The availability of new commercial instruments have provided further advancement in this technique for practical application. Some important applications are outlined below.

2.10.1 *Amino Acids*

Jorgenson and Lukacs were pioneers in the field of CE and demonstrated the high resolution separation of fluorescent derivatives of amino acids [162-164]. Since then numerous researchers investigated the analysis of amino acids by CE. These studies include the separation of dansylated derivatives [162-175], phenylthiohydantoin derivatives [176-179], naphthalene dicarboxyldehyde [180-182], 4,4-dimethylamino azobenzene-4'-sulfonyl chloride [183-185], fluorescein isothiocynate [186-188], ortho-phthaldialdehyde [182,187-189], fluorescamine [187,190,191], and 9-fluorenylmethylchloroformate derivatives [187,192]. Separation of dansylated amino acids can be accomplished with high efficiency using an electrophoretic buffer at neutral pH. Under these conditions, the amino acids have a negative charge and separation is based on differences in charge.

2.10.2 *Peptides*

Jorgenson and Lukacs demonstrated the use of CE for the separation of fluorescamine derivatives of dipeptides [163], and peptides from tryptic digests of ovalbumin [163-165]. Novotny and Cobb used CE for high sensitivity peptide mapping [193]. Ludi *et al.* employed CE for the analysis of recombinant insulin-like growth factor and recombinant hirudin [194]. Grossman *et al.* found that buffer pH was the primary parameter affecting the selectivity of the separation of a peptide mixture [195]. The results also proved that differences in the neutral amino acid composition and sequence of a peptide could be detected by CE.

Florance *et al.* studied the effects of different buffers and pH on the migration times and resolution of a gut hormone motilin [196] (Figure 2.14). The citrate buffer at pH 2.5 was

found to provide best resolution for the peptide. Other applications include the separation of multiple antigen peptides (MAPS) [197], histine containing compounds [198], bioactive peptides including neurotensin and angiotensin 1 [199]. The separation of chiral dipeptides by CE and MECC was achieved by derivatization with L-and D-Marfeys reagent [200] or simply by adding the reagent into the electrophoretic buffer [201]. CE-MS is another technique used frequently for the analysis of peptides [202-208]. Volatile buffers (ammonium acetate and ammonium formate) of low concentration (15-20 mM) and containing high organic modifier content (5-30% CH_3CN) or methanol were found to be more suitable for electrospray ionization (ESI). Mosely *et al.* used CE-MS with continuous flow fast atom bombardment (CF-FAB) for the analysis of peptides [207,208].

2.10.3 *Proteins*

The separation of proteins by CE represents an area of tremendous interest in recent years. Several reviews have appeared which described the application of CE in protein separations [209-211]. Researchers have found that reproducibility was affected by adsorption of protein to the capillary walls. Green and Jorgenson used additives such as metal salts in the run buffer to reduce wall adsorption [212]. However the resulting increase in conductivity

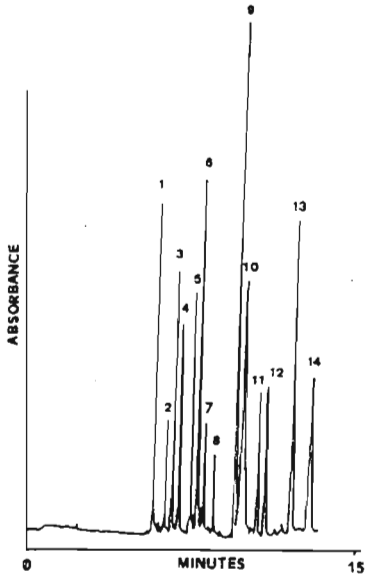

Figure 2.14 Electropherogram of 14 motilin peptides. Operating conditions: citrate buffer; pH 2.5; 20 kV applied voltage; UV detection at 200 nm [196].

necessitated the use of lower operating voltages and capillaries of smaller diameter to provide adequate heat dissipation.

Emmer *et al.* used a cationic fluorosurfactant to reduce the adsorption of basic proteins in CZE [213]. A charge reversal occurred and proteins were repelled from the wall. McCormick utilized poly(vinylpyrrolidone)-coated capillaries for the separation of 15 proteins [214]. However, insulin, ovalbumin and chymotrypsinogen could not be separated because of analyte adsorption. Hjerten and co-workers reported the use of gel-filled capillaries for separation based on molecular size with sodium dodecyl sulphate-polyacrylamide gels (SDS-PAGE) [215,216].

2.10.4 *Nucleic Acids*

Nucleic acids are the fundamental genetic material in all living organisms. They are generally long chained polymers consisting of a phosphoric acid group, a sugar component (ribose or deoxyribose) and purine (adenine, guanine and cytosine) and pyrimidine (thymine or uracil) bases. The use of CE for the separation of nucleic acids has been described in several reviews [166,217,218].

Row *et al.* used MECC with SDS for the separation of modified nucleic acid constituents. The optimum conditions were determined as 0.075 M SDS in 0.01 M phosphate-0.006 M borate buffer (pH 8.9), at a separation voltage of 10 kV [219]. Liu *et al.* investigated the effect of surfactant type for the analysis of phosphorylated nucleosides [220]. Hjerten *et al.* investigated the CE separation of nucleic acids and their degradation products [221]. CGE has also been used extensively for the separation of oligonucleotides [222-224]. Lui *et al.* separated twelve nucleotides (Figure 2.15) by MECC [225].

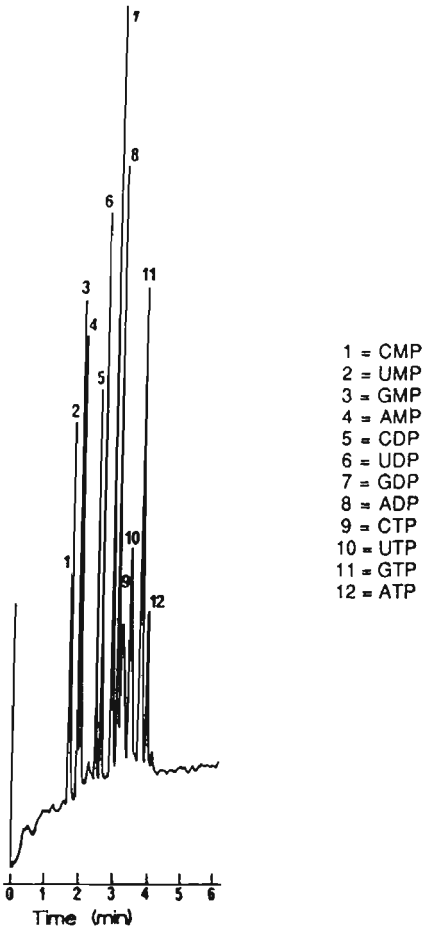

Figure 2.15 MECC separation of common nucleotides with a cationic surfactant. Operating conditions: 100 mM DTAB in 10 mM TRIS/phosphate buffer; pH 7.05, -18 kV; UV detection at 254 nm [225].

2.10.5 *Pharmaceuticals and Drugs*

Due to limitations such as the complexity and time consuming nature, the high degree of variability, the low separation efficiency or lack of sensitivity with conventional methods of analysis, there has been growing interest in CE for the analysis of pharmaceuticals and drugs. Table 2.2 show some selected types of pharmaceutical compounds analyzed by CE.

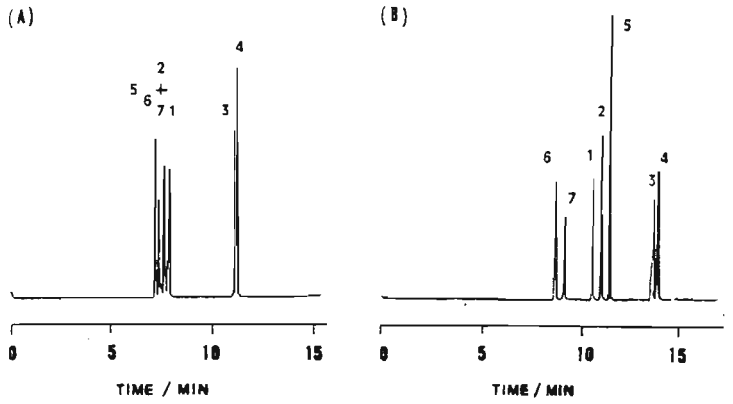

Figure 2.16 (A) Separation of 7 penicillins by CZE and (B) by MECC. Operating conditions 0.02 M borate-phosphate buffer, 0.1 M SDS, pH 8.5, UV detection at 210 nm [226].

Table 2.2 Pharmaceuticals analyzed by CE

Publication Year [Reference]	Authors	Application
1986 [227]	Fujiwara *et al.*	Cinnamic acid and analogues
1987 [228]	Fujiwara *et al.*	Analgestic preparations
1990 [229]	Honda *et al.*	Crude drug
1991 [230]	Yeo *et al.*	Antibiotics
1991 [231]	Snopek *et al.*	Chiral drugs
1991 [232]	Nishi *et al.*	Corticosteroids
1990 [233]	Nishi *et al.*	Benzodiazepine and benzothiazepine
1991 [234]	Thormann *et al.*	Barbiturates
1989 [235]	Nakagawa *et al.*	Cefpiramide
1988 [170]	Roach *et al.*	Anticancer drugs
1989 [236]	Hjerten *et al.*	Basic drugs
1991 [237]	Salomon *et al.*	Antidepressant
1988 [238]	Fujiwara *et al.*	Water-soluble vitamins
1991 [239]	Mutton *et al.*	Echistain
1991 [240]	Weinberger *et al.*	Anti-inflammatory

Table 2.2 Continued

Publication Year [Reference]	Authors	Application
1991 [241]	Guzman *et al.*	Recombinant cytokine
1991 [242]	Pietta *et al.*	Flavonoids
1991 [243]	Hurni *et al.*	Vaccine production process monitoring
1991 [244]	Ackermans *et al.*	Selected drugs insoluble in water
1990 [245]	Weinberger *et al.*	Urinary porphyrins
1990 [246]	Wainwright *et al.*	Peptide drugs
1988 [247]	Tsuda *et al.*	Polyamines in urine
1991 [248]	Soini *et al.*	Cimetidine
1990 [249]	Atria *et al.*	Radiopharmaceuticals
1991 [250]	Swartz *et al.*	Robitussin
1989 [251]	S. Fanali	Aminophenol and diaminophenol
1991 [250]	Swartz *et al.*	Cough/cold formulation
1991 [252]	Ong *et al.*	Antihistimines

2.10.6 *Other Areas of Application*

Capillary electrophoretic methods have been used in many other application areas. CGE was used for the separation and detection of DNA sequencing samples [253] while CE of the tobacco mosaic virus was performed by Hjerten *et al.* [215] and red blood cells by Chen and Zhu [254]. Researchers have also used CE for the analysis of body fluids [255,256], anions [257,258], cations [259,260], metal chelates [261,262], hydrocarbons [89,252,263-267], organic acids [133,215,268-271] amines [272-274], carbohydrates [275-277], food analysis [278-280], environmental pollutants [252,281-284], polymers [252,285-288], natural products [289-291], chiral compounds [292-294], geometric and positional isomers [295-298], coal and fuels [299,300], dyes and textiles [301] and finally for toxin analysis [63,64].

Chapter Three

Experimental Techniques and Methods

3.1 Introduction

A number of techniques including high performance capillary electrophoresis (HPCE), micro-high performance liquid chromatography (μHPLC), supercritical fluid extraction (SFE), capillary electrochromatography (CEC) and high performance liquid chromatography (HPLC) were investigated during the course of this research project. In this chapter, the various experimental aspects of the project are described in full to enable duplication of the work or application of the methods in other studies. Detailed descriptions and schematic diagrams of the instrumentation used together with any instrument modifications are provided. The CE methods investigated required the use of a number of reagents, buffer solutions and calibration standards. Experimental procedures for their preparation and for extraction and clean-up of samples are described. Sample introduction was also an important focus of the CE work. The procedures for cleaning, rinsing, executing hydrodynamic injections, electrokinetic injections, and field amplified sample injections in MECC, as well as sample introduction and preparation methods such as on-line solid-phase extractions and electro-extraction are therefore described in detail.

3.2 Preparation of Toxin Standards

3.2.1 *The Toxin Standards*

Reference standards of MC LR (>96%), MC YR (98.7%), MC RR (>99%) and nodularin (>99%) were purchased from Calbiochem-Novabiochem (CA, USA). The toxins were stored dry at -20°C in amber coloured glass bottles until required for use.

3.2.2 *The Stock Standards*

Stock solutions of the toxin standards were prepared by dissolving the appropriate masses in HPLC grade methanol (Reidel de Haën) according to Table 3.1. Due to the minute

quantities of the standards available, physical massing was not practical. The entire content of the vial received from the supplier was transferred quantitatively into a volumetric flask and diluted to volume. The authenticity of each standard solution was verified on the basis of its UV spectrum (Appendix) obtained by HPLC analysis and photodiode array UV detection.

Table 3.1 Preparation of the toxin stock solutions

Compound	Mass (μg)	Volume (mL)	Concentration (ng/μL)
Nodularin	500	50.00	10
MC LR	500	50.00	10
MC YR	500	50.00	10
MC LR	5000	500.00	10

3.2.3 *The Primary Dilution Standard and Calibration Standards*

100 μL of each toxin stock solution was transferred into a 1.8 mL GC autosampler glass vial (Hewlett Packard, Little Falls Site, DE, USA) with the use of a 100 μL high precision syringe (Hamilton Company, Reno, NV, USA). The solvent was evaporated to dryness under a gentle stream of high purity nitrogen and resuspended in 10 μL of methanol. For electrokinetic injections, the standards were diluted with 30 mM di-sodium tetraborate (borax) buffer (BDH, Poole, UK), for field amplified injection, 3 mM borax was used, and doubly deionised water (Millipore Corp., Milford, MA, USA) for solid phase extractions. The calibration standards were prepared as indicated in Table 3.2.

Table 3.2 Preparation of calibration standards

Standard	Volume Stock (μL)	Final Volume (μL)	Concentration (ng/μL)
1	20	10	20
2	40	10	40
3	60	10	60
4	80	10	80

3.3 Preparation of Buffer Solutions

3.3.1 *The Phosphate Buffer (10 mM Na_2HPO_4, 10 mM NaH_2PO_4, 10 mM SDS)*

The phosphate buffer consisted of 0.12 g sodium dihydrogen phosphate (BDH, Poole, UK), 0.142 g disodium hydrogen phosphate (BDH) and 0.288 g sodium dodecyl sulphate (SDS) dissolved in doubly deionised water and diluted to 100 mL. The buffer solution was degassed for 10 minutes in an ultrasonic bath (Branson 1210, Connecticut, USA) and passed through a 0.45 μm syringe type filter (Millipore) prior to use.

3.3.2 *The Run Buffer (30 mM Borax, 9 mM SDS)*

The run or separation buffer consisted of 0.2595 g SDS (Merck) and 1.144 g of borax dissolved doubly deionised water and diluted to 100 mL. The buffer solution was degassed and filtered as in 3.3.1 above, prior to use.

3.3.3 *The Sample Buffer (3 mM Borax)*

0.1144 g of borax was dissolved in doubly deionised water and diluted to 100 mL. The buffer was degassed and filtered as described previously.

3.3.4 *Sodium Hydroxide (0.1 M)*

0.4 g of AR grade NaOH (Merck) was dissolved in doubly deionised water and diluted to 100 mL. The solution was transferred to a plastic bottle and stored for later use. Filtration was carried out prior to use.

3.4 Sample Extraction and Clean-Up

3.4.1 *Algal Scum Samples*

Algal scum samples were collected from kwaMakutha waste water treatment plant in Umlazi, kwaZulu Natal, South Africa in December 1996. The scum was filtered through glass fibre filter (Whatman International Ltd, Kent, UK), the residue freeze-thawed and stored at -20°C in the dark. Sample extraction was carried out using supercritical CO_2.

3.4.2 *Supercritical Fluid Extraction (SFE)*

Instrumentation: SFE was carried out on a laboratory built extraction system (Figure 3.1) comprising a Lee Scientific series 501 syringe pump (Dionex Corp., Sunnyvale, CA, USA) to deliver supercritical CO_2, and a thermostatically controlled Sigma 3B GC oven (Perkin-Elmer, CT, USA). The pump had a cylinder capacity of 150 mL and could deliver fluid up to a pressure of 400 atmospheres. The fluid pressure was controlled by an IBM 386 SX PC with Lee Scientific Software (Version 1.7). The pump head was cooled by circulating cold water between 8-10°C, using a cooling coil (Grant Inst., Cambridge, UK) placed inside a circulatory water bath. A 10 mL stainless steel extraction cell (Keystone Scientific, Bellefonte, PA, USA) fitted with finger tight fittings, PTFE seals and retaining frits, was used for sample extraction (Figure 3.2). SFC/SFE grade liquid CO_2 (Air Products, South Africa), was directed from the tank to the syringe pump via a piece of 1/8″ stainless steel tubing soldered to a piece of 1/16″ stainless steel tubing.

Extraction fluid leading from the pump was transported via 1/16″ stainless steel tubing to a four port valve (Valco Inst., TX, USA) fixed outside the GC oven. The outlet from the extraction vessel was connected to a two way valve (Supelco, Bellefonte, PA, USA) fitted outside the oven. This served to control extractions in the static and dynamic modes when the valve was closed and opened respectively. The cell pressure and fluid flow rate was controlled by the use of a 30 cm x 10 μm i.d. deactivated fused silica linear restrictor (SGE, Melbourne, Australia). This capillary was connected to the two way high pressure valve by threading it through a 3 cm length of 1/16″ o.d. polyetheretherketone (PEEK) sleeve (Upchurch Scientific, NJ, USA) which was then pushed through a 1/16″ stainless steel nut and ferrule. The end of the capillary was immersed into a 10 mL volumetric flask containing the collection solvent.

Sample Extraction: 100 μL of methanol was added to freeze - thawed algae (3.52 g) in the 10 mL supercritical fluid extraction SFE vessel. The algal scum was extracted with CO_2 at 400 atmospheres and 40°C for 60 minutes statically and 60 minutes dynamically. Static extraction was achieved by keeping the two way high pressure valve at the outlet end of the extraction vessel closed while the sample was exposed to supercritical CO_2 at 400

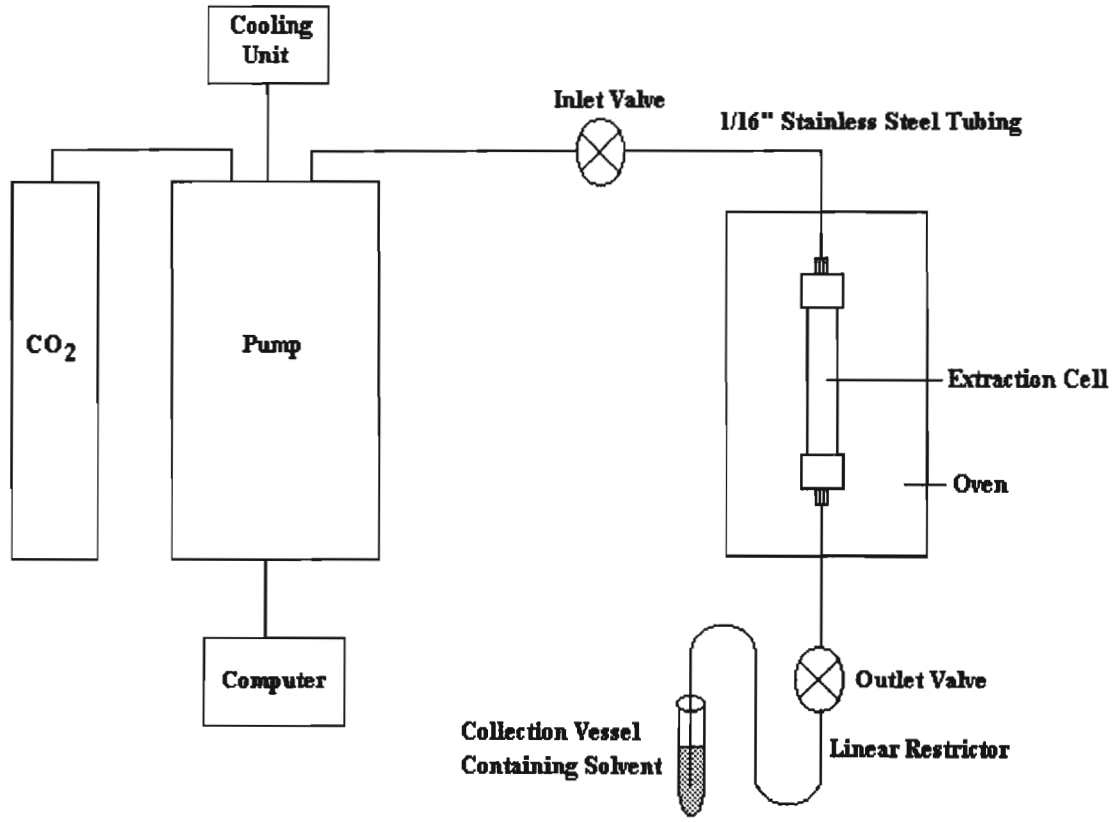

Figure 3.1 Schematic diagram of the supercritical fluid extraction system used for off-line sample extraction.

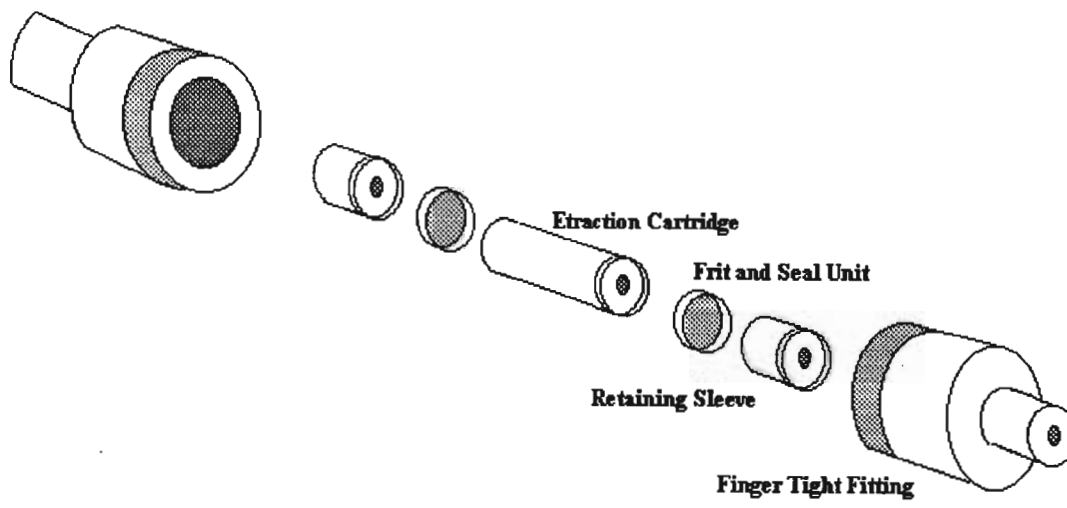

Figure 3.2 Schematic diagram of the stainless steel supercritical fluid extraction cell.

atmospheres. Dynamic extraction was achieved by opening the outlet valve while the sample was subjected to a supercritical CO_2 pressure of 400 atmospheres. Extracted components were transferred directly into a 10 mL volumetric flask containing methanol. The restrictor was heated periodically (5 minute intervals) with the use of a hot air blower to prevent plugging by ice formation. The extract was then evaporated to dryness and reconstituted in 10 mL of water.

3.4.3 *Sample Clean-Up*

A trifunctionally bonded C_{18} Sep-Pak Plus cartridge (Millipore Corp., Milford, MA, USA) was activated by passing 10 mL of methanol followed by 10 mL of deionised water through the cartridge with the use of a 25 mL disposable syringe. Thereafter, the crude extract from 3.4.2 was passed through the cartridge followed by 10 syringe volumes of air to remove traces of water from the sorbent. The toxins were then eluted with 2 mL of methanol. Activation, extraction, air drying and elution were carried out from the same inlet.

3.5 Capillary Electrophoresis System

Although some experience was gained on a Hewlett Packard HP ^{3D}CE system (experimental details regarding the use of this instrument are given in section 3.11), due to restricted access, most of the analyses with UV detection were performed on a laboratory built CE system comprising a perspex sampling cabinet and two vial holders fixed on opposite ends within the cabinet (Figures 3.3 and 3.4).

The Perspex Sampling Cabinet: The cabinet with a length of 450 mm, width of 220 mm and a height of 300 mm, was designed from 8 mm thick perspex. Two high voltage platinum electrodes, the capillary column, an inlet tray to contain the inlet buffer and sample reservoirs and an outlet tray for the outlet buffer reservoir, were housed inside the cabinet. The cabinet doors were fitted with interlocks for operator safety. The separation capillary and electrode connecting wires were threaded through drill holes made in the perspex material.

The Inlet Tray: The inlet tray had 8 positions which could be loaded with the sample and buffer reservoirs. The positions could be changed by manually rotating the tray. A groove and ridge arrangement on the underside of the inlet tray was designed to ensure that the vial positions and the electrode/capillary assembly was always aligned.

The Outlet Tray: The outlet tray had two positions which could be loaded with the sample and buffer reservoirs. The tray was movable along a central rod, allowing for the height to be lowered for sample introduction by hydrostatic pressure. A polyethylene screw was used to secure the tray at the desired height.

3.5.1 *High Voltage Power Supply*

A 0-30 kV power supply (Series 230, Bertan High Voltage, Hickville, NY USA) was used. The power supply had a 0-400 μA range and was activated remotely by the interlocking switches fixed to the sampling cabinet doors. Polarity reversal was achieved by switching the position of the two electrodes manually.

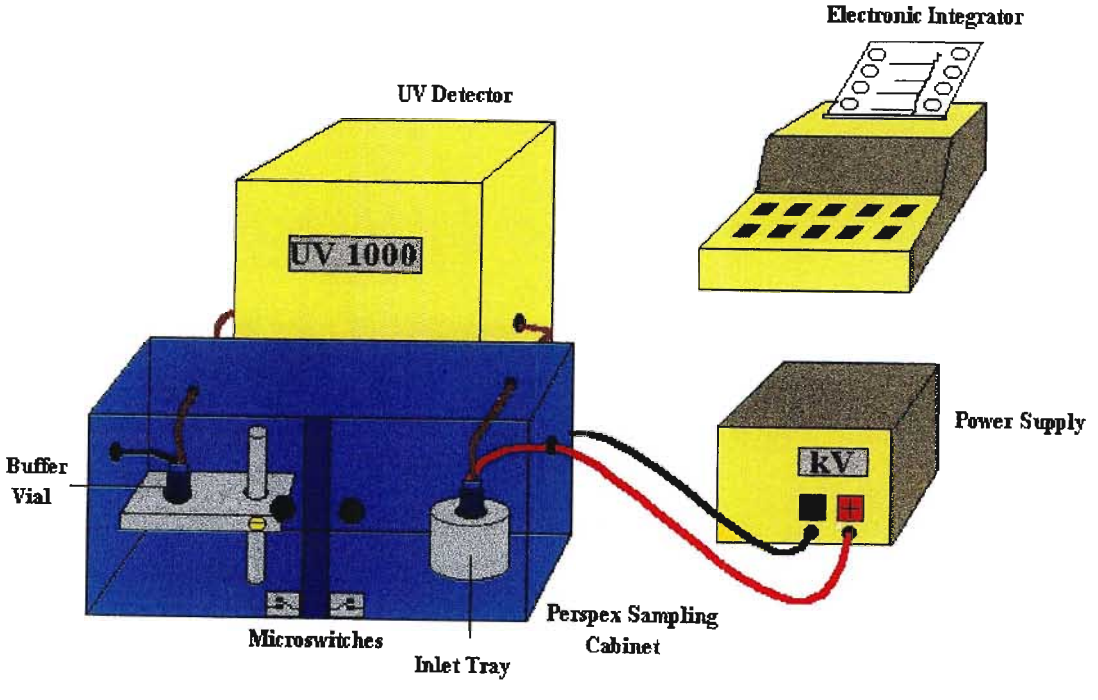

Figure 3.3 Diagrammatic representation of the laboratory built capillary electrophoresis system.

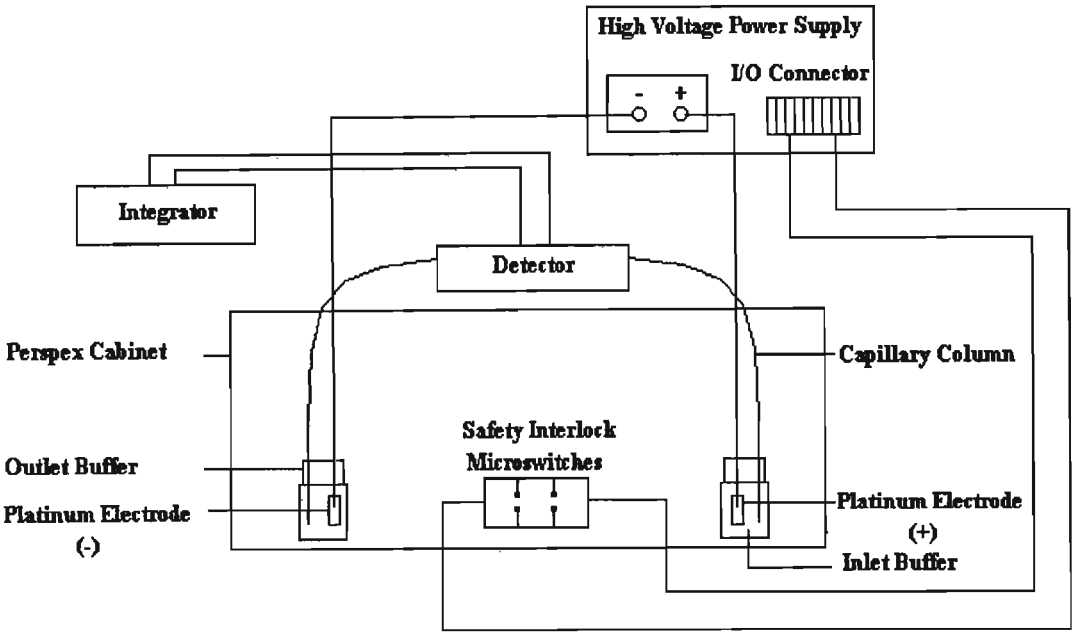

Figure 3.4 Schematic diagram of the laboratory built capillary electrophoresis system.

3.5.2 *UV Detector*

UV detection was achieved with a variable wavelength, dual beam UV detector (Spectra System UV 1000, Spectra Physics, San Jose, CA, USA) (Figure 3.5) fitted with an on-column capillary cell holder (Model 9550-0155, Linear Instruments, NY, USA) (Figure 3.6). The cell holder had a ball lens to focus the light on a small section of the capillary. The capillary was threaded through a sleeve made from 1/16 inch o.d. PEEK tubing and secured in position by a stainless steel nut and a 1/16 inch o.d. PEEK ferrule. A deuterium lamp source with a wavelength range from 190 to 380 nm was used. The wavelength for toxin analysis was set at 238 nm and the detector absorbance range was set at 0.0005 a.u.f.s.

3.5.3 *Data System*

Electropherograms were recorded with an electronic integrator (Model SP 4200, Spectra Physics).

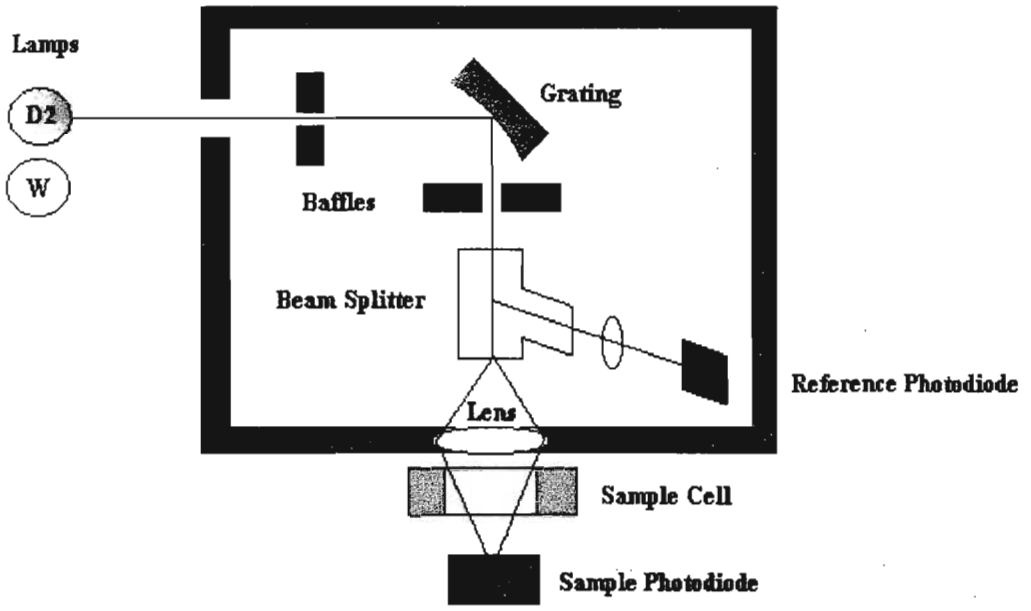

Figure 3.5 Schematic diagram of the optical system of the UV 1000 detector.

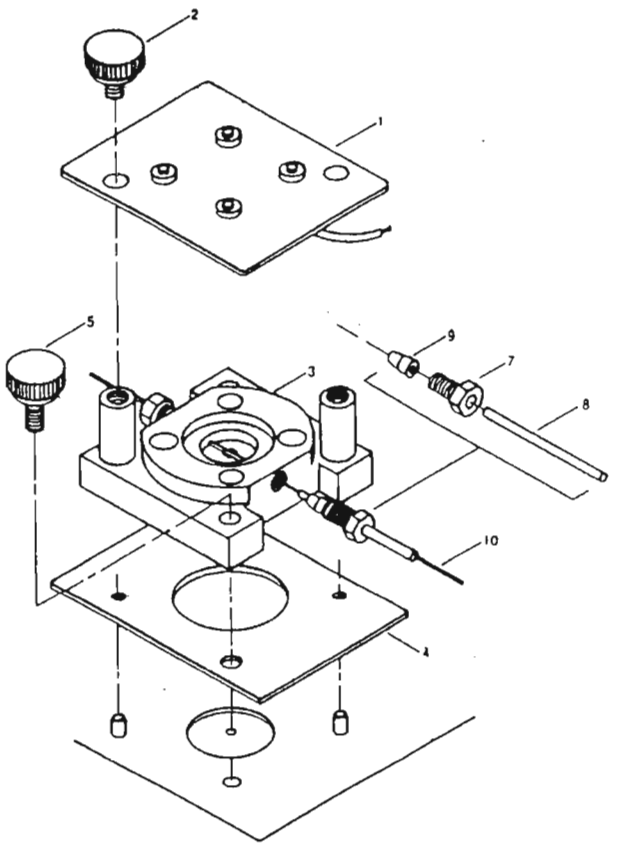

Figure 3.6 Diagram of the on-column capillary cell. 1 photodiode assembly; 2 photodiode mounting screw; 3 cell body; 4 capillary insulator; 5 flow cell mounting screw; 6 capillary column; 7 cell nut (stainless steel); 8 PEEK tubing; 9 1/16 inch o.d. PEEK ferrule; 10 sleeve [302].

3.5.4 *Capillary Filling Adapter*

An old septum equipped GC packed column injection port was modified for the purpose of capillary conditioning, buffer introduction and sample introduction for field amplification studies (Figure 3.7). It comprised a septum and nut assembly with a steel housing (vial holder) and rubber o-ring. The injector was attached to a cylinder of nitrogen (Air Products, South Africa) via a high pressure, low volume micro-valve (Scientific Systems, Inc., PA, USA). The capillary could easily be inserted into the adapter by piercing the septum. The positive N_2 pressure forced liquid into the column.

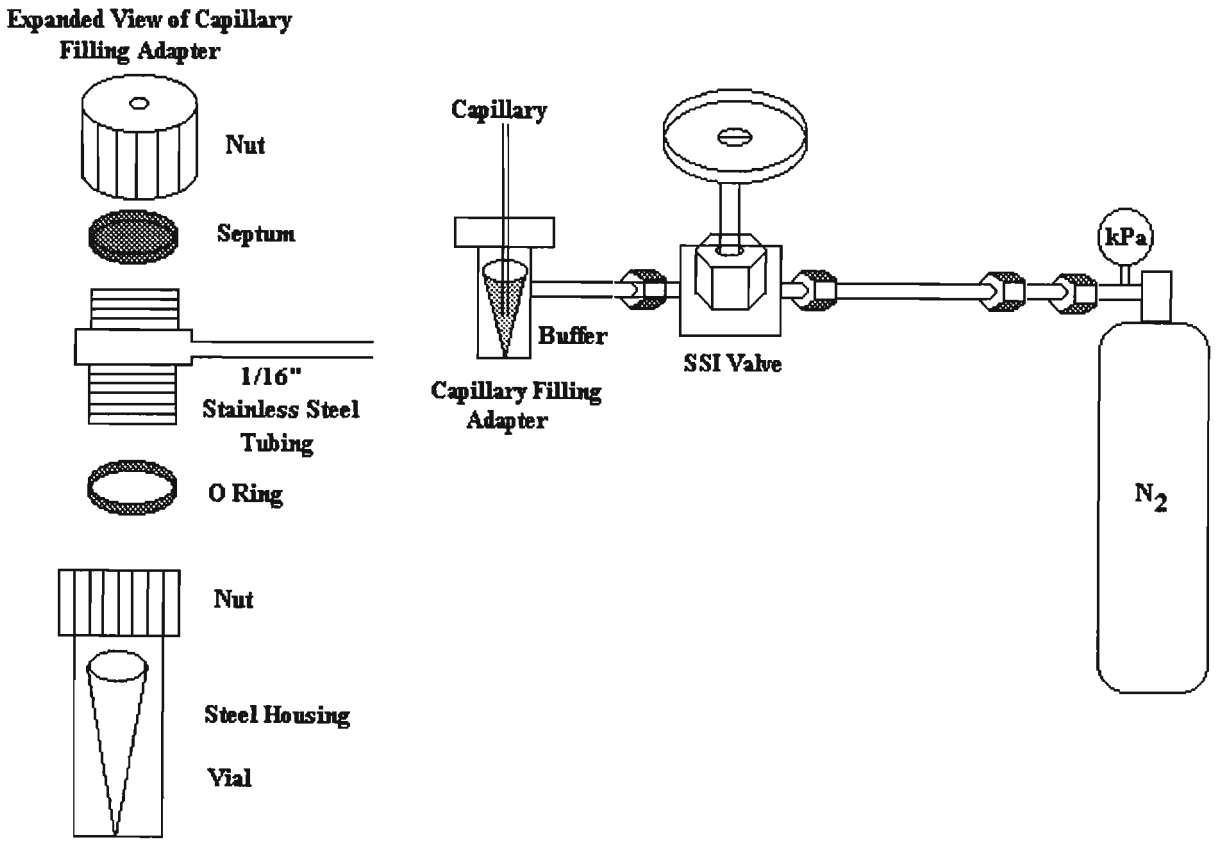

Figure 3.7 Schematic diagram of the capillary filling adapter.

3.5.5 *The Capillary Column*

Bare fused silica capillaries of dimensions 50 μm i.d. x 10 m were obtained from SGE (Melbourne, Australia). A 70 cm length of the capillary was cut with a ceramic capillary cutter (Hewlett Packard, Little Falls Site, DE, USA). A detection window was created at a

distance of 40 cm from the injection end of the column by charring a small section (ca 2.5 mm) of the polyimide coating. This was achieved by bending the column into a semicircle and placing the curved section into the flame of a Bunsen burner for no more than a second. The polyimide was removed from the column and the window was cleaned with a soft tissue moistened with acetone and carefully aligned with the optical path within the on-column capillary cell.

3.6 Column Conditioning

The inlet end of the column was pierced through the septum of the capillary filling adapter leading into a vial filled with 0.1 M NaOH (Figure 3.7). The valve (Scientific Systems Inc.) was opened, introducing a nitrogen head pressure of 400 kPa into the injection port. After five minutes, the micro-valve was closed, the pressure vented and the vial replaced with one containing doubly deionised water. The above procedure was repeated with the run buffer after which the column ends were immersed into the buffer reservoir together with their respective electrodes. The column was equilibrated at 30 kV for 10 minutes in the run buffer prior to sample analysis. At the end of each day, the column was rinsed with 0.1 M NaOH for five minutes followed by another five minute rinse with doubly deionised water and finally the column was dried by flushing with nitrogen for five minutes. The column was stored dry.

3.7 Sample Introduction by Hydrodynamic Injections

Samples were introduced by lowering the detector end of the capillary together with the buffer reservoir by 4 cm ($\Delta h = 4$ cm). The opposite end (injection end) of the capillary tube was then removed from the inlet buffer vial and immersed in the sample solution for a period of 5 s. The sample was introduced into the capillary by a siphoning action. Thereafter, the capillary was returned to its original level ($\Delta h = 0$) and the inlet capillary returned to the inlet buffer vial. The system was then ready for the application of a potential difference and electrophoresis.

3.8 Sample Introduction by Electrokinetic Injections

The inlet end of the capillary together with the anode was immersed into the analyte solution prepared in 30 mM borax. An injection voltage of 2.5 kV was applied for 5 s causing the analyte solution to enter into the column by electromigration. Both column and electrode were then returned to the separation buffer reservoir prior to electrophoresis.

3.9 CE with Laser Induced Fluorescence (LIF) Detection

3.9.1 *Instrumentation*

The CE-LIF work was performed on a Beckman P/ACE 5500 CE instrument (Beckman Instruments Inc., CA, USA). This instrument comprised an autosampler, a cartridge holder and interface, a high voltage power supply and electrodes, an optics module and detector, temperature control hardware, a sample injection mechanism and a controller with front panel display and function switches (Figure 3.8). Automated control of the instrument was permitted with the use of either System Gold Software or the Microsoft Windows based P/ACE Control Software.

The autosampler had two concentrically arranged trays that rotated independently in either direction. These trays held vials containing sample, buffer, column conditioning and rinse solutions. The capillary column was wound around a mandrel and housed in a cartridge. The ends of the capillary protruded through two sealed openings in the bottom of the housing. Near the outlet of the capillary, the polyimide coating was removed to create an optically transparent window. This section of the capillary was aligned with an opening in the housing for use with the detector optics. A liquid coolant flowed through the cartridge via two openings in the bottom of the cartridge. This fluid flowed around the capillary within the cartridge and maintained a preset temperature through convective heat removal.

The system could be operated either by the controller on the front panel of the instrument or by software. An inlet pressure of at least 80 psi nitrogen was required to actuate the pneumatic instrument functions. The power supply was capable of delivering a maximum

of 30 kV at 250 μA and the system could be operated in either constant voltage or constant current mode. The operation of the high voltage power supply was interlocked with the instrument doors and covers to disable the high voltage when a door or cover was opened. In this work, the instrument was fitted with the LIF detector, the laser module 488, and connecting fibre optic cable as shown in Figure 3.8. A schematic diagram of a typical LIF detection system is shown in Figure 3.9. A 3 mW argon-ion laser was used with an excitation wavelength of 488 nm and a 520 nm emission filter. Data capture was achieved using Systems Gold Software (Beckman Instruments).

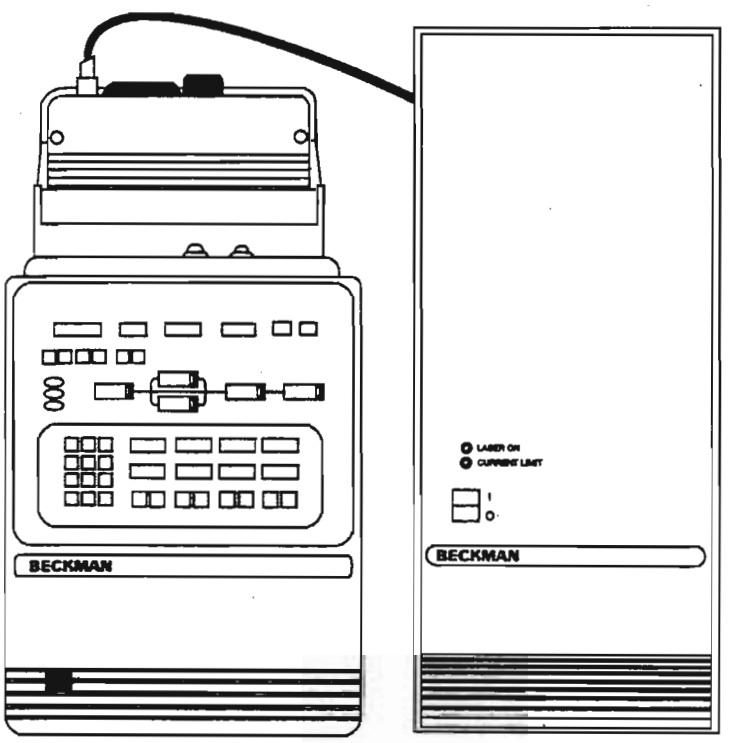

Figure 3.8 The Beckman P/ACE System with the laser module 488 and connecting fibre optic cable.

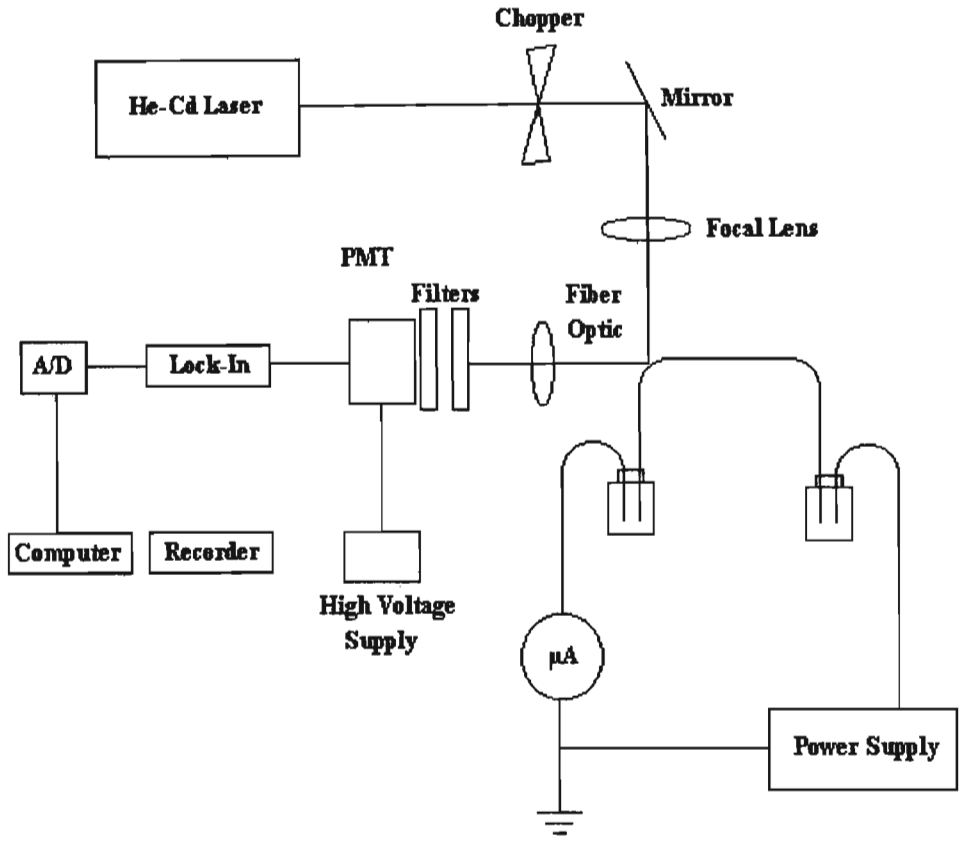

Figure 3.9 Schematic diagram of a typical capillary electrophoresis/laser induced fluorescence detection system [303].

3.9.2 *Derivatization procedure for tagging toxins with a fluorescent moiety*

A 5.5 x 10^{-4} M stock solution containing 0.00214 g of fluorescein isothiocynate (FITC) isomer 1 (Sigma Chemical Co., St Louis, MO, USA) was prepared in 10 mL HPLC grade acetone (Riedel de Haën). 10 μL of FITC reagent was then added to 1 mL of a toxin solution (1 ng/μL in 30 mM borax) and allowed to react overnight in a dark cupboard at ambient temperature according to the method of Dovichi *et al.* [304]. The resulting solution was analysed by CE-LIF. Instrument conditions were identical to those used in MECC.

3.10 Field Amplified Back and Forth MECC

The entire column was filled with analyte solution prepared in 3 mM borax using the modified capillary filling adapter (Figure 3.7). Thereafter, the column ends together with their respective electrodes were placed in the high ionic strength run buffer (30 mM borax, 9 mM SDS) and a potential difference of -30 kV applied. The current was monitored until it reached a maximum value (55 μA), after which, the polarity was switched to + 30 kV. This was achieved by manually changing the positions of the positive and negative electrodes. The applied voltage was therefore interrupted for a brief period.

3.11 Use of Hewlett Packard HP ^{3D}CE Instrument (UV detection)

During the course of this project, the author was fortunate enough to briefly use an HP ^{3D}CE instrument (Hewlett Packard, Waldbronn, Germany). The CE instrument comprised an autosampler, cartridge holder, high voltage power supply and electrodes, an optics module and a diode-array detector as shown in Figure 3.10. The capillary column was wound around six plastic posts which were part of the cartridge housing. The fused silica capillary ends were cut to a smooth, mirror-like finish using fibre optic technology. In addition, the polyimide outer coating was removed from the ends to minimise solute adsorption and help maintain sharp peak shapes. The column had a pre-made detection window and a built-in alignment stopper which allowed rapid and precise insertion into the alignment interface. The alignment interface simplified capillary exchange, protected the fragile detection window and ensured exact alignment of the window in the detector. The ends of the capillary protruded through two openings in the bottom of the housing. Temperature control was maintained by an air cooling system.

The instrument was completely controlled by the HP ^{3D}Chemstation Software. During initialisation, the instrument tested different functions and adjustments and the tray was moved to a defined position, and the UV lamp was switched on. The software displayed a diagram of the system showing the actual instrument status as shown in Figure 3.11. A replenishment system was used to automatically empty and refill vials with fresh buffer.

This was particularly useful in multiple analyses as it ensured a constant buffer composition. The sample tray could house 50 vials and could be operated either manually or via software. Electric field parameters such as polarity, voltage, current and power were fully controllable by the software while the timetable was used to set values for these parameters, at a certain time during a run.

As just described, the system was equipped with numerous advanced features and of particular importance for field amplification back and forth MECC, was the time programmable polarity switching facility. The method developed for field amplification back and forth MECC (as described in section 3.10) was therefore evaluated on this system.

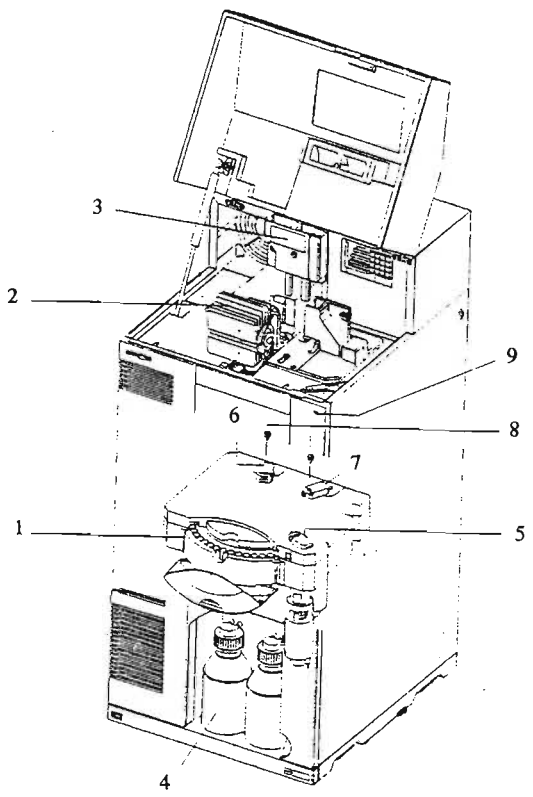

Figure 3.10 The HP ^{3D}CE system. Component 1 Tray; 2 Diode-Array Detector; 3 Capillary Cassette; 4 Replenishment Bottles; 5 Replenishment Lift; 6 Outlet Lift; 7 Inlet Lift; 8 Electrodes; 9 Status Display LED.

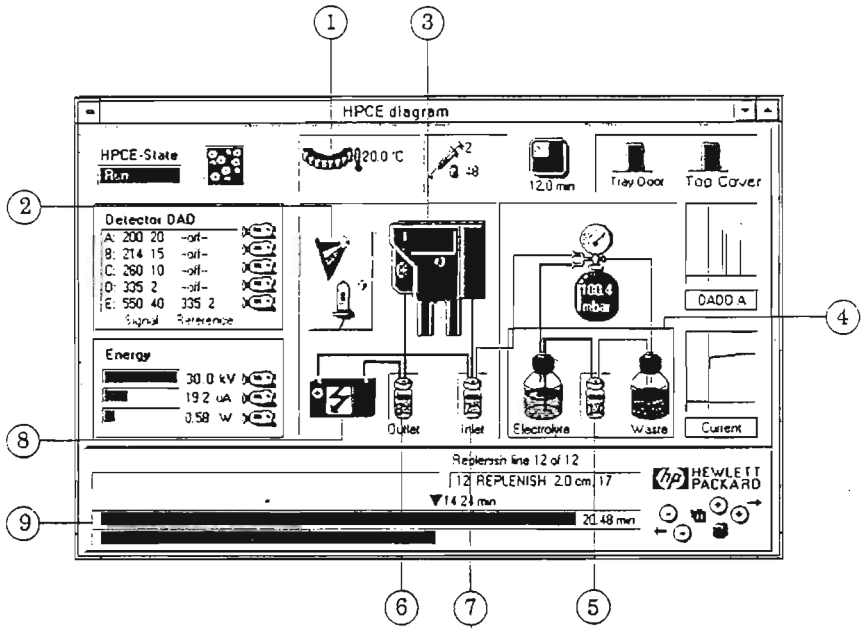

Figure 3.11 The instrument display screen on the HP ^{3D}CE system. Component labels are identical to Figure 3.10.

3.12 Field Amplified Back and Forth MECC on the HP ^{3D}CE system

Using 12 psi pressure, the entire column was filled with solute containing 1 ng/μL nodularin and 1 ng/μL MC LR, prepared in dilute sample buffer (3 mM borax). The system was programmed to begin electrophoresis with -30 kV at time zero with both column ends placed in the run buffer. At 4.3 minutes, the polarity was switched automatically to +30 kV. These two events caused stacking and electrophoresis respectively.

3.13 Field Amplified Sample Injection (FASI)

3.13.1 *Normal Polarity FASI*

The inlet end of the capillary together with the anode was immersed into a solution containing 1 ng/μL of the 4 toxins in 3 mM borax. An injection voltage of 10 kV for 15 s was applied for sample injection to occur. Both column and electrode were returned to the run buffer prior to electrophoresis.

3.13.2 *Reversed Polarity FASI*

The inlet end of the capillary together with the cathode was immersed into a solution containing 1 ng/μL of the 4 toxins in 3 mM borax. An injection voltage of 10 kV for 15 s was applied for sample introduction and solute stacking to occur. Both column and electrode were returned to the run buffer reservoir for normal polarity separation.

3.14 Electro-extraction

The injection end of the capillary column filled with 3 mM borax was immersed into a sample containing toxins dissolved in water while the detector end was placed in the run buffer containing 30 mM borax and 9 mM SDS. A potential difference of -30 kV was applied, causing solute to migrate from water and enter the column.

3.15 Off-Line Solid Phase Extraction

3.15.1 *Apparatus*

The vacuum manifold system (Millipore Corp., Milford, MA, USA) (Figure 3.12) comprised a glass vessel fitted with a vacuum control gauge and bleed valve assembly for vacuum and flow control, individually controlled valves to permit simultaneous processing of samples, adjustable rack assembly to accommodate a variety of collection vessels, a nylon manifold with luer fittings and a gasket. The manifold was designed to extract 24 samples simultaneously.

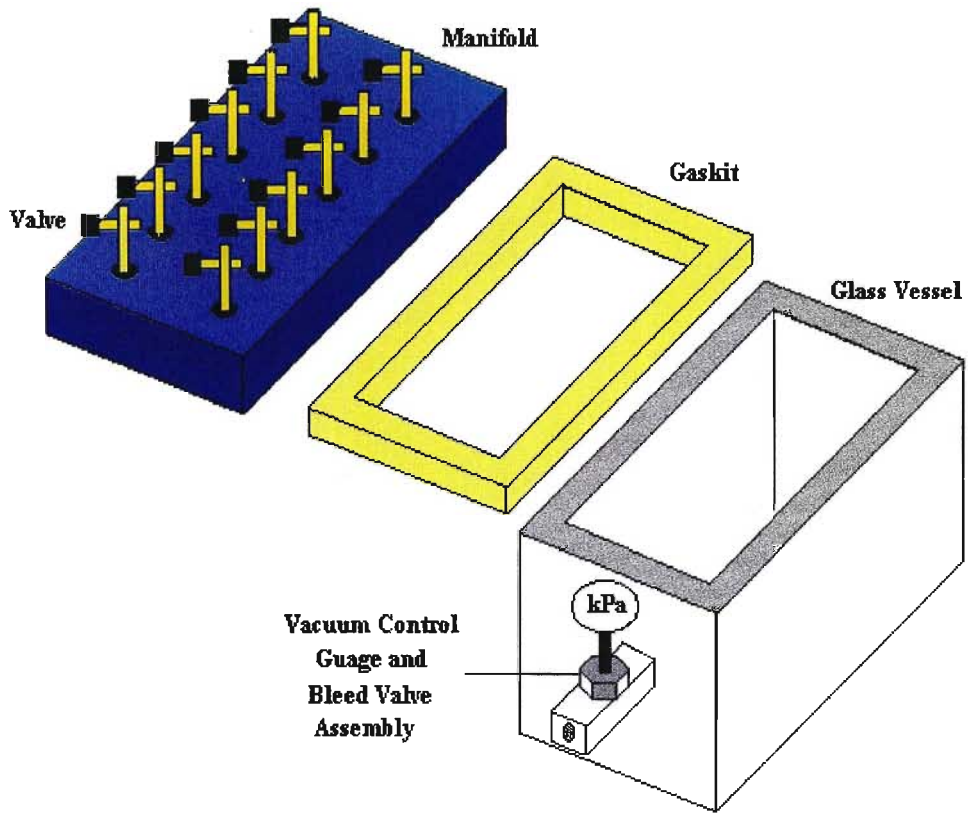

Figure 3.12 The vacuum manifold system for solid phase extraction.

3.15.2 *Sep-Pak Plus Cartridges*

The extraction cartridges contained 100 mg trifunctionally bonded C_{18} solid phase material (Millipore), were stored in a sealed packet to prevent contamination by volatiles present in the air. The cartridges were inserted into the Luer fittings directly on the manifold.

3.15.3 *Activation and Extraction*

A disposable 25 mL syringe was inserted on the cartridge to act as a solvent reservoir to which 10 mL of methanol was added. A vacuum of -5 kPa was applied causing the solvent to wet the C_{18} sorbent. Thereafter 10 mL deionised water was passed through to remove the excess solvent. The solvent reservoir was removed and one end of a piece of PTFE tubing attached to the cartridge while the opposite end immersed into the sample (0.002 ng/μL toxin in 1% methanol). Analyte solution was drawn through the cartridge with a pressure of -20 kPa vacuum (Figure 3.13). When all the sample had passed through the cartridge, room air was drawn through for 30 minutes to minimise the amount of water eluted with the solute.

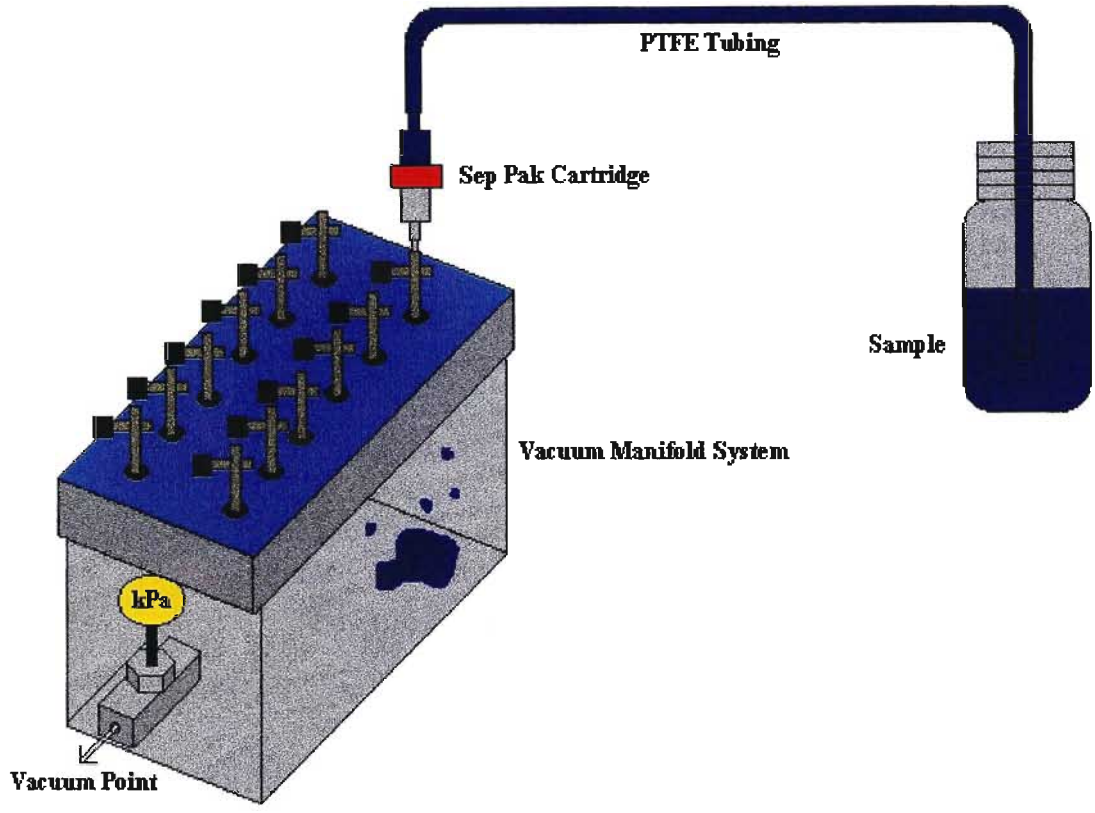

Figure 3.13 Schematic diagram of solid phase extraction.

3.15.4 *Elution*

The cartridge was removed from the manifold and attached to a 25 mL disposable syringe. The toxins were eluted from the solid sorbent with 3 x 1 mL aliquots of methanol. The solvent was then evaporated under a gentle stream of nitrogen to dryness and resuspended in 10 μL of methanol prior to MECC analysis.

3.16 On-Line Solid Phase Extraction

A solid phase extraction cartridge was fabricated from the packed capillary column prepared as described in 3.17.4. A 10 mm length was cut using a capillary column cutter and retaining frits inserted. The cartridge was joined to the CE column on one end and a piece

of deactivated fused silica column (50 mm x 50 μm i.d.) on the other end by inserting the column ends directly into Teflon sleeves made by cutting Teflon tubing into 6 mm lengths. Activation extraction and elution was executed by piercing the fused silica column into the septum of the capillary filling adapter. A nitrogen cylinder pressure of 400 kPa was used to drive liquid through the cartridge for the purpose of activation and extraction (Figure 3.14). The nitrogen pressure inlet valve (Scientific Systems Inc.) was closed and the capillary filling adapter allowed to depressurise slowly. The capillary inlet was then withdrawn from the septum and placed in the inlet buffer vial. A potential difference of +30 kV was applied for elution and subsequent MECC by the resulting electroosmotic flow.

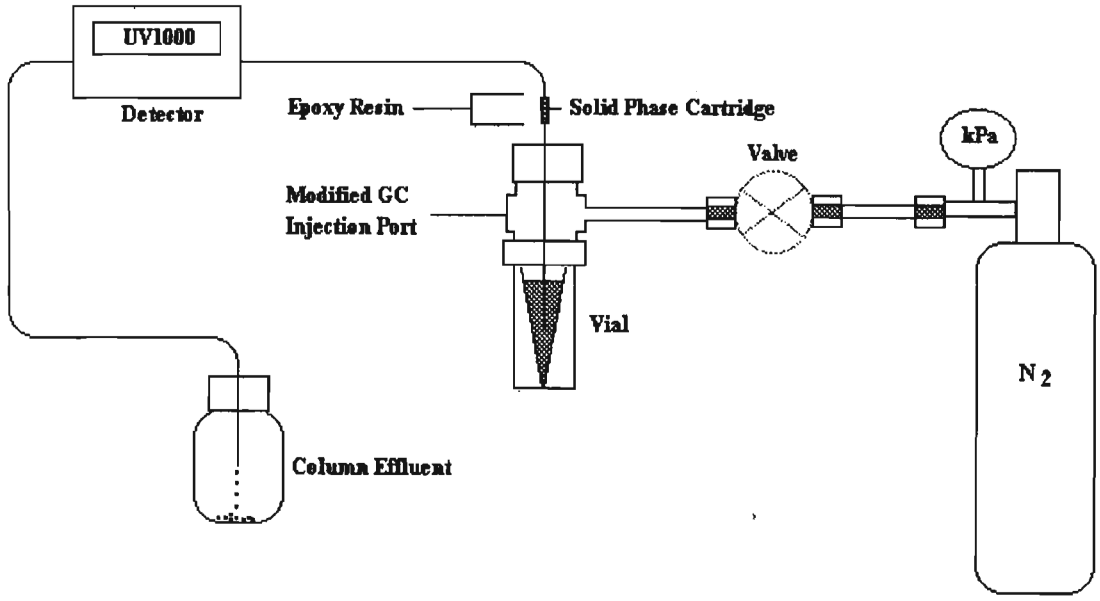

Figure 3.14 Apparatus used for on-line solid phase extractions.

3.17 Micro-High Performance Liquid Chromatography

3.17.1 *μHPLC Pump*

Mobile phase was driven through the column using a prototype pump, the RPT 9400 μSFC-LC pump (RPT, CA, USA) (Figure 3.15). This is a positive displacement type pump consisting of a pressure control pumping system for SFC and a flow control pumping system for μhigh performance liquid chromatography (μHPLC). Each pumping system was

constructed using a dual plunger, dual independent, bi-directional motor and lead screw linkage design. This allowed for the system to have independently programmable delivery and refilling cycles of both pump chambers. A host computer (IBM PC) and a servo controller board performed the electronic sensing, analysing, and control functions needed to operate the entire system. Information from the pressure transducers and optical encoder assemblies on the motor shafts were used to determine the motion of the plungers.

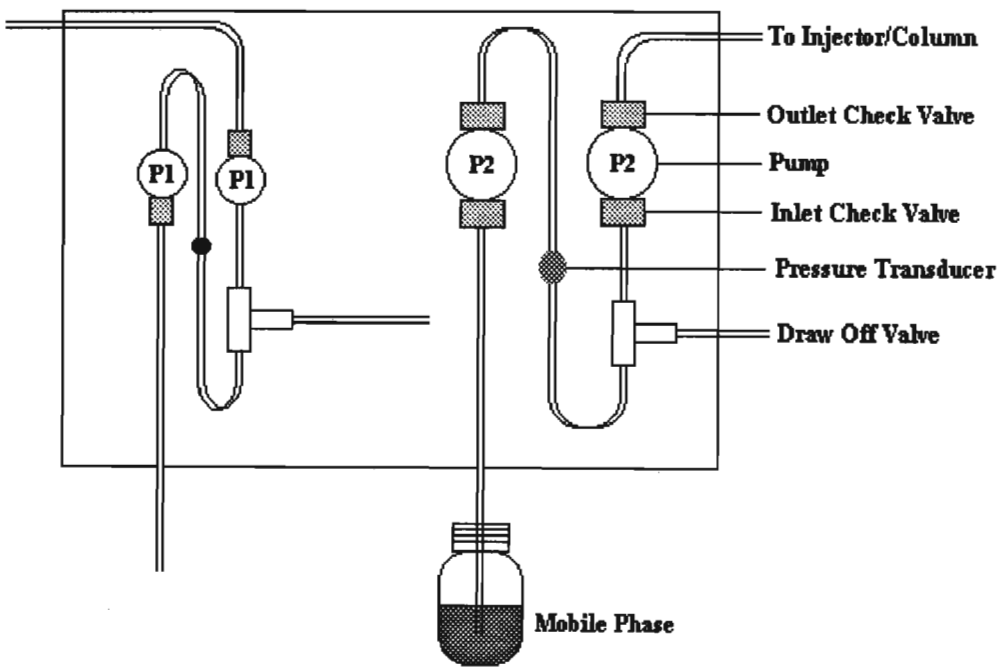

Figure 3.15 Schematic diagram of the μHPLC pump. The left hand part of the diagram is the pressure control pumping system for SFC as indicated in Section 3.17.1.

3.17.2 *μHPLC Control*

The SFC-LC user interface software program was based on a Windows environment. The program was designed to perform pressure and flow controls allowing pressures ranging from 1 to 350 bars and flow rates down to 1 μL/min. It provided the user with a graphic pump control display and an output pressure/flow histogram. It also enabled the user to select configuration settings such as fluid compressibility, plunger refill speed, refill volume and initial target pressure.

3.17.3 *Injection Valve*

Mobile phase was driven by the μpump via a 25 μm fused silica capillary to a C14W injection micro-valve (Valco Instruments, Texas, USA), containing a 60 nL internal volume rotor (Figure 3.16). The injector valve was operated manually by turning the valve to the load position, after which a small sample volume was transferred with a 10 μL syringe, thereby filling the sample loop, followed by rotation of the valve to the inject position. All capillary connections to the micro pump and injector where made using 1/16 inch o.d. polyetherether ketone (PEEK) and stainless steel ferrules.

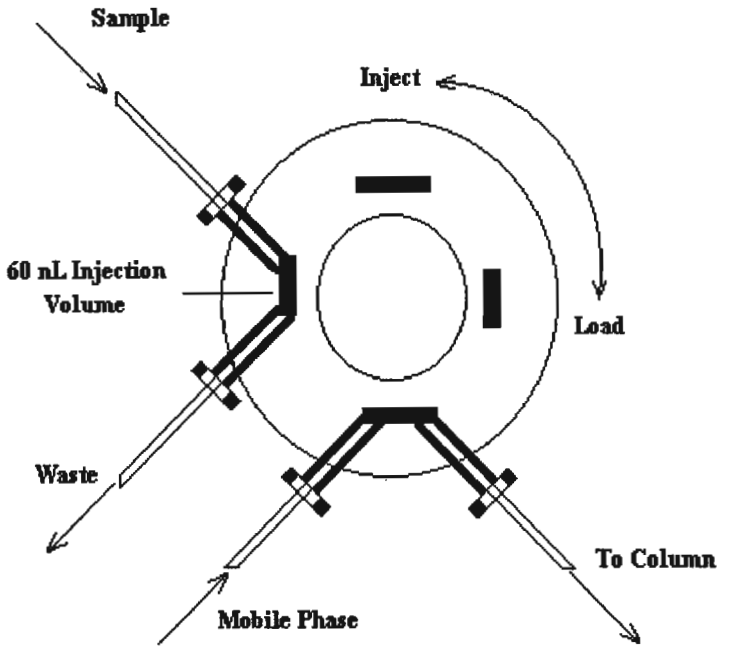

Figure 3.16 A schematic diagram of the Valco micro valve injector.

3.17.4 Packed Capillary Column Fabrication

Instrumentation: Supercritical CO_2 required for the packing process was directed from the injection port of a Lee Scientific Series 600 SFC/GC system to a packing reservoir. The reservoir was constructed from a 150 mm length of 1/8″ o.d. stainless steel tubing. Both ends were fitted with stainless steel ferrules and 1/8″ to 1/16″ reducing unions. A metal screen with 2 μm pores was placed inside the reducer at the inlet end of the reservoir to prevent backflushing of the packing material into the SFC pumping unit. A schematic

diagram is shown in Figure 3.17. A series 600 SFC computer based syringe pump (Lee Scientific, Salt Lake City) controlled by the Lee Scientific Series 600 controller was used for pressure programming of the mobile phase. The syringe pump had a volume of 150 mL. The pump head was cooled by a Grant Inst cooler (Grant, Cambridge, UK) which circulated a mixture of ethylene glycol/water (75:25 v/v), to approximately 10°C around the cylinder head. SFC grade CO_2 (Air Products, South Africa) was connected to the pump using 1/8 inch stainless steel tubing.

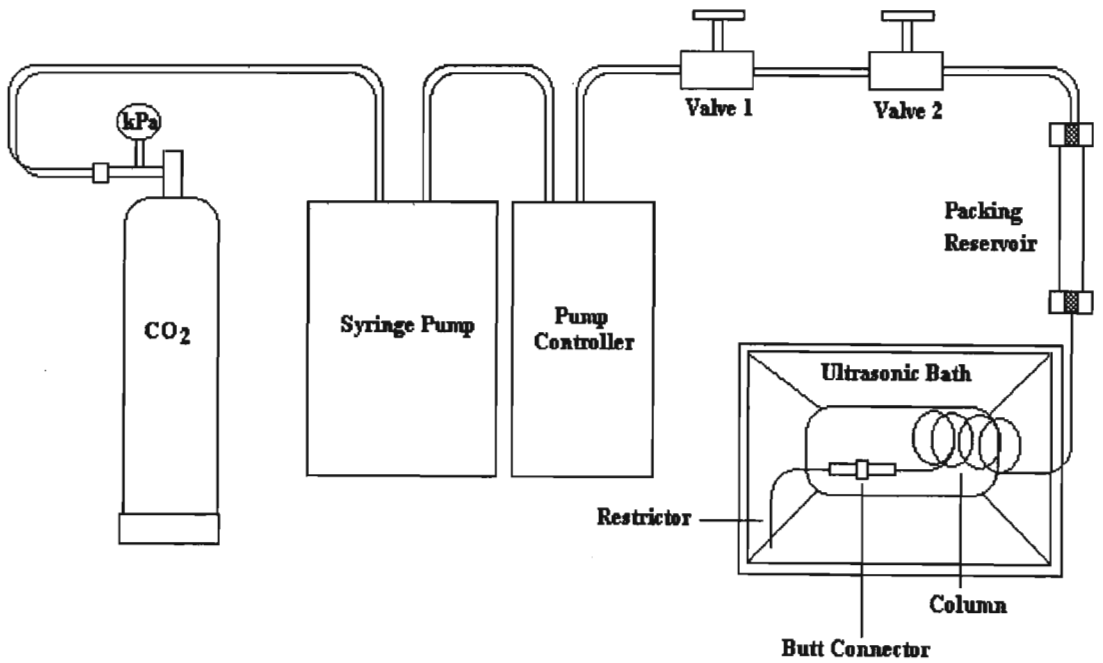

Figure 3.17 Apparatus used for packing micro-columns for μHPLC, CEC and on-line solid phase extractions.

Preparation of the Capillary Column: The fused silica capillary column of dimensions 50 cm x 50 μm i.d. was packed using supercritical CO_2 at 350 atmospheres [305]. The tubing was connected to a packing reservoir, cleaned with methanol and dried (Figure 3.18). The packing material (3 μm Spherisorb ODS 1, Phase Sep., Wales, UK) was placed in the reservoir. The reservoir containing a 2 μm screen was connected to a high pressure valve allowing the introduction of the CO_2 but preventing the backward movement of the packing

material towards the pump. The end of the column was butt-connected to a linear restrictor (15 cm x 10 μm i.d.) (SGE).

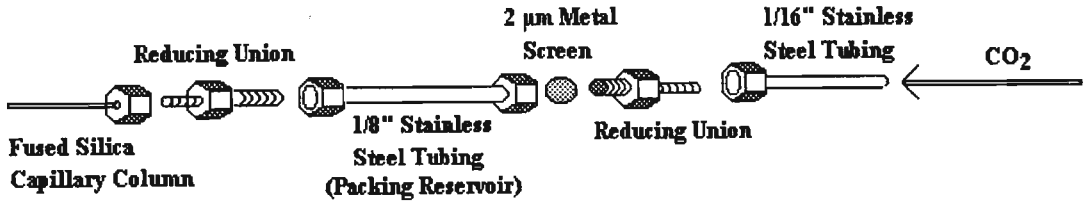

Figure 3.18 Schematic diagram of the packing reservoir.

To the outlet end of the capillary, a frit was inserted to retain the packing material (Figure 3.19). The frit (0.2 to 0.3 mm in length) was fabricated by repeated insertion of the capillary into a slurry of silica (5 μm Spherisorb 5W, Phase Separations Ltd, UK) in potassium silicate solution (80:20 K_2SiO_4:H_2O v/v). The material was then fused in a flame of a Bunsen burner.

This end was butt-connected to a linear restrictor to maintain the pressure inside the capillary. The column and the restrictor were immersed in an ultrasonic bath maintained at 40°C. Liquid CO_2 was introduced via two valves (Scientific Systems Inc., State College , PA 16803), the column sonicated and the pressure raised from 120 atmospheres to 350 atmospheres gradually in units of 20 atmospheres. Throughout the pressurisation procedure, the packing reservoir was tapped until the column had been packed to the required length. Sonication was then stopped and the pressure held for 30 minutes before depressurising. This was performed slowly (1 atmosphere per minute) to avoid backflushing of packing material. The pressure inside the column was monitored by immersing the restrictor into a beaker of water. After bubble formation ceased (usually overnight), the restrictor and packing reservoir was disconnected. The column was cut into 15 cm lengths and frits inserted on opposite ends (Figure 3.19) and this was connected to the electrophoresis column with a fused silica capillary column press fit connector (Hewlett Packard).

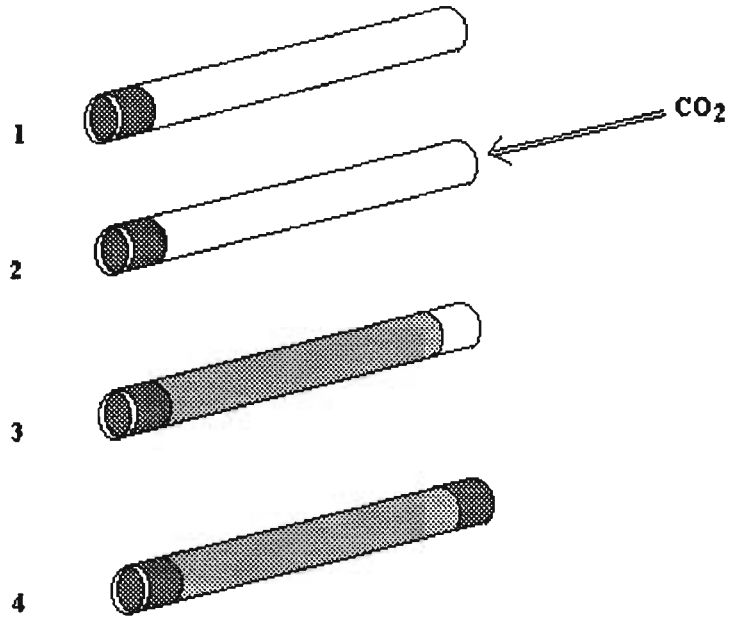

Figure 3.19 Diagrammatic representation of the packing process. 1 Formation of end frit; 2 Packing of column with high pressure supercritical CO_2; 3 Slow depressurisation; 4 Formation of retaining frit.

3.17.5 *μHPLC*

A schematic representation of the instrumental set up is illustrated in Figure 3.20. It comprised the RPT μSFC-HPLC pump, a length of fused silica tubing (25 μm x 300 mm) connecting the Valco C14W injection valve to the micro pump, the μHPLC column (50 μm i.d. x 150 mm piece cut from the column packed in 3.17.4 above), and the fused silica capillary joiner linking the micro LC column to the open tubular column and the UV detector. All capillary connections from the micro pump to the Valco injection valve were made using 1/16 inch o.d. PEEK sleeves together with stainless steel ferrules. The mobile phase contained 26% HPLC grade acetonitrile prepared in 0.1% AR grade ammonium acetate [306]. The flow rate was set at 1 μL/min at ambient temperature.

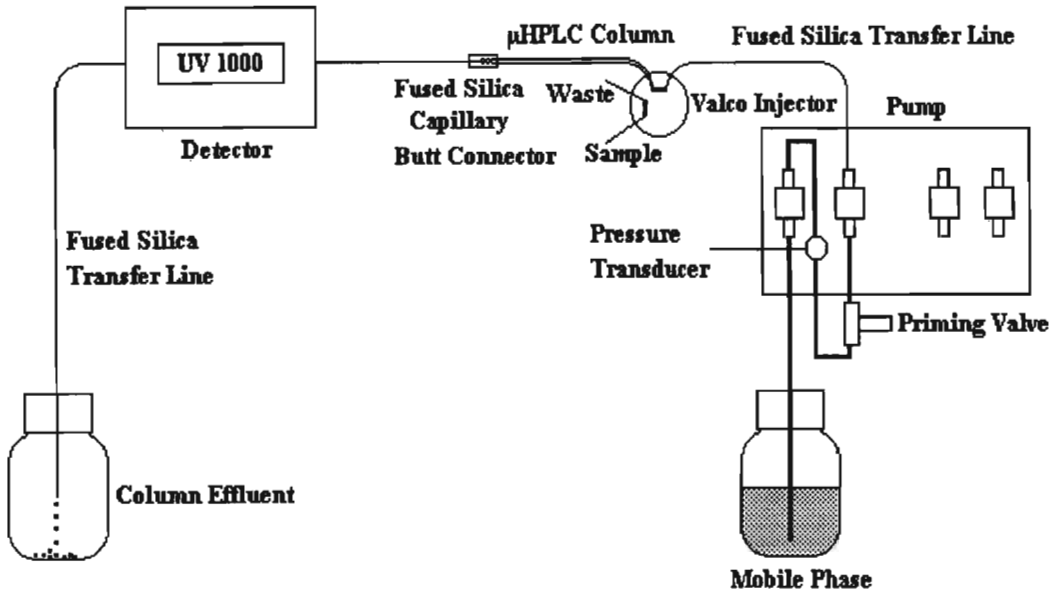

Figure 3.20 Schematic diagram of the μHPLC system.

3.18 CEC without Applied Pressure

The instrumental set-up was initially, identical to that in μHPLC (Figure 3.20). After sample introduction into the packed capillary column, using the 60 nL micro-valve injector, the RPT micro SFC-LC pump was switched off and allowed to depressurise slowly. The column was subsequently removed from the injector and attached to the open tubular capillary electrophoresis column with a fused silica capillary joiner. The opposite end of the packed column was immersed into the inlet buffer vial while that of the open tubular column placed in the outlet buffer vial. A potential difference of +30 kV was applied (Figure 3.21).

3.19 CEC with Applied Pressure

Figure 3.22 is a schematic illustration of the system used for performing capillary electrochromatography (CEC) with applied pressure. This system is a modified version of

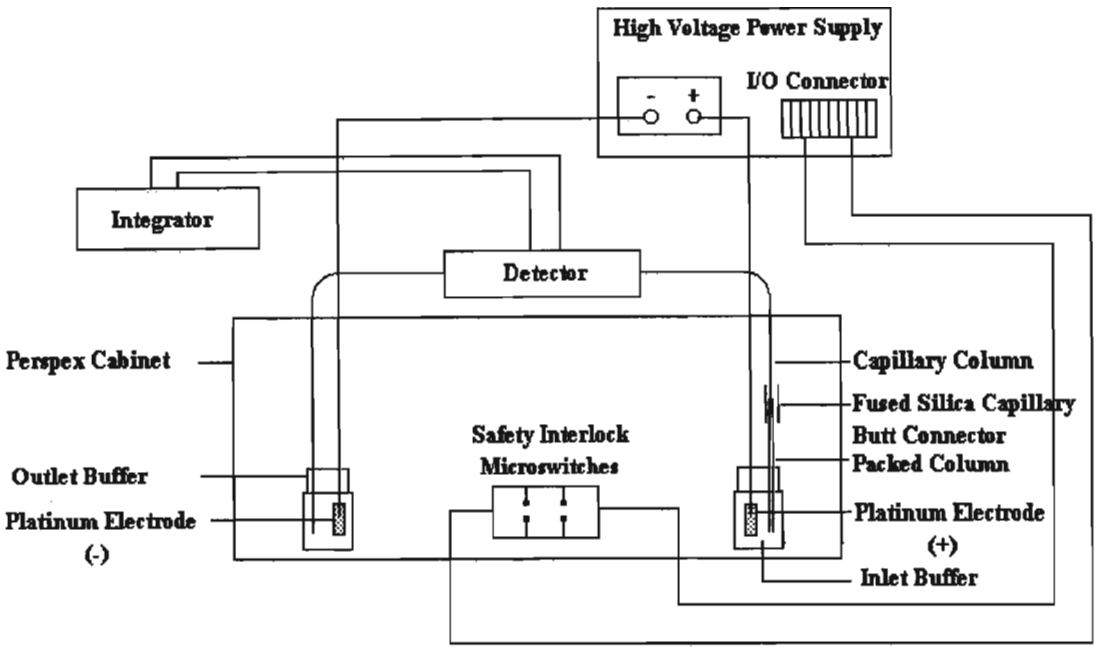

Figure 3.21 Schematic diagram of the CEC system without applied pressure.

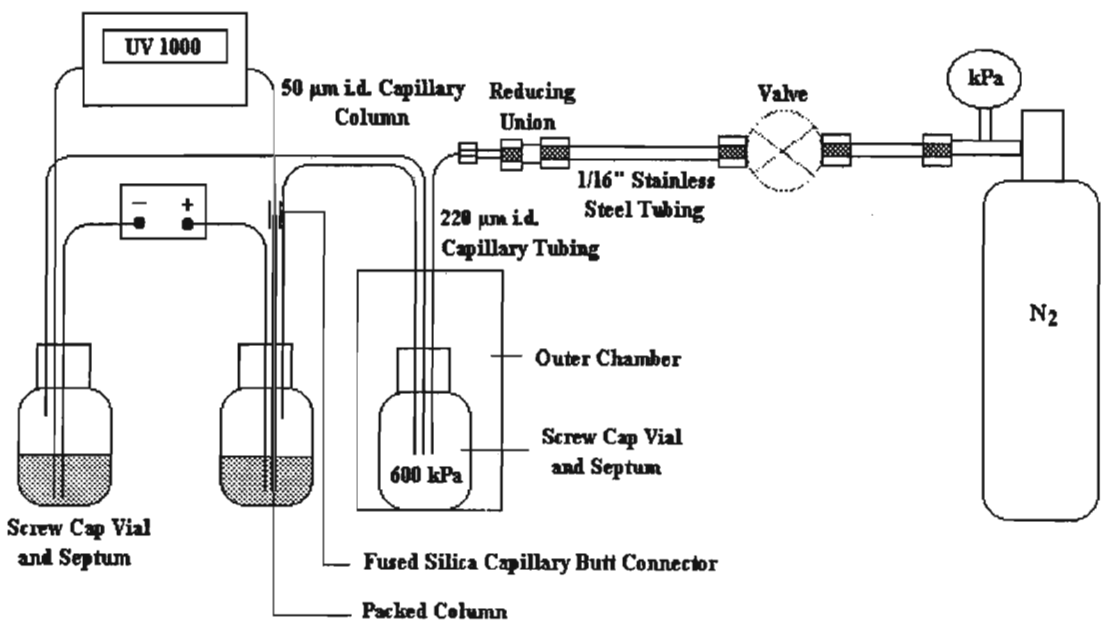

Figure 3.22 Schematic diagram of the laboratory built electrochromatography system with applied pressure.

that employed for MECC. Sample introduction was achieved using the instrumental set-up in the μHPLC mode (Figure 3.20). After sample introduction into the packed capillary column using the 60 nL Valco micro valve injector, the RPT micro SFC/HPLC pump was switched off and allowed to depressurise slowly. The column was then removed from the injector and pierced into the buffer vial through the septum. Similarly the opposite end of the capillary was pierced into the outlet buffer vial equipped with a septum and a screw cap. A third vial housed inside a safety chamber, as a precaution for explosion hazards during pressurisation, was pressurised to 600 kPa by directing a stream of nitrogen into the vial via a length of fused silica capillary tubing (220 μm i.d. x 200 mm). Another two tubes (220 μm i.d. x 300 mm) leading out of the pressurised vial were used to pressurise the buffer vials. Lastly both electrodes were inserted into the respective buffer vials by piercing them through the septum. The system was then pressurised and a voltage of 30 kV applied.

3.20 High Performance Liquid Chromatography (HPLC)

3.20.1 *Instrumentation*

HPLC analyses were carried out on a Waters system (Figure 3.23) equipped with a model 600E solvent delivery system, Model 710B WISP autosampler and a Model 991 photodiode array detector (Millipore Corporation, Waters Chromatography Division, Milford, MA, USA) at 200-400 nm. The system was computer driven using Millennium software. A Waters μBondapak C_{18} column of dimensions 300 mm x 3.9 mm i.d. and a particle size of 10 μm was used and maintained at 40°C with a Waters temperature control module. A run time of 60 minutes was found to be sufficient for the toxin analysis as well as conditioning of the column for the next analysis.

3.20.2 *Mobile Phase*

The eluents were water/0.05% trifluoroacetic acid (solvent A) and acetonitrile/0.05% trifluoroacetic acid (solvent B). Separation was achieved using a linear gradient as in Table 3.3 and a flow rate of 1 mL/min. The HPLC system was equipped with a special helium sparge line for solvent degassing. The solvents were degassed/sparged for 15 minutes after

which the gas was controlled automatically by introducing a sparge delay time of 10 minutes for the entire duration of the run.

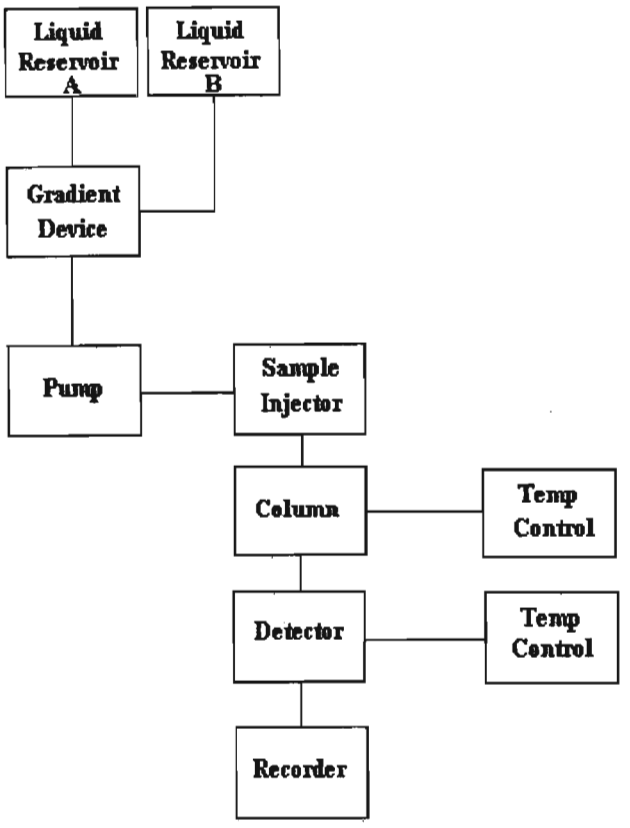

Figure 3.23 Block diagram of a typical HPLC system.

Table 3.3 Gradient elution profile

Time (min)	0	10	40	42	44	46	50
% A	70	65	30	0	0	70	70
% B	30	35	70	100	100	30	30

Chapter Four

Optimization and the Application of CE for Algal Toxin Analysis

4.1 Introduction

Up to now analytical methods for the determination of algal toxins have involved the use of high performance liquid chromatography [62,66,67]. The drawbacks of HPLC include long analysis times, low chromatographic efficiency and poor resolving power. Furthermore, the low diffusion coefficients (D_m) of large biomolecules in liquid mobile phases increases the contribution to the resistance to mass transfer term in the van Deemter equation, resulting in band broadening. Capillary electrophoretic techniques on the other hand are more efficient at separating these type of molecules. From equation 1.1, it is clear that a greater number of theoretical plates (N) will be produced from solutes with a low D_m [68]. Further, the other contributor to the large number of theoretical plates is that high operating voltages are permitted in CE because of the efficient heat dissipation capacity of the fused silica capillary columns. The two electroseparation modes, capillary zone electrophoresis (CZE) and micellar electrokinetic capillary chromatography (MECC) were investigated for the possible application to the analysis of algal toxins.

Parameters such as surfactant concentration, buffer ionic strength, buffer pH and operating voltage, were systematically optimized. Using these conditions, the practical application of this method for qualitative analysis was demonstrated on supercritical fluid extracts of freeze-thawed algal scum samples. HPLC work with photodiode array UV detection was conducted in parallel for the purposes of verification of results obtained by MECC.

4.2 Capillary Zone Electrophoresis

The three microcystin toxins have very closely related structures, charge, size and shape and as a consequence, a small difference in their electrophoretic mobility, μ_{ep}. Since this electro-separation mode is based on the differences in μ_{ep} resulting in different velocities of migration of ionic species, only nodularin could be sufficiently resolved from the microcystins (Figure 4.1). Attempts to optimize buffer ionic strength (Table 4.1 & 4.2) and, buffer pH (Table 4.3 & 4.4) had little effect on the migration time and migration time difference of the microcystins. The corresponding data illustrated graphically in Figure 4.2 show that an increasing buffer ionic strength increases the migration time difference of nodularin and MC YR to a reasonable extent. MC LR and MC RR are affected to a lesser extent and no observable changes to MC YR and MC LR occurred. Figure 4.3 showing pH effects on the migration time difference gives an almost identical relationship except the migration time difference decreases at high pH because of the associated increase in EOF. These findings can be accounted for by the fact that only nodularin has an electrophoretic mobility that is sufficiently different to that of the microcystins.

The use of a phosphate buffer had no observable effect on the resolution of the microcystins (Figure 4.4) and therefore further work using this technique was discontinued. Liu *et al.* however developed a CZE technique for the separation of MC RR, MC LR and [D-Asp^3] MC LR [63]. Fifty two different buffer solutions were evaluated and conditions such as pH, applied voltage, and concentration were optimized. Their findings revealed that an acetate buffer at pH 4 produced best results. These conditions were considered unsuitable for the purposes of this study as the amphoteric peptide toxins require a net negative charge for the purpose of field amplified sample stacking, a technique which must be used in order to attain sufficient sensitivity. This will be discussed in Chapter 5.

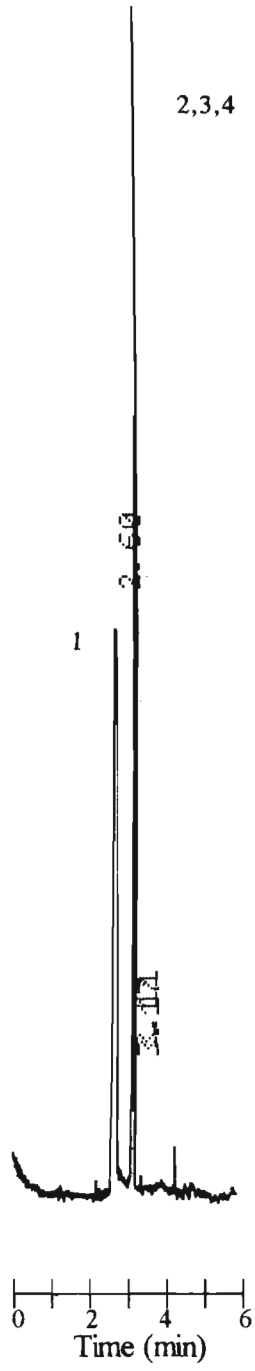

Figure 4.1 Electropherogram of four algal toxins using capillary zone electrophoresis and UV detection at 238 nm. Operating conditions: 30 mM borax; pH 9.18; 30 kV applied voltage; 10 s hydrodynamic injection; L_T 70 cm; L_{EFF} 40 cm. Peak identification: 1 nodularin; 2 MC YR; 3 MC LR; 4 MC RR.

Table 4.1 Migration time data for ionic strength optimization in CZE

	Migration Time (min)			
Borax (mM)	Nodularin	MC YR	MC LR	MC RR
10	2.18	2.63	2.62	2.69
20	2.58	3.22	3.22	3.26
30	3.17	4.15	4.15	4.29
40	3.7	5.1	5.1	5.33

Table 4.2 Migration time difference data for ionic strength optimization

	Migration Time Difference (min)		
Borax (mM)	Nod & MC YR	MC YR & MC LR	MC LR & MC RR
10	0.45	0	0.06
20	0.64	0	0.04
30	0.98	0	0.14
40	1.4	0	0.23

Table 4.3 Migration time data for pH optimization in CZE

	Migration Time (min)			
pH	Nodularin	MC YR	MC LR	MC RR
8.1	3.73	5.33	5.33	5.58
8.2	3.21	4.21	4.21	4.36
8.3	2.64	3.27	3.27	3.36
8.5	2.59	3.19	3.19	3.28
8.9	2.31	2.82	2.82	2.88
9.2	2.19	2.73	2.73	2.79
10.1	1.99	2.37	2.37	2.42

Table 4.4 Migration time difference data for pH optimization in CZE

	Migration Time Difference (min)		
pH	Nod & MC YR	MC YR & MC LR	MC LR & MC RR
8.1	1.6	0	0.25
8.2	1	0	0.15
8.3	0.63	0	0.09
8.5	0.6	0	0.09
8.9	0.51	0	0.06
9.2	0.54	0	0.06
10.1	0.38	0	0.05

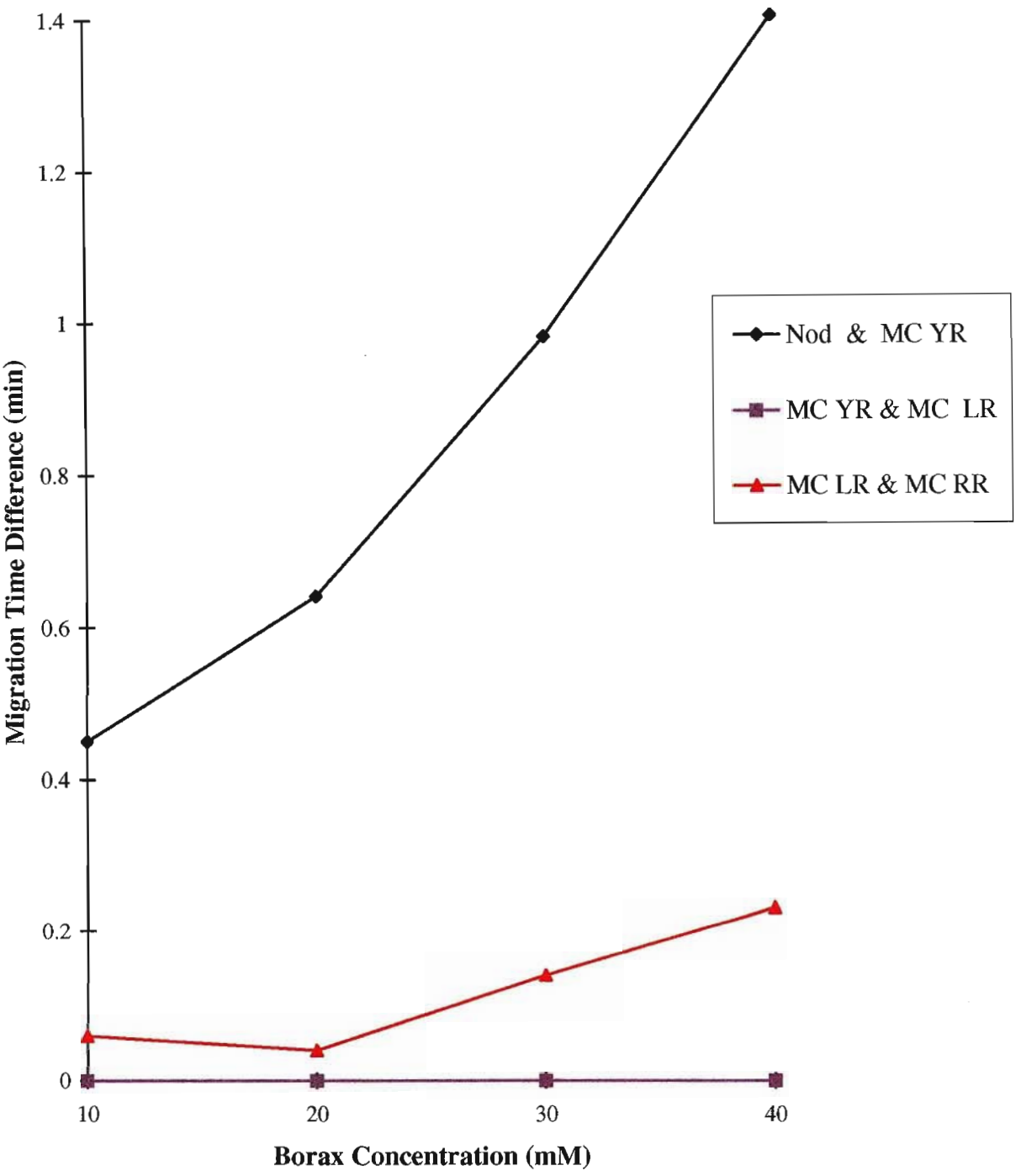

Figure 4.2 Variation of migration time difference with borax concentration.

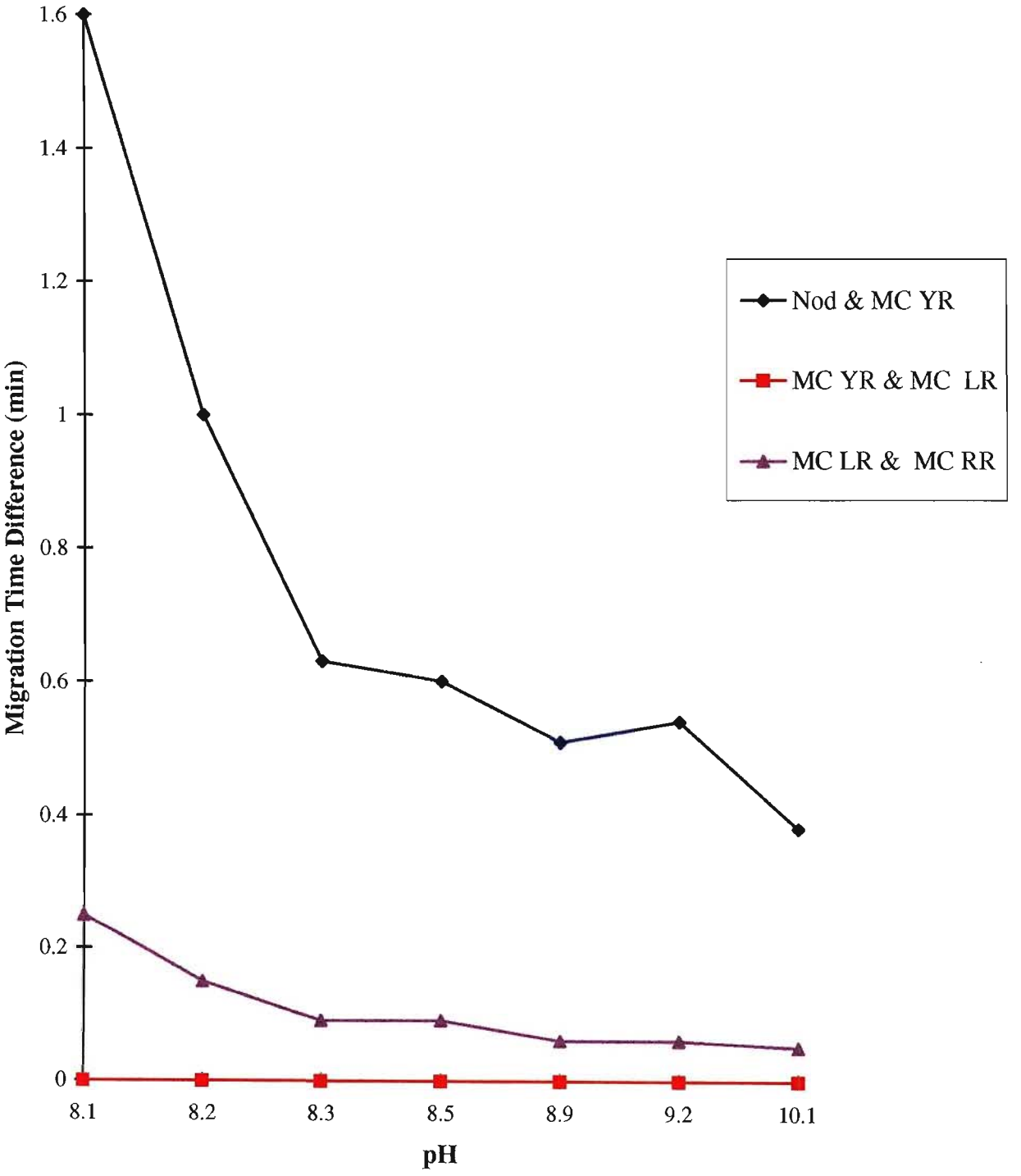

Figure 4.3 Variation of migration time difference with pH.

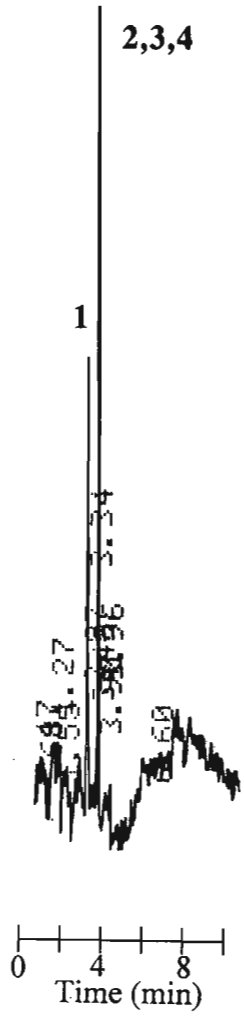

Figure 4.4 Electropherogram of four algal toxins using capillary zone electrophoresis and UV detection at 238 nm. Operating conditions: 10 mM Na_2HPO_4; 10 mM NaH_2PO_4; pH 7.97; 30 kV applied voltage; 10 s hydrodynamic injection; L_T 70 cm; L_{EFF} 40 cm. Peak identification: 1 Nodularin; 2 MC YR; 3 MC LR; 4 MC RR.

4.3 Micellar Electrokinetic Capillary Chromatography

Selectivity was enhanced by incorporating sodium dodecyl sulphate (SDS), an anionic surfactant in the run buffer. The toxins partition themselves between the micellar phase and the aqueous phase in a fashion analogous to reversed phase HPLC, during the normal course of electrophoresis (Figure 4.5). A combination of charge/mass ratios,

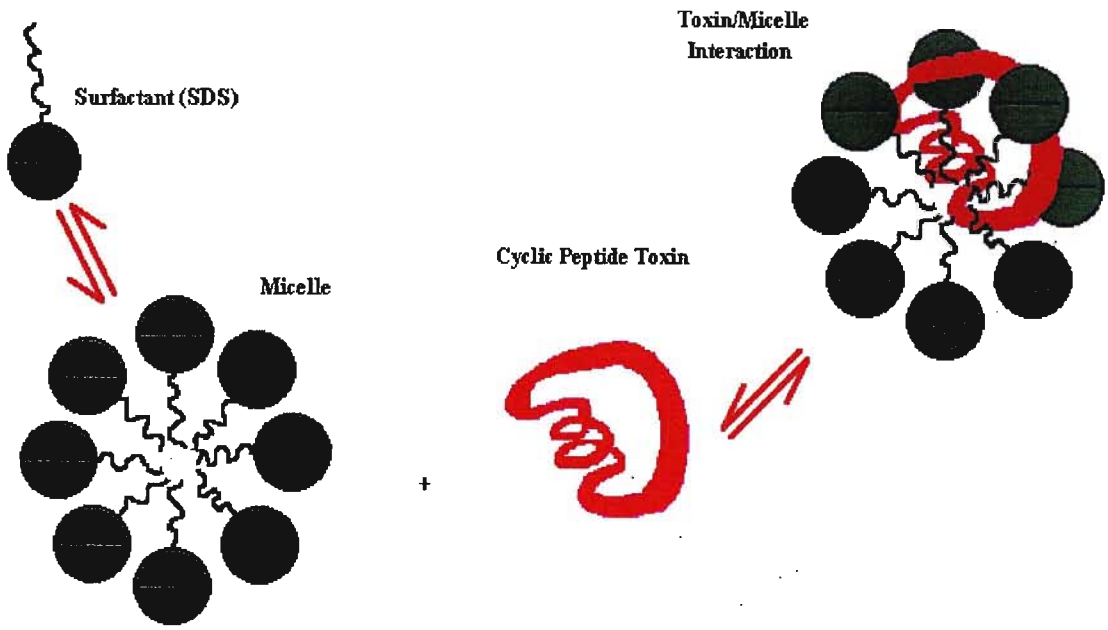

Figure 4.5 Schematic diagram of the mechanism of micelle formation and the toxin partition equilibrium.

hydrophobicity and charge interactions at the surface of the micelles combine to effect the separation of the analytes. Initial studies indicated that this electro-separation mode had potential for the separation of the toxins. Data presented in Table 4.5 were obtained for the optimization of SDS concentration. The corresponding capacity factors (Table 4.6) were calculated using the expression

$$k' = \frac{t_r - t_o}{t_o\left(1 - \frac{t_r}{t_{mc}}\right)} \qquad 4.1$$

Table 4.5 Retention time data obtained for SDS concentration optimization

0 mM SDS				
	t_r-t_o (min)			
t_o (min)	Nodularin	MC YR	MC LR	MC RR
2.6	0	0.51	0.51	0.57
2.65	0	0.51	0.51	0.57
2.66	0	0.5	0.51	0.56
mean	0	0.51	0.51	0.57
8 mM SDS				
2.67	2.77	3.73	3.97	4.84
2.78	2.69	3.6	3.83	4.62
2.76	2.7	3.59	3.81	4.6
mean	2.72	3.64	3.87	4.69
10 mM SDS				
2.8	3.42	4.4	4.63	5.31
2.69	3.26	4.18	4.42	5.14
2.73	3.39	4.34	4.58	5.32
mean	3.36	4.31	4.54	5.26
20 mM SDS				
2.56	4.02	4.66	4.86	5.13
2.56	4.13	4.81	5.02	5.33
2.6	4.39	5.09	5.29	5.56
mean	4.19	4.85	5.06	5.34
30 mM SDS				
2.71	5.28	5.82	6	
2.73	5.39	5.92	6.11	6.25
2.69	5.28	5.83	5.99	6.12
mean	5.32	5.86	6.03	6.18
40 mM SDS				
2.69	5.54	5.93	6.12	6.12
2.62	5.35	5.79	5.95	5.95
2.65	5.43	5.86	6.05	6.05
mean	5.44	5.86	6.04	6.04

Table 4.6 Capacity factors obtained during SDS concentration optimization

	k'			
SDS (mM)	Nodularin	MC YR	MC LR	MC RR
0	0	0.19	0.19	0.22
8	0.99	1.33	1.41	1.71
10	1.23	1.57	1.66	1.92
20	1.63	1.88	1.97	2.08
30	1.96	2.16	2.23	2.28
40	2.06	2.21	2.28	2.45

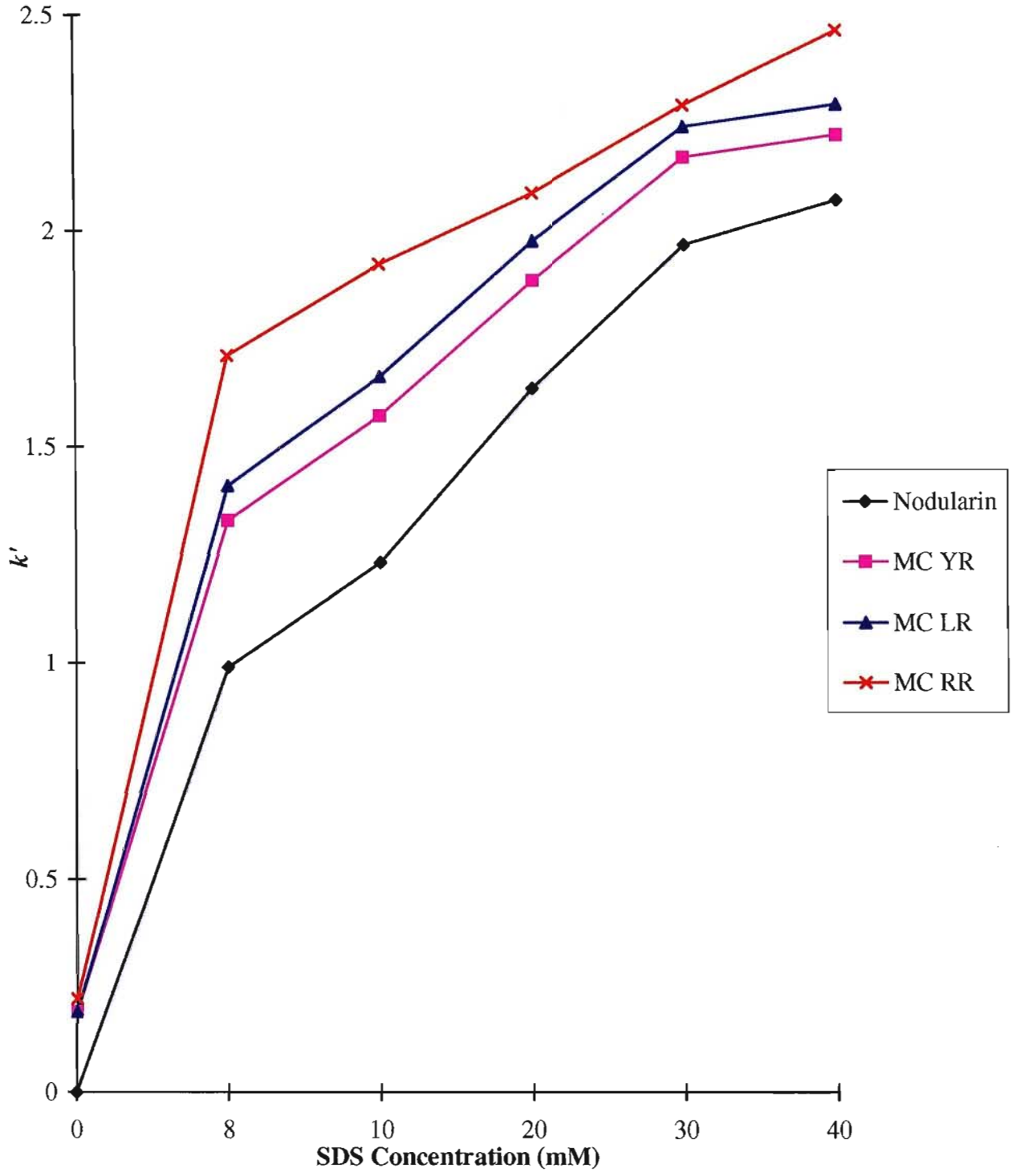

Figure 4.6 Variation of capacity factor as a function of SDS concentration.

where t_r is the solute retention time, t_o is the retention time of a neutral marker that does not interact with the micelle (formamide or methanol) and t_{mc} the retention time of a solute that is completely solubilized in the micelle (Sudan III) [94]. A graphical representation of k' variation with SDS concentration (Figure 4.6) illustrates that the best resolution lies in the range 8 to 10 mM. At a level below 8 mM, micelle formation did not occur as the critical micelle concentration for SDS is 8 mM. At concentrations greater than 10 mM SDS in the run buffer resulted in an increase in the toxin solubility in the micellar phase and produced a deterioration in resolution and increased k' values.

4.4 The Buffer Electrolyte System

Migration and resolution in CE are governed by the applied voltage, electrophoretic mobility of the analyte and the electroosmotic flow. In addition to this, the electrophoresis buffer is also very important because its composition determines the migration behavior of the analyte species and the magnitude of EOF. Two of the most commonly used buffer systems were considered for use. The phosphate buffer had an effective pH range in the region 1.1 to 3.1 and 6.2 to 8.2. As the analytes are amphoteric, a low pH buffer (pH < pI) would produce a net positive charge on the molecule. This is undesirable for two reasons. Firstly positively charged peptides are more susceptible to wall adsorption causing band spreading and secondly a net negative charge is a prerequisite for the purposes of field amplification as will be demonstrated in Chapter 5. Both the phosphate buffer (Figure 4.7), and borate buffers (pH 8.1 to 10.1) produced a separation of the four components, however, as will be shown in the remaining part of this chapter, borax was selected as the run buffer because it exhibited good selectivity, relatively low conductivity, short analysis time resulting from the high pH (Figure 4.12), and had an effective range where the toxins were negatively charged.

The following expression has been given for the dependence of electrophoretic mobility on concentration

$$\mu_{ep} \cong \frac{e}{3 \times 10^7 \times |Z| \eta \sqrt{c}} \qquad 4.2$$

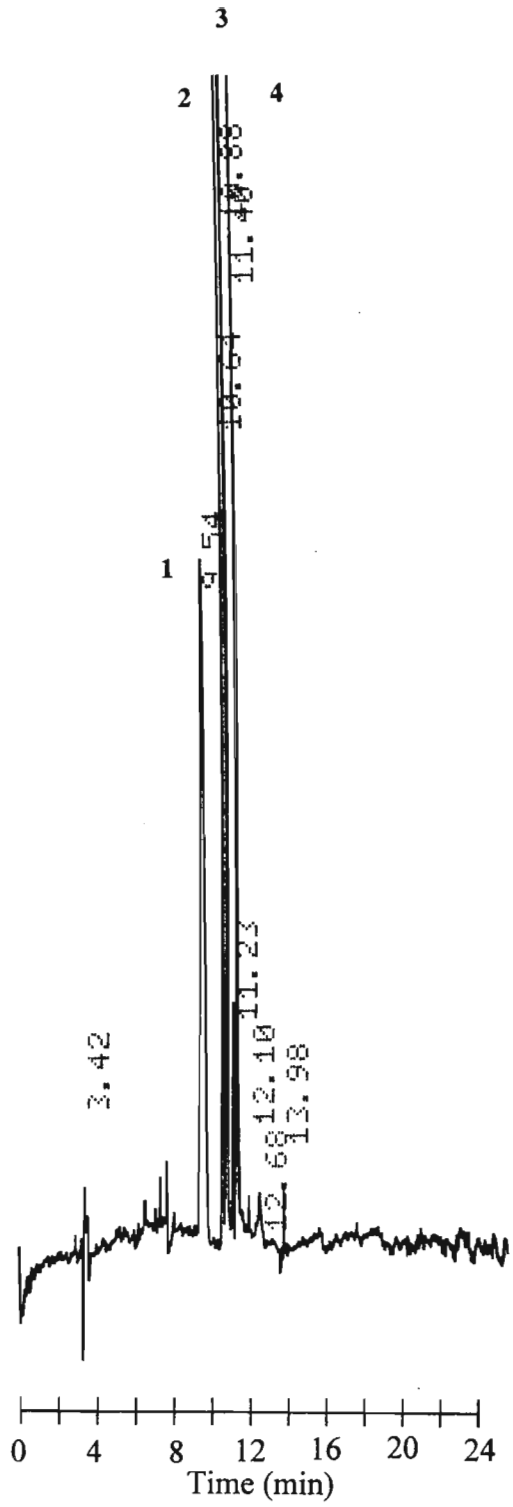

Figure 4.7 Electropherogram of four algal toxins toxins using MECC and UV detection at 238 nm. Operating conditions: 10 mM Na_2HPO_4; 10 mM NaH_2PO_4; 10 mM SDS; pH 7.97; 30 kV applied voltage; 10 s hydrodynamic injection; L_T 70 cm; L_{EFF} 40 cm. Peak identification: 1 Nodularin; 2 MC YR; 3 MC LR; 4 MC RR.

where μ_{ep} is the electrophoretic mobility, e the excess charge in solution per unit area, Z the effective charge on the ion, η the solution viscosity and c the concentration of the solution [307]. Equation 4.2 predicts changes in electrophoretic mobilities with the inverse of the square root of concentration. This relationship is based on the assumption that zeta potential is directly proportional to the thickness of the double layer. An added advantage of high concentration buffers is that the counter ions compete for active sites on the capillary surface thereby reducing analyte wall adsorption. This was demonstrated by Green and Jorgenson for the analysis of proteins [308]. Buffer concentration was therefore used as a tool for resolution optimization. Data for retention time changes as a function of borax concentration is presented in Table 4.7. The corresponding capacity factors were calculated (Table 4.8) and illustrated graphically in Figure 4.8.

The general trend observed was an increase in k' with buffer concentration. This is depicted by the increase in the separation of the k' values of each toxin. The relationship is non linear with the best resolution between components occurring at 40 mM borax. Further improvement in resolution is predicted at higher concentrations, however, Joule heating becomes the limiting factor especially when natural convection is used for heat dissipation. High ionic strength buffers produce good peak efficiency and symmetry because there is effective suppression of electrophoretic dispersion. The drawbacks include high conductivities, high temperatures, Joule heating and viscosity changes that result in poor retention time reproducibility. This necessitates the use of lower operating voltages and consequently, a relatively long analysis time may be required. A 30 mM borax buffer was selected as the optimum practical buffer concentration as higher values were associated with the generation of high currents resulting in excessive Joule heating.

4.5 The Determination of Electrophoretic Mobility

The electrophoretic mobility, μ_{ep}, is defined as the steady state velocity per unit field strength given by

$$\mu_{ep} = \frac{v_{ep}}{E} = \frac{v_{ep} L_T}{V} \qquad 4.3$$

Table 4.7 Retention time data obtained for buffer ionic strength optimization

10 mM Borax				
	t_r-t_o (min)			
t_o (min)	Nodularin	MC YR	MC LR	MC RR
2.33	1.5	2.13	2.24	3.14
2.36	1.29	1.84	1.94	2.76
2.46	1.04	1.58	1.69	2.51
mean	1.28	1.85	1.96	2.8
20 mM Borax				
2.23	2.3	3.01	3.18	3.92
2.38	2.3	3	3.17	3.85
2.33	2.3	3.01	3.18	3.89
mean	2.3	3.01	3.18	3.89
30 mM Borax				
2.77	2.3	3.12	3.38	4.14
2.44	2.59	3.39	3.64	4.4
2.42	2.59	3.38	3.63	4.39
mean	2.49	3.3	3.55	4.31
40 mM Borax				
2.3	2.55	3.3	3.59	4.4
2.4	2.48	3.3	3.62	4.44
2.35	2.54	3.38	3.72	4.54
mean	2.52	3.33	3.64	4.46

Table 4.8 Capacity factors obtained during buffer ionic strength optimization

	k'			
Borax (mM)	**Nodularin**	**MC YR**	**MC LR**	**MC RR**
10	0.54	0.78	0.82	1.17
20	0.99	1.3	1.37	1.68
30	0.97	1.3	1.4	1.69
40	1.07	1.42	1.55	1.9

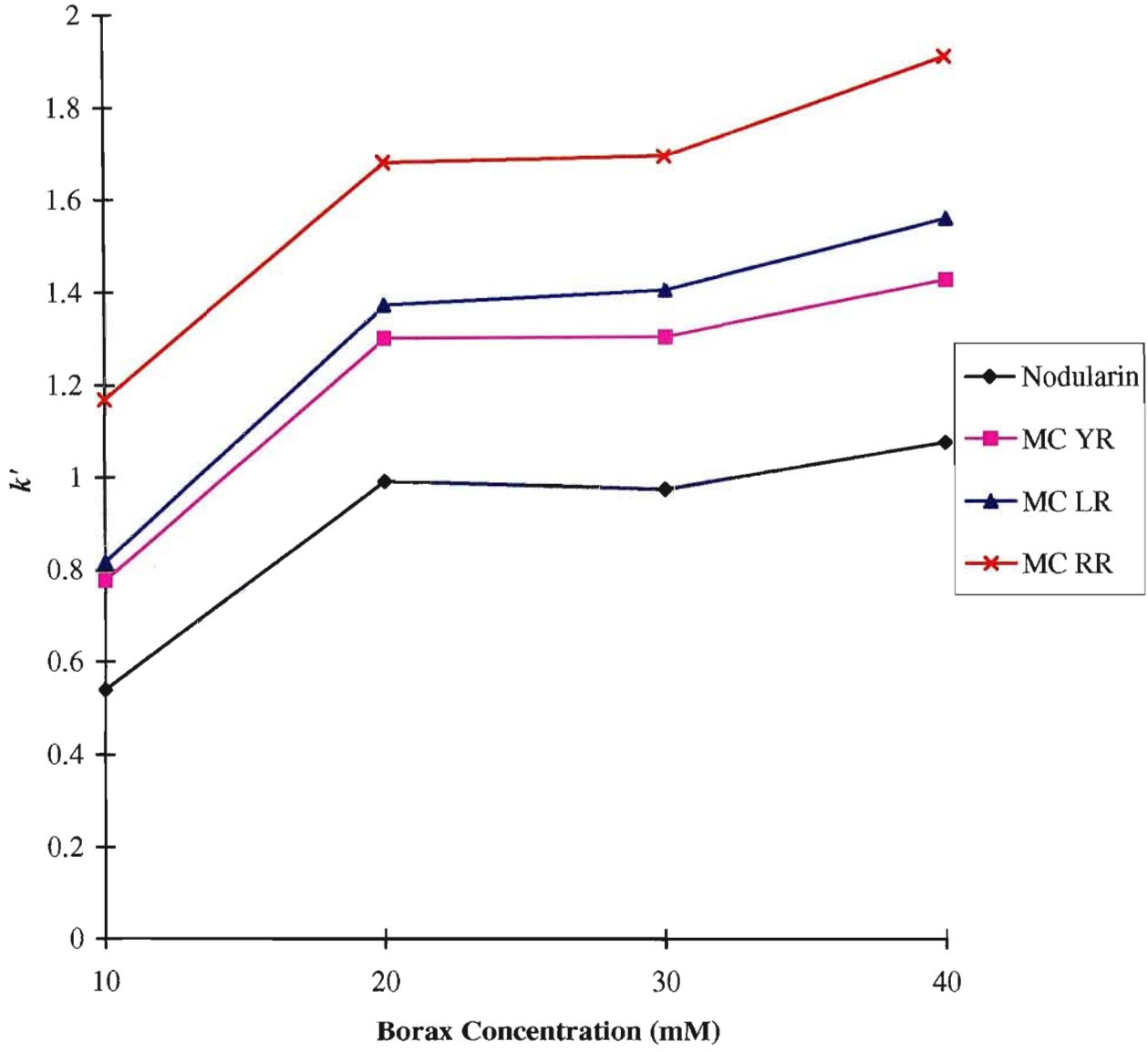

Figure 4.8 Variation in capacity factor as a function of buffer ionic strength.

where v_{ep} is the electrophoretic velocity, E the field strength, L_T the total column length and V the applied voltage. Although the determination of μ_{ep} using equations is extremely difficult, it can be easily calculated from an electropherogram. The electrophoretic velocity is first calculated using

$$v_{ep} = v_{net} - v_{eo} = \frac{L_{EFF}}{t_r} - \frac{L_{EFF}}{t_o} \qquad 4.4$$

where L_{EFF} is the column length from the injector to the detector, v_{net} the net electrophoretic velocity and v_{eo} the electroosmotic velocity. Table 4.9 shows data to be used for v_{ep} and μ_{ep} calculations. The negative sign indicates the relative direction of the electrophoretic and electroosmotic velocities. In practice, however, the negative sign is neglected. Substituting for v_{ep} in equation 4.3 gives μ_{ep}. The electrophoretic mobility of each toxin was determined and is presented in Table 4.11. It can be seen that μ_{ep} is essentially invariant over the buffer concentration range investigated and this value is a characteristic constant for each toxin (Figure 4.9). This is a very useful parameter and can be used for the verification of solute identity.

4.6 pH Optimization

The degree of ionization of the species present in the electrolyte system depends on the pH of the solution. Differences in the degree of ionization give rise to differences in μ_{ep} and μ_{eo}. Consequently, both the separation efficiency and flow velocities may be affected by the buffer pH and it is therefore considered as the most important separation parameter for changing the selectivity of the system.

4.6.1 The Borax/Sodium Hydroxide System (pH 9.18 - 10.1)

Boric acid and borax are functionally similar when titrated with sodium hydroxide.

$$Na_2B_4O_7 + 7H_2O \rightleftharpoons 2NaB(OH)_4 + 2H_3BO_3 \rightleftharpoons 2NaOH + 4H_3BO_3 \qquad 4.5$$

Table 4.9 Retention time changes with increasing buffer concentration

	10 mM Borax, t_o 143 s			
	Nodularin	**MC YR**	**MC LR**	**MC RR**
t_r (s)	219.8	254	260.6	311
	20 mM Borax, t_o 138.8 s			
t_r (s)	276.8	319.4	329.6	372.2
	30 mM Borax, t_o 152.6 s			
t_r (s)	302	350.6	365.6	411.2
	40 mM Borax, t_o 141 s			
t_r (s)	292.2	340.8	359.4	408.6

Table 4.10 Changes in electrophoretic velocity with buffer concentration

	v_{ep} (cm s^{-1})			
Borax (mM)	**Nodularin**	**MC YR**	**MC LR**	**MC RR**
10	-0.1	-0.12	-0.13	-0.15
20	-0.14	-0.16	-0.17	-0.18
30	-0.13	-0.15	-0.15	-0.16
40	-0.15	-0.17	-0.17	-0.18

Table 4.11 Electrophoretic mobility changes with buffer concentration

	μ_{ep} ($cm^2 V^{-1} s^{-1}$)			
Borax (mM)	**Nodularin**	**MC YR**	**MC LR**	**MC RR**
20	3.27×10^{-4}	3.73×10^{-4}	3.90×10^{-4}	4.22×10^{-4}
30	3.03×10^{-4}	3.46×10^{-4}	3.57×10^{-4}	3.85×10^{-4}
40	3.43×10^{-4}	3.87×10^{-4}	4.02×10^{-4}	4.34×10^{-4}
Mean	3.24×10^{-4}	3.69×10^{-4}	3.83×10^{-4}	4.14×10^{-4}

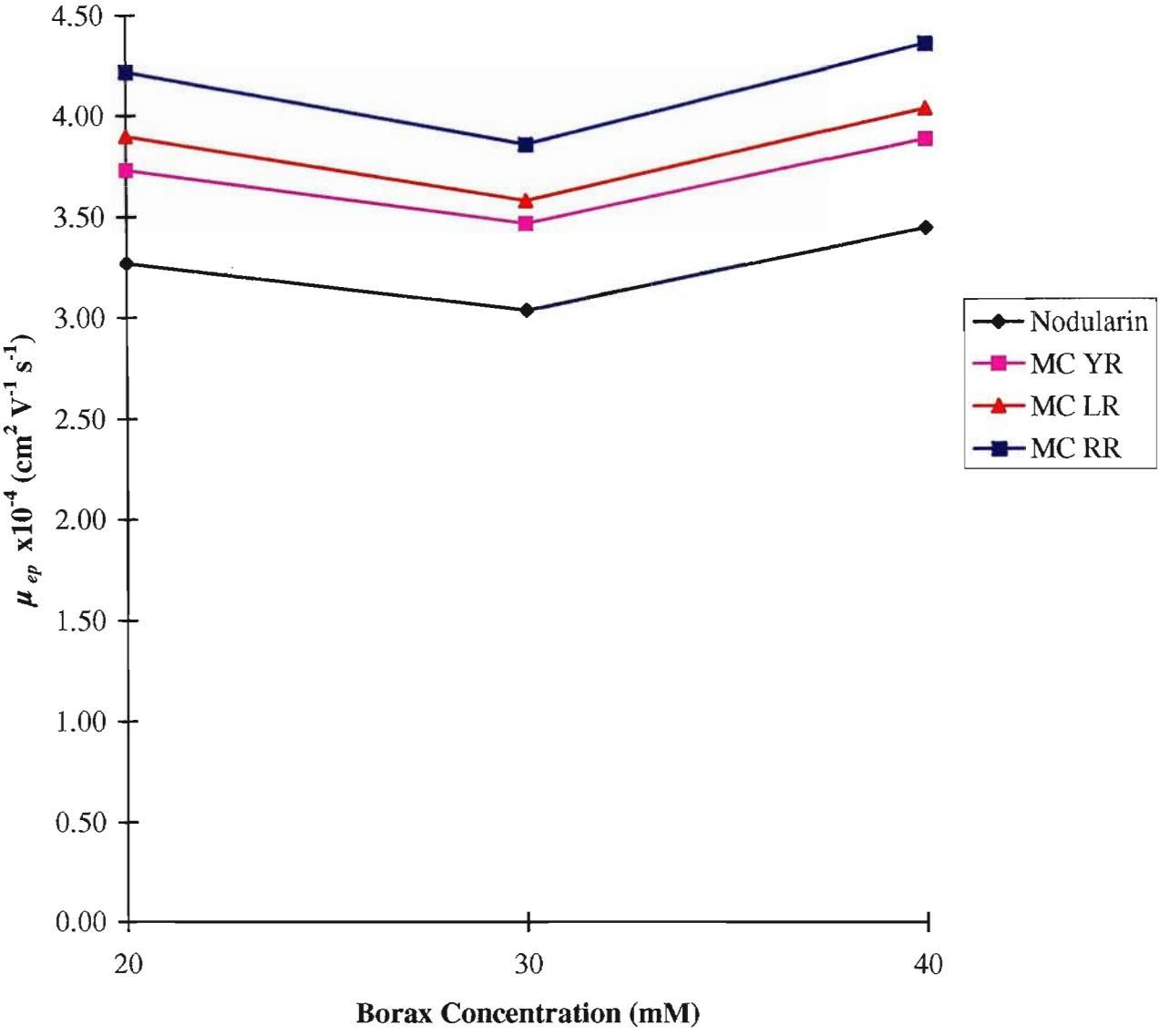

Figure 4.9 Electrophoretic behaviour as a function of buffer concentration.

Expressing the borax/sodium hydroxide system in terms of boric acid, the equilibrium reaction becomes

$$H_3BO_3 + NaOH \rightleftharpoons Na^+ + B(OH)_4^- \qquad 4.6$$

From this equation, it can be seen that an increase in pH is accompanied by an increase in the ionic strength. Unfortunately these effects (pH and ionic strength) can complicate resolution optimization by being co-operative in some cases and counteractive in others [15]. Table 4.12 contains retention time data as a function of pH. The corresponding k' values appear in Table 4.13 and a graphical representation is shown in Figure 4.10. This graph illustrates fairly constant k' values in the pH region 9.18 to 10.1. These results can be attributed to the fact that the surface silanol groups on the fused silica capillary are almost fully ionized, resulting in the production of a constant electroosmotic flow. Studies have shown that EOF changes are most significant in the pH range 3 to 8 (Figure 2.8). In addition to this, another contributing factor is that the electrophoretic mobility of the solutes in this pH region is constant, indicating that no further ionization of the toxins occurs.

4.6.2 The Borax HCl system (pH 8.07-9.18)

This system can be represented by the equilibrium reaction

$$2Na^+ + 2B(OH)_4^- + HCl \rightleftharpoons 2Na^+ + B(OH)_4^- + Cl^- + H_3BO_3 \qquad 4.7$$

During pH adjustment with HCl, the ionic strength remains constant and only the pH effect is noted [309]. A pH reduction protonates the charged SiO^- sites on the fused silica surface causing a reduction in the surface charge density, zeta potential and electroosmotic flow. This impacts on the net electrophoretic velocity and results in an increase in k'. Data plotted in Figure 4.10 correlate well with the predicted trend. The absence of sharp changes in k' indicates that the net charge on the toxins is unaffected by pH adjustment.

Table 4.12 Retention time data obtained for buffer pH optimization

pH 8.07				
	t_r-t_o (min)			
t_o (min)	Nodularin	MC YR	MC LR	MC RR
2.64	3.49	4.23	5.21	5.72
2.59	3.77	5.16	5.61	6.89
2.62	3.63	5.61	5.41	6.31
mean	3.63	5	5.41	6.31
pH 8.2				
2.68	3.61	5.06	5.44	6.94
2.68	3.87	5.41	5.84	7.38
2.6	3.66	5.04	5.43	7.01
mean	3.72	5.19	5.6	7.13
pH=8.57				
2.5	2.99	3.99	4.25	5.31
2.47	3.41	4.58	4.92	5.95
2.56	3.67	4.89	5.23	6.15
mean	3.56	4.49	4.8	5.8
pH 8.9				
2.5	3.05	4.03	4.31	5.2
2.36	3.01	3.99	4.28	5.2
2.53	3.09	4.15	4.44	5.41
mean	3.05	4.06	4.34	5.27
pH 9.18				
2.58	3.03	3.97	4.21	5.03
2.61	2.96	3.89	4.13	4.94
2.46	3.02	3.95	4.2	5
mean	3	3.94	4.18	4.99
pH 9.5				
2.48	3	3.97	4.24	5.07
2.48	3	3.94	4.19	4.98
2.33	3.17	4.11	4.35	5.13
mean	3.06	4.01	4.26	5.06
pH 9.7				
2.58	3.22	4.15	4.48	5.25
2.55	3.18	4.16	4.51	5.3
2.57	3.22	4.2	4.55	5.3
mean	3.21	4.17	4.51	5.28
pH 9.93				
2.44	2.87	3.71	4.13	4.91
2.53	2.98	3.91	4.36	5.28
2.39	2.9	3.74	4.18	5.07
mean	2.92	3.79	4.22	5.09

Table 4.12 Continued

	pH 10.1			
t_o (min)	Nodularin	MC YR	MC LR	MC RR
2.51	3.22	4.17	4.66	5.52
2.47	2.76	3.68	4.17	5.09
2.39	2.59	3.45	3.9	4.8
mean	2.86	3.77	4.24	5.14

Table 4.13 Variation of capacity factor as a function of pH

	k'			
pH	Nodularin	MC YR	MC LR	MC RR
8.07	1.39	1.8	2.07	2.41
8.2	1.4	1.95	2.1	2.68
8.57	1.46	1.84	1.97	2.38
8.9	1.24	1.65	1.76	2.14
9.18	1.18	1.54	1.64	1.96
9.5	1.26	1.65	1.75	2.08
9.7	1.25	1.62	1.76	2.06
9.93	1.19	1.54	1.72	2.07
10.1	1.16	1.53	1.73	2.09

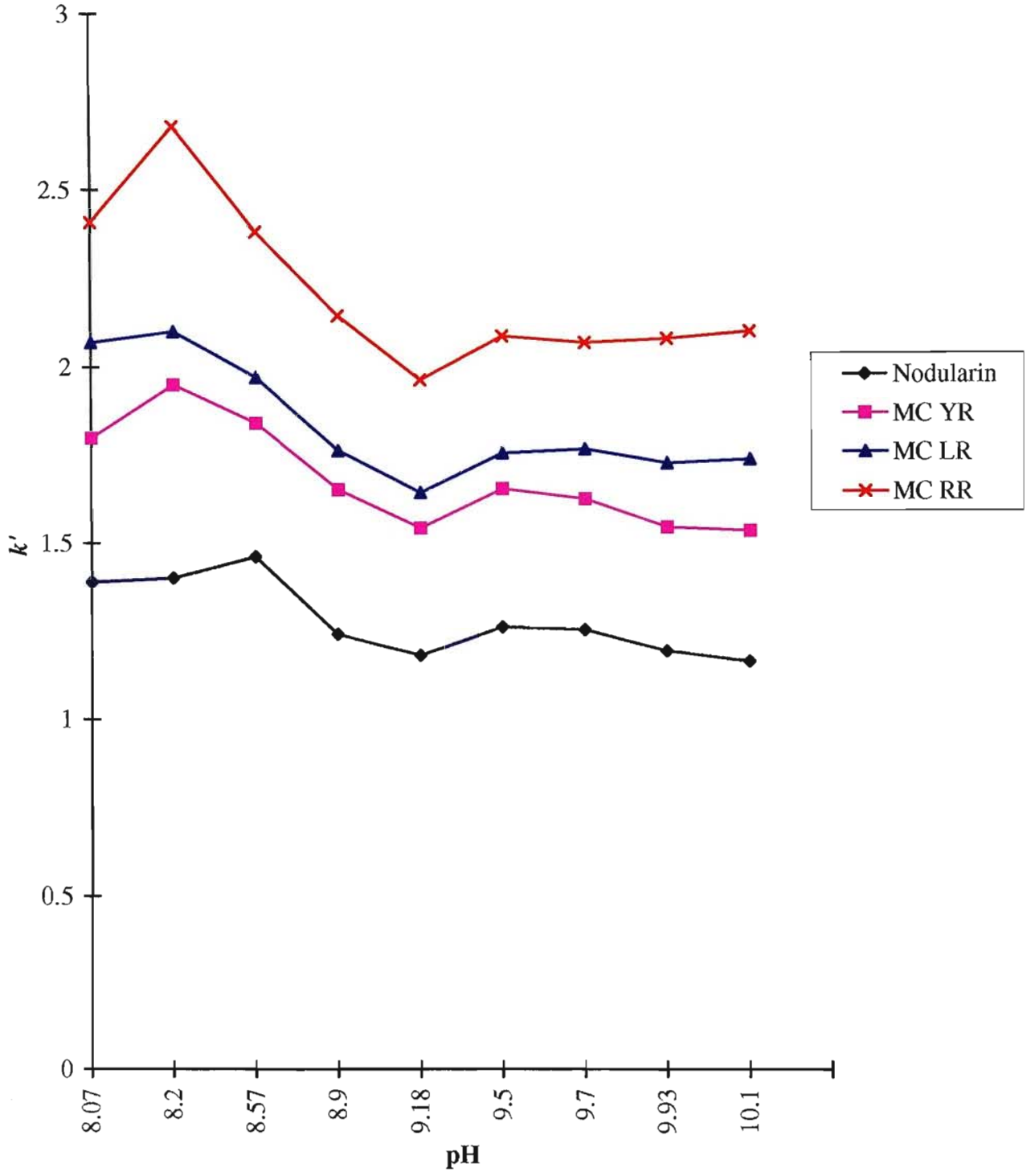

Figure 4.10 Variation in capacity factor as a function of buffer pH.

Combining the Borax/NaOH and Borax/HCl systems, good results were obtained at both pH extremes. However, at high pH, the ionic strength was increased, producing a high conductivity that resulted in excessive Joule heating. This enforced the use of lower operating voltages at the expense of peak efficiency and analysis time. Although the Borax/HCl system has a constant ionic strength, high electrophoresis currents are produced by the presence of the high mobility chloride ions. Once again the heat dissipation capacity of the capillary column became a limiting factor. Choosing the best operating conditions was complicated by the generation of high currents and excessive Joule heating. A compromise was reached between current, resolution, efficiency and analysis time. Since the net charge on the toxins remained the same in the buffer pH range, pH adjustment was deemed redundant.

4.7 Ohm's Law Plot

From equation 1.1, efficiency is directly proportional to the applied voltage. This theory is based on the assumption that higher applied voltages reduce elution times and thus reduce the time available for bands to broaden by diffusion. In addition to good peak shapes, the use of high operating voltages produces a significant reduction in analysis time. However, the limitation of high voltages are Joule heating, thermal degradation possibilities, micro air bubble formation and electrophoresis current disruptions caused by boiling of the solvent. Joule heating is responsible for an increase in the height equivalent to a theoretical plate at high fields due to the existence of a temperature gradient between the center of the capillary and the wall. The maximum applied voltage for the laboratory built CE system was established using firstly, natural convection and then forced air convection as the cooling mechanism (Table 4.14). From the *E-I* plot (Figure 4.11), it can be seen that better linearity and lower currents were achieved with forced air convection, making it the preferred method. Forced air convection permitted the used of higher operating voltages. With natural convection, curvature occurs in the region of 25 kV. This is due to the decrease in the column resistance with an increase in the electric field. The electrolyte continues to increase in temperature as the resistance decreases until the circuit is broken by

Table 4.14 Data obtained for Ohm's Law plot

	Current (μA)	
Voltage (kV)	Forced Air Convection	Natural Convection
13	2	3
14	4	5
15	7	8
16	9	11
17	11	13
18	14	16
19	16	19
20	19	22
21	22	26
22	25	30
23	28	35
24	32	40
25	36	45
25.5	38	48
26	39	51
26.5	42	54
27	44	57
27.5	46	61
28	48	63
28.5	51	68
29	54	74
29.5	56	78
30	59	81

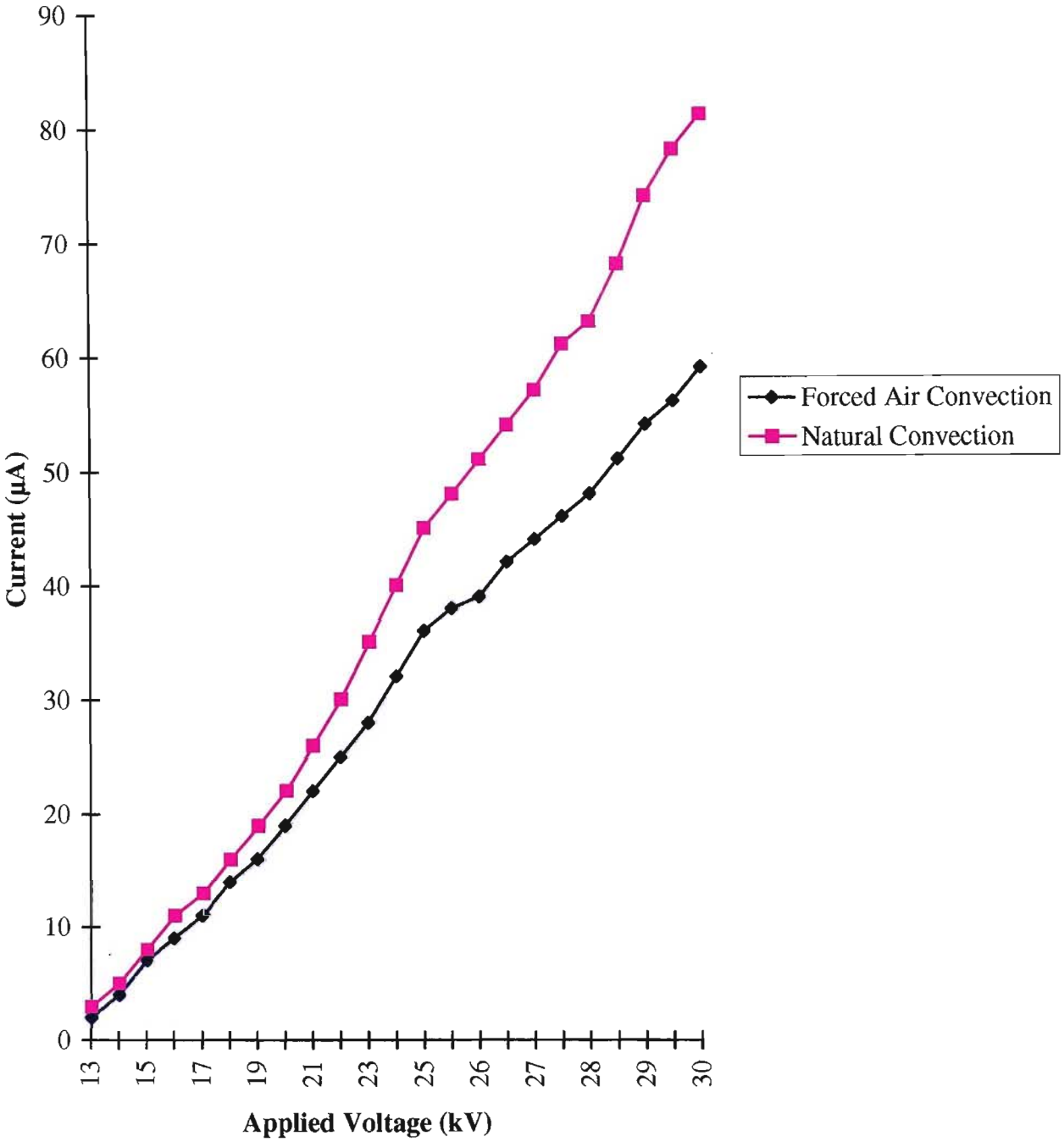

Figure 4.11 Ohm's law plots obtained with natural and forced air convection.

air bubble formation. The final operating voltage (30 kV) produced baseline resolution, high efficiency peaks, and short analysis time (Figure 4.12).

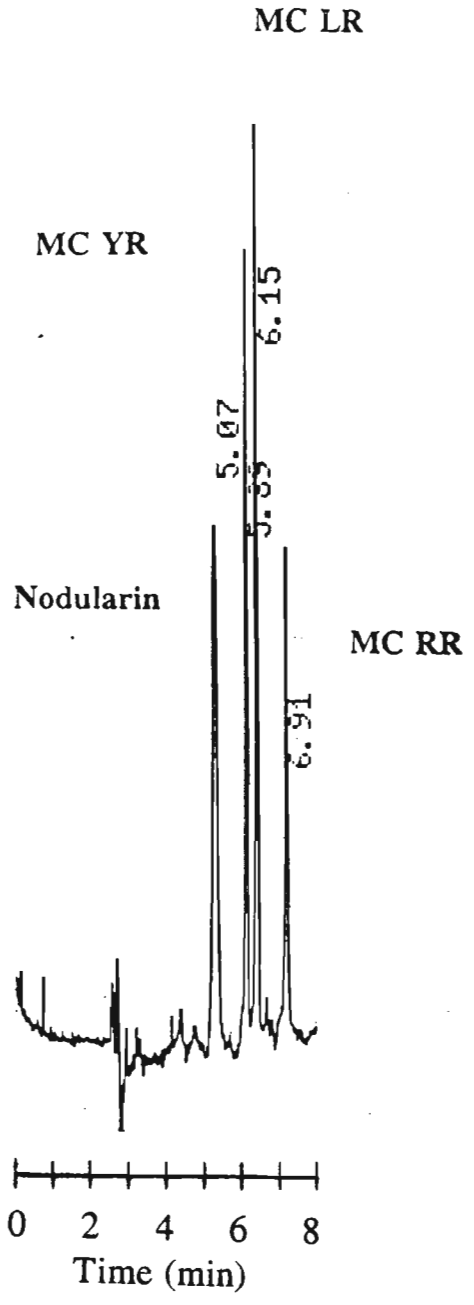

Figure 4.12 Electropherogram of four algal toxins using MECC and UV detection at 238 nm. Operating conditions: 30 mM borax; 9 mM SDS; pH 9.18; 30 kV applied voltage; 10 s hydrodynamic injection; L_T 70 cm; L_{EFF} 40 cm.

4.8 Precision

Comparison of peaks based on their retention times requires highly constant experimental conditions. Small changes in operational parameters such as temperature, buffer pH, buffer ionic strength and capillary pretreatment, alter the mobility of the analyte which may lead to misidentification of peaks. The following precautions were observed during reproducibility studies.

- The buffer ionic strength was kept constant by using fresh buffer between injections.
- Temperature was maintained constant by operating at constant current of 55 μA. As the laboratory built CE system did not have an automatic feature to operate in this mode, the voltage knob was physically adjusted during the course of a run. This unfortunately was not practical for the entire exercise.
- The column was rinsed with 0.1 M NaOH, water, and then buffer solution between injections.

Statistical treatment of retention time data (Table 4.15 and Table 4.16), indicate standard deviations ranging from 0.018 for nodularin to 0.054 for MC RR with the use of electrokinetic injections. Standard deviation values for relative migration time were not significantly different, however a slight improvement in precision was noted. The good reproducibility for both cases suggests that stable and reproducible experimental conditions were achieved producing a constant electroosmotic flow. A similar trend was observed for hydrodynamic injections. The standard deviation ranged from 0.069 for nodularin to 0.148 for MC RR. As expected, the migration time showed better precision by compensating for any changes in the electroosmotic flow. Comparing the two injection techniques, it is clear that electrokinetic injections produce far superior precision. In addition to a constant electroosmotic flow, electrokinetic injections could be executed with more control and more reproducibility than hydrodynamic injections. The retention times of both methods, however indicate good precision of the method.

Table 4.15 Retention time precision data for electrokinetic injections

		Retention Time (min)			
Replicate		**Nodularin**	**MC YR**	**MC LR**	**MC RR**
1	t_r	4.15	4.68	4.79	5.25
	t_r-t_o	1.32	1.85	1.96	2.42
2	t_r	4.17	4.72	4.83	5.33
	t_r-t_o	1.34	1.89	2.00	2.50
	t_r-t_o	1.38	1.95	2.07	2.57
4	t_r	4.17	4.72	4.85	5.35
	t_r-t_o	1.35	1.90	2.03	2.53
	t_r-t_o	1.35	1.92	2.04	2.56
6	t_r	4.16	4.70	4.82	5.32
	t_r-t_o	1.35	1.89	2.01	2.51
7	t_r	4.2	4.78	4.9	5.45
	t_r-t_o	1.38	1.96	2.08	2.63
8	t_r	4.17	4.72	4.84	5.34
	t_r-t_o	1.36	1.91	2.03	2.53
9	t_r	4.19	4.75	4.86	5.36
	t_r-t_o	1.36	1.92	2.04	2.54
10	t_r	4.18	4.74	4.86	5.38
	t_r-t_o	1.36	1.92	2.04	2.54
Mean t_r ±STDEV		4.18±0.018	4.74±0.033	4.85±0.035	5.36±0.054
Mean (t_r-t_o)±STDEV		1.36±0.017	1.91±0.032	2.03±0.034	2.53±0.054

Table 4.16 Retention time precision data for hydrodynamic injections

		Retention Time (min)			
Replicate		**Nodularin**	**MC YR**	**MC LR**	**MC RR**
1	t_r	5.53	6.65	6.86	7.91
	t_r-t_o	2.23	3.35	3.56	4.61
2	t_r	5.55	6.78	6.99	8.09
	t_r-t_o	2.25	3.48	3.69	4.79
3	t_r	5.6	6.75	6.96	8.04
	t_r-t_o	2.3	3.45	3.66	4.74
4	t_r	5.45	6.57	6.77	7.76
	t_r-t_o	2.21		3.53	4.52
5	t_r	5.43	6.54	6.73	7.61
	t_r-t_o	2.18	3.29	3.48	4.36
6	t_r	5.52	6.66	6.87	7.93
	t_r-t_o	2.27	3.41	3.62	4.68
7	t_r	5.57	6.73	6.93	8.02
	t_r-t_o	2.28	3.44	3.63	4.73
8	t_r	5.41	6.55	6.74	7.8
	t_r-t_o	2.2	3.34	3.53	4.59
9	t_r	5.41	6.54	6.74	7.78
	t_r-t_o	2.2	3.33	3.53	4.57
10	t_r	5.53	6.67	6.88	7.91
	t_r-t_o	2.26	3.4	3.61	4.64
Mean±STDEV		5.5±0.069	6.64±0.091	6.85±0.097	7.88±0.148
Mean (t_r-t_o)±STDEV		2.24±0.04	3.38±0.063	3.58±0.068	4.62±0.125

4.9 Application

The electropherogram of the algal scum extract (Figure 4.13A) illustrates the power of CE as an analytical technique. Extremely high peak capacity and efficiency can be noted. By comparison of their capacity factors with those of reference standards under identical conditions (Figure 4.13B), the presence of MC YR (t_r = 4.48 minutes) and MC LR (t_r = 4.68 minutes) was inferred. As diode array UV detection was unavailable on the home-built system, verification was accomplished by analyzing the extract using an established reversed phase HPLC method with photo diode array UV detection [62]. This method is currently being used routinely at Umgeni Water laboratories. A peak was noted at 16.295 minutes corresponding to that of MC LR (Figure 4.14). MC LR was positively identified on the basis of its UV spectrum (Figure 4.15). From the electropherogram, t_o was taken as 1.96 minutes, t_r as 4.68 minutes, L_{EFF} as 40 cm and L_T as 57 cm and substituting for these values in equation 3.3 and equation 3.4, the electrophoretic mobility was found to be 3.76 x 10^{-4} $cm^2\ V^{-1}\ s^{-1}$. This value lies close to the average value for μ_{ep} obtained from Table 4.11, which is further evidence of the presence of MC LR.

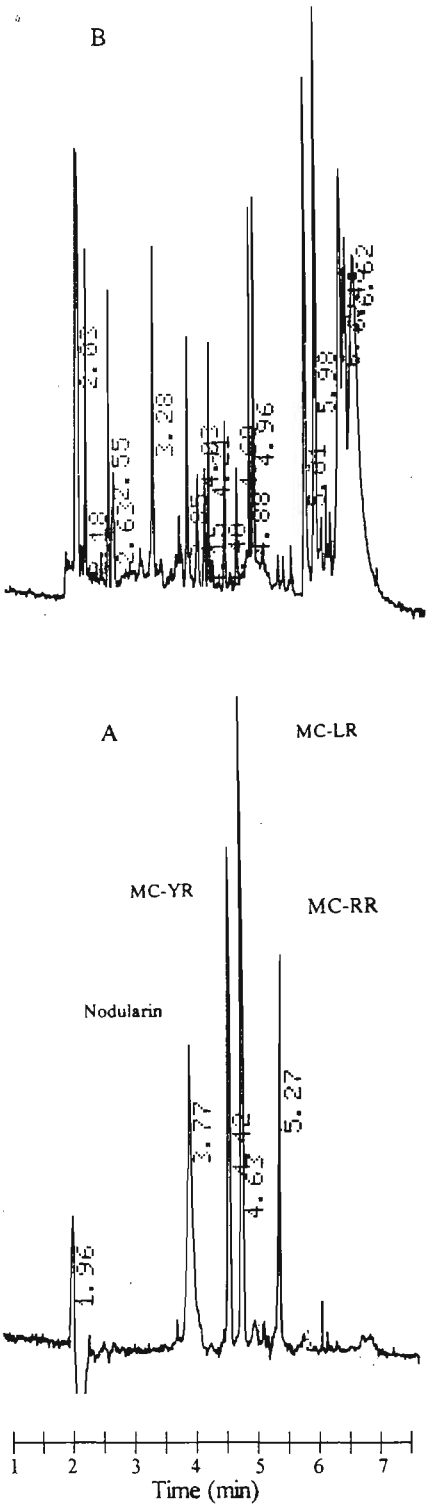

Figure 4.13 (A) Electropherogram of a typical reference standard of the four algal toxins under study and (B) Electropherogram of a supercritical fluid extract of a freeze-thawed algal scum sample obtained from kwaMakutha sewage treatment plant in Umlazi, kwaZulu Natal. Optimized conditions as in Figure 4.12 were used.

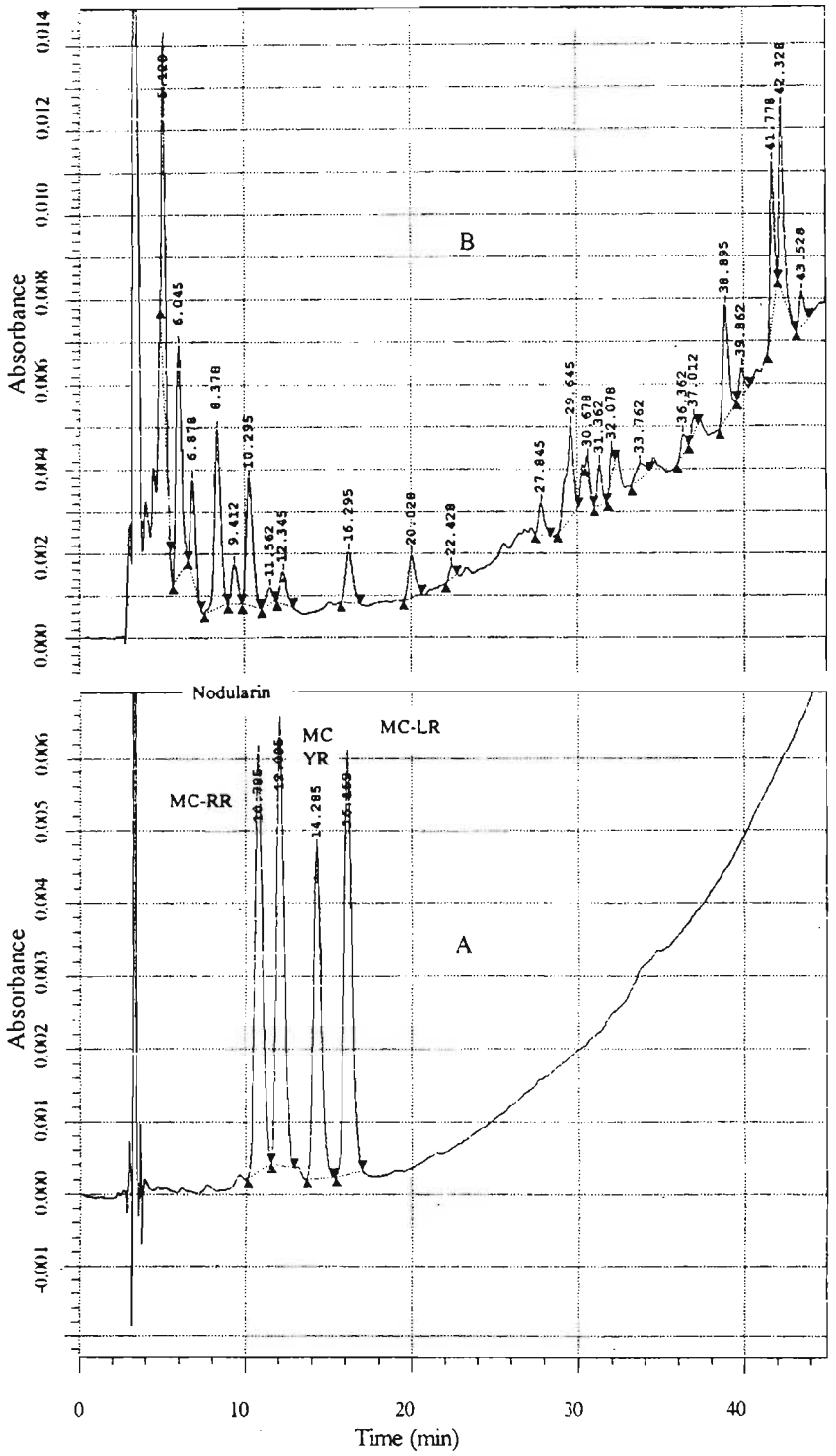

Figure 4.14 (A) Reversed phase HPLC chromatogram of a standard solution containing the four algal toxins and (B) HPLC chromatogram of the sample run under identical conditions. A 10 μL injection was used together with a linear gradient according to Table 3.3.

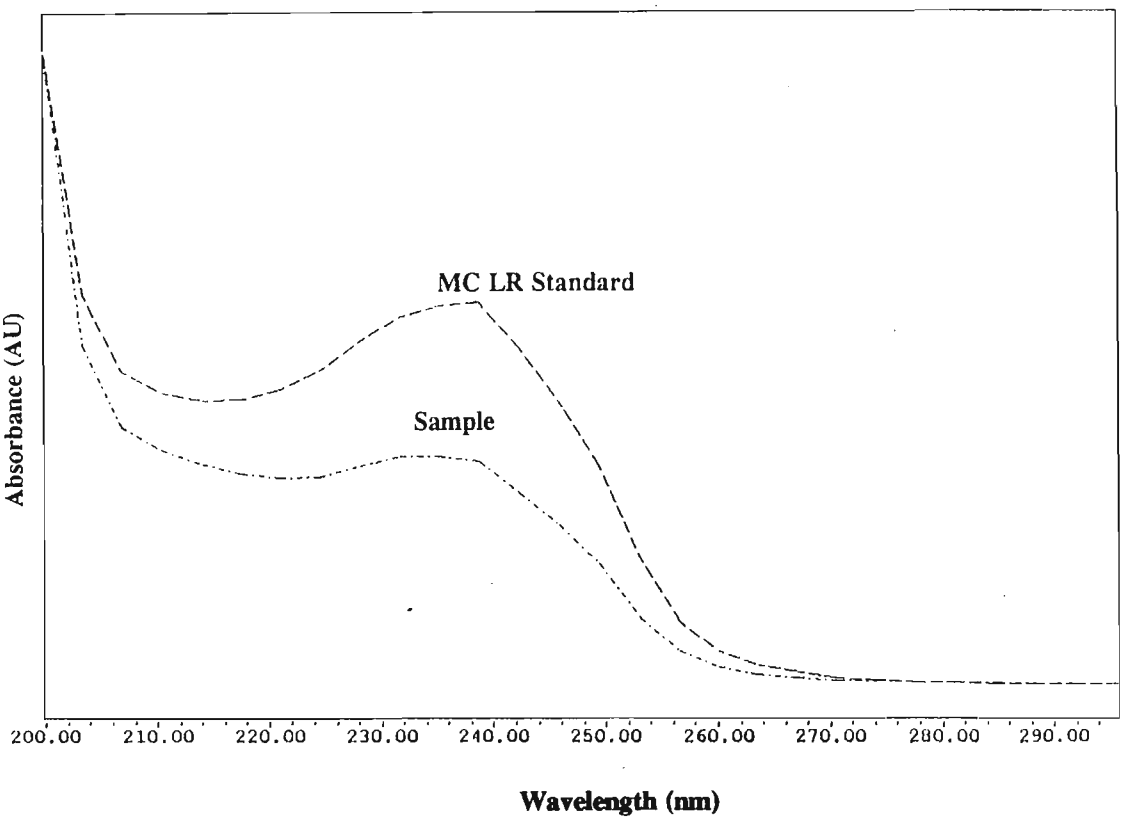

Figure 4.15 UV spectrum of MC LR superimposed on the UV spectrum of the unknown peak in the scum extract. Operating conditions were identical to that in Figure 4.14.

4.10 Conclusions

In contrast to capillary zone electrophoresis, micellar electrokinetic capillary chromatography can be used to separate the four fresh water algal toxins using a borax buffer system. The technique displays enormous efficiency, short analysis times, high peak capacity and coupled with simple instrumentation (no injector, pumps, mixers, or special detection cell), MECC is an attractive alternative or a complimentary technique to HPLC for the analysis of algal toxins. The optimum SDS concentration was chosen as 9 mM (Figure 4.6) while the optimum practical buffer concentration was chosen to be 30 mM borax. An operating voltage of 30 kV could be applied with forced air convection and the borax buffer system at pH 9.18. However, the major limitation of this technique is that

only small sample volumes can be loaded onto the capillary without deterioration of separation efficiency and loss of component resolution. The concentration sensitivity in the case of UV absorbance detection in conventional CE is in general approximately two orders of magnitude less than in HPLC. However this method was found to be suitable for the analysis of algal cell extracts containing high levels of toxins. These high levels were artificially derived by extracting a large mass of the algal scum. The presence of MC LR was verified by the use of HPLC and the UV spectrum. Based on calculated values, the electrophoretic mobility compared favourably with that of MC LR and the identity can be reported with a high degree of confidence.

Chapter Five

Improving Detection Sensitivity in MECC of Algal toxins

5.1 Introduction

The main limitation of CE arises as a direct consequence of the low sample capacity to be detected. Further, the optical path length is defined by the internal diameter of the capillary adding to poor detection sensitivity. Approaches to help address this problem can be divided into four categories, namely the use of alternative capillary geometries, alternative injection modes, sample concentration strategies or alternative detection modes.

According to Beer's law, the optical absorbance of a sample is directly proportional to the optical path-length through which the absorbance measurement is performed. Therefore, extension of the optical path-length should lead to increases in the detection sensitivity. However, simply increasing the inner diameter of the capillary is not always an attractive alternative because increased Joule heating can result with a corresponding loss of component resolution from increased peak widths. Methods based on increasing the optical path length include the use of axial beam illumination [310,311], the Z-shaped flow cell [312], the multi reflection cell [127], and the bubble cell [313]. However these methods only improve the sensitivity by two or three times. Recently Hewlett Packard introduced the high sensitivity cell for use with the HP ^{3D}CE system [335]. The capillary geometry of the HP high sensitivity cell improves detection sensitivity more than 10 fold over standard capillaries. The work described in this chapter focuses on improving the detection sensitivity for algal toxins by using alternative injection techniques, sample concentration strategies, and alternative detection techniques. Attempts at quantitative analysis were also made.

5.2 Sample Injection Techniques

5.2.1 *Hydrodynamic Injection*

This is the most widely used injection mode in which the sample is introduced by creating a pressure differential across the capillary with the use of a vacuum, positive pressure or by gravity. The total length of the injection plug, ℓ_{inj}, is limited by the impact of plug length on peak width. The relationship between plug length and the contribution to peak variance σ^2_{inj} is given by

$$\sigma^2_{inj} = \frac{\ell^2_{inj}}{12} \qquad 5.1$$

Therefore, if ℓ_{inj} becomes too large, σ^2_{inj} can negatively influence separation efficiency, although a sensitivity enhancement will be realised. Using injection time data from Table 5.1 peak efficiencies were calculated using the equation

$$N = 16\left(\frac{t_r}{w_b}\right)^2 \qquad 5.2$$

where N is the number of theoretical plates, t_r the retention time and w_b is the peak width. The average efficiency as a function of injection time appears in Table 5.2. The efficiency variation as a function of injection time illustrated in Figure 5.1 indicates a decrease in N with time. This is in agreement with equation 5.1 that predicts an increase in the peak variance σ^2_{inj} with injection plug length or injection time. Component resolution R was calculated from data in Table 5.1 using the equation

$$R = \frac{2(t_{r2} - t_{r1})}{w_{b1} + w_{b2}} \qquad 5.3$$

and the averages presented in Table 5.3. A corresponding decrease in resolution was noted (Figure 5.2). At injection times lower than 10 s, higher efficiencies were achieved at the expense of a significant amount of sensitivity. Data for efficiency and resolution calculations for injection times lower than 10 s were neglected because of poor precision.

Table 5.1 Efficiency and resolution data for hydrodynamic injections

10 s injection, Replicate 1				
	Nodularin	**MC YR**	**MC LR**	**MC RR**
t_r *(min)*	5.63	6.80	7.01	8.12
W_b	0.25	0.19	0.19	0.23
N	8114	20494	21780	19942
R	5.32	1.11	5.29	
Replicate 2				
t_r *(min)*	5.44	6.57	6.78	7.85
W_b	0.25	0.19	0.19	0.23
N	7576	19131	20374	18638
R	5.14	1.11	5.10	
Replicate 3				
t_r *(min)*	5.42	6.54	6.75	7.77
W_b	0.25	0.18	0.18	0.23
N	7520	21122	22500	18260
R	5.21	1.17	4.98	
Replicate 4				
t_r *(min)*	5.36	6.46	6.66	7.69
W_b	0.22	0.16	0.16	0.22
N	9497	26082	27722	19549
R	5.79	1.25	5.42	
Replicate 5				
t_r *(min)*	5.38	6.49	6.70	7.73
W_b	0.22	0.16	0.16	0.22
N	9568	26325	28056	19753
R	5.84	1.31	5.42	
20 s injection, Replicate 1				
t_r *(min)*	5.53	6.65	6.86	7.91
W_b	0.30	0.20	0.20	0.25
N	5437	17689	18824	16017
R	4.48	1.05	4.67	
Replicate 2				
t_r *(min)*	5.52	6.66	6.86	7.90
W_b	0.32	0.20	0.20	0.26
N	4761	17742	18824	14772
R	4.38	1.00	4.52	
Replicate 3				
t_r *(min)*	5.38	6.47	6.68	7.70
W_b	0.30	0.20	0.20	0.26
N	5146	16744	17849	14033
R	4.36	1.05	4.43	

Table 5.1 Continued

	Nodularin	MC YR	MC LR	MC RR
Replicate 4				
t_r *(min)*	5.50	6.65	6.87	7.94
W_b	0.28	0.20	0.20	0.26
N	6173	17689	18879	14922
R	4.79	1.10	4.65	
Replicate 5				
t_r *(min)*	5.36	6.44	6.64	7.62
W_b	0.28	0.20	0.20	0.26
N	5863	16589	17636	13743
R	4.50	1.00	4.26	
30 s injection, Replicate 1				
t_r *(min)*	5.40	6.51	6.70	7.68
W_b	0.33	0.22	0.22	0.27
N	4284	14010	14840	12945
R	4.04	0.86	4.00	
Replicate 2				
t_r *(min)*	5.42	6.51	6.71	7.72
W_b	0.34	0.23	0.22	0.27
N	4066	12818	14884	13081
R	3.82	0.89	4.12	
Replicate 3				
t_r *(min)*	5.48	6.58	6.77	7.84
W_b	0.34	0.23	0.23	0.27
N	4156	13095	13863	13490
R	3.86	0.83	4.28	
Replicate 4				
t_r *(min)*	5.61	6.89	7.14	8.35
W_b	0.32	0.25	0.24	0.27
N	4918	12153	14161	15303
R	4.49	1.02	4.75	
Replicate 5				
t_r *(min)*	5.37	6.45	6.66	7.73
W_b	0.34	0.24	0.24	0.26
N	3991	11556	12321	14143
R	3.72	0.88	4.28	

Table 5.2 Mean efficiency variation with hydrodynamic injection time

	Mean *N*			
Inj Time (s)	**Nodularin**	**MC YR**	**MC LR**	**MC RR**
10	8455	22631	24086	19229
20	5476	17291	18402	14697
30	4283	12727	14014	13792

Table 5.3 Mean resolution variation with hydrodynamic injection time

	Mean *R*		
Inj Time (s)	**Nod & YR**	**YR &LR**	**LR & RR**
10	5.46	1.19	5.24
20	4.5	1.04	4.51
30	3.99	0.89	4.29

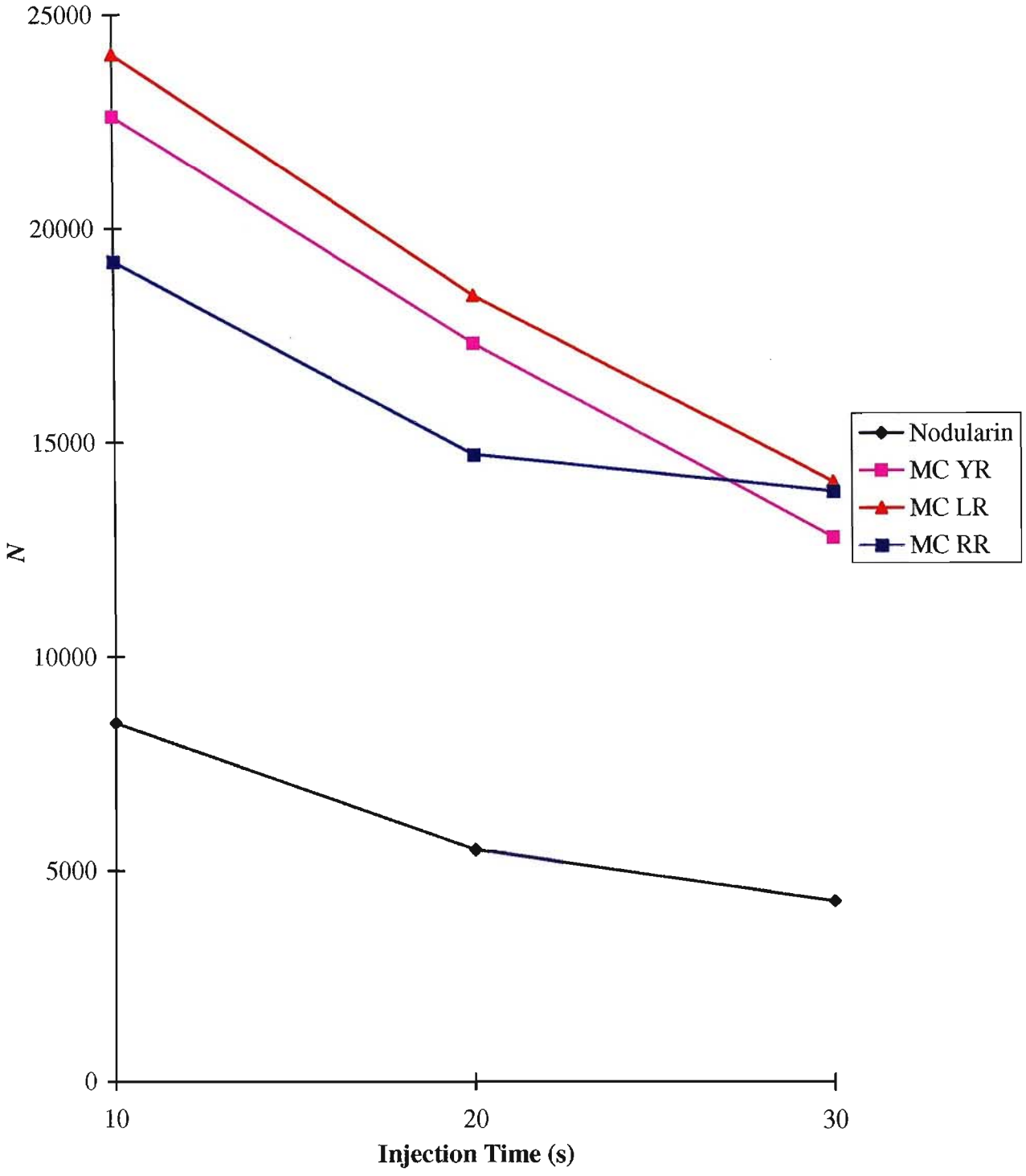

Figure 5.1 Efficiency variation as a function of hydrodynamic injection time.

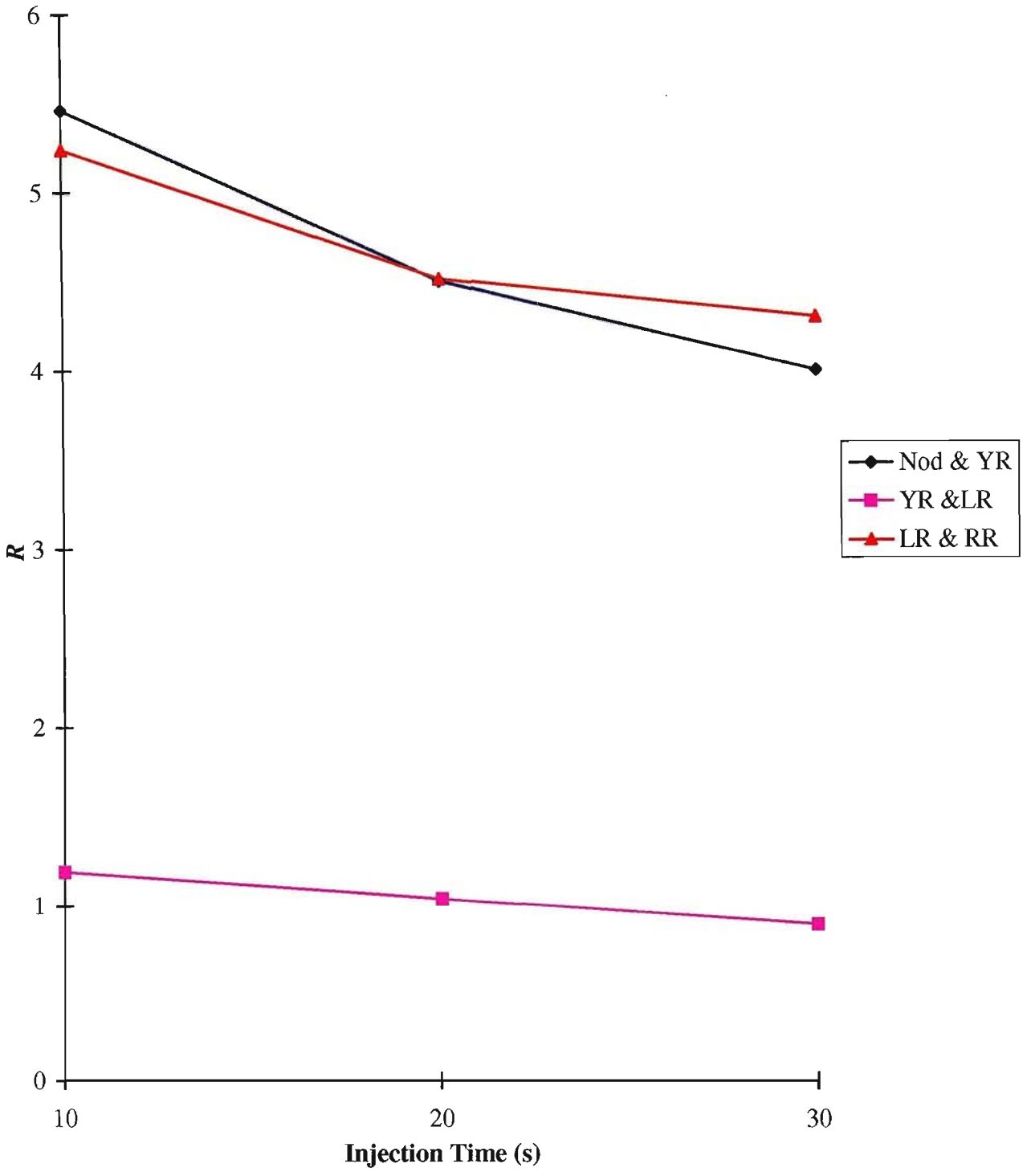

Figure 5.2 Resolution change as a function of hydrodynamic injection time.

and accuracy of physically measuring the extremely narrow peak widths. The electronic integrator did not give peak width values and these had to be measured manually. A compromise between sensitivity, resolution and efficiency was reached and 10 s was selected as the most suitable and practical injection time. Above 10 s, both efficiency and resolution dropped steadily because of the increase in the peak widths.

Using the optimized hydrodynamic injection conditions (10 s), detection limit data (Table 5.4) was collected with a 20 ng/μL toxin composite standard solution. The limits of detection (LOD) at a signal-to-noise ratio of 2 (s/n 2) based on peak height measurements, was 29.85 ng/μL for nodularin, 17.7 ng/μL for MC YR, 14.13 ng/μL for MC LR and 20.1 ng/μL for MC RR. Figure 5.3 shows an electropherogram of a toxin standard close to the detection limit.

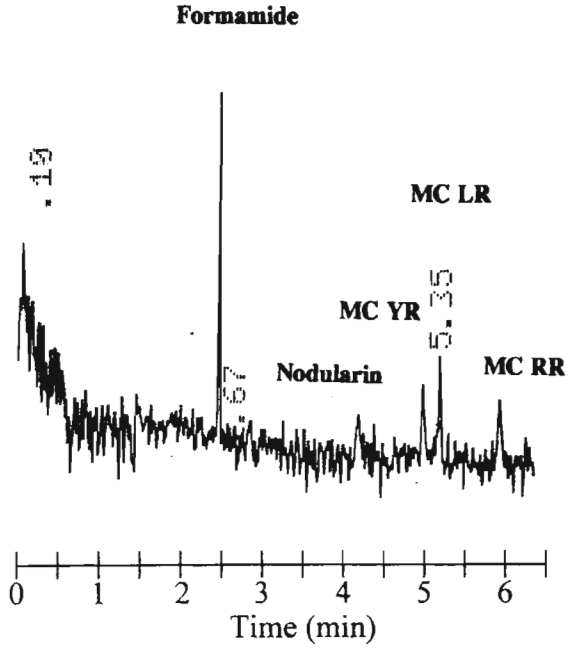

Figure 5.3 Electropherogram of a 20 ng/μL toxin composite standard close to the detection limit. Operating conditions: 30 mM borax; 9 mM SDS; pH 9.18; +30 kV applied voltage; 10 s hydrodynamic injection; bare fused silica capillary column; L_T 70 cm; L_{EFF} 40 cm; UV detection at 238 nm.

Table 5.4 Detection limit data based on peak heights, for hydrodynamic injections collected with a 20 ng/μL toxin standard

	Nodularin	MC YR	MC LR	MC RR	Mean
Replicate 1					
Signal	3	6	10	6	
Noise	2	2	2	2	2
s/n	1.50	3.00	5.00	3.00	
Replicate 2					
Signal	6.5	10.2	14	9	
Noise	5.5	4	5	5.5	5
s/n	1.30	2.04	2.80	1.80	
Replicate 3					
Signal	8	16	14.5	10	
Noise	7	5.5	7	6	6.38
s/n	1.25	2.51	2.27	1.57	
Replicate 4					
Signal	9	11	12	10	
Noise	7	5	6	6	6
s/n	1.50	1.83	2.00	1.67	
Replicate 5					
Signal	6	10	11	10	
Noise	6	4.5	5.5	5	5.25
s/n	1.14	1.90	2.10	1.90	
mean s/n	1.34	2.26	2.83	1.99	

Detection Limit Calculations

$$LOD_{nodularin} = \frac{2}{1.34} \times 20\ ng/\mu L = 29.85\ ng/\mu L$$

$$LOD_{MC\ YR} = \frac{2}{2.26} \times 20\ ng/\mu L = 17.70\ ng/\mu L$$

$$LOD_{MC\ LR} = \frac{2}{2.83} \times 20\ ng/\mu L = 14.13\ ng/\mu L$$

$$LOD_{MC\ RR} = \frac{2}{1.99} \times 20\ ng/\mu L = 21.10\ ng/\mu L$$

5.2.2 *Electrokinetic Injection*

With electrokinetic injections, in addition to injection time, injection voltage was optimised since both parameters contribute to the length of the injection plug. Efficiency and resolution was calculated from Table 5.5 and the mean presented in Tables 5.6 and 5.7 respectively. Figures 5.4 and 5.5 are graphical representations of the mean efficiency variation and the mean resolution as a function of injection time, respectively. The trends observed are consistent with that obtained with hydrodynamic injections. A steady drop in both efficiency and resolution is noted and has been attributed to the increase in the peak variance. The graphs predict higher efficiency and resolution at injection times less than 5 s, however sensitivity is reduced. In addition errors in peak width measurements are anticipated. A drop in efficiency ranging from 17% for nodularin to 40% for MC RR is observed on going from a 5 s to a 10 s injection. For this reason 5 s was found to be the optimum electrokinetic injection time.

With electrokinetic injections, injection voltage is an additional parameter that governs the volume of sample injected, and hence efficiency and resolution. The average efficiency and average resolution was calculated from Table 5.8 and presented in Tables 5.9 and 5.10 respectively. Plots of average efficiency and average resolution as a function of injection voltage are illustrated in Figures 5.6 and 5.7 respectively, with the injection time kept constant at 5 s. The trend observed is very similar to that of injection time variation because of the impact of injection voltage on peak variance. Good results were obtained at 2.5 kV. Below this value, there was a significant loss in sensitivity due to the small sample volume injected as a result of the reduced EOF. In addition, the precision and accuracy with which peak width measurements were taken, was poor.

Using optimised injection conditions of 2.5 kV for 5 s, detection limit data (Table 5.11) was collected with a 20 ng/μL toxin composite standard solution. The LOD (s/n 2) for nodularin was calculated from s/n data as 6.03 ng/μL, 1.95 ng/μL for MC YR, 1.42 ng/μL for MC LR and 1.76 ng/μL for MC RR. By comparison with the LODs in hydrodynamic injections, the improvement in detection sensitivity ranged from 4.95 times for nodularin to 19.85 times for MC LR. The electropherogram in Figure 5.8A and 5.8B shows a comparison of sensitivities of the two modes of injection.

Table 5.5 Efficiency and resolution data for electrokinetic injections at 2.5 kV

5 s injection, Replicate 1				
	Nodularin	**MC YR**	**MC LR**	**MC RR**
t_r *(min)*	4.15	4.68	4.79	5.25
W_b *(min)*	0.19	0.12	0.12	0.14
N	7633	24336	25493	22500
R	3.42	0.92	3.54	
Replicate 2				
t_r *(min)*	4.17	4.72	4.85	5.35
W_b *(min)*	0.2	0.11	0.12	0.14
N	6956	29459	26136	23365
R	3.55	1.13	3.85	
Replicate 3				
t_r *(min)*	4.2	4.78	4.9	5.45
W_b *(min)*	0.2	0.11	0.12	0.13
N	7056	30213	26678	28121
R	3.74	1.04	4.40	
10 s injection, Replicate 1				
t_r *(min)*	4.17	4.72	4.83	5.33
W_b *(min)*	0.22	0.14	0.14	0.18
N	5748	18186	19044	14029
R	3.06	0.79	3.13	
Replicate 2				
t_r *(min)*	4.19	4.76	4.88	5.4
W_b *(min)*	0.22	0.13	0.15	0.17
N	5804	21451	16935	16144
R	3.26	0.86	3.25	
Replicate 3				
t_r *(min)*	4.17	4.72	4.84	5.34
W_b *(min)*	0.21	0.14	0.15	0.18
N	6309	18186	16658	14082
R	3.14	0.83	3.03	
20 s injection, Replicate 1				
t_r *(min)*				
W_b *(min)*	4.16	4.7	4.82	5.32
N	0.24	0.16	0.16	0.18
R	4807	13806	14520	13976
	2.70	0.75	2.94	
Replicate 2				
t_r *(min)*	4.08	4.6	4.71	5.16
W_b *(min)*	0.24	0.16	0.16	0.18
N	4624	13225	13865	13148
R	2.60	0.69	2.65	

Table 5.5 Continued

		Replicate 3		
	Nodularin	**MC YR**	**MC LR**	**MC RR**
t_r *(min)*	4.09	4.62	4.72	5.17
W_b *(min)*	0.24	0.16	0.16	0.18
N	4647	13340	13924	13199
R	2.65	0.62	2.65	
		30 s injection, Replicate 1		
t_r *(min)*	4.11	4.62	4.73	5.22
W_b *(min)*	0.26	0.17	0.17	0.2
N	3998	11817	12386	10899
R	2.37	0.65	2.65	
		Replicate 2		
t_r *(min)*	4.13	4.65	4.74	5.25
W_b *(min)*	0.26	0.17	0.17	0.2
N	4037	11971	12439	11025
R	2.42	0.53	2.76	
		Replicate 3		
t_r *(min)*	4.11	4.62	4.73	5.22
W_b *(min)*	0.26	0.17	0.17	0.2
N	3998	11817	12386	10899
R	2.37	0.65	2.65	

Table 5.6 Mean efficiency variation with electrokinetic injection time at 2.5 kV

	Mean *N*			
Inj Time (s)	**Nodularin**	**MC YR**	**MC LR**	**MC RR**
5	7215	28003	26102	24662
10	5954	19275	17546	14752
20	4693	13457	14103	13441
30	4465	12928	13537	12608

Table 5.7 Mean resolution variation with electrokinetic injection time at 2.5 kV

	Mean *R*		
Inj Time (s)	**Nod & MC YR**	**MC YR & MC LR**	**MC LR & MC RR**
5	3.57	1.03	3.93
10	3.15	0.82	3.14
20	2.65	0.69	2.75
30	2.39	0.61	2.68

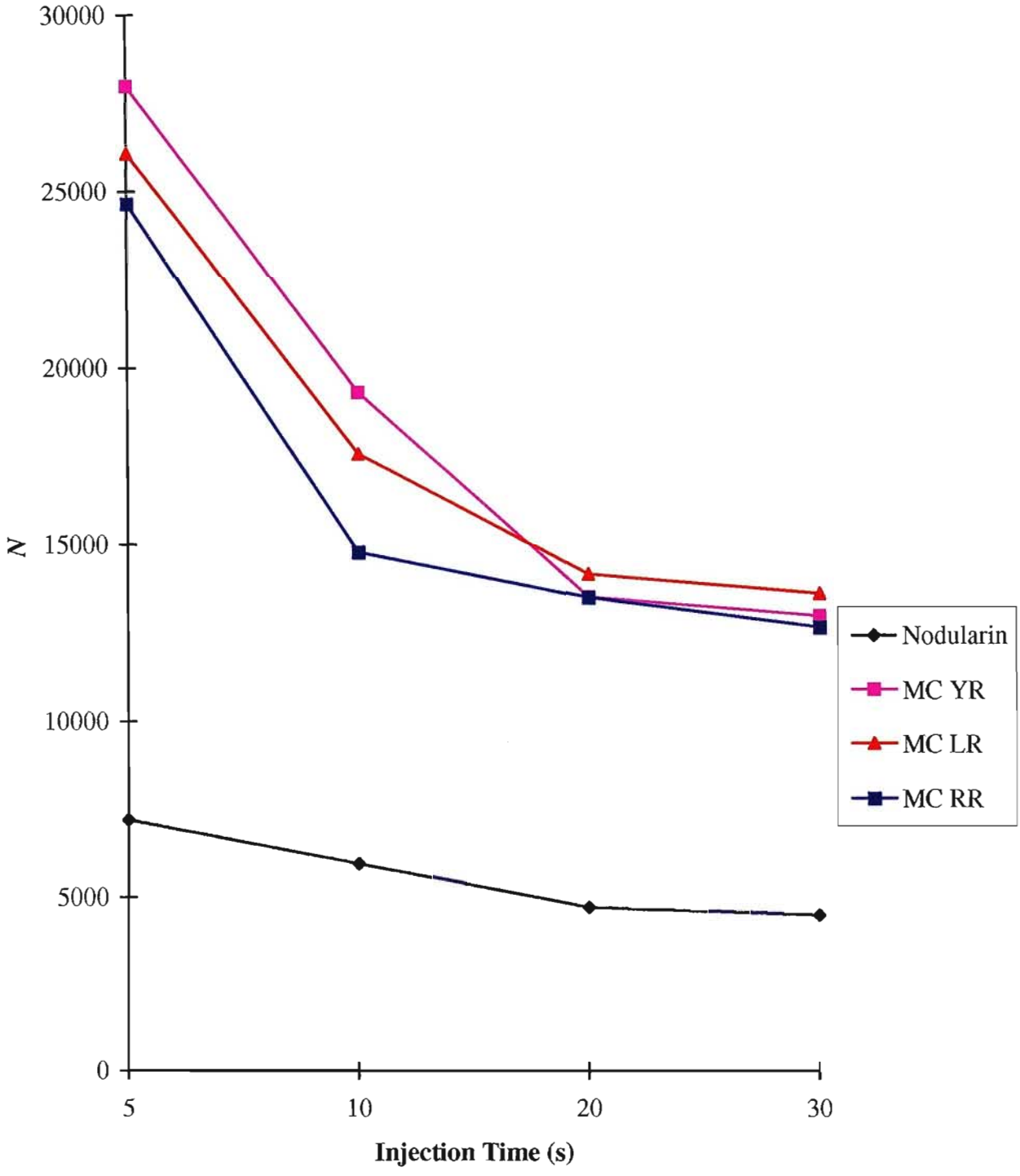

Figure 5.4 Efficiency variation as a function of electrokinetic injection time.

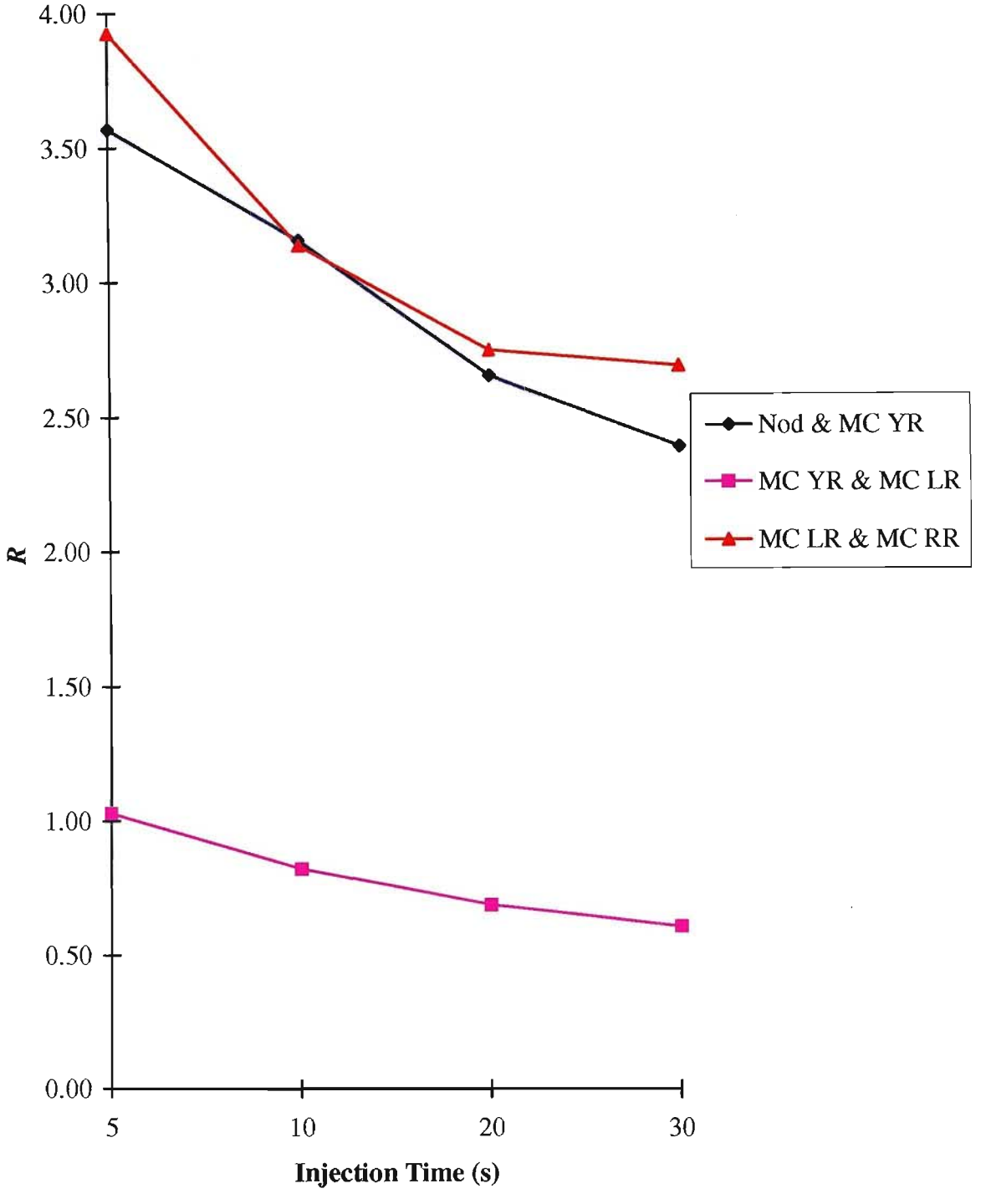

Figure 5.5 Resolution change as a function of electrokinetic injection time.

Table 5.8 Efficiency and resolution data variation with injection voltage using a fixed injection time of 5 s

2.5 kV, Replicate 1				
	Nodularin	**MC YR**	**MC LR**	**MC RR**
t_r *(min)*	5.11	6.05	6.26	7.11
W_b *(min)*	0.27	0.14	0.14	0.14
N	5731	29880	31990	41267
R	4.59	1.50	6.07	
Replicate 2				
t_r *(min)*	4.78	5.62	5.83	6.64
W_b *(min)*	0.2	0.1	0.1	0.1
N	9139	50535	54382	70543
R	5.6	2.1	8.1	
Replicate 3				
t_r *(min)*	4.74	5.54	5.75	6.57
W_b *(min)*	0.22	0.11	0.11	0.12
N	7427	40584	43719	47961
R	4.85	1.91	7.13	
5 kV, Replicate 1				
t_r *(min)*	4.87	5.79	6.01	6.88
W_b *(min)*	0.29	0.14	0.15	0.18
N	4512	27367	25685	23375
R	4.28	1.52	5.27	
Replicate 2				
t_r *(min)*	4.73	5.59	5.8	6.61
W_b *(min)*	0.26	0.14	0.14	0.15
N	5295	25509	27461	31070
R	4.30	1.50	5.59	
Replicate 3				
t_r *(min)*	4.52	5.33	5.52	6.33
W_b *(min)*	0.28	0.13	0.12	0.14
N	4169	26896	33856	32709
R	3.95	1.52	6.23	
7.5 kV, Replicate 1				
t_r *(min)*	4.73	5.59	5.8	6.61
W_b *(min)*	0.3	0.15	0.15	0.19
N	3977	22221	23922	19365
R	3.82	1.40	4.76	
Replicate 2				
t_r *(min)*	5.09	6.18	6.41	7.42
W_b *(min)*	0.3	0.15	0.15	0.19
N	4606	27159	29218	24402
R	4.84	1.53	5.94	

Table 5.8 Continued

	Nodularin	MC YR	MC LR	MC RR
Replicate 3				
t_r *(min)*	4.52	5.28	5.48	6.25
W_b *(min)*	0.3	0.13	0.15	0.19
N	3632	26394	21355	17313
R	3.53	1.43	4.53	
10 kV, Replicate 1				
t_r *(min)*	5.01	6.09	6.31	7.29
W_b *(min)*	0.32	0.16	0.16	0.2
N	3922	23180	24885	21258
R	4.50	1.38	5.44	
Replicate 2				
t_r *(min)*	5	5.95	6.17	7.1
W_b *(min)*	0.35	0.17	0.16	0.22
N	3265	19600	23793	16664
R	3.65	1.33	4.89	
Replicate 3				
t_r *(min)*	5.17	6.26	6.49	7.58
W_b *(min)*	0.32	0.17	0.19	0.22
N	4176	21696	18668	18994
R	4.45	1.28	5.32	

Table 5.9 Mean efficiency variation with injection voltage and a 5 s injection time

	Mean *N*			
Inj Voltage (kV)	**Nodularin**	**MC YR**	**MC LR**	**MC RR**
2.5	7433	40333	43364	53257
5	4659	26590	29001	29051
7.5	4072	25258	24832	20360
10	3788	21492	22449	18972

Table 5.10 Mean resolution variation with injection voltage and a 5 s injection time

	Mean *R*		
Inj Voltage (kV)	**Nod & YR**	**YR & LR**	**LR & RR**
2.5	5.01	1.84	7.10
5	4.18	1.51	5.70
7.5	4.07	1.45	5.08
10	4.20	1.33	5.22

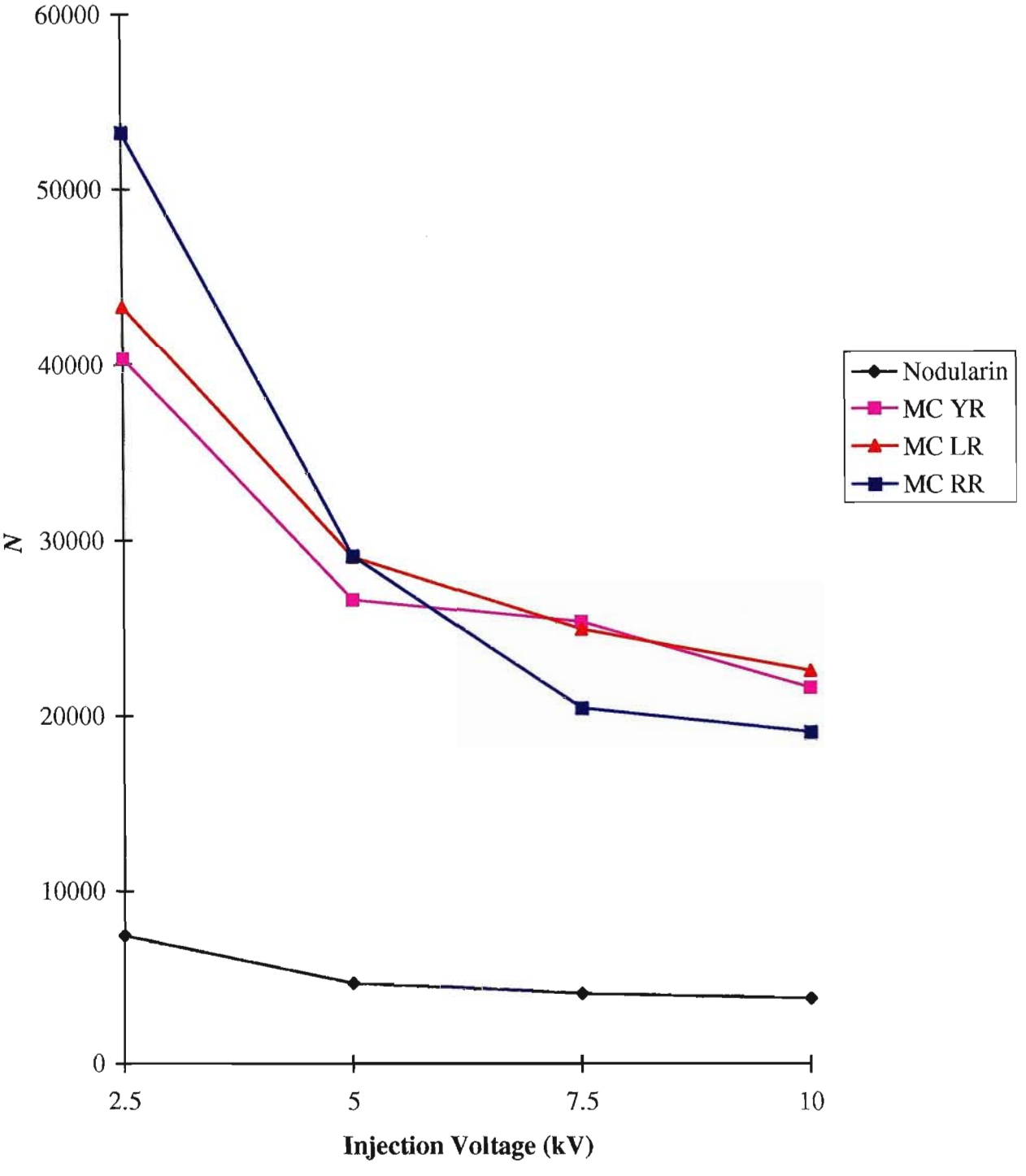

Figure 5.6 Efficiency variation as a function of electrokinetic injection voltage.

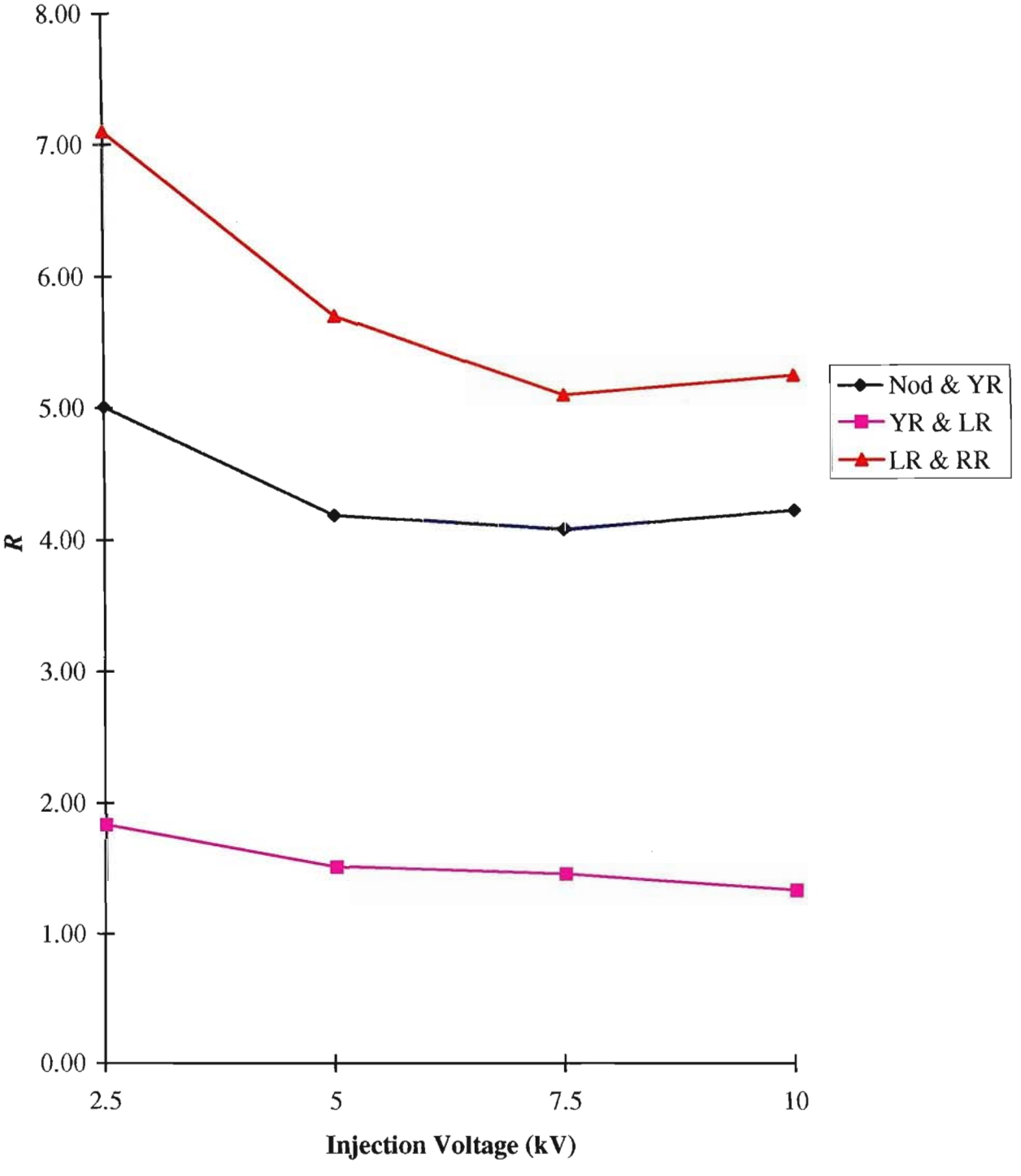

Figure 5.7 Resolution change as a function of electrokinetic injection voltage.

Table 5.11 Detection limit data for electrokinetic injections collected with a 20 ng/μL toxin standard

Replicate 1					
	Nodularin	MC YR	MC LR	MC RR	Mean
Signal	14	44	86.5	50	
Noise	3	2	2.5	3.5	2.75
s/n	5.09	16.00	31.45	18.18	
Replicate 2					
Signal	21	31.5	44.5	33	
Noise	4	4	4	4	4.00
s/n	5.25	7.88	11.13	8.25	
Replicate 3					
Signal	29.8	70	117	81	
Noise	5	5.5	4.5	5	5.00
s/n	5.96	14.00	23.40	16.20	
Replicate 4					
Signal	34	136	148	148	
Noise	5	6	6	5	5.50
s/n	6.18	24.73	26.91	26.91	
Replicate 5					
Signal	34	98	143	118	
Noise	5	5	5	5	5.00
s/n	6.80	19.60	28.60	23.60	
Replicate 6					
Signal	37	112	159	148	
Noise	4	5	5.5	4	4.63
s/n	8.00	24.22	34.38	32.00	
Replicate 7					
Signal	37	145.5	151	110	
Noise	4	3.5	5.5	4	4.25
s/n	8.71	34.24	35.53	25.88	
Replicate 8					
Signal	32	87	142	112	
Noise	8	4	3	5	5.00
s/n	6.40	17.40	28.40	22.40	
Replicate 9					
Signal	36	113	163	122	
Noise	5	5	5	5	5.00
s/n	7.20	22.60	32.60	24.40	

Table 5.11 Continued

	Nodularin	MC YR	MC LR	MC RR	Mean
			Replicate 10		
Signal	34	111	156	135	
Noise	4.5	5.5	5.5	5	5.13
s/n	6.63	21.66	30.44	26.34	
			Replicate 11		
Signal	37	138	150	146	
Noise	5	6	6	5	5.50
s/n	6.73	25.09	27.27	26.55	
mean s/n	6.63	20.67	28.19	22.79	

Detection Limit Calculations

$$LOD_{Nodularin} = \frac{2}{6.63} \times 20\ ng/\mu L = 6.03\ ng/\mu L$$

$$LOD_{MC\ YR} = \frac{2}{20.67} \times 20\ ng/\mu L = 1.95\ ng/\mu L$$

$$LOD_{MC\ LR} = \frac{2}{28.19} \times 20\ ng/\mu L = 1.42\ ng/\mu L$$

$$LOD_{MC\ RR} = \frac{2}{22.79} \times 20\ ng/\mu L = 1.76\ \text{ng}/\mu\text{L}$$

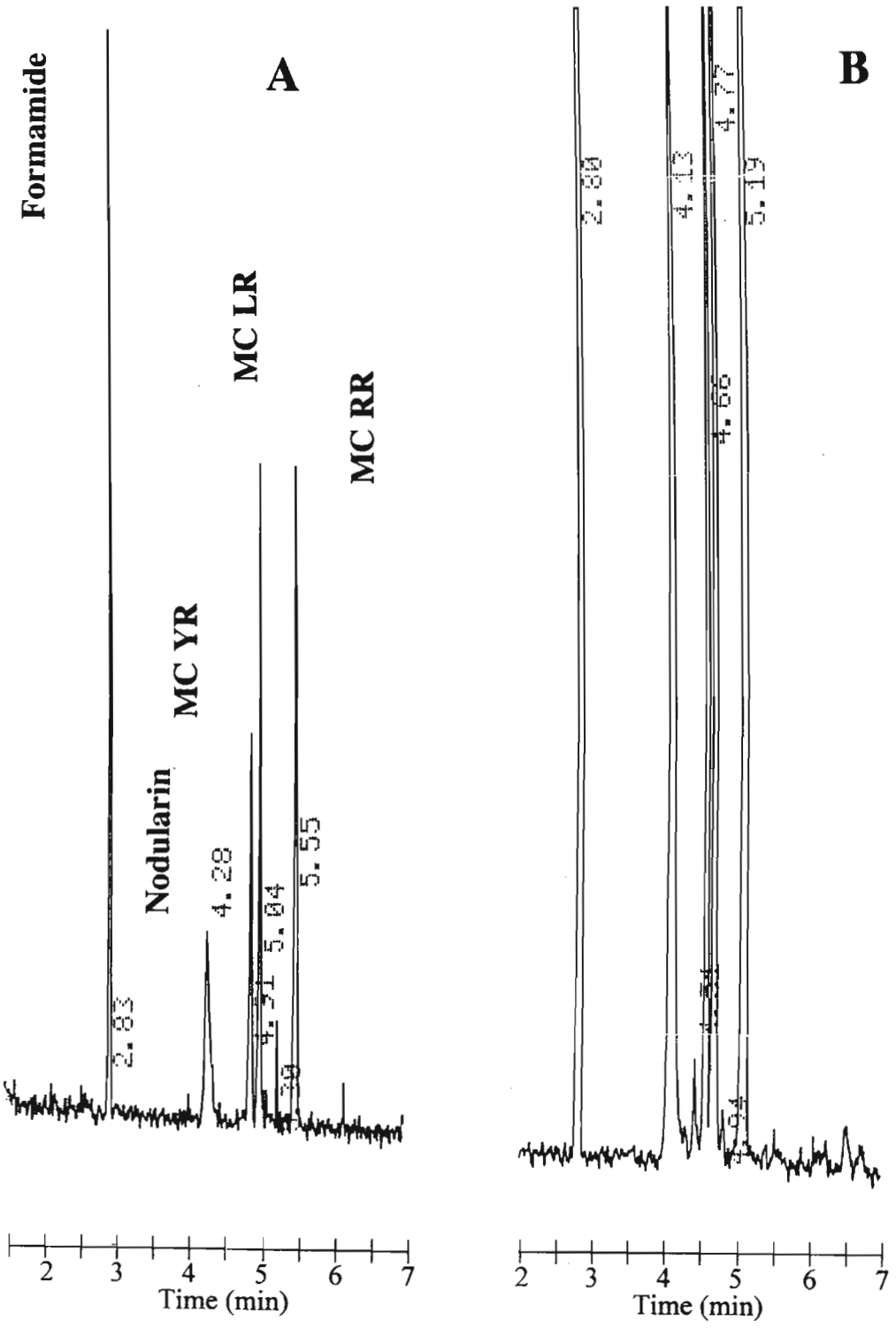

Figure 5.8 (A) Electropherogram of a 60 ng/μL toxin composite standard using a 10 s hydrodynamic injection and (B) Using a 2.5 kV electrokinetic injection for 5 s. The remaining operating conditions were similar to that used in Figure 5.3.

5.3 Sample Concentration Strategies

5.3.1 *Field Amplified Sample Stacking*

A solution of low ionic strength has a low conductivity or a high resistance. This solution can be viewed in terms of an electrical resistor. A high resistance implies that there is a greater potential difference across that resistor which is given by the Ohm equation

$$V = IR \tag{5.4}$$

where V is the potential difference, I the current and R the electrical resistance. From the expression

$$E = \frac{V}{L} \tag{5.5}$$

it can be inferred that the field strength is high in the region of low conductivity and low in the region of high conductivity. In practice, the field strength E can be controlled by varying the buffer ionic strength. This fact was exploited to advantage in improving sensitivity. Initial studies involved filling the entire column with solute dissolved in a dilute buffer (also referred to as the sample buffer, 2 mM borax) and then immersing the column ends into the run buffer (30 mM borax). Upon the application of a potential difference of +30 kV, the current increased from less than 1 μA to 55 μA. A single peak was observed in the electropherogram (Figure 5.9). An explanation of this phenomenon can be made by studying the events in Figures 5.10A and 5.10B.

Figure 5.10A represents a CE column filled with analyte dissolved in sample buffer. When a voltage of +30 kV is applied (Figure 5.10B), two electrokinetic effects occur with opposing velocities. Electroosmosis originates at the anodic end of the column and hence the column begins to fill with the concentrated run buffer. At the same time, electrophoresis of the negatively charged toxins occurs. The column contains a discontinuous buffer system that results in a high field strength in the buffer of low conductivity and a low field strength in the concentrated buffer. Electrophoresis is the dominating electrokinetic effect in the region of low conductivity because of the high field

strength and solutes acquire a net velocity toward the cathode. Solute velocity decreases rapidly at the interface of the two buffer regions because of a decrease in the field strength, with the result that analyte stacking occurs. As stacking

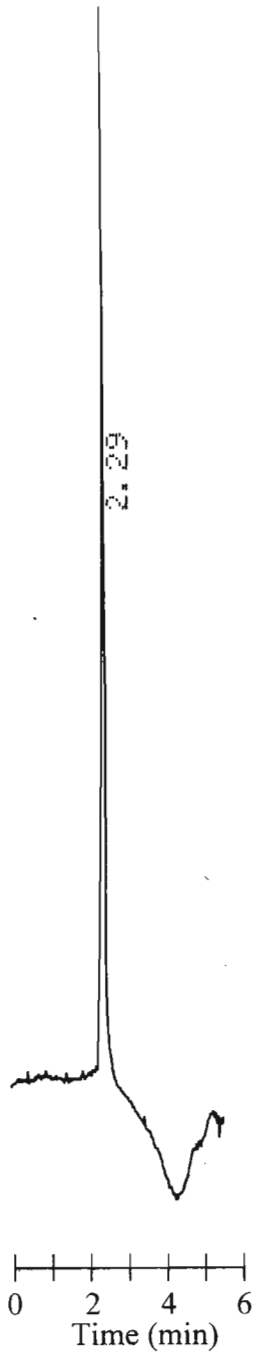

Figure 5.9 Electropherogram of analytes stacked in a single band. Operating conditions: 30 mM borax; 9 mM SDS; +30 kV operating voltage; bare fused silica column; L_T 70 cm; L_{EFF} 40 cm; UV detection at 238 nm.

progresses, the local conductivity increases, resulting in a further decrease in the field strength. Electroosmosis becomes the dominating electrokinetic effect and the net electrophoretic velocity reduces to zero and then negative. All solute species remain in this tight band and eventually pass the detection window giving rise to the peak that is seen in Figure 5.9. Although sample concentration occurred, electrophoretic separation was never achieved.

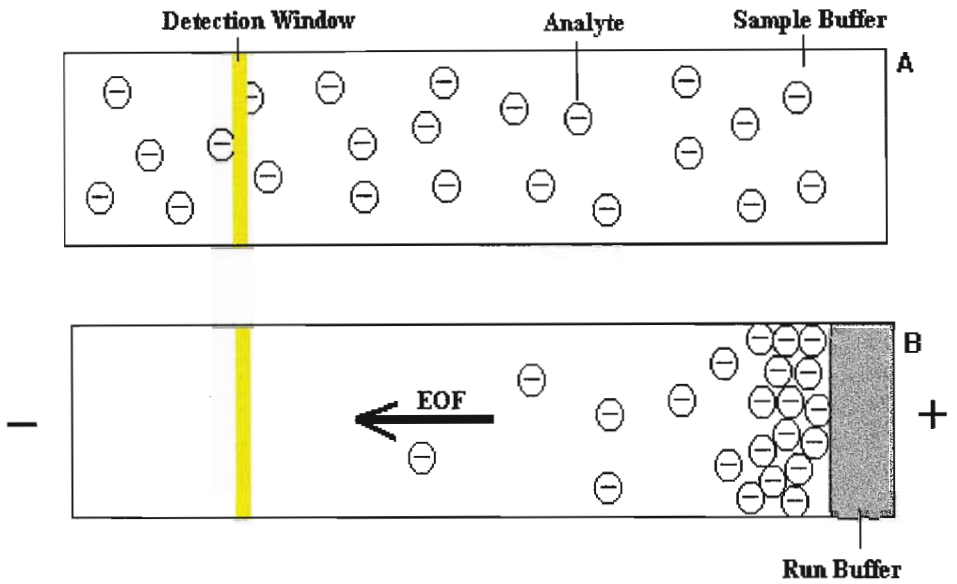

Figure 5.10 (A) Diagrammatic representation of the CE column filled with analyte dissolved in the sample buffer and (B) Stacking of the analytes at the interface of the two buffer regions upon the application of a potential difference of +30 kV. UV absorbance measurements were taken at 238 nm.

5.3.2 *Field Amplified Back and Forth MECC*

A second approach utilising field amplified sample stacking was used to achieve sample stacking as well as separation. The column filled with analyte dissolved in the diluted sample buffer [Figure 5.11A], was immersed into the more concentrated run buffer at both ends and a potential difference of -30 kV applied. Two electrokinetic effects with opposing velocities occurred. EOF originated at the detector end and resulted in a flow of sample buffer into the column. The negatively charged toxins accelerated rapidly toward the

electrode of opposite polarity due to the high electric field strength, and stacked at the interface of the two buffer regions (Figure 5.11B). Due to analyte stacking the local conductivity at the interfacial region increased, resulting in a decrease in the electric field strength and consequently electrophoretic velocity, v_{ep}. EOF then became the dominating electrokinetic effect in this region and the analyte band acquired a net velocity in the direction of electroosmosis. When all the sample buffer had been displaced with the run buffer (Figure 5.11C), which was monitored by observing the rise in the current to a maximum value of 55 μA, the voltage was switched to +30 kV (Figure 5.11D). At this stage in time, the solutes were focused in a narrow band at the injector end of the capillary, while the entire length of the column contained the run buffer. The toxins were then separated in a homogeneous electric field (Figure 5.11E).

As shown in Figures 5.12A and 5.12B, a sensitivity enhancement of over two orders of magnitude was recorded in comparison with the hydrodynamic mode of injection. The peak profile is different to that achieved with normal MECC. This has been attributed to the differences in the extent to which stacking occurs, which is in turn defined by the μ_{ep} of the solute, electroosmotic flow (μ_{eo}), the injection plug length (l_{inj}), and the differences in the ionic strengths of the discontinuous buffer system. Solutes with high μ_{ep} stack more efficiently and produce high efficiency peaks (MC RR). The ultimate effectiveness of the stacking is limited by the trade off between resolution and injection plug length while sensitivity enhancement is due to stacking of toxins from *ca.* 1.4 μL (total column volume) to *ca.* 10 nL (typical injection volume). This method is particularly useful because it can be performed without any modification to the electrophoresis equipment. Normalised peak area data from Table 5.12 and Table 5.13 were used to compare the sensitivity enhancement of hydrodynamic injections and field amplification. A sensitivity enhancement of 749 times was achieved for nodularin, 777 times for MC YR, 657 times for MC LR and 197 times for MC RR. The low sensitivity for MC RR could suggest that the polarity was reversed too late and, being the solute with highest electrophoretic mobility, part of this solute band could have migrated out of the injection end of the column. From the data in Table 5.14, the retention time precision for field amplification sample stacking was found to range from

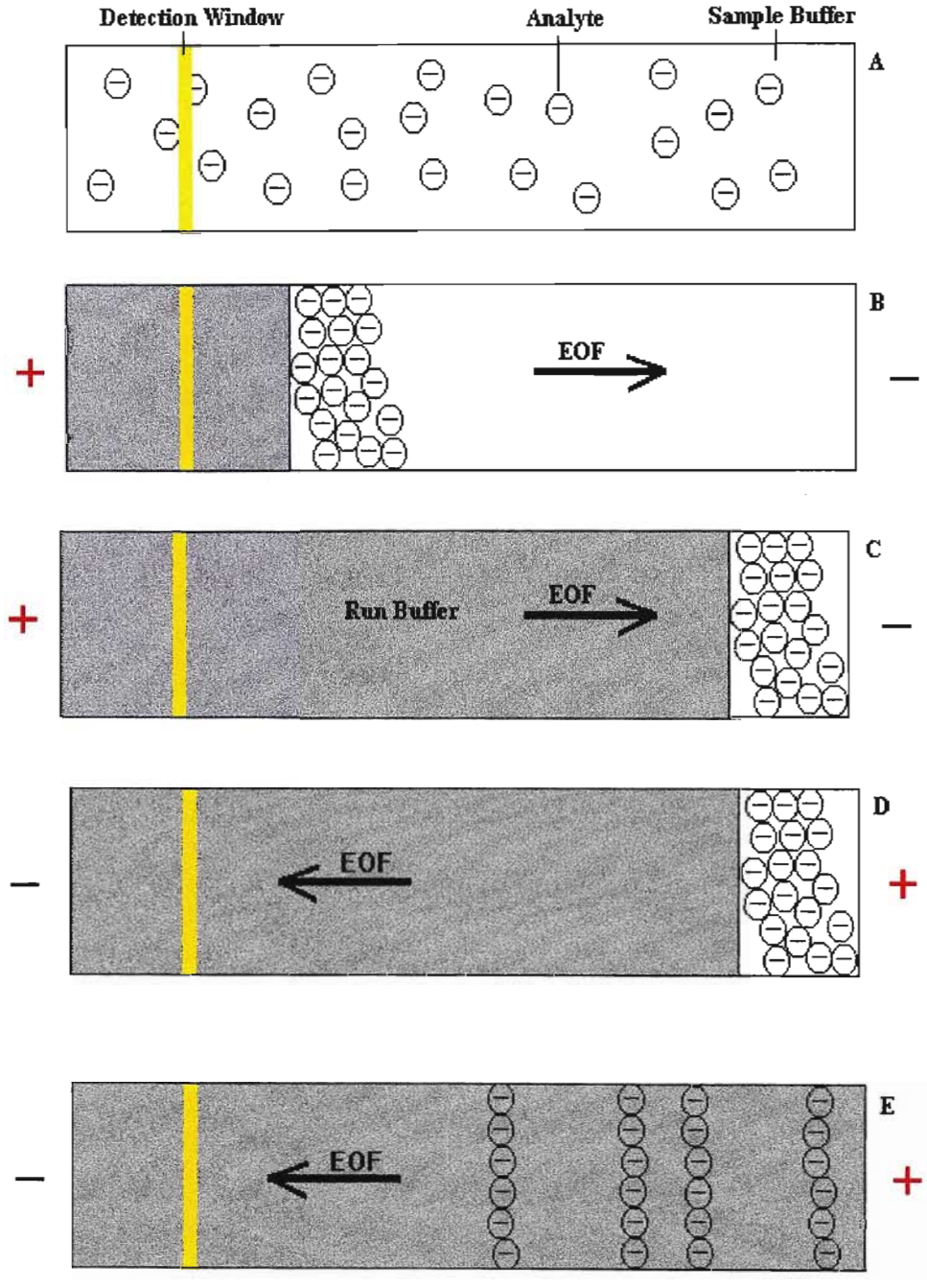

Figure 5.11 (A) Diagrammatic representation of the CE column filled with analyte dissolved in the sample buffer (B) Application of -30 kV cause the analyte to stack in a single band at the interface of the two buffer regions (C) EOF displaces the sample buffer with the run buffer (D) When the analyte band is at the injection end of the column, the polarity is switched to +30 kV and (E) Toxins separate in a homogeneous electric field.

1.96% and 2.25% RSD indicating good precision of the method. Area precision, however was not as good and was attributed to the tedious procedure of manually switching the electrodes to reverse the polarity.

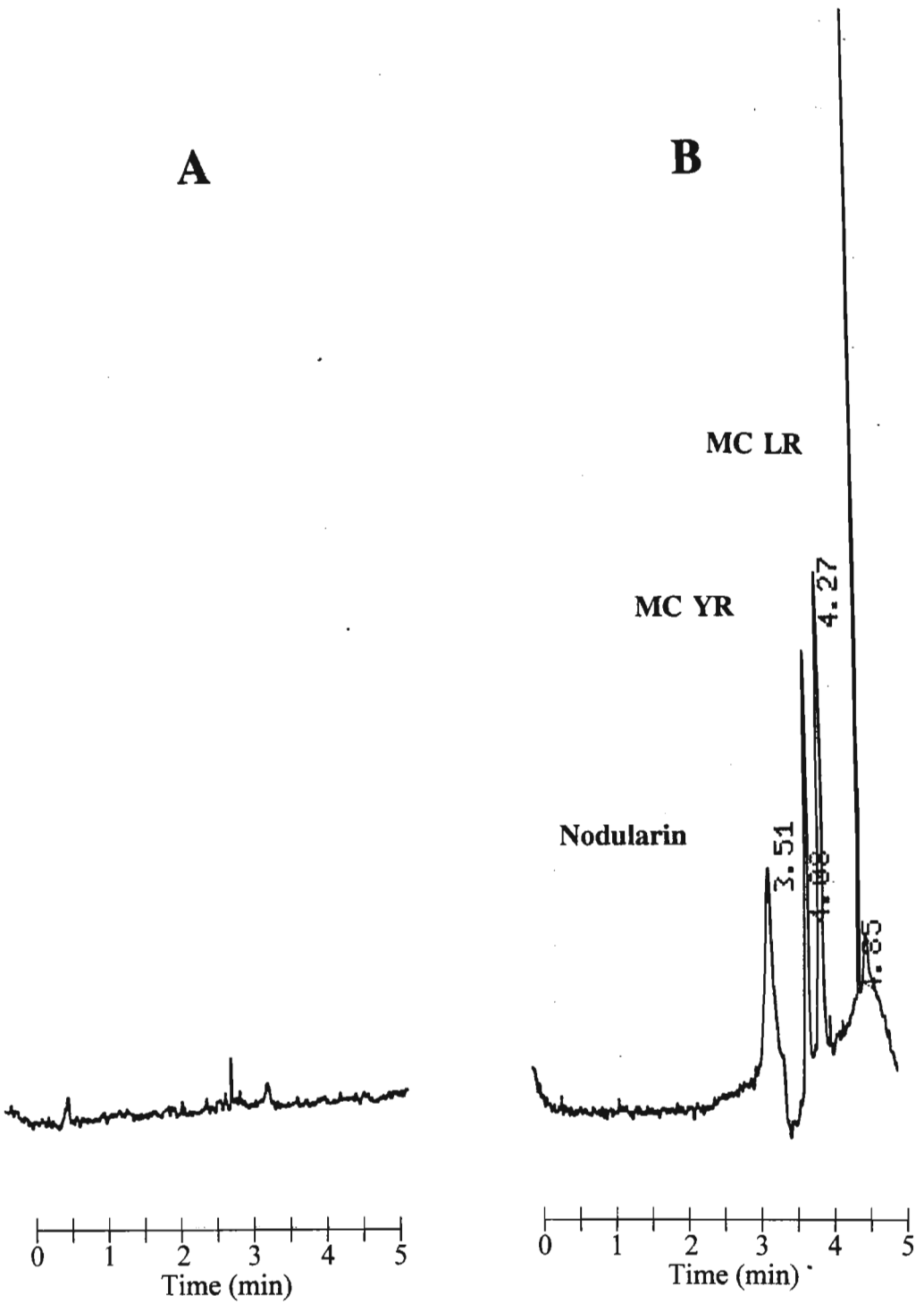

Figure 5.12 (A) Electropherogram of a 1 ng/μL toxin composite standard using a 30 s hydrodynamic injection and (B) Using field amplified back and forth MECC.

Table 5.12 Area and normalised peak area data for hydrodynamic injections using a 100 ng/μL toxin standard solution

	Nodularin	MC YR	MC LR	MC RR
Replicate 1				
Area	7315	8064	10525	17647
t_r	4.52	5.26	5.46	6.11
Area/t_r	1618	1533	1928	2888
Replicate 2				
Area	8008	9011	11752	24556
t_r	4.57	5.48	5.69	6.43
Area/t_r	1752	1644	2065	3819
Replicate 3				
Area	8723	8237	9676	18142
t_r	4.93	5.58	5.74	6.15
Area/t_r	1769	1476	1686	2950
Replicate 4				
Area				
t_r	10444	7270	12099	22983
Area/t_r	4.35	5.39	5.58	6.18
	2401	1349	2168	3719
Replicate 5				
Area	13915	18876	17596	21142
t_r	5.31	5.49	6.11	6.16
Area/t_r	2621	3438	2880	3432
Replicate 6				
Area	9602	15712	20058	34081
t_r	4.57	5.35	5.54	6.17
Area/t_r	2101	2937	3621	5524
Mean Area	9668	11195	13618	23092
Mean Area/t_r	2044	2063	2391	3722

Table 5.13 Area and normalised peak area data for field amplified sample stacking using a 1 ng/μL toxin standard

	Nodularin	MC YR	MC LR	MC RR
Run 1				
Area	56634	36400	46830	35244
t_r	3.34	3.86	4.44	5.47
Area/t_r	16956	9430	10547	6443
Run 2				
Area	48787	66688	89641	45042
t_r	3.75	4.35	4.52	5.61
Area/t_r	13010	15331	19832	8029
Run 3				
Area	59034	76190	99712	38236
t_r	3.71	4.3	4.47	5.33
Area/t_r	15912	17719	22307	7174
Run 4				
Area	44334	41628	64090	43558
t_r	3.71	4.15	4.26	5.37
Area/t_r	11950	10031	15045	8111
Run 5				
Area	66680	33438	54216	38994
t_r	3.85	4.25	4.39	5.38
Area/t_r	17319	7868	12350	7248
Run 6				
Area	70720	169172	70012	38032
t_r	4.22	4.73	4.93	5.37
Area/t_r	16758	35766	14201	7082
Mean Area	57698	70586	70750	39851
Mean Area/t_r	15318	16024	15714	7348

Sensitivity enhancements with field amplification

$$Nodularin = \frac{15318 \times 100}{2044} = 749 \qquad MC\ YR = \frac{16024 \times 100}{2063} = 777$$

$$MC\ LR = \frac{15714 \times 100}{2391} = 657 \qquad MC\ RR = \frac{7348 \times 100}{3722} = 197$$

Table 5.14 Retention time precision data for field amplification using a 1 ng/μL toxin composite standard

	Retention Time (min)			
Replicate	**Nodularin**	**MC YR**	**MC LR**	**MC RR**
1	3.86	4.33	4.44	5.47
2	3.75	4.35	4.52	5.61
3	3.71	4.3	4.47	5.33
4	3.71	4.15	4.26	5.37
5	3.85	4.25	4.39	5.38
Mean	3.776	4.276	4.416	5.432
STDEV	0.07	0.08	0.10	0.11
%RSD	1.96	1.87	2.25	2.06

5.3.3 *Field Amplified Back and Forth MECC on the Hewlett Packard CE System*

Due to the increasing popularity of CE methods, numerous commercial instruments have been introduced. The HP ^{3D}CE system was of particular importance in this work as it was equipped with the feature of time programmable polarity reversal. This particular feature was employed in sample preconcentration studies discussed below.

Using 12 psi pressure, the entire column was filled with a composite standard (1 ng/μL) prepared in 3mM borax buffer. The system was programmed to begin electrophoresis with -30 kV at time zero with both column ends placed in the run buffer. At 3.3 minutes, the polarity was switched automatically to +30 kV. These two events caused stacking and destacking respectively. As shown by the electropherogram in Figure 5.13A, the small peak at 0.504 minutes, indicates the stacked solute zone. The low intensity peak in the electropherogram indicates that stacking was still in progress and only a small proportion of the solute was stacked before passing the detector. This figure not only shows the electropherogram (Figure 5.13A), but also a trace of the electrophoresis current profile (Figure 5.13B). When reversed polarity was applied, the electrophoresis current reading was reflected on the negative part of the y-axis. Initially the column contained solute in the dilute sample buffer resulting in the production of a current whose magnitude was close to zero. As stacking progressed, the run buffer began to fill the column and this was monitored by observing a rise in the current. The polarity was automatically reversed at 3.3 minutes to +30 kV. The value of the current reading also changed from -22 μA to +22 μA and this is reflected on the positive part of the y-axis. The Figure also indicates that there was a further rise in the current to a maximum of 36 μA before stabilizing. This is evidence that the system still contained dilute sample buffer at the point of polarity reversal. The impact of this discontinuous buffer system is that the solute band remained in the stacked zone because of inhomogeneities in the electric field strength, resulting in incomplete resolution.

When polarity reversal was executed at 3.6 minutes, all analytes except MC YR and MC LR displayed good resolution (Figure 5.14A). The loss in resolution was a small compromise for the gain in sensitivity. The plot of the electrophoresis current as a function of time (Figure 5.14B) is therefore a very useful feature and gives invaluable information.

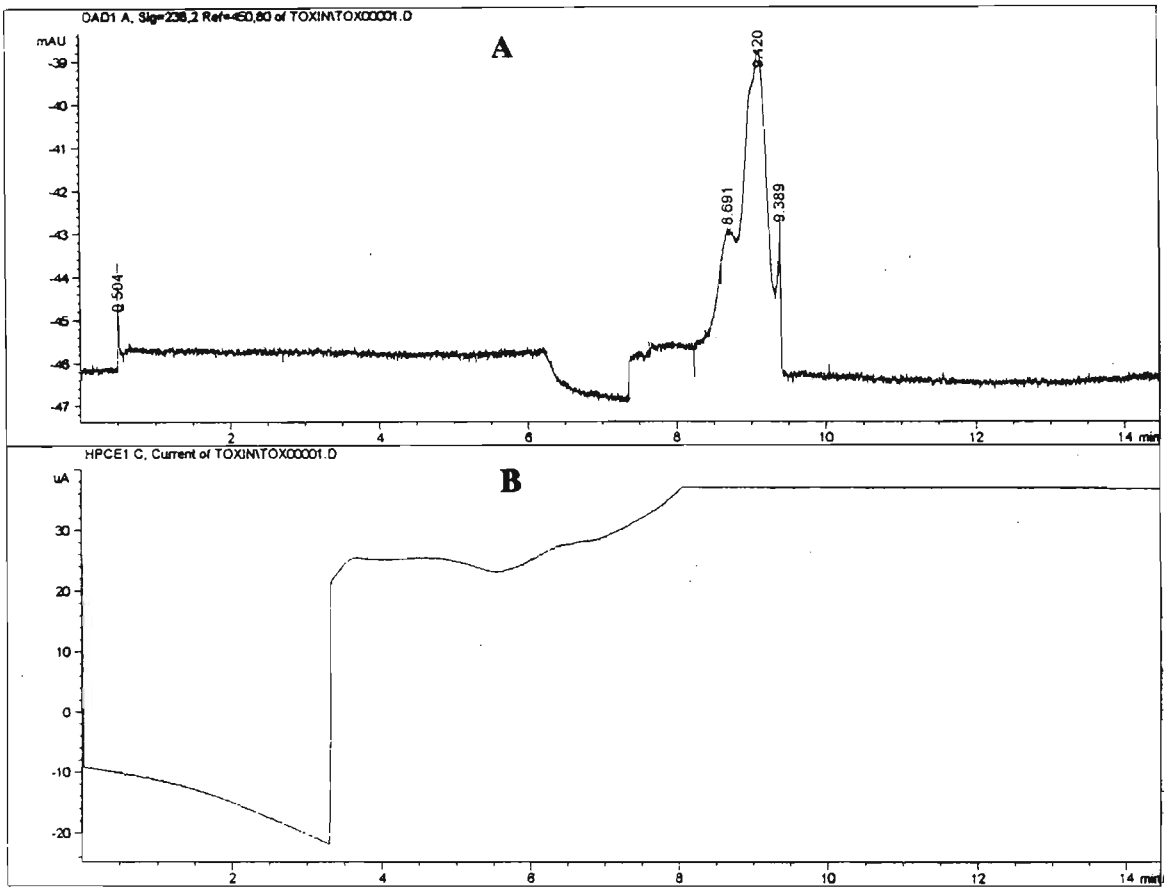

Figure 5.13 (A) Electropherogram of a 1 ng/μL toxin composite standard using field amplified back and forth MECC. The operating conditions: 30 mM borax; 9 mM SDS; 3 mM borax sample buffer; time zero -30 kV; time 3.3 minutes +30 kV; PVA coated column; L_T 64.5 cm; L_{EFF} 56 cm; 50 μm i.d.; PDA UV detection 200-300 nm and (B) The resulting electrophoresis current for the system in Figure 5.13A.

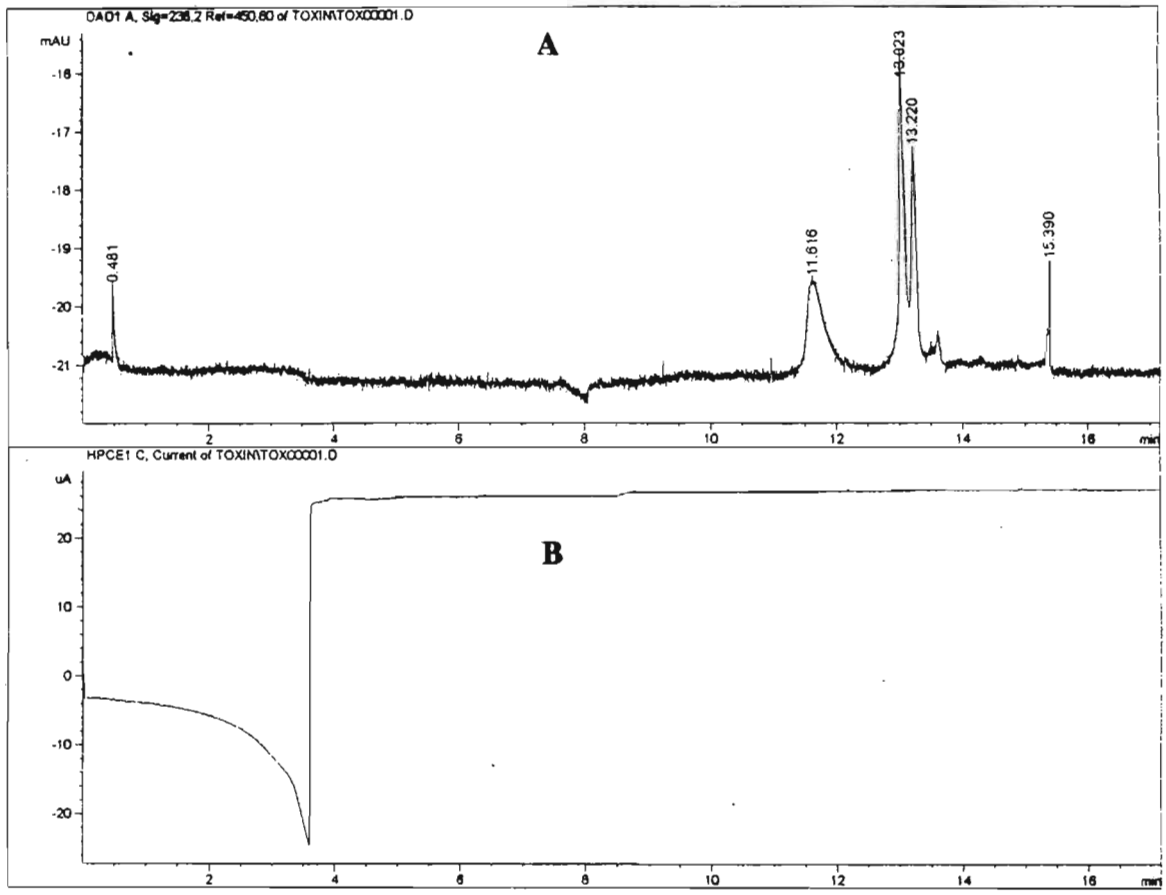

Figure 5.14A Electropherogram of a 1 ng/μL toxin composite standard with PDA UV detection at 200-300 nm. Operating conditions: time zero -30 kV; time 3.6 minutes +30 kV; the remaining parameters were as in Figure 5.13 and (B) The resulting electrophoresis current for the system in Figure 5.14A.

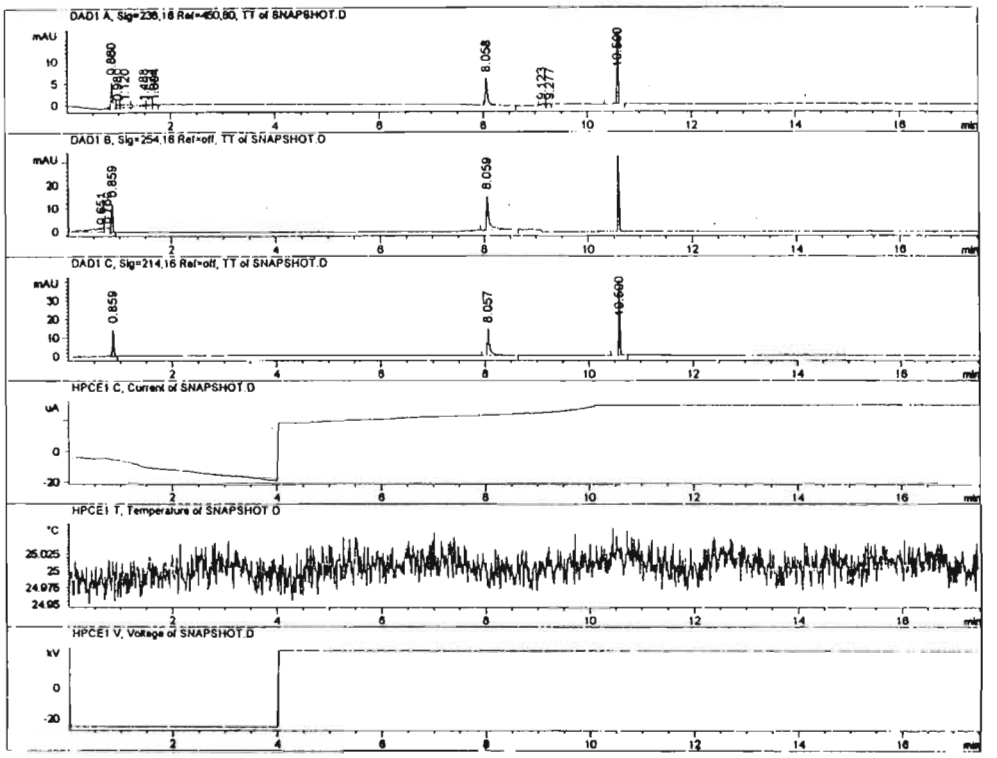

Figure 5.15 Electropherogram of nodularin and MC LR recorded at 238 nm, 254 nm and 214 nm. A recording of the current, temperature, and voltage is also provided. Operating conditions were as in Figure 5.14.

Under normal operation modes, rapid fluctuation in the current is indicative of excessive Joule heating that results in boiling of the solvent. In field amplification back and forth MECC, the current profile can be used as an indicator for polarity reversal. The current recording in Figure 5.13B, show that polarity reversal was executed too early as there is a further rise in the electrophoresis current until it reaches the stable plateau region. The impact of this can be seen by the poor resolution of the stacked analyte zone. In contrast, Figure 5.14B, shows a stable current reading after polarity reversal and this results in good resolution of components. Figure 5.15 illustrates the capability of the HP ^{3D}CE for performing photo diode array detection, monitoring of electrophoresis currents, monitoring of operating voltage and temperature recordings. The electropherogram was recorded at 238 nm, 254 nm and 214 nm. All three traces show similar intensity peaks. Both the recordings of electrophoresis current and operating voltage show good stability, verifying the absence of excessive Joule heating. The capillary column was air cooled and maintained at 25 ±0.05°C during these experiments.

5.3.4 *Field Amplified Sample Injection (FASI)*

Field amplified sample injection is a special case of electrokinetic injection in which the sample and run buffers are of different ionic strengths. Upon the application of a potential difference, the electric field strength in the low conductivity sample medium is higher than that in the run buffer. Solute can migrate rapidly to the interface between the lower and higher conductivity zones. Upon reaching the interface, the analytes then slow down causing contraction of the sample zone. The effectiveness of the stacking depends on the difference in ionic strengths of the run and sample buffers, electroosmotic flow velocity (v_{eo}) and the injection plug length. Conditions for stacking are as follows:

- v_{eo} is slow and in the same direction as v_{ep}, good stacking
- $v_{eo} = 0$, better stacking
- v_{eo} in opposite direction, best stacking
- $v_{eo} >> v_{ep}$, no stacking occurs if both effects are in the same direction

The last case applies to most countermigration separations including the cyanobacterial toxins and no injection takes place. With positive polarity, negatively charged ions will tend to migrate out of the injection end of the capillary. Reversing the polarity, causes anions to stack at the sample/buffer interface, however EOF immediately carries the anionic species out of the column. Hence the method is of little use to the algal toxins.

5.3.5 *Electro-extraction*

Electro-extraction is the third field amplification technique investigated. Using this technique, solute dissolved in water was extracted using an electric field and concentrated in a narrow band at the injection end of the column. Electroosmosis originating at the anodic end introduces a plug of high ionic strength run buffer into the column containing only sample buffer. At the interface of the two regions, electrophoresis tends toward zero and analyte stacking occurs. As the stacking proceeds, the local conductivity at the interface increases. The potential difference across this region is small and as a consequence, the field strength E is small. When the entire column is filled with run buffer, a band of analyte exists at the injection end. Separation of the extracted components was achieved under normal polarity conditions. Table 5.15 shows the detection limits achieved with this technique. Sensitivity enhancements recorded were 50.6 times for nodularin, 65.6 times for MC YR, 38.2 times for MC LR and 19.5 times for MC RR, when compared to hydrodynamic injections (Table 5.4). Figure 5.16 is a typical electropherogram of toxins stacked by electro-extraction. This procedure is similar to field amplification back and forth MECC except for the fact that the analyte is extracted from water using the electric field rather than being stacked from within the capillary column. A homogeneous buffer system is used. There is also a subtle difference to FASI that requires a discontinuous buffer system (dilute sample buffer and concentrated run buffer). In contrast, electro-extraction requires a normal buffer system with solute dissolved in water instead of sample buffer.

Table 5.15 Detection limit data based on peak heights, for electro-extractions

	Nodularin	MC YR	MC LR	MC RR	Mean
			Replicate 1		
Signal	8	18	13	5	
Noise	2	2.5	2.5	2	2.1
s/n	3.76	8.47	6.12	2.35	
			Replicate 2		
Signal	8	15	11	3	
Noise	2	2.5	2.5	2.5	2.4
s/n	3.33	6.25	4.58	1.25	
			Replicate 3		
Signal	8	20	14	5	
Noise	2.5	2	2.5	2.5	2.40
s/n	3.33	8.33	5.83	2.08	
			Replicate 4		
Signal	8	16	12	5	
Noise	2.5	2.5	2.5	2.5	2.5
s/n	3.20	6.40	4.80	2.00	
			Replicate 5		
Signal	8	18	14	4	
Noise	2.5	2.5	2.5	2.5	2.5
s/n	3.20	7.20	5.60	1.60	
mean s/n	3.38	7.33	5.39	1.86	

Detection Limit Calculations

$$LOD_{nodularin} = \frac{2}{3.38} \times 1\ ng/\mu L = 0.59\ ng/\mu L$$

$$LOD_{MC\ YR} = \frac{2}{7.33} \times 1\ ng/\mu L = 0.27\ ng/\mu L$$

$$LOD_{MC\ LR} = \frac{2}{5.39} \times 1\ ng/\mu L = 0.37\ ng/\mu L$$

$$LOD_{MC\ RR} = \frac{2}{1.86} \times 1\ ng/\mu L = 1.08\ ng/\mu L$$

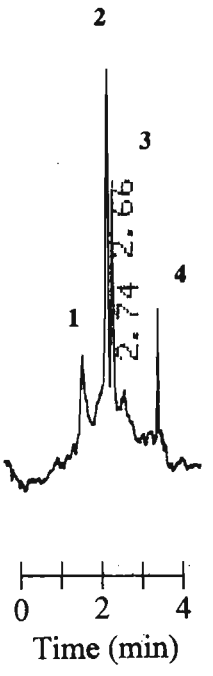

Figure 5.16 Electropherogram of a 1 ng/μL toxin solution using electro-extraction and UV detection at 238 nm. Extraction was carried out at -30 kV and separation was achieved at +30 kV. Peak identification: 1 Nodularin; 2 MC YR; 3 MC LR; 4 MC RR.

5.3.6 *On-Line Solid Phase Extraction*

Attempts at performing on-line solid phase extractions were complicated by technical problems. Firstly the cartridge comprised a 10 mm length of the packed capillary column prepared in section 3.17.4. Due to miniaturization, it was an extremely intricate task to insert frits on such a small section of capillary. Not only was it difficult to handle physically, the packing was often disrupted during fusion of the frits in the Bunsen flame. After numerous attempts, a solid phase cartridge was successfully fabricated. More problems were encountered with connecting the cartridge to the electrophoresis column. This was done by inserting the capillary column and cartridge into a Teflon sleeve that was cut from a length of tubing. Although the electrophoresis column and cartridge were secured into position with epoxy resin, there were problems associated with leakages resulting from pressurization of the system during solid phase conditioning and solid phase extraction (Figure 3.14). The extraction capacity of the preconcentration column was first

evaluated using pressure as the driving force. Initially a plug of methanol was introduced to activate the C_{18} solid sorbent, followed by a plug of water to remove the excess methanol. The toxins were then injected and allowed to concentrate on the solid. Run buffer containing 30 mM borax and 30 % (v/v) methanol was used as the elution solvent. A single peak was observed (Figure 5.17A), indicating that preconcentration of the solute was successful. It was thought that SDS that formed hydrophobic micelles would have the potential for eluting the toxins from the solid phase. Replacing methanol with SDS did indeed elute the toxins (Figure 5.17B). This was a very useful property of SDS, in that it could be used not only for improving selectivity in MECC, but also as the elution solvent. Borax buffer alone, however, did not elute toxins retained on the solid sorbent (Figure 5.17C).

On-line solid phase extraction was then repeated except electroosmosis was used as the driving force to elute the toxins, that was subsequently subjected to micellar electrokinetic capillary chromatography. Unfortunately, the Teflon sleeve joining the packed and electrophoresis columns formed a small non-conducting section in the capillary system and an electrophoresis current was never observed. This was verified by joining a piece of capillary tubing (50 mm x 50 μm i.d.) to the CE column. No current was observed when a potential difference was applied indicating that the Teflon sleeve was of no use as a capillary column connector. Ideally, the packed section should be part of the main CE column with no joins. Difficulty was experienced in fabricating frits within the column. Attempts to design a frit formation device with the resources available failed due to oxidation of a tungsten filament that was used as an electrical heating coil.

5.3.7 *Off-Line Solid Phase Extraction*

Trace toxin enrichment was achieved using a C_{18} solid-phase extraction cartridge. The successful extraction and elution of the solute species was dependent on numerous factors. After activation with methanol, the excess solvent was washed with water to prevent premature elution of solute. Extraction was performed immediately thereafter to prevent the sorbent from drying up. The sorbent was kept wet during the extraction by the presence of 1% (v/v) methanol in the sample. Thereafter, room air was drawn through the cartridge

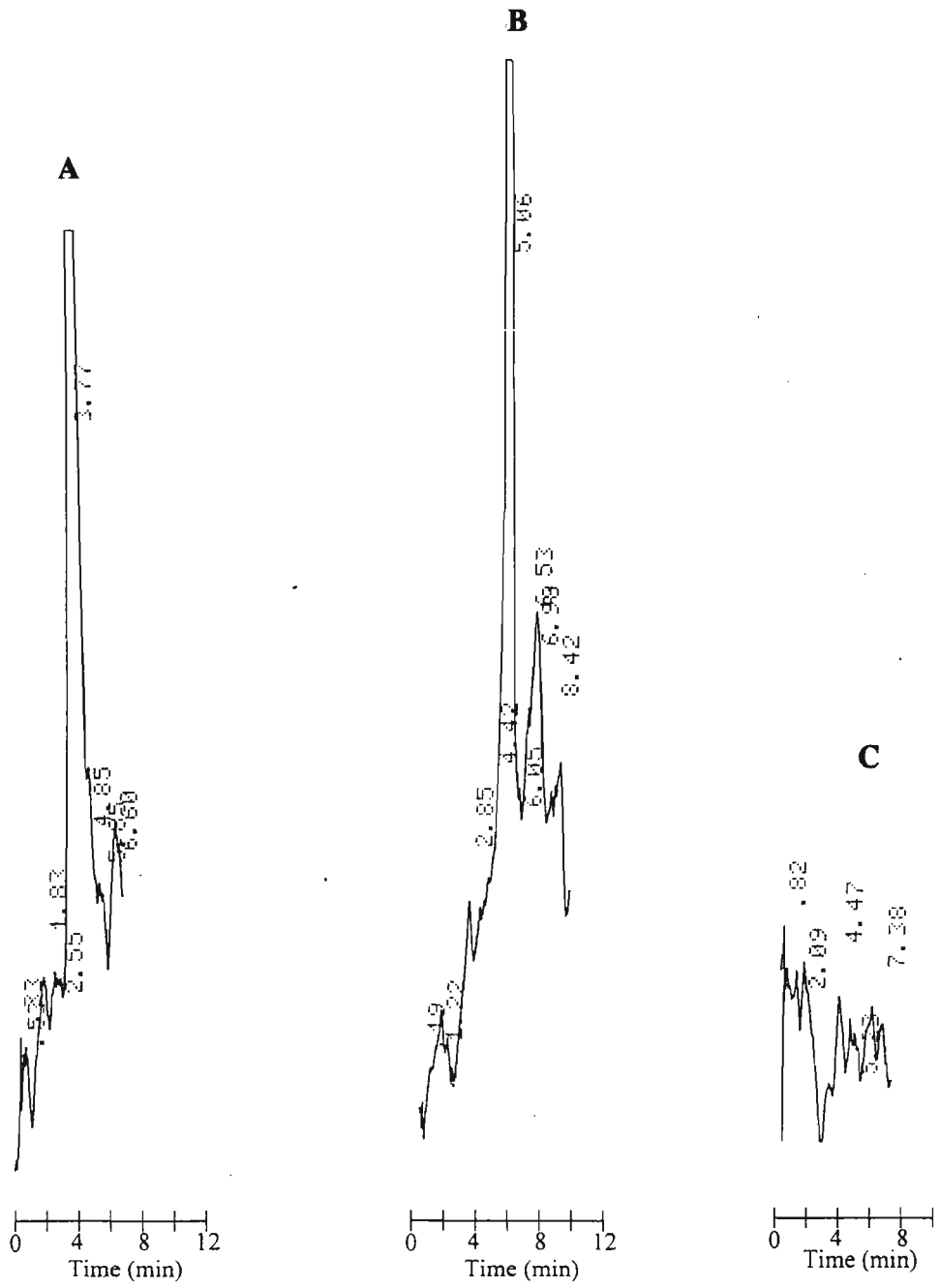

Figure 5.17 (A) Peak resulting from the elution of toxins trapped on the preconcentration column. Absorbance measurements were taken at 238 nm with the run buffer containing 30 % (v/v) methanol, (B) Peak resulting from the elution of toxins trapped on the preconcentration column. Absorbance measurements were taken at 238 nm with the run buffer containing 9 mM SDS instead of the methanol and (C) Trace resulting from elution of toxins from the solid sorbent with the run buffer containing 30 mM borax only.

for 15 minutes to remove the excess water. Elution was performed with 3 small aliquots of methanol rather than one large volume for a more efficient toxin recovery. The concentration detection limit based on Figure 5.18 was less than 0.002 ng/μL. The fact that the relative peak intensities are not consistent with Figure 4.12 suggests that the extraction efficiencies with which the individual toxins were recovered were not equal.

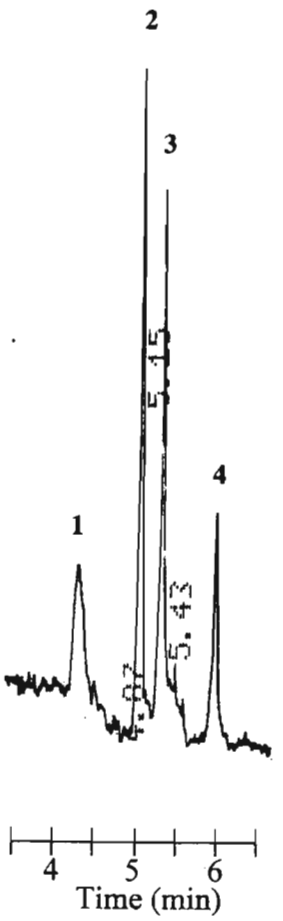

Figure 5.18 Electropherogram of a toxin composite standard after solid phase extraction from a water sample spiked with algal toxins to give a concentration of 0.002 ng/μL. Optimum hydrodynamic injection conditions as in Figure 4.12 were used. Peak identification: 1 Nodularin, 2 MC YR, 3 MC LR, 4 MC RR.

5.4 Alternative Detection

5.4.1 *Laser Induced Fluorescence (LIF)*

The use of high intensity light sources provides an alternative to extending the optical path length for sensitivity enhancement as they offer superior focusing capabilities, which allow the excitation energy to be more effectively applied to very small sample volumes [129,130,314,315]. Another useful feature of lasers is that they possess better monochromaticity which reduces stray light. Their limitation is that only a few wavelengths are available and there are possibilities of photodegradation of analytes caused by the high intensity light. Using LIF, detection limits as low as 1 to 2 zeptomoles (approximately 600 molecules) were reported by Dovichi *et al.* for derivatized amino acids [316]. Zare and co-workers were first to use LIF [169,170] and they achieved detection limits of 2 fmol for dansyl amino acids with the use of a He-Cd laser, while Jorgenson and co-workers were able to detect close to 1 attomol of FITC labelled amino acids [171]. Since the microcystin toxins under study do not possess intense native fluorescence, the FITC fluorophore was used in an attempt to derivatize the solutes. This fluorophore was selected because its excitation and emission wavelengths matched that of the argon ion laser of the electrophoresis system. FITC reacts with primary amines under alkaline conditions to form the fluorescein thiocarbamyl (FTC) derivatives as shown in Scheme 1.

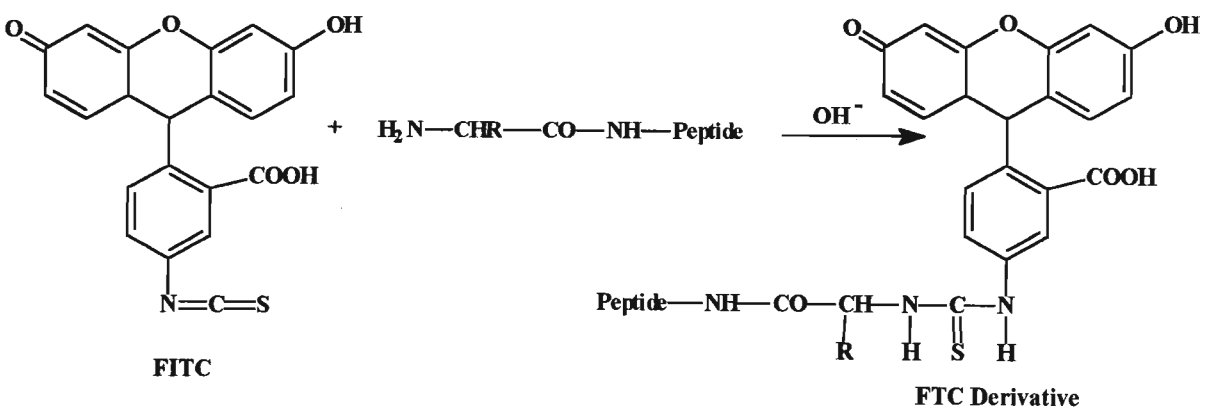

Scheme 1 The fluorescence derivatization reaction for the peptide toxins.

Reports from various publications demonstrate that FITC provides extremely good sensitivity for primary amines. Unfortunately however, the toxin derivatization reaction did not occur and a large artefact signal due to the free FITC was observed in the electropherogram (Figure 5.19). A plausible explanation for the failed reaction is that the free primary amine group on the toxin is in a sterically hindered position, thereby preventing the bulky FITC label from approaching the reaction site. This was concluded after the free amino acid arginine was subjected to the same derivatization conditions and analysed. The derivative formation was successful (Figure 5.20). Although other workers in the field of toxin analysis confirm our results [317], they are in direct conflict with that obtained by James *et al.*, who reported the successful derivatization of the microcystin toxins [49]. They, however attributed the low sensitivity of the method to the intense background fluorescence originating from the sample matrix. The fluorescamine derivatives produced by Wright *et al.* [64] were of a concentration (100 pg) easily detected by UV and therefore defeated the purpose of using LIF.

5.4.2 *Indirect Fluorescence*

Fluorescence detection can be used in an indirect format in which a fluorescent additive is combined with the buffer electrolyte. With this method, it is possible to broaden the applicability of these selective and sensitive detectors and can be used as a general detector. No derivatization or chemical manipulation is necessary, making quantification easier. The main disadvantage is that the linear dynamic range is limited. In this study FITC was added to the run buffer to create a high background fluorescence. By the mechanism of analyte or charge displacement of the fluorophore, a reduction in the background fluorescence and the production of a negative peak was anticipated. However, stability of the background fluorescence signal was extremely poor, causing low sensitivity with the result that no peaks could be detected at a toxin concentration of 1 ng/μL. LIF detection of toxins above this concentration was of little use since UV detection could quite easily be used. For this reason, all further fluorescence work was abandoned.

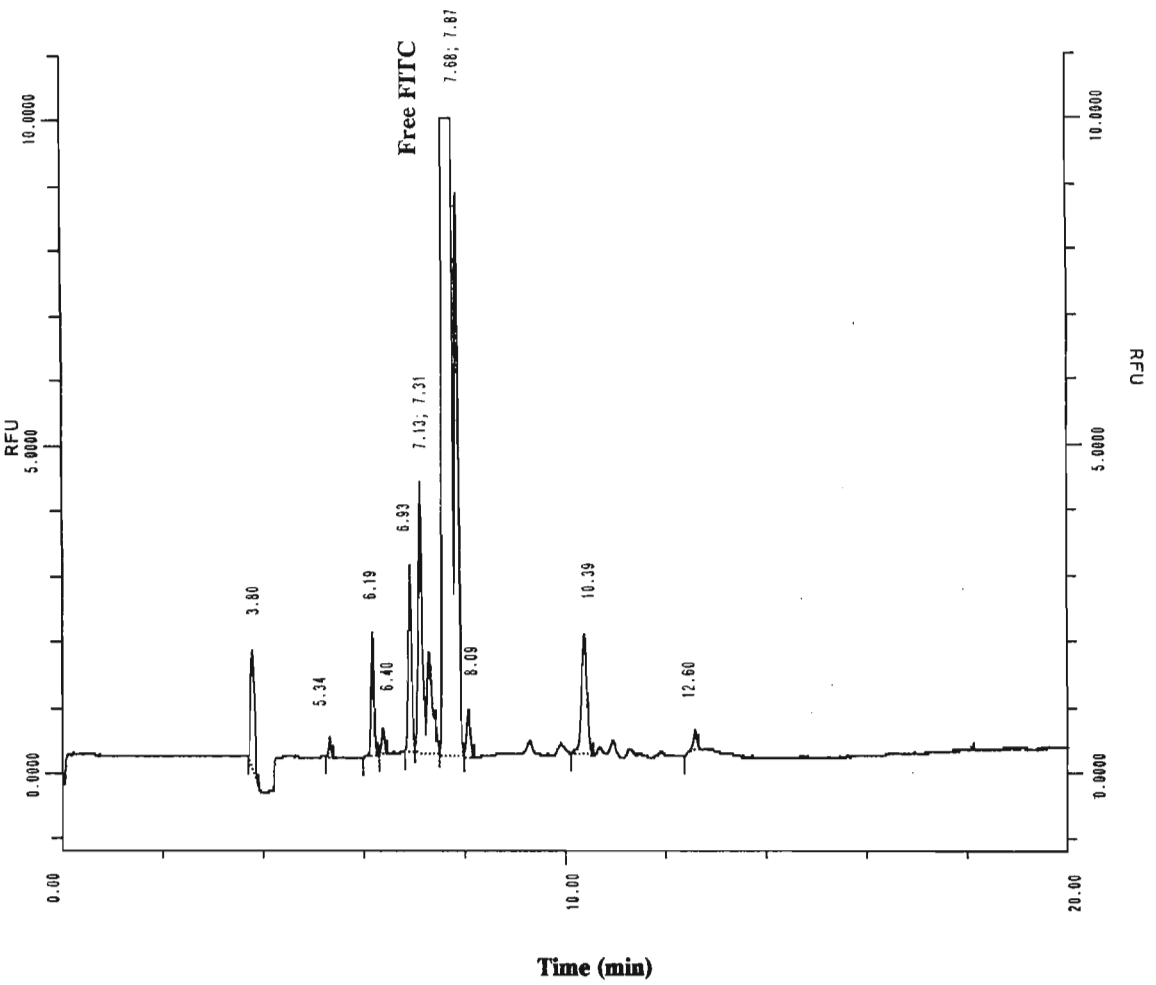

Figure 5.19 Electropherogram of a 1 ng/μL toxin composite standard after derivatization with FITC isomer 1. LIF detection was used with an excitation wavelength of 418 nm and an emission filter of 520 nm. Optimized electrophoresis conditions were used as described in Figure 5.3.

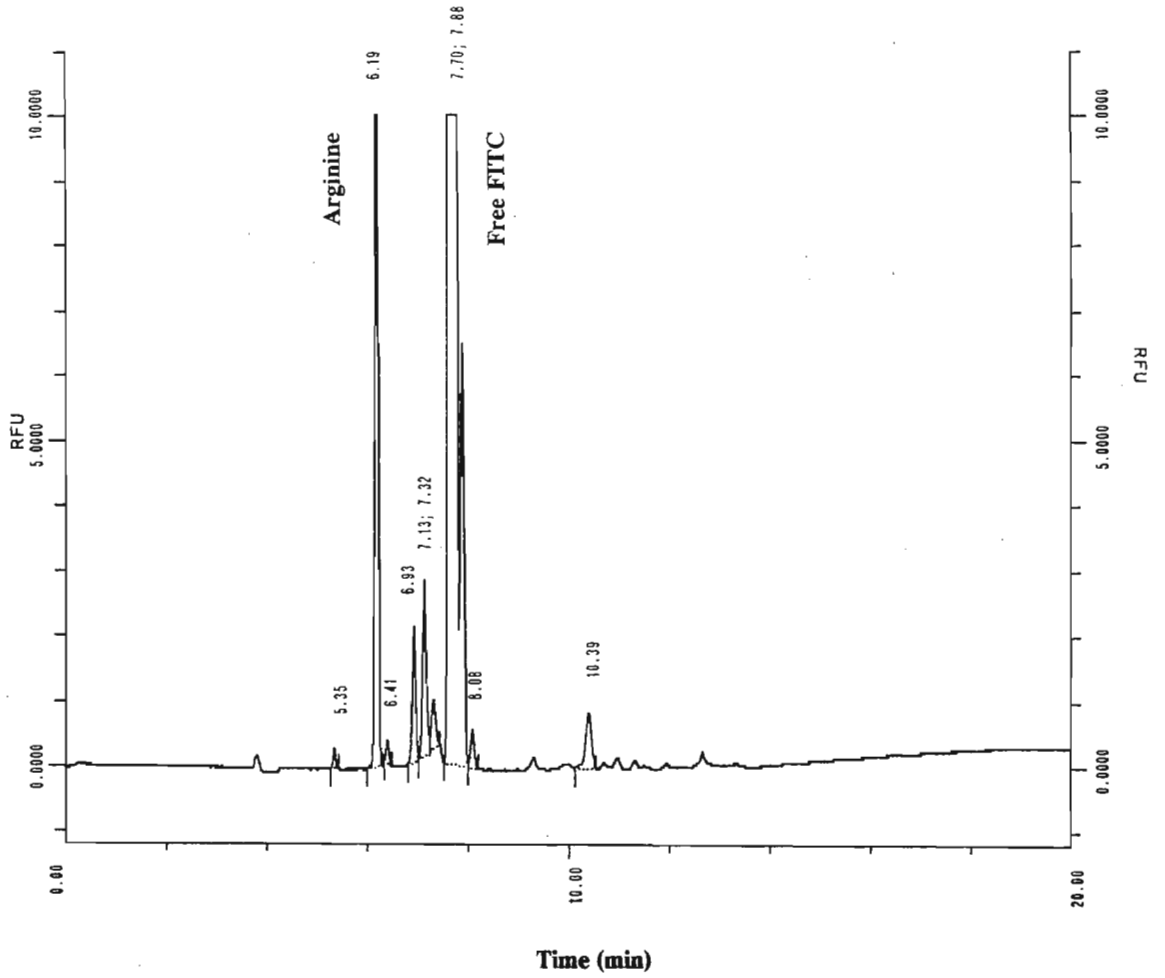

Figure 5.20 Electropherogram of arginine at a concentration of 1 ng/μL. Derivatization and detection were as in Figure 5.19.

5.5 Calibration and Quantitation

Quantitative analysis provides information about the concentration of a substance in a given sample. This information is obtained from peak height or peak area measurements. Quantitative methods employing MECC represent an area still in the development stages of the technique. However the separating power and the low mass detection limits are well researched and documented. The main concerns of the early investigators were with optimisation and evaluation of the advantages and disadvantages of the procedures. Only recently have the possibilities for quantitative applications been explored.

In contrast to chromatographic separation techniques, solute zones in CE migrate at a velocity given by the electrophoretic velocity of the solute and the electroosmotic velocity of the background electrolyte. This results in time related peak widths in an electropherogram that do not necessarily denote different zone volumes of analyte. To compensate for the influence of velocity variations, the concept of normalised peak areas (area/t_r), were introduced. Prior to collecting calibration data, the two injection modes studied previously were evaluated in terms of peak area and normalised peak area precision using a 100 ng/μL standard and experimental conditions as in Figure 5.8. Data for hydrodynamic injections (Table 5.16), show RSD values ranging from 83% to 97%, indicating poor precision. Hydrodynamic injections on the laboratory built system was a very tedious procedure and could not be controlled or reproduced easily (injection time and Δh). Although this is believed to be the main cause of the poor results, evaporation losses were another contributory factor since slight evaporation impacts significantly on the small sample volumes (10 μL) used. There is however no significant difference in the RSDs for peak area and normalised peak area, suggesting that migration time did not contribute significantly to peak areas. Electrokinetic injections (Table 5.17) produced much improved precision. The RSD values ranged from 11% to 18.7%. The improved precision over hydrodynamic injections can be attributed to better reproducibility of injections because injection voltage and time could be controlled precisely. In addition, there was no need to alter Δh. Both peak areas and normalised peak areas were not significantly different,

Table 5.16 Area precision data for hydrodynamic injections

	Nodularin	MC YR	MC LR	MC RR
Run 1				
t_r *(min)*	6.11	7.5	7.74	9.05
area	7075	9875	11371	14838
area/t_r	1158	1317	1469	1640
Run 2				
t_r *(min)*	5.59	6.75	6.95	8.01
area	19217	14889	16244	23483
area/t_r	3438	2206	2337	2932
Run 3				
t_r *(min)*	5.2	6.16	6.34	7.29
area	19978	14403	15144	23091
area/t_r	3842	2338	2389	3167
Run 4				
t_r *(min)*	5.18	6.18	6.38	7.41
area	5801	4121	5353	2272
area/t_r	1120	669	839	307
Run 5				
t_r *(min)*	5.6	6.75	6.96	8.04
area	2554	2655	3126	3914
area/t_r	456	393	449	487
Run 6				
t_r *(min)*	5.52	6.66	6.87	7.93
area	712	2757	3009	3680
area/t_r	129	414	438	464
Run 7				
t_r *(min)*	5.41	6.54	6.74	7.78
area	2896	3232	3933	4681
area/t_r	535	494	584	602
Run 8				
t_r *(min)*	5.34	6.43	6.64	7.61
area	5642	4285	6091	8530
area/t_r	1056	666	917	1120
Run 9				
t_r *(min)*	5.35	6.43	6.64	7.65
area	3535	4287	5551	7152
area/t_r	661	667	836	935

Table 5.16 Continued

Run 10				
t_r *(min)*	5.31	6.41	6.61	7.63
area	3511	4065	5187	7043
area/t_r	661	634	785	923
Run 11				
t_r *(min)*	5.42	6.53	6.73	7.78
area	5965	6100	7452	10113
area/t_r	1100	934	1107	1300
Run 12				
	Nodularin	**MC YR**	**MC LR**	**MC RR**
t_r *(min)*	5.33	6.41	6.61	7.58
area	2311	25870	29319	39961
area/t_r	434	4036	4436	5272
Mean Area	6600	8045	9315	12396
STDEV	6342	7082	7712	11238
%RSD	96	88	83	91
Mean Area/t_r	1216	1230	1382	1596
STDEV	1180	1102	1164	1481
%RSD	97	90	84	93

Table 5.17 Area precision data for electrokinetic injections at 2.5 kV for 5 s

	Nodularin	MC YR	MC LR	MC RR
Run 1				
t_r *(min)*	4.62	5.39	5.58	6.3
area	4147	4391	6346	5195
area/t_r	898	815	1137	825
Run 2				
t_r *(min)*	4.69	5.49	5.68	6.37
area	3636	3802	5341	4763
area/t_r	775	693	940	748
Run 3				
t_r *(min)*	4.75	5.66	5.89	6.81
area	3859	3907	4524	5075
area/t_r	812	690	768	745
Run 4				
t_r *(min)*	4.6	5.46	5.69	6.5
area	4993	5565	7532	7400
area/t_r	1085	1019	1324	1138
Run 5				
t_r *(min)*	4.55	5.34	5.55	6.3
area	3894	3948	5266	5709
area/t_r	856	739	949	906
Run 6				
t_r *(min)*	4.36	5.12	5.33	6.11
area	3819	4445	7170	6613
area/t_r	876	868	1345	1082
Run 7				
t_r *(min)*	4.45	5.23	5.43	6.21
area	4455	5679	7582	5935
area/t_r	1001	1086	1396	956
Run 8				
t_r *(min)*	4.49	5.3	5.51	6.29
area	4317	4073	5766	5455
area/t_r	961	768	1046	867
Run 9				
t_r *(min)*	4.46	5.25	5.45	6.22
area	3462	4368	5809	5604
area/t_r	776	832	1066	901

Table 5.17 Continued

Run 10				
t_r *(min)*	4.52	5.35	5.57	6.39
area	4255	4554	6684	6416
area/t_r	941	851	1200	1004
Run 11				
t_r *(min)*	4.57	5.38	5.59	6.44
area	4770	5474	8025	7291
area/t_r	1044	1017	1436	1132
Mean Area	4146	4564	6368	5951
STDEV	456.06	684.6	1146.24	880.75
%RSD	11	15	18	14.8
Mean Area/t_r	911	852	1146	937
STDEV	104.77	136.32	214.30	140.55
%RSD	11.5	16	18.7	15

suggesting once again that migration time did not affect peak areas to any measurable extent. Due to financial constraints, toxin standards could not be acquired in abundance and only hydrodynamic injections could be performed on the small volumes of the calibration standards (10 μL) that were available. Electrokinetic injections required a minimum volume of 100 μL so that both the column end and the respective electrode could be immersed in the standard solution during injections. Another problem with calibration and quantitation was that after an extensive literature search, a suitable internal standard could not be found. It was therefore decided to use one of the analytes as the internal standard. MC RR was chosen because this toxin was found infrequently in the various strains of blue-green algae in the Umgeni Water operational area. Although hydrodynamic injections produced poor area precision, as demonstrated by the RSD values, it was hoped that the internal standard would compensate for the poor reproducibility of injections. Three separate calibrations were performed. Calibration data are presented in Tables 5.18, 5.19, and 5.20. Based on MC RR as the internal standard, the average normalised peak area ratios were determined (Tables 5.18B, 5.19B and 5.20B). Linearity for the method calibration graphs are indicated by the correlation between increasing concentration and the corresponding change in the normalised peak areas. The calculated correlation coefficients, R^2 values and linear regression equations are shown in Table 5.21.

The calibrations embrace a very small range due to the limited availability of toxin solutions. It is for this reason that the linear dynamic range of the method was not established. This was deemed to be of little importance for this specific application since experience has shown that algal toxins were present in trace levels in the algal scums and toxin contaminated waters. From the results presented, it is quite clear that quantitative work is unacceptable. It is however anticipated that better quantitative work can be done with the use of an automated system.

Table 5.18A Calibration data for run 1

Std 100 ng/μL, Replicate 1				
	Nodularin	**MC YR**	**MC LR**	**MC RR**
Area	9736	8098	10330	29012
t_r	5.43	6.19	6.43	6.86
area/t_r	1793	1308	1607	4229
std/istd	0.42	0.31	0.38	
Replicate 2				
Area	4853	8103	11521	34854
t_r	4.89	6.02	6.26	6.69
area/t_r	992	1346	1840	5210
std/istd	0.19	0.26	0.35	
Replicate 3				
Area	11709	11503	15514	38485
t_r	5.33	6.08	6.33	6.79
area/t_r	2197	1892	2451	5668
std/istd	0.39	0.33	0.43	
Std 80 ng/μL, Replicate 1				
Area	6767	6388	8355	32287
t_r	5.61	6.38	6.63	7.08
area/t_r	1206	1001	1260	4560
std/istd	0.26	0.22	0.28	
Replicate 2				
Area	8282	4987	6679	32483
t_r	4.77	5.44	5.66	6.07
area/t_r	1736	917	1180	5351
std/istd	0.32	0.17	0.22	
Replicate 3				
Area	14105	10796	11919	42480
t_r	4.73	5.37	5.6	5.99
area/t_r	2982	2010	2128	7092
std/istd	0.42	0.28	0.30	
Std 60 ng/μL, Replicate 1				
Area	10415	4462	6515	33272
t_r	4.73	5.38	5.59	5.97
area/t_r	2202	829	1165	5573
std/istd	0.40	0.15	0.21	
Replicate 2				
Area	3676	2493	4317	27168
t_r	4.79	5.43	5.65	6.04
area/t_r	767	459	764	4498
std/istd	0.17	0.10	0.17	

Table 5.18A Continued

Replicate 3				
	Nodularin	**MC YR**	**MC LR**	**MC RR**
Area	3752	3513	5494	27330
t_r	4.83	5.47	5.68	6.07
area/t_r	777	642	967	4502
std/istd	0.17	0.14	0.21	
Std 40 ng/μL, Replicate 1				
Area	5391	5876	7688	53214
t_r	4.53	4.99	5.19	5.57
area/t_r	1190	1178	1481	9554
std/istd	0.12	0.12	0.16	
Replicate 2				
Area	172825	63607	61143	96325
t_r	4.27	4.85	5.05	5.45
area/t_r	40474	13115	12108	17674
std/istd	2.29	0.74	0.69	

Table 5.18B Mean area and amount ratios for the calibration run 1

Amnt Std/Amnt istd	**Area std /Area istd**		
	Nodularin	**MC YR**	**MC LR**
0.8	1.21	0.43	0.42
1.2	0.25	0.13	0.20
1.6	0.42	0.28	0.30
2	0.33	0.30	0.39

Table 5.19A Data for calibration run 2

Std 80 ng/μL, Replicate 1				
	Nodularin	**MC YR**	**MC LR**	**MC RR**
Area	8405	4351	5259	16167
t_r	5.46	6.01	6.17	6.42
area/t_r	1539	724	852	2518
std/istd	0.61	0.29	0.34	
Replicate 2				
Area	11426	5650	5937	15384
t_r	5.53	6.13	6.27	6.52
area/t_r	2066	922	947	2360
std/istd	0.88	0.39	0.40	
Replicate 3				
Area	16214	12101	9861	21833
t_r	5.63	6.19	6.37	6.63
area/t_r	2880	1955	1548	3293
std/istd	0.87	0.59	0.47	
Std 60 ng/μL, Replicate 1				
Area	7448	3978	4719	7864
t_r	5.63	6.23	6.39	6.66
area/t_r	1323	639	738	1181
std/istd	1.12	0.54	0.63	
Replicate 2				
Area	9812	4509	5948	9231
t_r	5.58	6.17	6.33	6.61
area/t_r	1758	731	940	1397
std/istd	1.26	0.52	0.67	
Replicate 3				
Area	8917	5011	6092	10465
t_r	5.73	6.34	6.5	6.77
area/t_r	1556	790	937	1546
std/istd	1.01	0.51	0.61	
Std 40 ng/μL, Replicate 1				
Area	5876	2496	2729	15480
t_r	5.69	6.3	6.46	6.74
area/t_r	1033	396	422	2297
std/istd	0.45	0.17	0.18	

Table 5.19A Continued

	Replicate 2			
	Nodularin	**MC YR**	**MC LR**	**MC RR**
Area	4322	2297	2700	14566
t_r	5.75	6.36	6.54	6.81
area/t_r	752	361	413	2139
std/istd	0.35	0.17	0.19	
		Replicate 3		
Area	5063	2874	3445	18140
t_r	5.65	6.25	6.43	6.72
area/t_r	896	460	536	2699
std/istd	0.33	0.17	0.20	

Table 5.19B Mean area and amount ratios for calibration run 2

Amnt std/Amnt istd	**Area std /Area istd**		
	Nodularin	**MC YR**	**MC LR**
1.2	0.38	0.17	0.19
1.6	1.13	0.53	0.63
2	0.79	0.42	0.40

Table 5.20A Data for calibration run 3

Std 100 ng/μL, Replicate 1				
	Nodularin	**MC YR**	**MC LR**	**MC RR**
Area	8048	4248	5783	6729
t_r	5.52	6.48	6.73	7.54
area/t_r	1458	656	859	892
std/istd	1.63	0.73	0.96	
Replicate 2				
Area	8096	4281	5514	6932
t_r	5.37	6.31	6.57	7.41
area/t_r	1508	678	839	935
std/istd	1.61	0.73	0.90	
Replicate 3				
Area	7557	3826	6002	7392
t_r	5.86	6.93	7.17	8
area/t_r	1290	552	837	924
std/istd	1.40	0.60	0.91	
Std 80 ng/μL, Replicate 1				
Area	5218	2550	3542	6049
t_r	5.63	6.59	6.84	7.63
area/t_r	927	387	518	793
std/istd	1.17	0.49	0.65	
Replicate 2				
Area	3724	3382	4636	8886
t_r	5.56	6.58	6.83	7.67
area/t_r	670	514	679	1159
std/istd	0.58	0.44	0.59	
Replicate 3				
Area	8892	5586	8362	15563
t_r	5.63	6.61	6.87	7.68
area/t_r	1579	845	1217	2026
std/istd	0.78	0.42	0.60	

Table 5.20A Continued

Std 60 ng/μL, Replicate 1				
Area	2093	2005	1988	4781
t_r	5.73	6.7	6.96	7.79
area/t_r	365	299	286	614
std/istd	0.60	0.49	0.47	
Replicate 2				
Area	4672	1886	2449	6529
t_r	5.65	6.66	6.91	7.73
area/t_r	827	283	354	845
std/istd	0.98	0.34	0.42	
Replicate 3				
	Nodularin	**MC YR**	**MC LR**	**MC RR**
Area	3447	2651	2864	9752
t_r	5.36	6.31	6.56	7.35
area/t_r	643	420	437	1327
std/istd	0.48	0.32	0.33	
Std 40 ng/μL, Replicate 1				
Area	1656	1218	1941	1955
t_r	5.28	6.34	6.59	7.4
area/t_r	314	192	295	264
std/istd	1.19	0.73	1.11	
Replicate 2				
Area	1839	1444	2183	7078
t_r	5.1	6.05	6.3	7.1
area/t_r	361	239	347	997
std/istd	0.36	0.24	0.35	
Replicate 3				
Area	1788	1759	1830	14756
t_r	5.52	6.05	6.29	7.03
area/t_r	324	291	291	2099
std/istd	0.15	0.14	0.14	

Table 5.20B Mean area and amount ratios for calibration run 3

Amnt std/Amnt istd	Area std / Area istd		
	Nodularin	**MC YR**	**MC LR**
0.8	0.57	0.37	0.53
1.2	0.69	0.38	0.40
1.6	0.84	0.45	0.61
2	1.55	0.69	0.92

Table 5.21 Regression statistics for calibration runs one to three

Run	Correlation Coefficient	R^2	Linear Regression Equation
		Nodularin	
1	0.7185	0.5163	y=-0.62x + 1.417
2	0.54595	0.2980	y=0.51x - 0.053
3	0.9108	0.8253	y=0.77x - 0.169
		MC YR	
1	0.2521	0.0636	y=-0.06x + 0.369
2	0.6776	0.4591	y=0.31x - 0.127
3	0.8906	0.7932	y=0.26x + 0.112
		MC LR	
1	0.01302	0.0002	y=0.0025x + 0.324
2	0.47711	0.2276	y=0.26x - 0.0133
3	0.8062	0.6499	y=0.34x + 0.132

5.6 Conclusions

Under optimised conditions of injection time and voltage, electrokinetic injections produced greater than an order of magnitude better sensitivity than hydrodynamic injections, with the exception of nodularin. Since the solutes had similar electrophoretic mobilities, no discrimination occurred during injections and this method of sample introduction was preferred. Additionally, the injections could be executed more reproducibly, giving improved area precision and better peak shapes. The use of field amplified back and forth MECC indicates that large sample volumes can be loaded on a CE column without causing serious deterioration of separation efficiency and loss of component resolution. Sensitivities were improved by over two orders of magnitude compared with hydrodynamic injections. Electro-extraction produced a 10 fold increase in detection sensitivity over hydrodynamic injections. Laser fluorescence detection was unsuccessful and this was attributed to the

stereochemistry of the toxins. FASI was also unsuccessful because of the negative charge on the toxins. Lastly, sample enrichment with the use of solid phase extraction technology provides a useful method for the analysis of trace level algal toxins by MECC. However, due to technical difficulties, the method could not be applied on-line.

Due to poor area precision with hydrodynamic injections, non linear calibration graphs were obtained, rendering this method of little use for quantitative work. This is in agreement with the work of previous researchers who compared quantitative work obtained from the laboratory system with that of the Beckman P/ACE 2000 system [318]. However the calibration graph for limonin glucoside and nomilinic acid glucoside showed better linearity than that obtained for the algal toxin study [318]. It is very likely that the quantitation problem, due to lack of automation, was compounded by the fact that the toxin standards were made up to a final volume of 10 μL and small changes in volume by evaporation resulted in significant changes in concentration.

Chapter Six

Comparative Study of HPLC, μHPLC, CEC and MECC for Algal Toxin Analysis

6.1 Introduction

This chapter deals with a comparative study of HPLC, μHPLC, CEC and MECC for the analysis of algal toxins. While HPLC is the established technique used routinely in the laboratory of the author, μHPLC, CEC and MECC are novel techniques for the separation of these toxins. Miniaturisation is a common feature in modern analytical science. The tremendous interest in microcolumn separations stems from the fact that there are numerous advantages, which include high column efficiencies, improved detector sensitivity, reduced flow rates, and the ability to work with smaller sample volumes and mobile phase volumes. These microcolumns provide a compromise between conventional packed and open tubular columns.

6.2 HPLC

A gradient HPLC programme (Table 3.3) recommended by researchers Lawton, Edward and Codd [62], was used to separate the 4 toxins. Figure 6.1 is a typical chromatogram obtained. Some features of this chromatogram are low peak capacity, column efficiency (peak width >1 minute), and resolution. Furthermore the total analysis time including column equilibration time is 60 minutes. The main reason for band spreading in HPLC arises as a direct consequence of its characteristic parabolic flow profile. In addition, large biomolecules such as the algal toxins under study possess low diffusion coefficients and result in an increase in the contribution to the resistance to mass transfer, and hence band spreading.

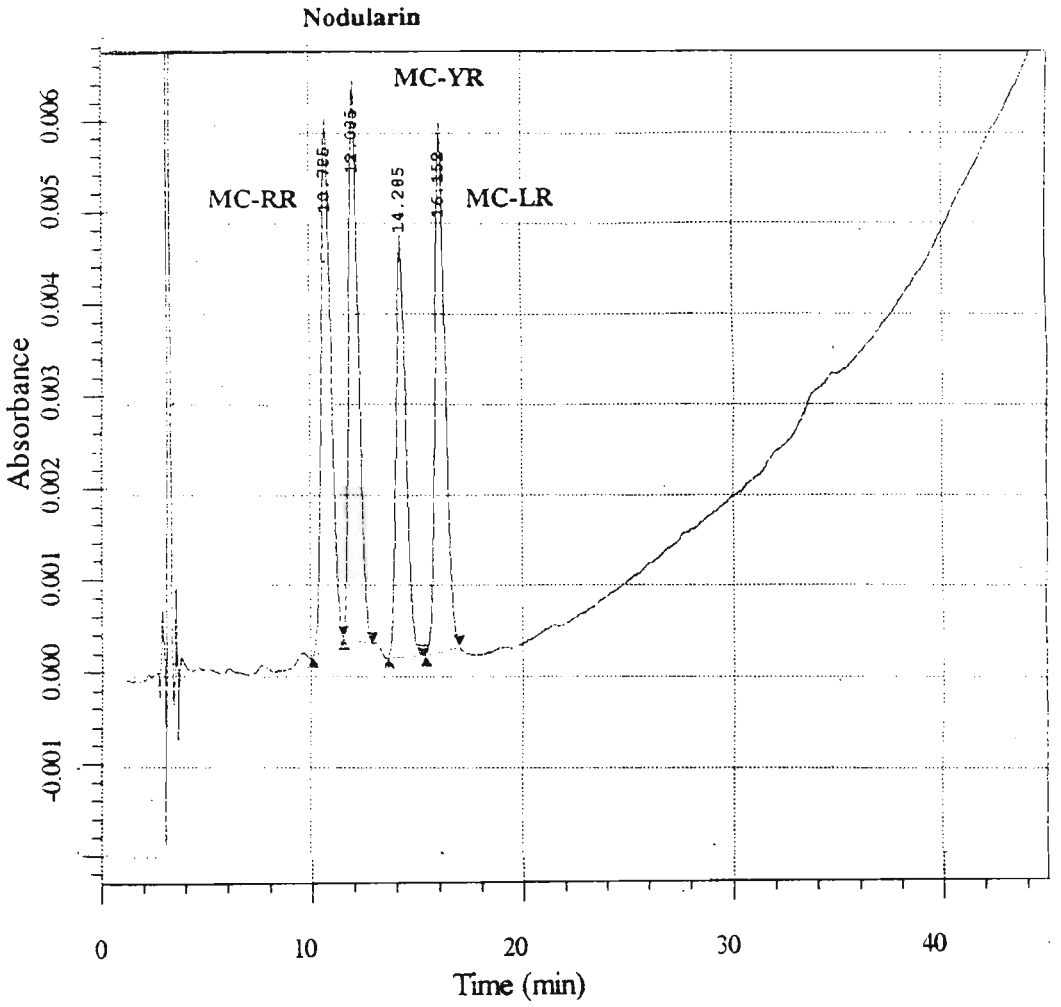

Figure 6.1 HPLC chromatogram of a 1 μg/L toxin composite standard acquired with PDA UV detection at a wavelength ranging from 200 to 400 nm. A 10 μL injection was used and a linear gradient as described in Table 3.3.

Retention time precision data in Table 6.1 indicate % RSDs ranging from 0.12 to 0.64. This shows better precision than that obtained with either injection modes in MECC and for both absolute and relative migration times (Tables 4.15 and 4.16). Both methods are of acceptable precision in terms of retention time reproducibility. Area precision (Table 6.2) was determined to range from 1.78 to 2.86 % RSD, making HPLC far superior to MECC for quantitative work using either injection technique (Tables 5.16 and 5.17), part of the problem being the lack of an automated sample introduction system on the laboratory built system. Peak efficiency under the recommended HPLC conditions (Table 6.3) ranged from 5470 plates for MC RR to 13186 plates for MC LR. MECC produces higher efficiency and shorter analysis times (Table 5.2 and 5.6). Resolution was calculated from Table 6.3.

Although adequate resolution between the toxins was achieved, problems with impurities eluting close to the analyte peak were anticipated as peak widths were of the order of about one minute. The concentration detection limit was found to range from 0.022 ng/μL to 0.041 ng/μL (Table 6.4), while MECC with hydrodynamic injection ranged from 14.13 to 29.85 ng/μL (Table 5.4) and electrokinetic injections, 1.42 ng/μL to 6.03 ng/μL (Table 5.11). The mass detection limits for a 25 μL injection ranged from 0.55 ng to 1.025 ng. Calculations for MECC mass detection limits based on a 10 nL electrokinetic injection volume ranged from 0.0142 to 0.0603 ng, indicating high mass detection sensitivity for this method. HPLC shows superiority in concentration sensitivity and is attributed to the high sample capacity to be loaded as well as a longer optical path length flow cell.

6.3 μHPLC

Most researchers produce columns by the slurry packing method. A number of problems associated with this technique have been highlighted particularly when packing small diameter tubes with small diameter particles, the main problems being the difficulty of packing reproducibly a column of consistent performance. In this study, the methodology developed by Bartle *et al.* on packing columns with supercritical fluid carbon dioxide (CO_2) as the carrier gas in the packing procedure was used [305]. The column prepared for use in electrochromatography and on-line solid phase extraction was first evaluated for performance using μHPLC. A typical chromatogram obtained with an isocratic run indicated incomplete resolution between the peak with a retention time of 6.93 and that with a retention time of 7.48 minutes (Figure 6.2). From a visual inspection of the peak profile, the MC RR peak at 22.02 minutes indicates poor efficiency. Due to the fact that the micro SFC/LC pump could not be used to perform gradient elution, peak efficiency and resolution could not be optimized. By increasing the strength of the mobile phase, the peak efficiency was enhanced, and the retention time decreased from 22.02 minutes to 13.82 minutes. However there was a decrease in the resolution of peaks 1, 2 and 3 (Figure 6.3). The results of this study revealed that the column had potential for use in electrochromatography. Although poor efficiency and resolution were observed with

Table 6.1 Retention time precision data for the HPLC analysis of algal toxins

	Retention Time (min)			
Replicate No.	**MC RR**	**Nodularin**	**MC YR**	**MC LR**
1	16.50	20.10	22.18	23.93
2	16.15	19.87	22.00	23.79
3	16.14	19.84	21.97	23.76
4	16.14	19.86	21.98	23.76
5	16.16	19.86	21.97	23.77
6	16.17	19.85	21.99	23.77
7	16.16	19.86	21.99	23.77
8	16.13	19.84	21.98	23.76
9	16.11	19.83	21.94	23.73
10	16.08	19.81	21.93	23.71
Mean	16.14	19.85	21.97	23.76
STDEV	0.029	0.018	0.021	0.024
RSD	0.12	0.18	0.1	0.64

Table 6.2 Area precision data for the HPLC analysis of algal toxins

	Area Counts			
Replicate No.	**MC RR**	**Nodularin**	**MC YR**	**MC LR**
1	33971	41322	35169	42522
2	31431	40129	33860	40656
3	32096	39735	32650	40183
4	31812	38993	33028	39254
5	33395	39200	34070	39336
6	32962	40301	33930	39651
7	31626	39705	33458	39609
8	33094	39841	33441	39105
9	32941	38920	33426	38268
10	33143	39545	33343	40004
Mean	32647	39769	33638	39859
STDEV	847.60	709.60	684.47	1140.07
RSD	2.60	1.78	2.03	2.86

Table 6.3 Peak efficiency and resolution data for the HPLC analysis of algal toxins

Replicate 1				
	MC RR	**Nodularin**	**MC YR**	**MC LR**
t_r *(min)*	16.5	20.1	22.183	23.933
W_b *(min)*	0.883	0.916	0.783	0.85
N	5587	7704	12842	12685
R	4.00	2.45	2.14	
Replicate 2				
t_r *(min)*	16.152	19.868	22.002	23.785
W_b *(min)*	0.85	0.95	0.783	0.834
N	5777	6998	12633	13014
R	4.13	2.46	2.21	
Replicate 3				
t_r *(min)*	16.14	19.84	21.973	23.757
W_b *(min)*	0.883	0.916	0.75	0.85
N	5346	7506	13733	12499
R	4.11	2.56	2.23	
Replicate 4				
t_r *(min)*	16.142	19.858	21.975	23.758
W_b *(min)*	0.884	0.917	0.75	0.817
N	5335	7503	13736	13530
R	4.13	2.54	2.28	
Replicate 5				
t_r *(min)*	16.155	19.855	21.972	23.772
W_b *(min)*	0.883	0.917	0.783	0.817
N	5356	7501	12599	13546
R	4.11	2.49	2.25	
Replicate 6				
t_r *(min)*	16.168	19.852	21.985	23.768
W_b *(min)*	0.883	0.95	0.767	0.816
N	5364	6987	13146	13575
R	4.02	2.48	2.25	
Replicate 7				
t_r *(min)*	16.155	19.855	21.988	23.772
W_b *(min)*	0.85	0.917	0.766	0.817
N	5780	7501	13184	13546
R	4.19	2.53	2.25	

Table 6.3 Continued

Replicate 8				
t_r *(min)*	16.125	19.842	21.975	23.758
W_b *(min)*	0.884	0.917	0.75	0.817
N	5324	7491	13736	13530
R	4.13	2.56	2.28	
Replicate 9				
t_r *(min)*	16.11	19.827	21.943	23.727
W_b *(min)*	0.867	0.916	0.783	0.817
N	5524	7496	12566	13495
R	4.17	2.49	2.23	
Replicate 10				
t_r *(min)*	16.075	19.808	21.925	23.708
W_b *(min)*	0.883	0.917	0.767	0.85
N	5303	7466	13074	12447
R	4.15	2.51	2.21	
Mean N	5470	7415	13125	13186
Mean R	4.11	2.51	2.23	

Table 6.4 Detection limit data for the HPLC analysis of algal toxins collected with a 0.2 ng/μL standard solution

			Replicate 1		
	MC RR	**Nodularin**	**MC YR**	**MC LR**	**Mean**
Signal	13	16	18	28	
Noise	2	1	1.2	1.8	1.5
s/n	8.67	10.67	12.00	18.67	
			Replicate 2		
Signal	14	16	17	25	
Noise	2	1	1.2	1.3	1.38
s/n	10.14	11.59	12.32	18.12	
			Replicate 3		
Signal	13	15	17	23	
Noise	2	1	1	1	1.25
s/n	10.40	12.00	13.60	18.40	
			Replicate 4		
Signal	13	16	17	25	
Noise	2	1	1	1	1.25
s/n	10.40	12.80	13.60	20.00	
			Replicate 5		
Signal	13	16	17	25	
Noise	2	1.5	1.5	1.2	1.55
s/n	8.39	10.32	10.97	16.13	
			Replicate 6		
Signal	13	16	17	24	
Noise	2	1	1	1	1.25
s/n	10.4	12.8	13.6	19.2	
Mean s/n	9.73	11.70	12.68	18.42	

Detection Limit Calculations

$$LOD_{MC\ RR} = \frac{2 \times 0.2}{9.73} = 0.041\ ng/\mu L$$

$$LOD_{NOD} = \frac{2 \times 0.2}{11.7} = 0.034\ ng/\mu L$$

$$LOD_{MC\ YR} = \frac{2 \times 0.2}{12.68} = 0.032\ ng/\mu L$$

$$LOD_{MC\ LR} = \frac{2 \times 0.2}{18.42} = 0.022\ ng/\mu L$$

μHPLC, it was hoped that CEC would help overcome this problem with the additional selectivity introduced by the interaction with a stationary phase. In addition, improved efficiency was anticipated since it is assumed that the flow profile is mixed Poiseuille and plug flow.

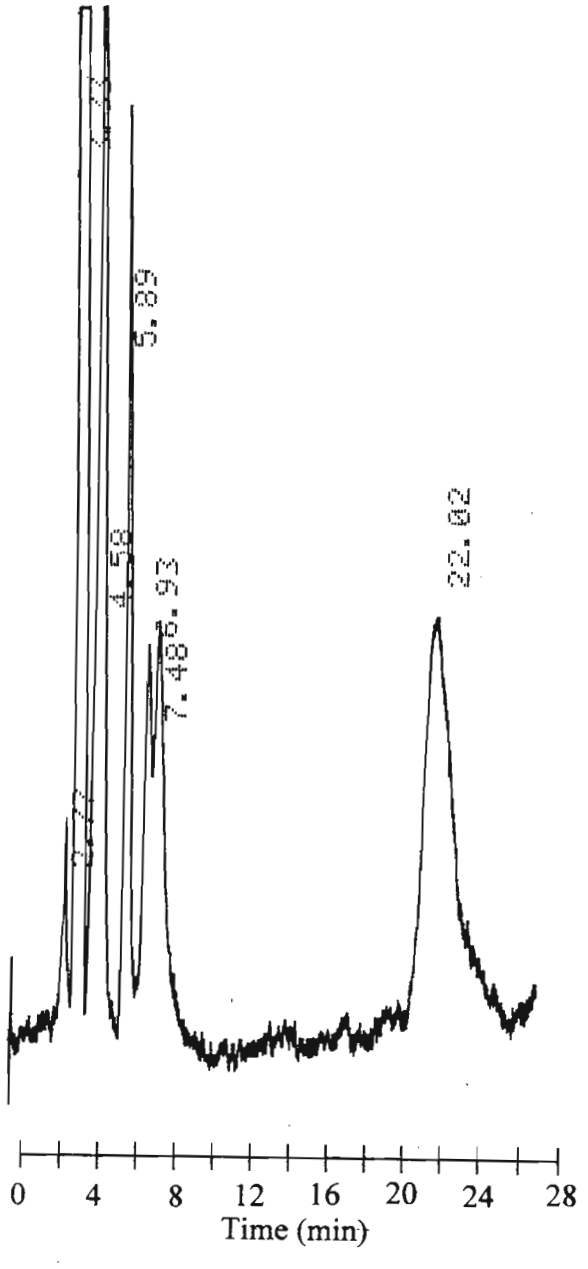

Figure 6.2 μHPLC chromatogram of a 50 ng/L toxin composite standard solution with UV detection at 238 nm. The mobile phase used contained 26% acetonitrile prepared in 0.1% ammonium acetate. The flow rate was 1 μL/minute at ambient temperature. Peak identification:- nodularin (5.89 minutes); MC LR (6.93 minutes); MC YR (7.48 minutes); MC RR (22.02 minutes) (see reference 306).

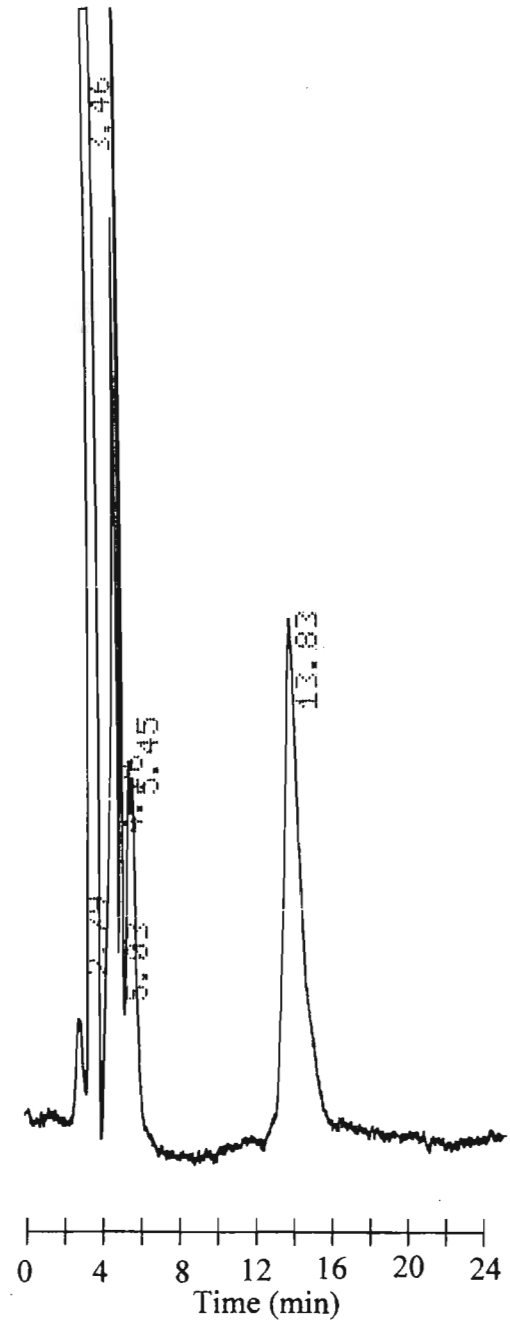

Figure 6.3 μHPLC chromatogram of a 50 ng/L toxin composite solution with UV detection at 238 nm. The mobile phase contained 35% acetonitrile prepared in 0.1% ammonium acetate. Peak identification: nodularin (4.76 minutes); MC LR (5.03 minutes); MC YR (5.45 minutes); MC RR (13.83 minutes).

6.4 CEC

CEC is a hybrid separation technique combining the stationary phase of HPLC with the electrolytically driven mobile phase transport of capillary electrophoresis. Separation is based both on electrophoretic processes and interactions with a stationary phase, such as adsorption, partition and gel permeation. The principle is in close analogy with conventional HPLC with packed columns, except the mobile phase is driven by electroosmosis rather than pressure. Unlike pressure driven systems, movement of the mobile phase through a packed CEC column is not subject to back pressure. This enables the use of longer columns and smaller diameter particles may be employed, producing enormously high efficiencies. A schematic representation of electrochromatography is shown in Figure 6.4. Solute partitioning occurs in the same way as in HPLC. Thus selectivity is identical for neutral analytes, but differs for ionic analytes due to additional electrophoretic migration. Yamamoto *et al.* reported 197000 plates per metre for a retained peak, using a 50 μm column packed with 3 μm Hypersil ODS particles [319]. Efficiencies of 370000 plates were obtained for a non retained peak, using a 50 μm column packed with 1.6 μm Monospher ODS particles. Knox and Grant [91] and Yan *et al.* [320] have demonstrated improved efficiencies in CEC in comparison with μHPLC. Smith and Evans [322] have observed very high plate numbers with CEC on columns packed with silica bonded with a strong cation exchanger. A variety of applications of CEC have been shown [323,324].

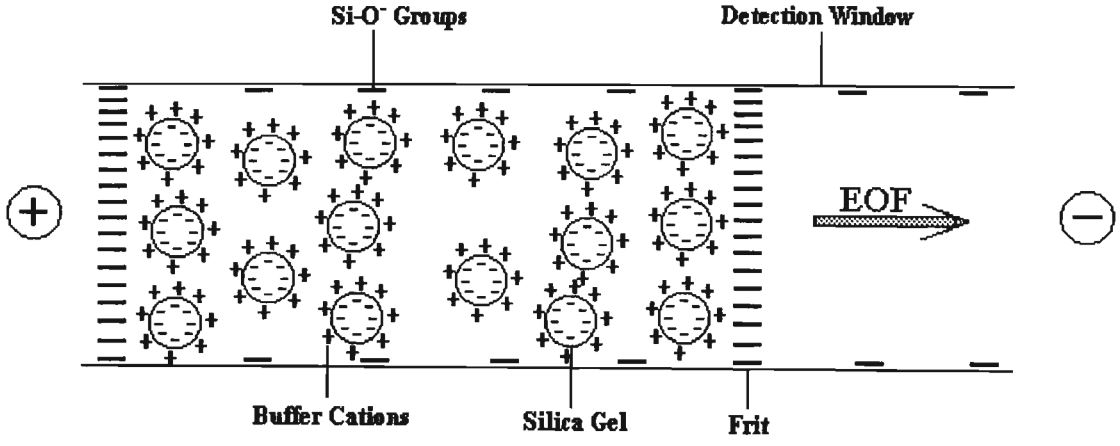

Figure 6.4 Schematic representation of CEC in capillaries packed with a stationary phase [321].

This study was performed to investigate the possible application of electrochromatography for the high resolution separation of algal toxins. The application of this method for the separation of toxins was plagued with technical problems such as columns breakages, frit fabrication, air bubble formation at the frit, and excessively high back pressure resulting from a homogeneous densely packed column using supercritical CO_2 at 350 atmospheres. Bubble formation in the column during electroseparation was the main cause of a failed separation. This was attributed to Joule heating as well as to the difference in pressure between the packed and unpacked regions of the capillary column, as suggested by Rebscher and Pyell [325]. The rate of bubble formation was found to increase with applied voltage because of a corresponding increase in Joule heating. While some researchers recommended the use of dilute buffers (<2 mM), others used a pressurized system for performing CEC without the risk of bubble formation. After the column had been equilibrated with mobile phase, the sample was injected. Thereafter the micro SFC/LC pump was stopped, and the system allowed to depressurize slowly to prevent rearrangement of the bed packing and damage to the frits.

CEC was carried out by removing the column from the injector and inserting it into the mobile phase (Figure 3.21). After the application of +30 kV, a current was observed briefly (1 minute) after which a section of the column began to dry up resulting in a breakage in the current.

6.5 CEC with Applied Pressure

CEC was then attempted with the application of pressure on either side of the column (Figure 3.22). This procedure resulted in the production and sustenance of a constant and stable current. However no peaks were detected, indicating that solute did not pass the detector but remained in the column. Tsuda *et al.* found that in electrochromatography, it was possible to retain a solute in a column during operation under pressurized flow if the velocity due to its mobility toward the inlet of the column was higher than that due to pressurized flow toward the outlet of the column [88]. This technique was used to preconcentrate solute in the column during a period of several injections to improve

detection sensitivity. To overcome the effect of solute retention, the pressure applied to the injection end of the column was increased, producing a net solute movement toward the outlet end of the column. Some degree of success was achieved with this method. Figures 6.5 and 6.6 show a peak for MC LR using μHPLC and CEC with applied pressure respectively. Purely by inspection of the electropherogram, it can be noticed that there was an improvement in peak symmetry and efficiency. However the problems of bubble formation were never completely resolved. A breakage in the current occurred after 6 minutes and this can be observed as spikes in the electropherogram.

Although CEC in packed columns is a developing technique that promises great potential in future chromatographic separations, it is difficult and less convenient. Jorgenson expressed doubt whether the performance increases in CEC would justify the increased technical difficulty experienced [84]. However, modern instrumentation equipped with automated features have certainly addressed a number of the problems, making CEC a more practical technique for routine work. A number of researchers have taken full advantage of this, with the result that numbers of publications in CEC are increasing. In fact researchers have proceeded a step further and attempted gradient elution in CEC. Zare *et al.* developed a system for delivering electroosmotically driven solvent gradients [326]. Dynamic gradients with nanolitre per minute flow rates were generated by merging two electroosmotic flows that were regulated by computer controlled voltages. This technique was used for the separation of 16 polycyclic aromatic hydrocarbons (PAHs). These researchers, however, point out clearly that to deliver such minute gradient flows into a capillary column is a delicate problem. In addition, due to changes in the electrophoresis buffer composition, fluctuations in the electrophoretic and electroosmotic mobilities occur, resulting in peak broadening.

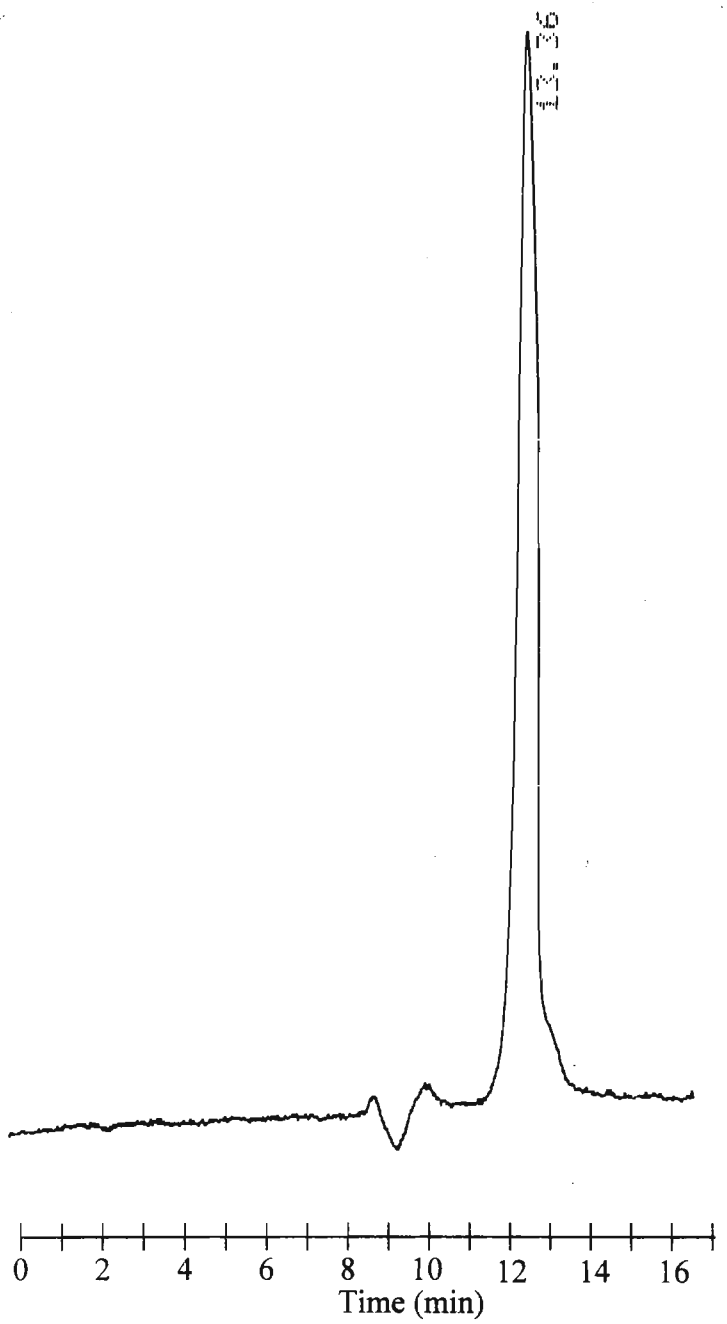

Figure 6.5 μHPLC chromatogram of a 100 ng/μL MC LR solution with UV detection at 238 nm. Operating conditions were identical to that in Figure 6.2.

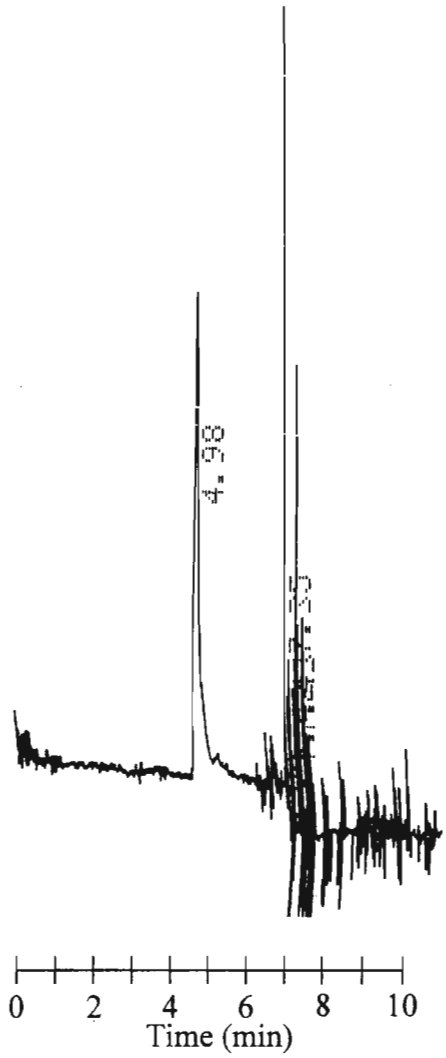

Figure 6.6 CEC electropherogram of 100 ng/μL MC LR solution with UV detection at 238 nm. The operating voltage was 20 kV and the mobile phase was the same as in Figure 6.2.

6.6 Conclusions

This study reveals that while HPLC is an established technique for the analysis of algal toxins, μHPLC, CEC and MECC are novel techniques that can also be used. The fundamental differences between HPLC and MECC are that the latter produces higher peak efficiency and shorter analysis times than the former. In terms of instrumentation, however, HPLC is equipped with automated features allowing sample injection times and

volumes to be precisely controlled. In HPLC, the volume of injected solution can be exactly measured while in MECC, there is no injection valve and the sample volume have to be determined by calculation. Additionally, with electrokinetic injections, the amount of sample introduced into the capillary is affected by injection voltage and time, whereas with the hydrodynamic injection mode, the injection amount is affected by the pressure differential across the capillary column as well as the injection time. These parameters were difficult to control on the laboratory built CE system and contributed to the poor peak area precision. Retention times in MECC also show lower precision than that obtained by HPLC. Performing manual injections was tedious and extremely difficult to reproduce. Furthermore, the electronic integrator had to be activated independently and manually, adding to the relatively low retention time precision. However with the use of modern day automated systems, it is anticipated that both retention time and peak area precision can be comparable to that achieved with HPLC. The concentration detection limit for HPLC is superior to MECC, while the reverse applies for the mass detection limits.

The use of μHPLC demonstrated that miniaturized packed columns have potential for algal toxin analysis. Efficiency and resolution was not optimized because of the lack of a gradient elution pump. CEC could not be used without pressure due to Joule heating and bubble formation. The technique is possible with applied pressure and exhibits higher efficiency than μHPLC. Once again, with the development of modern instrumentation, CEC has become a viable, highly efficient separation technique with enormous potential in analytical chemistry.

Chapter Seven

Concluding Remarks

Initial studies have shown that CZE lacked selectivity to sufficiently resolve the three microcystins from each other at basic pH. Attempts to optimize operating conditions had little effect on the resolution of these components. However, changing to MECC proved to be far superior for the analysis of the microcystins and nodularin. Operating conditions were systematically optimized and the best conditions (30 mM borax; 9 mM SDS; pH 9.18; 30 kV applied vlotage) produced adequate resolution, high efficiency peaks, and a short analysis time. The method was applied successfully to the analysis of algal toxins from a real sample containing algal scum.

Even though the problems associated with the HPLC analysis of algal toxins have been highlighted, the method was used for the verification of the results acquired by MECC. It is therefore important to note that the CE analysis of these compounds should be regarded as a complementary technique and not a replacement technique.

A number of researchers have dedicated their work to addressing what is thought to be the main limitation in CE; the poor detection sensitivity, and this study is no exception. Various approaches were evaluated and some remarkable sensitivity enhancements were recorded. In the simplest case, electrokinetic injections displayed approximately 20 times better sensitivity than hydrodynamic injections. Field amplification, a more complicated procedure, produced a sensitivity enhancement of up to 777 times compared with hydrodynamic injections. Attempts at tagging the toxins with a fluorescent moiety were unsuccessful and this was attributable to steric hindrance. This was rather unfortunate as a sensitivity enhancement of at least 3 orders of magnitude was anticipated with LIF detection, compared with UV detection. The results obtained for quantitative work on the laboratory built CE system were unsatisfactory and the instrument can therefore be recommended only for qualitative algal toxin analysis.

The final part of this project shows that even though HPLC has disadvantages for algal toxin analysis, it is an old and well established technique that offers superiority in terms of precision, accuracy and concentration detection sensitivity. The use of packed capillary columns, as in μHPLC and CEC, are potential new methods for the separation of algal toxins. However further work is required to refine the use of these techniques for algal toxin analysis particularly as regards to gradient elution.

On-line precolumn concentration with the use of reversed phase HPLC packing materials or polymeric membrane type materials, represents an area with scope for further development in improving CE detection limits. From the tremendous potential offered by CE with LIF detection, it may well be a very rewarding exercise to investigate fluorescence derivatization from a new perspective.

CE is clearly one of the most powerful separation methods ever developed and is rapidly establishing itself as a major instrumental technique. While exciting advances are being made rapidly in CE, the technique is still in a development and growth stage. One aspect that is still in need of improvement is concentration sensitivity, especially when CE is used in conjunction with commonly used on-column UV-VIS absorption detection. A tremendous amount of research has been done in addressing this problem. Special injection techniques using sample stacking and large volume injections were investigated by numerous researchers. Others preferred the use of on-line preconcentration by packing a bed of chromatographic material such as C_{18} or C_8 in a small section of the CE column or by incorporating an adsorptive membrane such as polymeric styrene divinylbenzene (SDB) in the CE column. Other areas of focus include temperature programming, pH gradient programming, gradient elution, voltage programming, EOF control by the application of an external field, analyte velocity modulation and pulsed field CE. Interesting developments have also been made in column technology. Capillaries coated with Chiral-Dex were used for the separation of enantiomers [336]. The preparation of fritless packed columns by radical copolymerization is also a concept that is being used by a few laboratories. The stationary phase is chemically bonded directly onto the capillary wall and this removes problems associated with the frit construction [327].

Other exciting and new advances made to date include the interfacing of a CE instrument to a Raman microprobe to form a CE/Raman detection system for the analysis of nucleosides and nucleotides [328]. Lee *et al.* describe the advances made in time of flight mass spectrometry that have made it possible for use in microcolumn separations [329]. Capillary electrophoresis inductively coupled plasma mass spectrometry (CE-ICP-MS) is another area of great interest. Olesik *et al.* used this technique for the speciation of a number of metals [330]. A final observation is the growing interest in microfabricated devices for performing CE. Several groups have reported the use of such microchip devices over the past few years [331-334]. These miniature devices have been shown to perform just as well as conventional CE equipment.

With the new developments rapidly being made, the future of CE is difficult to anticipate. As new research is presented, a greater knowledge and understanding of the strength as well as the limitations of the technique are acquired. CE is likely to become a principal tool in DNA sequencing and due to its great speed, may well play a crucial role in sequencing the human genome. The successes achieved so far in interfacing CE with mass spectrometers promise remarkable capabilities for unraveling the structures of complex macromolecules with unsurpassed speed, accuracy and sensitivity.

Reference List

1 G.A. Codd, W.C. Brooks, L.A. Lawton, K.A. Beattie, Watershed '89, *The Future for Water Quality in Europe*, ed. D. Wheeler, M.J. Richardson, J. Bridges, Pergamon Press, Oxford, UK, Vol. 2, 1989, p211.

2 W.E. Scott, *Water Sci, Technol.*, **23** (1991) 175.

3 W.W. Carmichael, I.R. Falconer, *Algal Toxins in Seafood and Drinking Water*, ed. I.R. Falconer, Academic Press, London, UK, 1993, p187.

4 M. Schwimmer, D. Schwimmer, *Algae, Man and the Environment*, ed. D.F. Jackson, Syracuse University Press, New York, USA, 1968, p279.

5 H. Utkileu, *Photosynthetic Prokaryotes*, ed. N.H. Mann, N.G. Carr, Plenum Press, New York, USA, 1992, p211.

6 H.D. Rodger, T. Turnbull, C. Edwards, G.A. Codd, *J. Fish Dis.*, **17** (1994) 177.

7 C. Edwards, K.A. Beattie, C.M. Schwimmer, G.A. Codd, *Toxicon*, **30** (1992) 1165.

8 S.G. Bell, G.A. Codd, *Rev. Med. Microbiol.*, **5** (1994) 256.

9 M.V. Veldee, *Am. J. Publ. Health*, **21** (1931) 1227.

10 P.C. Turner, A.J. Gammie, K. Hollinrake, G.A. Codd, *Br. Med. J.*, **300** (1990) 1440.

11 S.Z. Yu, Toxic Cyanobacteria: *Current Status of Research and Management*, Proceedings of an International Workshop, ed. D.A. Steffeesen, B.C. Nicholson, Australian Center for Water Quality Research, Adelaide, Australia, 1994

12 D.G. Steyn, *S. Afr. J. Sci.*, **41** (1945) 243.

13 E.L. Stevens, *Trans. R. Soc. Afr.*, **32** (1949) 105.

14 M. Pillay, *Water Quality Report No. 5*, Umgeni Water, Pietermaritzburg, South Africa, 1995, p12.

15 W. Carmichael, C.L.A. Jones, N.A. Mahmood, W.C. Theis, *CRC Crit. Rev. Envir. Control*, **15** (1985) 275.

16 W.M. Repavich, W.C. Sonzogni, J.H. Standridge, R.E. Wedepohl, L.F. Meisner, *Water Res.*, Vol. 24, **2** (1990) 225.

17 W. Carmicael, *Handbook of Natural Toxins, Marine Toxins and Venoms*, Vol. 3, Marcel Dekker Inc., New York, USA, 1988, p121-147.

18 D.P. Botes, A.A. Tuinman, P.L. Wessels, C.C. Viljoen, H. Kruger, D.H. Williams, S. Santikarn, R.J. Smith, S.J. Hammond, *J. Chem. Soc. Perkin Trans I*, 1984, 2311.

19 K. Harada, K. Ogawa, K. Matsuura, H. Nagai, H. Murata, M. Suzuki, Y. Itezono, N. Nakayama, M. Shirai, M. Nakano, *Toxicon*, **29** (1991) 479.

20 R. Luukainen, K. Sivonen, M. Namikoshi, M. Fardig, K.L. Rinehart, S.I. Niemela, *App. Environ. Microbiol.*, 59 (1993) 2204.

21 M. Namikoshi, K.L. Rinehart, R. Sakai, *J. Org. Chem.*, **57** (1992) 866.

22 D.P. Botes, H. Kruger, P.L. Wessels, M.T.C. Runnegar, S. Suntikarn, R.J. Smith, J.C.C. Barna, D.H. Williams, *J. Chem. Soc., Perkin Trans I,* 1985, 2747.

23 K.L. Rinehart, K.I. Harada, M. Namikoshi, C. Chen, C.A. Harvis, M.H.G. Munro, J.W. Blunt, P.E. Mulligan, V.R. Beasley, A.M. Dahlem, W.W. Carmichael, *J. Am. Chem. Soc.*, **110** (1988) 8557.

24 M. Namikoshi, K.L. Rinehart, R. Sakai, R.R. Stotts, A.M. Dahlem, V.R. Beasley, W.W. Carmichael, W.R. Evans, *J. Org. Chem.*, **57** (1992) 866.

25 M. Namikoshi, K. Sivonen, W.R. Evans, W.W. Carmichael, L. Rouhiainen, R. Luukkainen, K.L. Rinehart, *Chem. Res. Toxicol.*, **5** (1992) 661.

26 K. Sivonen, W.W. Carmichael, M. Namikoshi, K.L. Rinehart, A.M. Dahlem, S.I. Niemela, *Appl. Environ. Microbiol.*, **56** (1990) 2650

27 K. Sivonen, M. Namikoshi, K. Kononen, A.M. Dahlem, W.W. Carmichael, K. Kiviranta, S.I. Niemela, R. Luukkainen, K.L. Rinehart, *Appl. Environ. Microbiol.*, **55** (1989) 1990.

28 W.W. Carmichael, *J. Appl. Bacteriol.*, **72** (1992) 445.

29 M.F. Watanabe, S. Oishi, K. Harada, K. Matsuura, H. Kawai, M. Suzuki, *M. Toxicon*, **26** (1988) 1017.

30 I.R. Falconer, A.R.B. Jacson, J. Langley, M. Runnegar, T. Aust. *J. Biol. Sci.*, **34** (1981) 179.

31 A.M. Dahlem, *Ph.D Thesis*, University of Illinois, IL, USA, pp.135-148.

32 A.J. Van der Westhuizen, J. N. Eloff, G.H. Kruger, *South Afr. J. Bot.*, **54** (1988) 372.

33 J.N. Eloff, A.J. Van der Westhuizen, *The Water Environment, Algal Toxins and Health*, Plenum Press, New York, 1981, USA, pp.343-364.

34 R.E. Harris, P.R. Gorham, *Unpublished Data*, 1965, quoted in reference 45.

35 P. R. Gorham, *Algae and Man*, Plenum Press, New York, USA, 1964, pp.307-336.

36 P.J. Brown, *Ph.D Thesis*, Texas A&M University, College Station, TX, USA 1974.

37 M.T. Runnegar, I.R. Falconer, A.R. Jackson, A. McInnes, *Toxicon*, **3** (1983) 377.

38 A.J. Van der Westhuizen, *Ph.D Thesis*, University of Orange Free State, South Africa, 1984.

39 A.J. Van der Westhuizen, J.N.Z. Eloff, *Pflanzenphysiol.*, **110** (1983) 157.

40 A.J. Van der Westhuizen, J.N. Eloff, *Planta*, **163** (1985) 55.

41 A.J. Van der Westhuizen, J.N. Eloff, G.H. Kruger, *Arch. Hydrobiol.*, **108** (1986) 145.

42 M.F. Watanabe, S. Oishi, *Bull. Jpn. Soc. Sci. Fish.*, **49** (1983) 1759.

43 M.F. Watanabe, S. Oishi, *Appl. Environ. Microbiol.*, **49** (1985) 1342.

44 M.F. Watanabe, K. Harada, K. Matsuura, M. Suzuki, *J. Appl. Phycol.*, **1** (1989) 161.

45 R.J. Wicks, P.G. Thiel, *Environ. Technol.*, **24** (1990) 1413.

46 J.H. Hoffmann, *Water SA.*, **2** (1976) 58.

47 A.M. Keijola, K. Himberg, A.L. Esala, K. Sivonen, L. Hiisvirra, *Toxicity Assessment,* **3** (1988) 102.

48 K. Himberg, A.M. Keijola, L. Hiisvirta, H. Pyysalo, K. Sivonen, *Wat. Res.*, **23** (1989) 979.

49 H.A. James, C.P. James, J. Hart, *Detection Methods for Cyanobacterial Toxins*, WRC, Buckinghamshire, 1992, UK, pp.12.

50 W. Lampert, *Verh. Int. Verein, Limnol.*, **21** (1981) 1436.

51 L.A. Lawton, S.P. Hawser, K. Jamel Al-Layl, K.A. Beattie, C. MacKintosh, G.A. Codd, *Proc. 2nd Water Quality Symp.*, ed. G. Castillo, V. Ampos, L. Herrera, University of Santiago, Chile, 1990, pp.83.

52 W.R. DeMott, Q.X. Zhang, W.W. Carmichael, *Limnol. Oceanogr.*, **36** (1991) 1346.

53 L.A. Lawton, D.L. Cambell, K.A. Beattie, G.A. Codd, *Lett. Appl. Microbiol.*, **11** (1990) 205.

54 W.O.K. Gabow, W.C. DuRandt, O.W. Prozesky, W.E. Scott, *Appl. Environ. Bacteriol.*, **43** (1982) 225.

55 G.A. Codd, W.P. Brooks, I.M. Priestley, G.K. Poon, S.G. Bell, J.K. Fawell, *Toxic. Assess.*, **4** (1989) 499.

56 J.E. Eriksson, H. Hagerstrand, B. Isomaa, *Biochim, Biophys. Acta*, **930** (1987) 304.

57 K. Henning, H. Meyer, G. Kraatz-Wadsack, J. Cremer, *Curr. Microbiol.*, **25** (1992) 129.

58 C. MacKintosh, R.W. Mackintosh, *Detection Methods for Cyanobacterial Toxins*, ed. G. A. Codd, T.M. Jefferies, C.W. Keevil, E. Potter, Royal Society for Chemistry, Cambridge, UK, 1994, p90.

59 G.J. Jones, P.T. Orr, *Wat. Res.*, **28** (1994) 871.

60 F.S. Chu, X. Huang, R.D. Wei, *J. Assoc. Anal. Chem.*, **73** (1990) 451.

61 R.P. Gregson, R.R. Lohr, *Comp. Biochem. Physiol., C: Comp. Pharmacol. Toxicol.*, **74** (1983) 413.

62 L.A. Lawton, C. Edwards, G.A. Codd, *Analyst*, **119** (1994) 1525.

63 H. Liu, H. Siren, M.L. Riekkola, K. Sivonen, *Poster Presentation, Proc. 18th Int. Symp. Cap. Chromatogr.*, Riva del Garda, Italy, 20-24 May, 1996, Huthig, Germany.

64 B.W. Wright, G.A. Ross, R.D. Smith, *J. Micro. Sep.*, **1** (1989) 85.

65 W. Linder, V. Seidel, B. Bohs, *Chromatographia*, **41** (1995) 631.

66 H.A. James, C.P. James, *Report No.R0224, Foundation for Water Research*, Allen House, The Listons, Listons Road, Marlow, Buckinghamshire, UK, 1991.

67 K. Harada, K. Matsuura, M. Suzuki, H. Oka, M.F. Watanabe, S. Oishi, A.M. Dahlem, V.R. Beasley, W.W. Carmichael, *J. Chromatogr.*, **449** (1988) 275.

68 J. Vindevogel, P. Sandra, *Introduction to Micellar Electrokinetic Capillary Chromatography*, Huthig, Heidelberg, Germany, 1993, p31.

69 R. Kuhn, S. Hoffstetter-Kuhn, *Capillary Electrophoresis, Principles and Practice*, Springer-Verlag, Heidelberg, Germany, 1993, p24.

70 D.S. Stegehuis, H. Irth, U.R. Tjaden, J van der Greef, *J. Chromatogr.*, **538** (1991) 393.

71 M. Firestone, P. Michand, R. Carter, W. Thormann, *J. Chromatogr.*, **407** (1987) 363.

72 T. McDonnell, J. Pawliszyn, *J. Chromatogr.*, **559** (1991) 489.

73 T. Izumi, T. Nagahari, T. Okuyama, *J. High Resol. Chromatogr.*, **14** (1991) 351.

74 S. Maysushita, M. Sushita, I. Motooka, Y. Kanagi, *J. Chromatogr.*, **586** (1991) 363.

75 A.S. Cohen, B.L. Karger, *J. Chromatogr.*, **397** (1987) 409.

76 A.S. Cohen, A. Paulus, B.L. Karger, *Chromatographia*, **24** (1987) 14.

77 S. Hjerten, K. Elenbring, F. Kiler, J.L. Liao, A.J.C. Chen, C.J. Siebert, M.D. Zhu, *J. Chromatogr.*, **403** (1987) 1987.

78 J.R. Mazzeo, I.S. Krull, *Biotechniques*, **10** (1991) 638.

79 S. Hjerten, M.D. Zhu, *J. Chromatogr.*, **346** (1985) 265.

80 S. Hjerten, J.L. Liao, K. Yao, *J. Chromatogr.*, **387** (1987) 127.

81 J.R. Mazzeo, I.S. Krull, *Biotechniques*, **10** (1991) 638.

82 K.W. Yim, *J. Chromatogr.*, **559** (1991) 401.

83 V. Pretorius, B.J. Hopkins, J.D. Schieke, *J. Chromatogr.*, **99** (1974) 23.

84 J.W. Jorgenson, K.D. Lukacs, *J. Chromatogr.*, **218** (1981) 209.

85 S. Otsuka, L. Listowsky, *Anal. Biochem.*, **102** (1980) 419.

86 P.H. O'Farrell, *Science*, **227** (1985) 1586.

87 T. Tsuda, *Anal. Chem.*, **60** (1988) 1677.

88 T. Tsuda, Y. Muramatsu, *J. Chromatogr.*, **515** (1990) 645.

89 T. Tsuda, K. Nomura, G. Nakagawa, *J. Chromatogr.*, **248** (1982) 241.

90 W.D. Pfeffer, E.S. Yeung, *J. Chromatogr.*, **557** (1991) 317.

91 J.H. Knox, I.H. Grant, *Chromatographia*, **32** (1991) 317.

92 J.H. Knox, I.H. Grant, *Chromatographia*, **24** (1987) 135.

93 S. Terabe, K. Otsuka, K. Ichikawa, A. Tsuchiya, T. Ando, *Anal. Chem.*, **56** (1984) 111.

94 S. Terabe, K. Otsuka, T. Ando, *Anal. Chem.*, **57** (1985) 834.

95 R.S. Ramsey, G.A. Kerchner, *J. High Resol. Chromatogr.*, **17** (1994) 4.

96 K.H. Row, W.H. Griest, M.P. Maskarinec, *J. Chromatogr.*, **409** (1987) 193

97 A.F. Lecoq, C. Leuratti, E. Marafante, S. DiBiase, *J. High Resol. Chromatogr.*, **14** (1991) 667.

98 K. Otsuka, S. Terabe, T. Ando, *J. Chromatogr.*, **332** (1985) 219.

99 D.E. Burton, M.J. Sepaniak, M.P. Maskarinec, *J. Chromatogr. Sci.*, **25** (1987) 514.

100 T. Tsuda, *J. High Resol. Chromatogr.*, **10** (1987) 622.

101 J. Liu, K.A. Cobb, M. Novotny, *J. Chromatogr.*, **519** (1990) 189.

102 J. Vindevogel, P. Sandra, *J. High Resol. Chromatogr.*,**13** (1990) 295.

103 A. Loregian, C. Scremin, M. Schiavon, A. Marcello, G. Palu, *Anal. Chem.*, **66** (1984) 2981.

104 M.E. Swartz, *J. Liq. Chromatogr.*, **14** (1991) 923.

105 G.M. McLaughlin, J.A. Nolan, J.L. Lindahl, R.H. Palmieri, K.W. Anderson, S.C. Morris, J.A. Morrison, T.J. Bronzert, *J. Liq. Chromatogr.*, **15** (1992) 961.

106 J.A. Zweigenbaum, *Beckman Instruments, Technical Information,* Harbour Boulevard, CA, USA, DS-804, 1991.

107 D.F. Swaile, D.E. Burton, A.T. Balchunas, M.J. Sepaniak, *J. Chromatogr. Sci.*, **26** (1988) 406.

108 D. Lambert, C. Adjalla, F. Felden, S. Benhayoun, J.P. Nicholas, J.L. Gueant, *J. Chromatogr.*, **608** (1992) 311.

109 S. Fujiwara, S. Iwase, S. Honda, *J. Chromatogr.*, **447** (1988) 133.

110 S.F. Y. Li, Y.F. Yik, F.K. Lee, S.B. Khoo, *J. Chromatogr.*, **585** (1995) 139.

111 S.F.Y. Li, *Capillary Electrophoresis Principles, Practice and Applications, Journal of Chromatography Library*, Vol. 52, Elsevier, Amsterdam, The Netherlands, 1993, p31.

112 E. Grushka, R.M. McCormick, *J. Chromatogr.*, **471** (1989) 421.

113 M. Deml, F. Foret, P. Bocek, *J. Chromatogr.*, **320** (1985) 159.

114 J. Tehrani, R. Macomber, L. Day, *J. High Resol. Chromatogr.*, **14** (1991) 10.

115 T. Tsuda, T. Mizuma, J. Akiyama, *Anal. Chem.*, **59** (1987) 799.

116 T. Verheggen, J. Beckers, F. Everaerts, *J. Chromatogr.*, **452** (1988) 615.

117 R.A. Wallingford, A.G. Ewing, *Anal. Chem.*, **60** (1988) 1972.

118 R.A. Wallingford, A.G. Ewing, *Anal. Chem.*, **60** (1988) 678.

119 A.G. Ewing, R.A. Wallingford, T.M. Olefirowicz, *Anal. Chem.*, **61** (1989) 292A.

120 R.A. Wallingford, A.G. Ewing, *Adv. Chromatogr.*, **29** (1990) 1.

121 C.A. Monnig, D.M. Dohmeier, J.W. Jorgenson, *Anal. Chem.*, **63** (1991) 802.

122 F.E.P. Mikkers, F.M. Everaerts, T.P.E.M. Verheggen, *J. Chromatogr.*, **169** (1979) 1.

123 S.E. Moring, J.C. Colburn, P.D. Grossman, H.H. Laner, *LC-GC Intl.*, **3** (1990) 46.

124 R.L. Chien, D.S. Burgi, *Anal. Chem.*, **64** (1992) 489A.

125 X. Huang, M. Gordon, R.A. Zare, *Anal. Chem.*, **60** (1988) 375.

126 T. Wang, J.H. Aiken, C.W. Huie, R.A. Hartwick, *Anal. Chem.*, **14** (1991) 1372.

127 D.J. Rose, J.W. Jorgenson, *J. Chromatogr.*, **447** (1988) 117.

128 M. Albin, R. Weinberger, E. Sapp, S. Moring, *Anal. Chem.*, **63** (1991) 417.

129 S. Wu, N.J. Dovichi, *Talanta*, **39** (1992) 173.

130 S. Hjerten, *Chromatogr. Rev.*, **9** (1967) 122.

131 B.J. Herren, S.G. Shafer, J. van Alstine, J.M. Harris, R.S. Snyder, *J. Colloid Interface Sci.*, **115** (1987) 46.

132 S. Hjerten, *J. Chromatogr.*, **347** (1985) 191.

133 K.A. Kobb, V. Dolnik, M. Novotny, *Anal. Chem.*, **62** (1990) 2476.

134 R.M McCormick, *Anal. Chem.*, **60** (1988) 2322.

135 G.J.M. Bruin, J.P. Chang, R.H. Kihlman, K. Zegers, J.C. Kraak, H. Poppe, *J. Chromatogr.*, **471** (1988) 429.

136 R. Kuhn, S. Hoffstetter-Kuhn, *Capillary Electrophoresis, Principles and Practice*, Springer-Verlag, Heidelberg, Germany, 1993, p27.

137 K.A. Cobb, V. Dolnik, M. Novotny, *Anal. Chem.*, **62** (1990) 2478.

138 S. Hjerten, *J. Chromatogr.*, **270** (1983) 1.

139 G.M. Bruin, J.P. Chang, R.H. Kuhlmann, K. Zegers, J.C. Kraak, H. Poppe, *J. Chromatogr.*, **471** (1989) 429.

140 S.A. Swedberg, *Anal. Biochem.*, 5 (1990) 185.

141 M.M. Bushey, J.W. Jorgenson, *J. Chromatogr.*, **480** (1989) 301.

142 F.A. Chen, *J. Chromatogr.*, **559** (1991) 445.

143 S. Hjerten, *Arkiv. Kemi*, **13** (1958) 151.

144 J.E. Wiktorowicz, J.C. Colburn, *Electrophoresis*, **11** (1990) 769.

145 S. Hjerten, *J. Chromatogr.*, **347** (1985) 189.

146 A. Balchunas, M. Sepaniak, *Anal. Chem.*, **59** (1987) 1466.

147 S. Swedberg, *Anal. Biochem.*, **185** (1990) 51.

148 G. Bruin, R. Huisden, J. Kraak, H. Poppe, *J. Chromatogr.*, **480** (1989) 339.

149 Y.F. Maa, K. Hyver, S. Swedberg, *J. High Resol. Chromatogr.*, **14** (1991) 65.

150 F. Regnier, J. Towns, *J. Chromatogr.*, **516** (1990) 69.

151 D. Bentrop, J. Kohr, H. Engelhardt, *Chromatographia*, **32** (1991) 171.

152 R. Kuhn, S. Hoffstetter-Kuhn, *Capillary Electrophoresis, Principles and Practice*, Springer-Verlag, Heidelberg, Germany, 1993, p44.

153 J. Knox, *Chromatographia*, **26** (1988) 329.

154 R. Virtanen, *Acta Polytechnica Scand.*, **123** (1974) 1.

155 X. Huang, W.F. Coleman, R. Zare, *J. Chromatogr.*, **480** (1989) 95.

156 A. Vinther, H. Soeberg, *J. Chromatogr.*, **559** (1991) 3.

157 R. Kuhn, S. Hoffstetter-Kuhn, *Capillary Electrophoresis, Principles and Practice*, Springer-Verlag, Heidelberg, Germany, 1993, p53.

158 R. Kuhn, S. Hoffstetter-Kuhn, *Capillary Electrophoresis, Principles and Practice*, Springer-Verlag, Heidelberg, Germany, 1993, p63.

159 J. Colburn, B. Black, S.M. Chen, D. Demorest, J.W. Wiktorowicz, K. Wilson, *Applied Biosystems Research News*, Issue 1, 1990.

160 J.W. Jorgensons, *ASC Symp. Ser.*, **335** (1987) 182.

161 S. Hoffstetter-Kuhn, A. Paulus, E. Gassmann, H.M. Widmer, *Anal. Chem.*, **63** (1991) 1541.

162 J.W. Jorgenson, K.D. Lukacs, *Anal. Chem.*, **53** (1981) 1298.

163 J.W. Jorgenson, K.D. Lukacs, *Clin. Chem.*, **27** (1981) 1551.

164 J.W. Jorgenson, K.D. Lukacs, *J. Chromatogr.*, **218** (1982) 209.

165 A.S. Cohen, A. Paulus, B.L. Karger, *Chromatographia*, **24** (1987) 15.

166 Y. Walbroehl, J.W. Jorgenson, *J. Microcol.Sep.*, **1** (1989) 41.

167 J. Green, J.W. Jorgenson, *J. High Resol. Chromatogr.*, **7** (1984) 529.

168 E. Gassmann, J. Kuo, R. Zare, *Science*, **230** (1985) 813.

169 M. Roach, P. Gozel, R. Zare, *J. Chromatogr.*, **426** (1988) 129.

170 P. Gozel, E. Gassman, H. Michelson, R.N. Zare, *Anal.Chem.*, **59** (1987) 44.

171 J.W. Jorgenson, K.D. Lukacs, *HRC*, **4** (1981) 230.

172 P. Camilleri, G. Okafo, *J. Chromatogr.*, **541** (1991) 489.

173 C. Fujimoto, Y. Muramatsu, M. Suzuki, K. Jinno, *J. High Resol. Chromatogr.*, **14** (1991) 178.

174 Y. Kurosu, K. Hibi, T. Sasaski, M. Saito, *J. High Resol. Chromatogr*, **14** (1991) 186.

175 Y. Miyashita, S. Terabe, *Chromatographia*, **11** (1990) 6.

176 J. Liu, K. Cobb, M. Novotny, *J. Chromatogr.*, **468** (1988) 219.

177 K. Otsuka, S. Terabe, T. Ando, *J. Chromatogr.*, **332** (1985) 219.

178 H.E. Meyer, E. Hoffmann-Posorske, H. Korte, A. Donella-Deana, A.M. Brunati, L.A. Pinna, J. Coull, J. Perich, R.M. Valerio, R.B. Johns, *Chromatographia*, **30** (1990) 691.

179 K. Otsuka, S. Terabe, *J. Chromatogr.*, **515** (1990) 221.

180 R.T. Kennedy, M.D. Oates, B.R. Cooper, B. Nickerson, J.W. Jorgenson, *Science*, **246** (1989) 57.

181 B. Nickerson, J.W. Jorgenson, *J. High Resol. Chromatogr.*, **11** (1988) 533.

182 B. Nickerson, J.W. Jorgenson, *J. High Resol. Chromatogr.* , **11** (1988) 878.

183 M. Yu, N. Dovichi, *Anal. Chem.*, **61** (1989) 37.

184 M. Yu, N. Dovichi, *Microchim. Acta*, **111** (1988) 27.

185 M. Yu, N. Dovichi, *J. Appl. Spectrosc.*, **43** (1989) 146.

186 N.J. Dovichi, Y.F. Cheng, *Am. Biotechnol. Lab.*, **7** (1989) 196.

187 M. Albin, R. Weinberger, E. Sapp, S. Morig, *Anal. Chem.*, **63** (1991) 417.

188 D.S. Stegehuis, H. Irth, U.R. Tjaden, J van der Greef, *J. Chromatogr.*, **538** (1991) 393.

189 S. Pentoney, X. Huang, D. Burgi, R. Zare, *Anal. Chem.*, **60** (1988) 2625.

190 R. Wallingford, A.G. Ewing, *Anal. Chem.*, **59** (1987) 678.

191 L. Hernandez, R. Marquina, J. Escalona, N.A. Guzman, *J. Chromatogr.*, **502** (1990) 247.

192 J.T.K. Pang, D.J. Kramer, T.R.Tullsen, *Curr. Res. Protein Chem: Tech., Struct., Funct.*,. ed. J.J. Villafranca, Academic Press, San Diego, CA, USA, 1989, p11-22

193 K.A. Kobb, M. Novotny, *Anal. Chem.*, **61** (1989) 2226.

194 H. Ludi, E. Gassman, H. Grossenbacher, W. Marki, *Anal. Chim. Acta*, **213** (1988) 215.

195 P. Grossman, K. Wilson, G. Petrie, H. Lauer, *Anal. Biochem.*, **173** (1988) 265.

196 J.R. Florance, Z.D. Konteatis, M.J. Macielag, R.A. Lessor, A. Galdes, *J. Chromatogr.*, **559** (1991) 391.

197 A. Pessi, E. Bianchi, L. Chiappinelli, A. Nardi, S. Fanal, *J. Chromatogr.*, **557** (1991) 307.

198 F. Stover, B. Haymore, R. McBeath, *J. Chromatogr.*, **470** (1989) 241.

199 T. Satow, A. Mechida, K. Funakushi, R. Palmieri, *J. High Resol. Chromatogr.*, **14** (1991) 276.

200 A.D. Trans, T. Blanc, E.J. Leopold, *J. Chromatogr.*, **516** (1990) 241.

201 E. Leopold, L. Gouesclou, *Spectra 2000*, **156** (1991) 27.

202 R.D. Smith, J.A. Olivares, N.T. Nguyen, H.R. Udseth, *Anal. Chem.*, **60** (1988) 436.

203 E.D. Lee, W. Mueck, J. Henion, T. Covey, *Biomed. Environ. Mass Spectrom.*, **18** (1989) 844.

204 R. Smith, J. Loo, C. Barinaga, C. Edmonds, H. Udseth, *J. Chromatogr.*, **480** (1989) 211.

205 R.D. Smith, H.R. Udseth, C.J. Barinaga, C.G. Edmonds, *J. Chromatogr.*, **559** (1991) 197.

206 R.D. Smith, J.A. Loo, R.R.O. Loo, M. Busman, H.R. Udseth, *Mass Spectrom Rev.*, **10** (1991) 359.

207 M. Moseley, L. Deterding, K. Tomer, J. Jorgenson, *J. Chromatogr.*, **480** (1989) 197.

208 M.A. Mosley, L.J. Deterding, K.B. Tomer, J.W. Jorgenson, *Anal. Chem.*, **63** (1991) 109.

209 B.L. Karger, *Nature*, **339** (1989) 641.

210 W. Steuer, I. Grant, F. Erni, *J. Chromatogr.*, **507** (1990) 125.

211 J.R. Mazzeo, I.S. Krull, *Biotechniques*, **10** (1991) 638.

212 J. Green, J. Jorgenson, *J. Chromatogr.*, **478** (1989) 63.

213 L.Emmer, M. Jansson, J. Roeraade, *J. Chromatogr.*, **547** (1991) 544.

214 R. McCormick, *Anal. Chem.*, **60** (1988) 2322.

215 S. Hjerten, K. Elenbring, F. Killar, J. Liao, A. Chen, C. Siebert, M. Zhu, *J. Chromatogr.*, **403** (1987) 47.

216 S. Hjerten, M. Zhu, *Protides Biol.*, **33** (1985) 537.

217 P. Gebauer, W. Thormann, *J. Chromatogr.*, **558** (1991) 423.

218 W. Kuhr, *Anal. Chem.*, **62** (1990) 403R.

219 K.H. Row, W.H. Griest, M.P. Maskarinec, *J. Chromatogr.*, **409** (1987) 193.

220 J. Liu, J. Banks, M. Novotny, *J. Microcol. Sep.*, **1** (1989) 136.

221 S. Hjerten, *Nucleosid. Nucleot.*, **9** (1990) 319.

222 A. Cohen, D. Nagarian, A. Paulus, A. Guttman, J. Smith, B. Karger, *Proc. Natl. Acad. (USA)*, **85** (1988) 9660.

223 A. Paulus, J. Ohms, *J. Chromatogr.*, **507** (1990) 113.

224 A. Paulus, E. Gassmann, M.J. Field, *Electrophor.*, **11** (1990) 702.

225 J. Liu, M. Novotny, *J. Microcol. Sep.*, **1** (1989) 136.

226 R. Kuhn, S. Hoffstetter-Kuhn, *Capillary Electrophoresis, Principles and Practice*, Springer-Verlag, Heidelberg, Germany, 1993, p228.

227 S. Fujiwara, S. Honda, *Anal. Chem.*, **58** (1986) 1811.

228 S. Fujiwara, S. Honda, *Anal. Chem.*, **59** (1987) 2773.

229 S. Honda, K. Suzuki, M. Kataoka, A. Makino, K. Kakehi, *J. Chromatogr.*, **515** (1990) 653.

230 S.K. Yeo, H.K. Lee, S.F.Y. Li, *J. Chromatogr.*, **585** (1991) 133.

231 I. Snopek, H. Soini, M. Novotny, E. Smolkova-Keulemansova, I. Jelinek, *J. Chromatogr.*, **559** (1991) 215.

232 H. Nishi, M. Matsuo, *J. Liq. Chromatogr.*, **14** (1991) 973.

233 H. Nishi, T. Fukugama, M. Matsuo, S. Terabe, *J. Chromatogr.*, **513** (1990) 279.

234 W. Thormann, P. Meier, C. Marcolli, F. Binder, *J. Chromatogr.*, **545** (1991) 445.

235 T. Nakawa, Y. Oda, A. Shibukawa, H. Tanaka, *Chem. Pharm. Bull.*, **37** (1989) 707.

236 S. Hjerten, L. Valtcheva, K. Elenbring, D. Eaker, *J. Liq. Chromatogr.*, **12** (1989) 2471.

237 K. Salomon, D.S. Burgi, J.C. Helmer, *J. Chromatogr.*, **549** (1991) 375.

238 S. Fujiwara, S. Iwase, S. Honda, *J. Chromatogr.*, **447** (1988) 419.

239 I.M. Mutton, *Poster Presentation, HPCE '91*, San Diego, CA, USA, 3-6 February, 1991.

240 R. Weinberger, M. Albin, *J. Liq. Chromatogr.*, **14** (1991) 953.

241 N.A. Guzman, H. Ali, J. Moschera, K. Iqbal, A.W. Malick, *J. Chromatogr.*, **559** (1991) 307.

242 P.G. Pietta, P.L. Mauri, A. Rava, G. Sabbatini, *J. Chromatogr.*, **549** (1991) 123.

243 W.M. Hurni, W.J. Miller, *J. Chromatogr.*, **559** (1991) 337.

244 M.T. Ackermans, F.M. Everaerts, J.L. Beckers, *J. Chromatogr.*, **585** (1991) 123.

245 R. Weinberger, E. Sapp, S. Moring, *J. Chromatogr.*, **516** (1990) 271.

246 A. Wainwright, *J. Microcol. Sep.*, **2** (1990) 169.

247 T. Tsuda, Y. Kobayashi, A. Hori, T. Matsumoto, O. Suzuki, *J. Chromatogr.*, **456** (1988) 375.

248 H. Soini, T. Tsuda, M. Novotny, *J. Chromatogr.*, **559** (1991) 547.

249 K.D. Atria, C.E. Simpson, A.K. Bharij, A.E. Theobald, *Electrophor.*, **11** (1990) 732.

250 M.E. Swartz, *HPCE '91*, San Diego, CA, USA, 3-6 February, 1991.

251 S. Fanali, *J. Chromatogr.*, **470** (1989) 123.

252 C.P. Ong, C.L. Ng, H.K. Lee, S.F.Y. Li, *J. Chromatogr.*, **542** (1991) 473.

253 H. Swerdlow, R. Gesteland, *Nucl. Acid Res.*, **18** (1990) 1415.

254 A. Zhu, Y. Chen, *J. Chromatogr.*, **470** (1989) 251.

255 E. Jellum, A.K. Thorsrud, E. Time, *J. Chromatogr.*, **559** (1991) 455.

256 N.A. Guzman, M.A. Trebilcock, J.P. Advis, *J. Liq. Chromatogr.*, **14** (1991) 997.

257 F. Foret, S. Fanali, L. Ossicini, P. Bocek, *J. Chromatogr.*, **470** (1989) 299.

258 M. Deml, F. Foret, P. Bocek, *J. Chromatogr.*, **320** (1985) 159.

259 X. Huang, M.J. Gordon, R.N. Zare, *Anal. Chem.*, **60** (1988) 357.

260 X. Huang, M. Gordon, R. Zare, *J. Chromatogr.*, **425** (1988) 385.

261 T. Saitoh, H. Hoshino, T. Yotsuyanagi, *J. Chromatogr.*, **469** (1989) 175.

262 K. Saitoh, C. Kiyohara, N. Suzuki, *J. High Resol. Chromatogr.*, **14** (1991) 245.

263 S. Terabe, H. Ozaki, K. Otsuka, T. Ando, *J. Chromatogr.*, **332** (1985) 211.

264 S. Terabe, Y. Miyashita, O. Shibata, E.R. Barnhart, L.R. Alexandra, D.G. Paterson, B.L. Karger, K. Hosaya, N. Tanaka, *J. Chromatogr.*, **516** (1990) 23.

265 Y. Walbroehl, J. Jorgenson, *Anal. Chem.*, **58** (1986) 479.

266 G.J.M. Bruin, P.P.H. Tock, J.C. Kraak, H. Poppe, *J. Chromatogr.*, **517** (1990) 557.

267 R. Szucs, J. Vindevogel, P. Sandra, *J. High Resol. Chromatogr.*, **14** (1991) 692.

268 S. Hjerten, L. Valtcheva, K. Elenbring, D. Eaker, *J. Liq. Chromatogr.*, **12** (1989) 2471.

269 M.J. Gordon, X. Huang, L. Pentoney, R.N. Zare, *Science*, **242** (1988) 224.

270 X. Huang, R.N. Zare, S. Sloss, A.G. Ewing, *Anal. Chem.*, **63** (1991) 189.

271 S. Hjerten, *J. Chromatogr.*, **270** (1983) 1.

272 A.T. Balchunas, M.J. Sepaniak, *Anal. Chem.*, **60** (1988) 617.

273 M.J. Sepaniak, D.F. Swaile, A.C. Powell, R.O. Cole, *J. High Resol. Chromatogr.*, **13** (1990) 679.

274 A.C. Powell, M.J. Sepaniak, *J. Microcol. Sep.*, **2** (1990) 278.

275 S. Honda, S. Iwase, A. Makino, S. Fujiwara, *Anal. Biochem.*, **176** (1989) 72.

276 J. Liu, O. Shirota, M. Novotny, *Anal. Chem.*, **63** (1991) 223.

277 W. Nashabeh, Z. El Rassi, *J. Chromatogr.*, **536** (1991) 31..

278 D.R. Rose, J.W. Jorgenson, *J. Chromatogr.*, **447** (1988) 117.

279 J. Vindvogel, R. Szucs, P. Sandra, *J. High Resol. Chromatogr.* , **14** (1991) 584.

280 C.W. Earle, N.J. Dovichi, *J. Liq. Chromatogr.*, **12** (1989) 2575.

281 C.D. Gaitonde, P. Pathak, *J. Chromatogr.*, **514** (1990) 389.

282 C.P. Ong, C.L Ng, N.C. Chong, H.K. Lee, S.F.Y. Li, *J. Chromatogr.*, **516** (1990) 263.

283 Y.F. Yik, H.K. Lee, S.F.Y. Li, *J. High Resol. Chromatogr.* , **15** (1992) 198.

284 F. Foret, V. Sustacek, P. Bocek, *Electrophoresis.*, **11** (1990) 95.

285 B. VanOrmann, G. McIntire, *J. Microcol. Sep.*, **1** (1989) 289.

286 H.K. Jones, N.E. Ballou, *Anal. Chem.*, **62** (1990) 2484.

287 L.N. Amankwa, J. Scholl, W.G. Kuhr, *Anal. Chem.*, **62** (1990) 2189.

288 R.M. McCormick, *J. Liq. Chromatogr.*, **14** (1991) 939.

289 S. Honda, K. Suzuki, M. Kataoka, A. Makino, K. Kakehi, *J. Chromatogr.*, **515** (1990) 653.

290 P.G. Pietta, P.L. Mauri, A. Rava, G. Sabbatini, *J. Chromatogr.*, **549** (1991) 367.

291 C.P. Ong, C.L. Ng, H.K. Lee, S.F.Y. Li, *J. Chromatogr.*, **588** (1991) 335.

292 K. Otsuka, S. Terabe, *Jasco Rep.*, **33** (1991) 1.

293 K.O. Otsuka, S. Terabe, *Electrophor.*, **11** (1990) 982.

294 K. Otsuka, J. Kawahara, K. Takekawa, S. Terabe, *J. Chromatogr.*, **559** (1991) 209.

295 M. Verheggen, A.C. Schoots, F.M. Everaerts, *J. Chromatogr.*, **503** (1990) 245.

296 M.W.F. Nielen, *J. Chromatogr.*, **542** (1991) 173.

297 R.R. Chadwick, J.C. Hsieh, *Anal. Chem.*, **63** (1991) 2377.

298 M. Bushey, J. Jorgenson, *J. Microcol. Sep.*, **1** (1989) 125.

299 Y. Walbroehl, J. Jorgenson, *J. Chromatogr.*, **315** (1984) 135.

300 B. Wright, G. Ross, R. Smith, *Energy and Fuels*, **3** (1989) 428.

301 E.D. Lee, W. Mueck, J. Henion, T. Covey, *Biomed. Environ. Mass Spectrom.*, **18** (1989) 253.

302 *On-Column Capillary Cell Owner's Manual*, Linear Instruments Corporation, Nevada, USA, 1989.

303 J. Liu, O. Shirotu, M. Novotny, *Anal. Chem.*, **63** (1991) 413.

304 N.T. Dovichi, Y.F. Cheng, *Science*, **242** (1988) 562.

305 M.M Robson, S. Roulin, S.M. Shariff, M.W. Raynor, K.D. Bartle, A.A. Clifford, P. Myers, M.R. Euerby, C.M. Johnson, *Chromatographia*, 43 (1996) 313.

306 A. Ohtake, M. Shirai, T. Aida, N. Mari, K. Harada, K. Matsuura, M. Suzuki, M. Nakano, *Applied and Environmental Microbiology*, December 1989, 3202.

307 H. Issaq, I. Atamma, G. Muschik, G. Janini, *Chromatographia*, **32** (1991) 155.

308 J.S. Green, J.W. Jorgenson, *J. Chromatogr.*, **478** (1989) 63.

309 J. Vindevogel, P. Sandra, *Introduction to Micellar Electrokinetic Capillary Chromatography*, Huthig, Heidelberg, Germany, 1993, p39.

310 I.H. Grant, W. Steuer, *J. Microcol. Sep.*, 2 (1990) 74.

311 X. Xi, E.S. Yeung, *Appl. Spectrosc.*, 45 (1991) 1199.

312 J.P. Chevret, R.E.J. van Soest, M. Ursem, *J. Chromatogr.*, 543 (1991) 439.

313 Handbook on Capillaries, Reagents and Supplies for Capillary Electrophoresis, Hewlett Packard, Waldbronn, Germany, 1995.

314 S. Wu, N.J. Dovichi, *J. Chromatogr.*, 480 (1989) 141.

315 Y.F. Cheng, N.J. Dovichi, *Science*, 242 (1988) 562.

316 J.Z. Zhauh, D.Y. Chen, S. Wu, H.R. Harke, N.J. Dovichi, *Anal. Chem.*, 37 (1991) 1942.

317 E. Sydenam, Medical Research Institute, Tygerberg, South Africa, Personal Communication.

318 V.E. Moodley, M.Sc. Thesis, University of Natal, Durban, South Africa, 1995,

319 H. Yamamoto, J. Baunmann, F. Erni, *J. Chromatogr.*, **593** (1992) 313.

320 C. Yan, R. Dadoo, H. Zhao, R.N. Zare, D.J. Rakestraw, *Anal. Chem.*, **67** (1995) 2026.

321 R. Kuhn, S. Hoffstetter-Kuhn, *Capillary Electrophoresis, Principles and Practice*, Springer-Verlag, Heidelberg, Germany, 1993, p213.

322 N.W. Smith, M.B. Evans, *Chromatographia*, **41** (1995) 197.

323 N.W. Smith, M.B. Evans, *Chromatographia*, **38** (1994) 649.

324 S.J. Lane, R. Boughtflower, T. Underwood, *Rapid Comm. Mass Spec.*, **9** (1995) 1288.

325 H. Rebscher, U. Pyell, *Chromatographia*, **38** (1994) 737

326 R.N. Zare, C. Yan, R. Dadoo, D.J. Rakestraw, D.S. Anex, *Anal. Chem.*, 68 (1996) 2726.

327 C. Fujimoto, Y. Fujise, E. Matsuzawa, *Anal. Chem.*, **68** (1996) 2753.

328 M.D. Morris, P.A. Walker, J.M. Shaver, H.M. Li, *Proc. 19th Int. Symp. Capillary Chromatography and Electrophoresis*, Wintergreen, Virginia, USA, 18-22 May, 1997, p128.

329 E.D. Lee, A.L. Rockwood, J.P. Fabbi, J.C.H. Sin, J. Jones, C. Ogden, H. Tolley, H.G. Lee, *Proc. 19th Int. Symp. Capillary Chromatography and Electrophoresis*, Wintergreen, Virginia, USA, 18-22 May, 1997, p124.

330 J.W. Olesik, J.A. Kinzer, E.J. Grunwald, *Proc. 19th Int. Symp. Capillary Chromatography and Electrophoresis*, Wintergreen, Virginia, USA, 18-22 May, 1997, p120.

331 S.C. Jacobson, R. Hergenroder, L.B. Koutny, R.J. Warmack, J.M. Ramsey, *Anal. Chem.*, **66** (1994) 1107.

332 S.C. Jacobson, R. Hergenroder, L.B. Koutny, J.M. Ramsey, *Anal. Chem.*, **66** (1994) 1114.

333 S.C. Jacobson, A.W. Moore, J.M. Ramsey, *Anal. Chem.*, **67** (1995) 2059.

334 S.C. Jacobson, J.M. Ramsey, *Electrophoresis*, **16** (1995) 481.

335 Handbook on Capillaries, Reagents and Supplies for Capillary Electrophoresis, Hewlett Packard, Waldbronn, Germany, 1996.

336 J. Snopek, I. Jelink, E. Smolkova, J. Chromatogr., 609 (1992) 1.

APPENDIX A

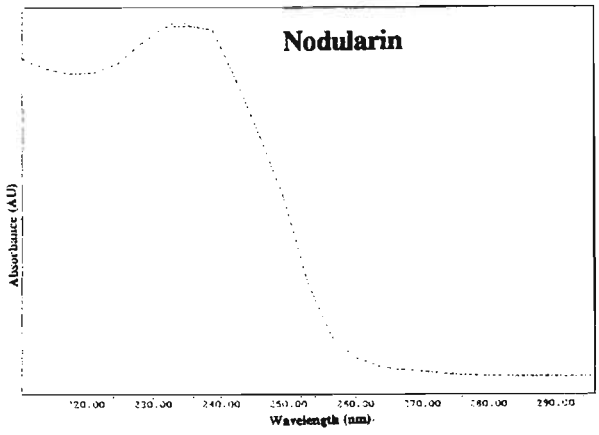

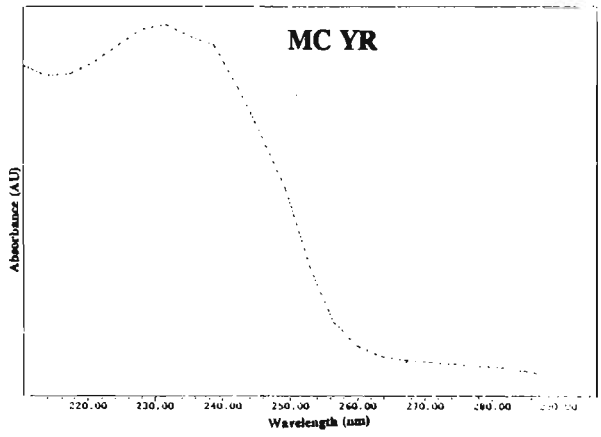

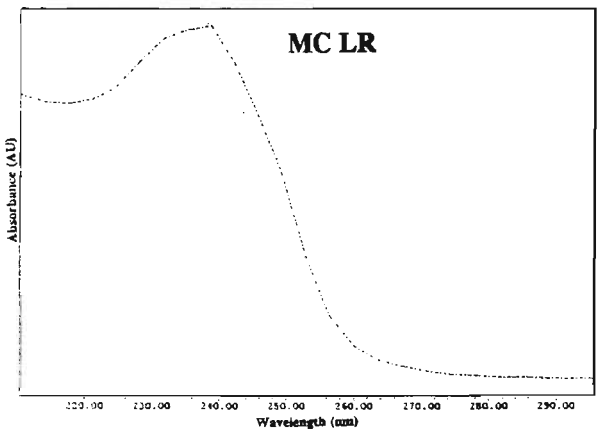

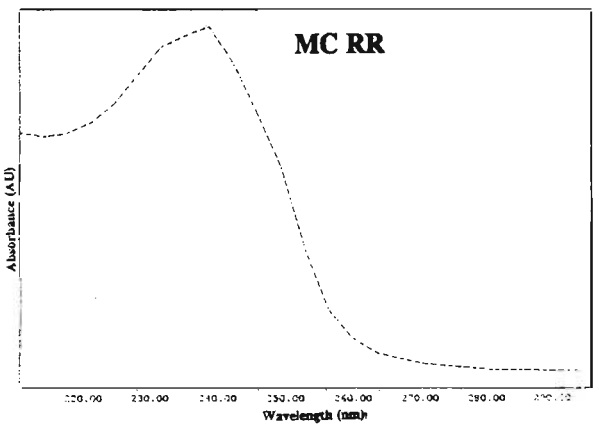

UV SPECTRA OF ALGAL TOXINS ACQUIRED AT A WAVELENGTH RANGING FROM 200-300 NM. A LINEAR GRADIENT AS DESCRIBED IN TABLE 3.3 WAS USED.